EXPERIMENTS AND COMPUTER MODELLING IN STICK-SLIP

by

ADRIAN BOWYER

A thesis submitted for the degree of

DOCTOR OF PHILOSOPHY

of the University of London

and also for the

DIPLOMA OF IMPERIAL COLLEGE

JUNE 1979

Lubrication Laboratory

Mechanical Engineering Department

Imperial College

London SW7

HEIGHT (MM)

0.000275

0.000150

0.000025

-0.000100

FRONTISPIECE

A CONTOUR MAP OF EN58B STAINLESS STEEL GROUND AND THEN ABRADED WITH 400 GRIT EMERY.

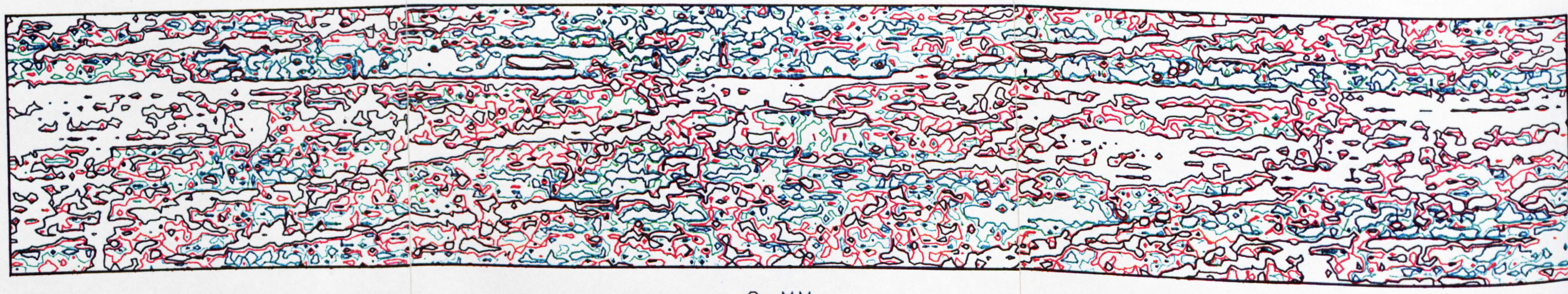

0.5 MM

3 MM

ABSTRACT

An apparatus was built for producing stick-slip and recording the time dependent variables associated with it, in order to investigate its causes.

A theory was devised to explain stick-slip behaviour based on the results of experiments and also on the literature discussed in Chapter One.

A novel computer model of sliding was written to test this theory, based on the work of Sayles and Thomas (46)* to cover the sliding of two real rough surface maps over one another after loading them together.

The results are presented in the following chapters.

* Numbers in brackets refer to references at the back of this thesis.

ACKNOWLEDGEMENTS

The author would like to thank the following people:

His supervisor, Professor A. Cameron, for his constant help and encouragement.

All members of the Imperial College Lubrication Laboratory for their good humoured assistance, especially Reg Dobson and Tony Wymark for their technical help.

His wife, Christine, for her patience and toleration in the face of all his eccentricities.

Doctors Robin Hiley, Hugh Spikes and Alan Syrop for many hours of interesting conversation on matters tribological and otherwise.

G.K.N. Limited for their sponsorship.

Judith Glushanok for the typing.

Professor K.L. Johnson for his suggestions for corrections and improvements.

CONTENTS

† See also corrections in the Addendum, p159

LIST OF FIGURES

SYMBOLS AND ABREVIATIONS

M	Mass
V_o	Constant slider velocity
L	Load
k	Spring constant
μ	Friction coefficient
μ_s	Static friction coefficient
μ_d	Dynamic friction coefficient
x	Displacement in direction of sliding
$\dot{x}$	Velocity
$\ddot{x}$	Acceleration
y	Length in a direction perpendicular to sliding
t	Time
z	Height values of a surface map
z_1	Lowest peak of upper map
z_2	Highest peak of lower map
Δz	Increment of height
h	Vertical displacement of slider
CLA	Center line average
μm	Micro meters
ADC	Analogue to digital converter
RMS	Root mean square
ACF	Auto correlation function
ψ	Plasticity index
E	Young's modulus
H	Hardness
ν	Poisson's ratio
A	Real area of contact

a_i	Element of real area of contact
p_s	Yeild shear stress
p_c	Yeild compression stress
LVDT	Linear variable displacement transducer
P	Pressure
l	Sample length

INTRODUCTION

Friction induced vibration, or stick-slip as it was called by Bowden and Leben (1), is a well known phenomenon. Creaking doors, brake squeal, chalk scraping on a blackboard and the music of instruments of the violin family (2) are some examples that are common in everyday life. With the exception of the last case stick-slip is unwanted. It causes inaccuracies in servomechanisims and in machining operations. It can increase the wear rate and fatigue of sliding components and usually makes an unpleasant noise.

CHAPTER ONE

GENERAL PRINCIPLES AND LITERATURE SURVEY

1.1 Fundamental principles

To investigate the mechanism of stick-slip a general mathematical model of sliding systems is needed.

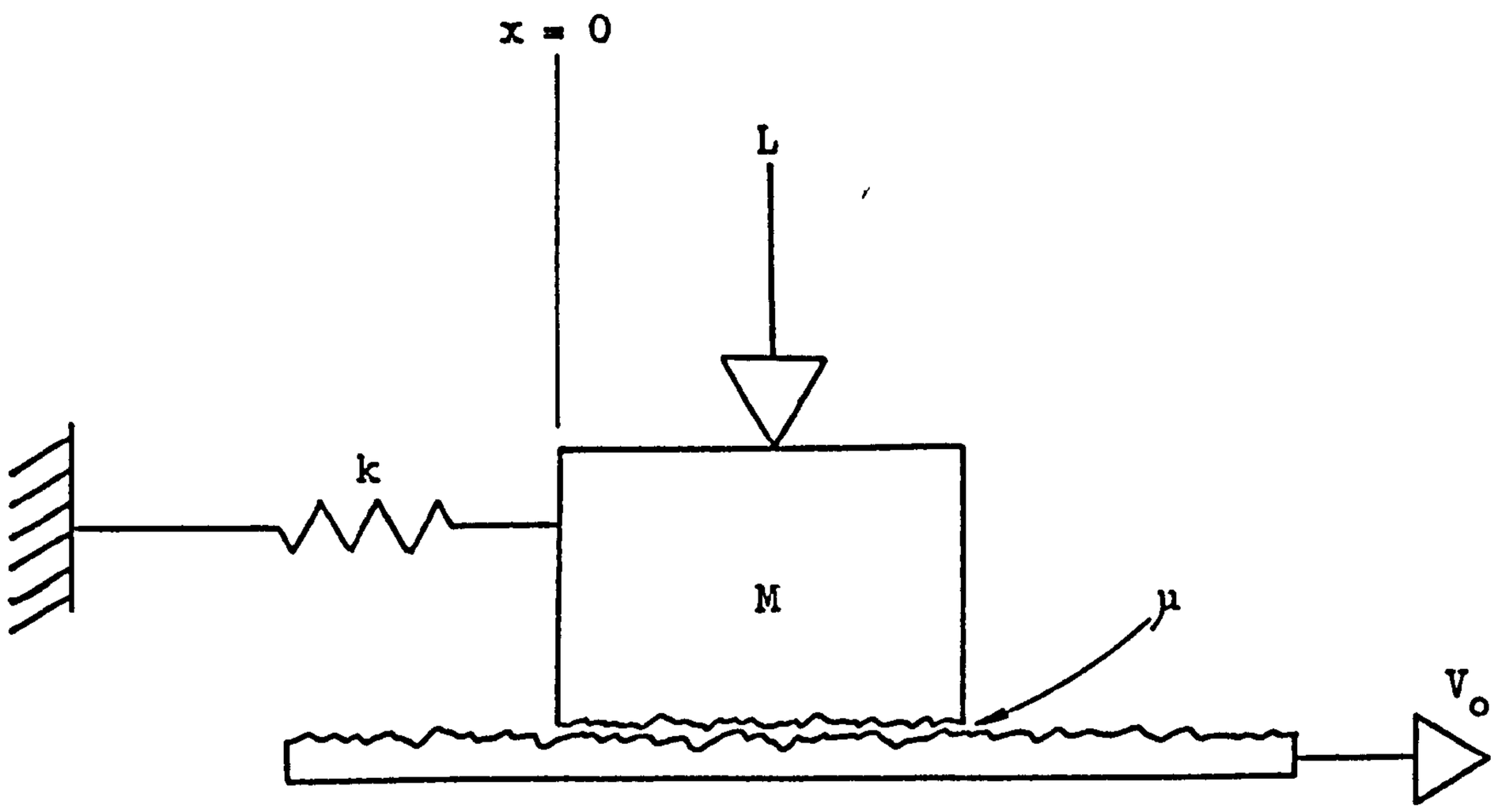

Fig. 1.1 A sliding system

Consider the system shown in fig. 1.1. A slider, of mass M, is forced against a surface moving at a velocity V_o, by a load L. M is restrained by a spring of stiffness k, and the mutual coefficient of friction between M and the lower surface is μ. When M is in the position x=0 the spring is relaxed. External damping will, for the moment, be ignored. Any damping forces that occur in the frictional contact can legitimately be considered part of the variable μ. Apart from external damping, this model and its polar equivalent are completely general. All real sliding

systems must have some mass and some finite stiffness.

Consider the horizontal forces acting on M (fig. 1.2).

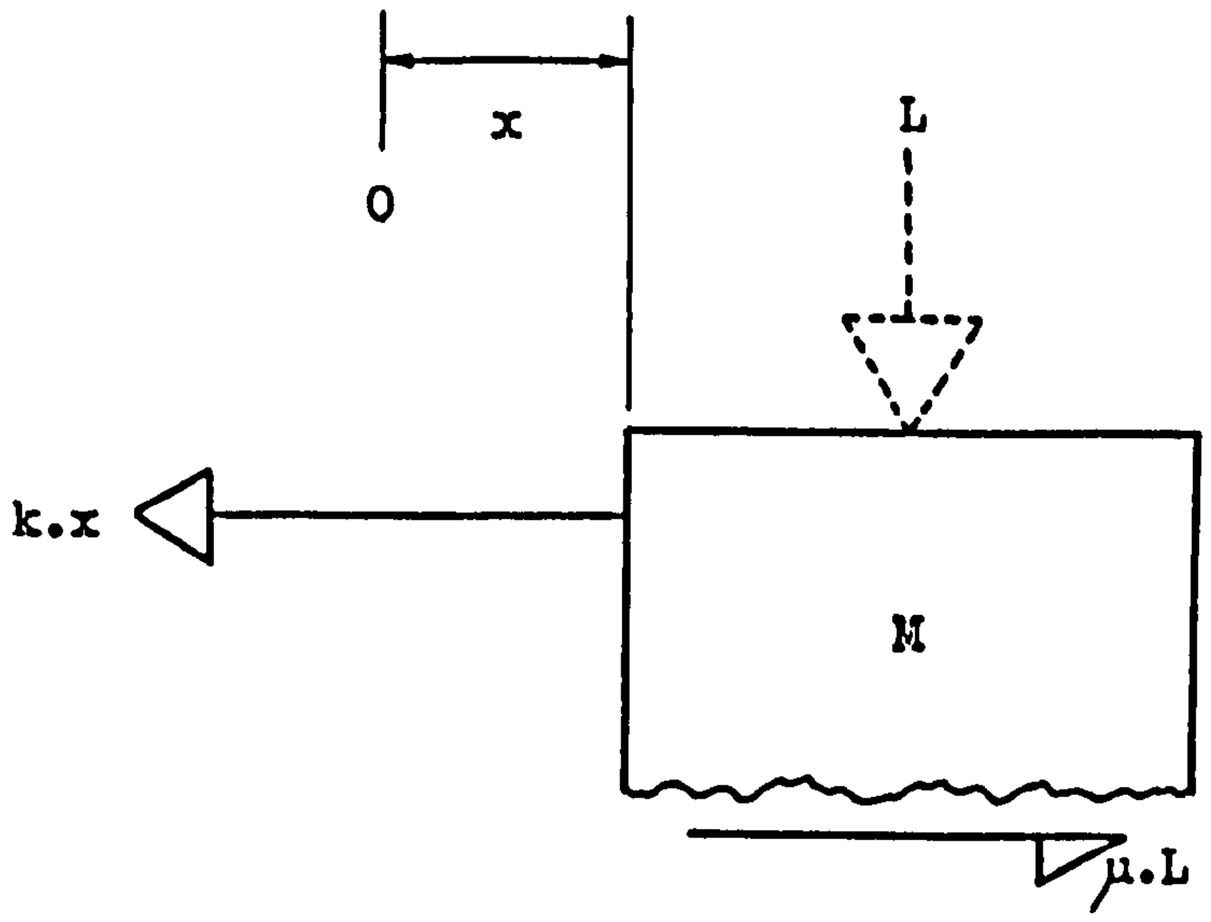

Fig. 1.2 Horizontal forces on M

If M is displaced by an amount x, there will be a force in the spring of

$$-k.x$$ (action to the right being considered +ve)

The force on M from the action of friction, μ, will be (neglecting the effect of gravity on M)

$$+\mu.L$$

These forces will cause M to accelerate and, from Newton's Second Law:

$$\mu.L - k.x = M.\ddot{x} \quad \ldots\ldots\ldots \quad (1)$$

This is the equation of motion of M (or, more properly, the force balance equation).

If μ were a constant, as predicted by the classical laws of friction from Amontons (1699) and Coulomb (1785), the system would be stable when

$$\mu.L = k.x \quad \ldots\ldots\ldots\ldots\ldots \quad (2)$$

M would slide steadily on the lower surface with the spring stretched by an amount

$$x = \frac{\mu.L}{k} \quad \ldots\ldots\ldots\ldots\ldots \quad (3)$$

If M were displaced by a small amount it would undergo a decaying oscillation (3). The system would not undergo self-excited vibrations, i.e. it would not stick-slip.

In 1835 Morin (4) proposed, from the results of experiments, two coefficients of friction: a high, static coefficient that applied to bodies at rest relative to each other, μ_s, and a lower, dynamic coefficient that applied to bodies in relative motion, μ_d.

A sliding system with these characteristics can stick-slip. The mechanism is as follows: As the lower surface starts to move at V_o with the spring relaxed, the spring force is zero and, as there is no relative sliding, the relevant friction coefficient is the high, static one. The force in the spring will be less than the maximum force that friction can provide and the two surfaces will move, stuck together, at V_o, friction just balancing the spring force ($O \longrightarrow P_1$, fig. 1.3). A point (P_1, fig. 1.3) will be reached when k.x equals μ_s.L and the surfaces will start to

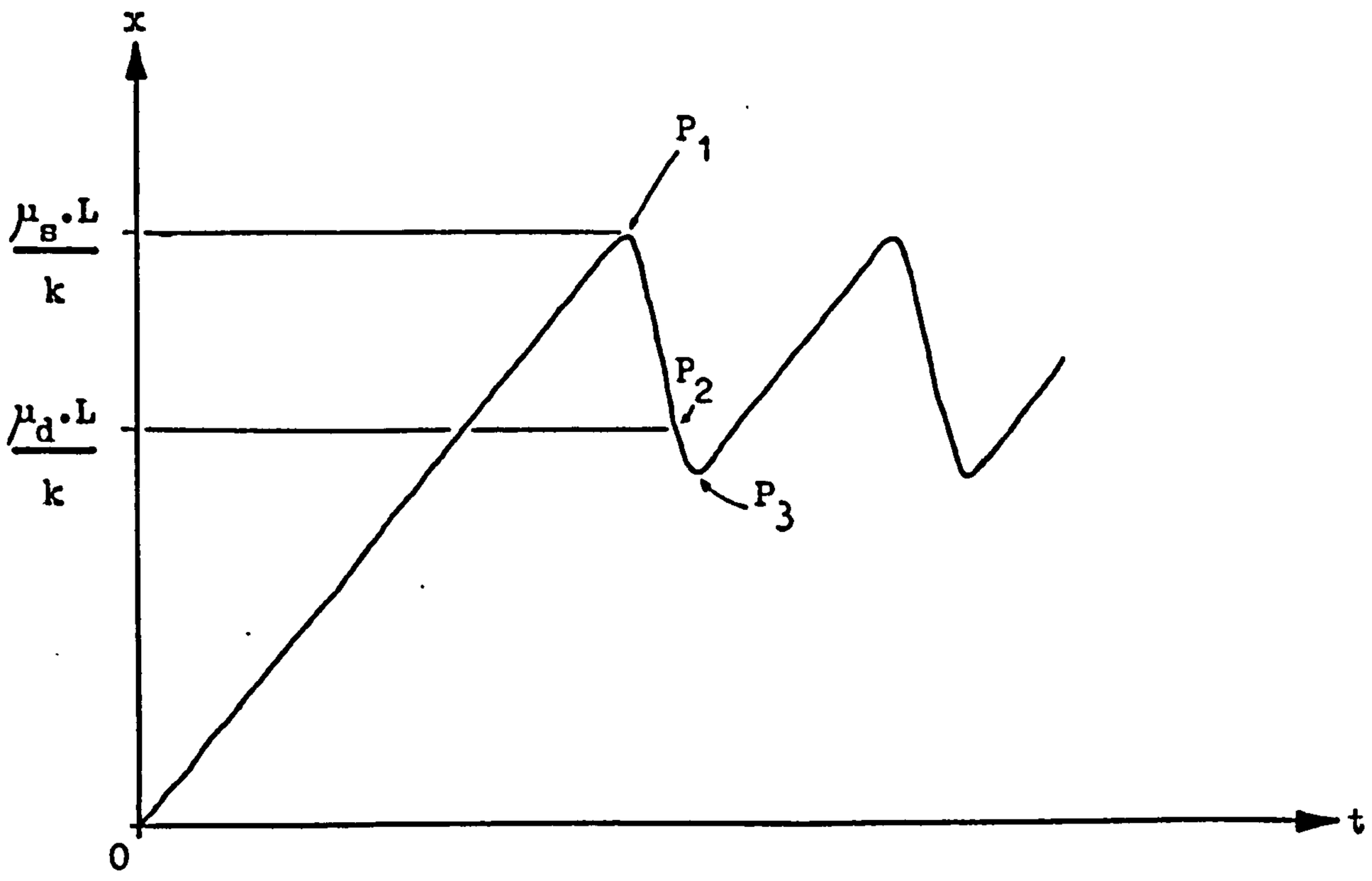

Fig. 1.3 Displacement-time graph for stick-slip

slide relative to each other. As soon as relative sliding commences, the lower, dynamic friction coefficient, μ_d takes over from μ_s. Consequently k.x will be greater than μ_d.L and M will accelerate until k.x reduces to be equal to μ_d.L (P_2, fig. 1.3).

As M continues to move under its stored kinetic energy, k.x will reduce further and will become smaller than μ_d.L. Therefore, M will decelerate, finally coming to rest, relative to the lower sliding surface, at P_3. As soon as it comes to rest, the higher, static coefficient, μ_s, takes over and the process repeats itself, giving rise to the sawtooth type of waveform shown in fig. 1.3.

Wells (5) noticed the occurrence of stick-slip in experiments he was conducting to measure dynamic coefficients of friction of lubricated and unlubricated surfaces with a variety of finishes.

Thomas (6) analysed the process described above and arrived at an equation giving an oscillation similar to that shown in fig. 1.3. He also pointed out the similarity of the waveform to that obtained from a violin (2). Rowson (7) has also analysed Morin's model.

Bowden and Leben (1) carried out a variety of friction tests on similar and dissimilar metals and produced experimental waveforms (fig. 1.4) similar to those shown in fig. 1.3.

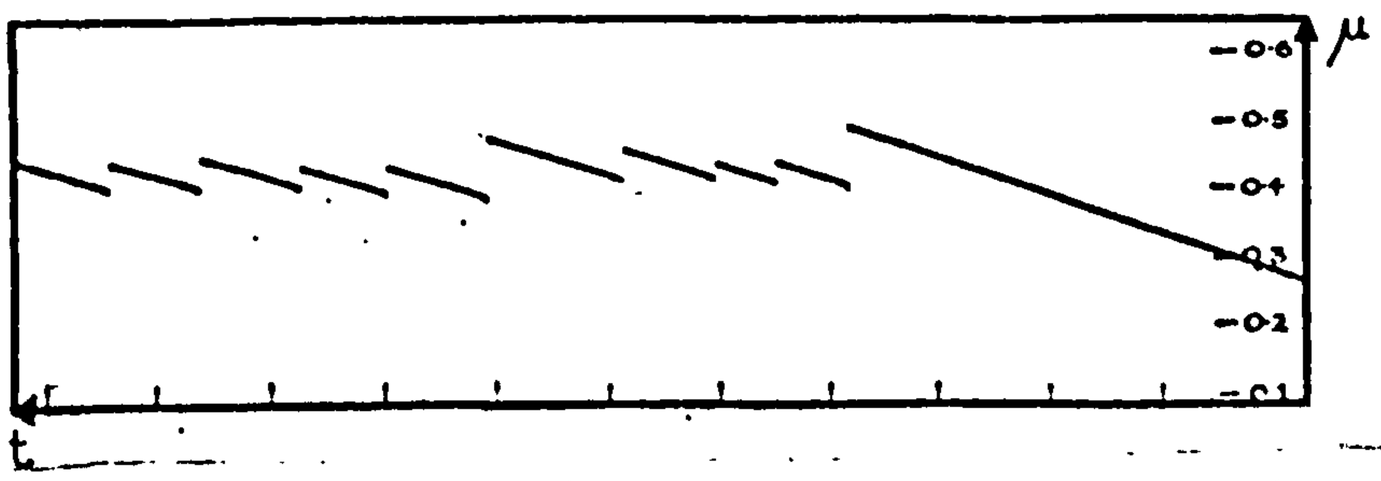

Fig. 1.4 Stick-slip of steel on steel from Bowden and Leben (1)

However, they make the mistake of converting the values of displacement to values of friction force (ordinate, fig. 1.4) by

multiplying by the spring constant of their system. Whilst this is accurate when there is no relative movement between the sliding surfaces, as soon as slip commences accelerations are present and inertial, as well as spring, forces have to be accounted for in evaluating friction (see eq. 1, p. 14).

1.2 Friction as a function of velocity

Rabinowicz (8) points out that frictional behaviour is more complicated than Morin's theory (fig. 1.5a) allows.

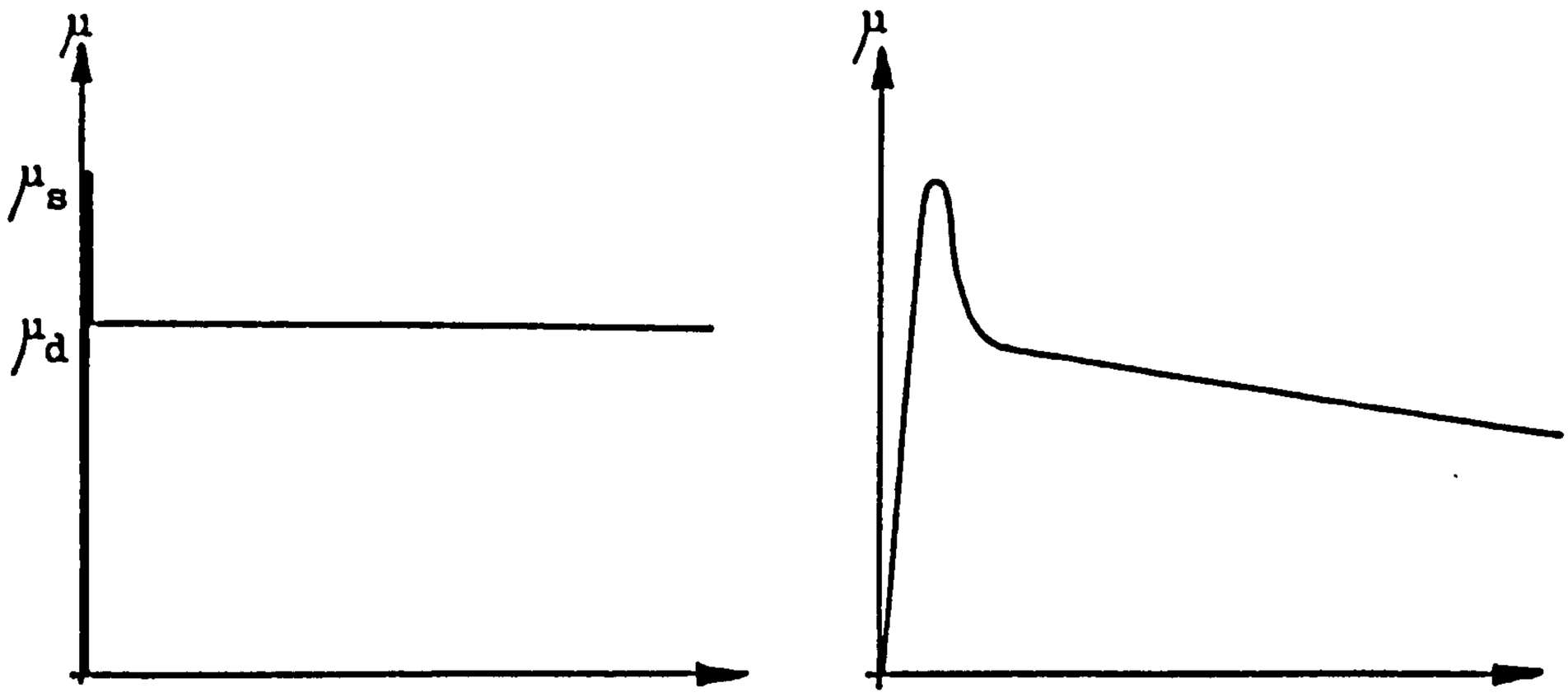

a: Morin's theory

b: Rabinowicz's theory

Fig. 1.5 Friction vs. velocity

Rabinowicz gives the variation of friction with relative sliding velocity as a continuous function (fig. 1.5b).

The initial, steep slope is caused by minute elastic/plastic movement between the sliding surfaces and, as real sliding starts, the friction coefficient falls relatively gradually. Antoniou (9) demonstrates, and quotes other work (10) to show that any sliding system where friction gets smaller as relative sliding velocity gets larger is capable of exhibiting stick-slip (11), (12), (13).

The idea that friction is a function of relative sliding

velocity, i.e.:

$$\mu = \mu\ (\dot{x} - V_0) \quad \ldots\ldots\ldots\ (4)$$

where $\dot{x}$ is the velocity of the slider, M, relative to the fixed support (see fig. 1.1) and V_0 is the velocity of the lower sliding surface, can be incorporated in equation 1. When rearranged this gives

$$\boxed{\frac{M.\ddot{x} + k.x}{L} = \mu\ (\dot{x} - V_0) \quad \ldots\ldots\ldots\ (5)}$$

Sampson, Morgan, Reed and Muskat (14) made one of the first attempts to solve this equation for $\mu\ (\dot{x} - V_0)$ using experimental stick-slip data. They measured displacement, x, and, with only partial success, velocity, $\dot{x}$. They then tried to differentiate these to give $\ddot{x}$ by drawing tangents. The results of this process were rather scattered so they had to use a smoothing curve fit to produce results. They obtained the function shown in fig. 1.6.

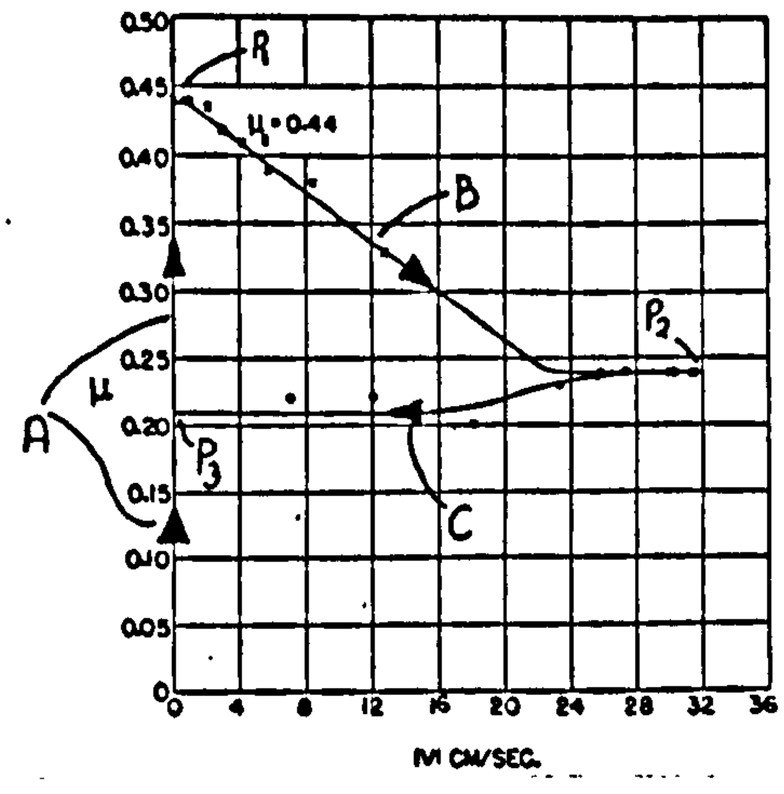

Fig. 1.6 The function $\mu\ (\dot{x} - V_0)$ from Sampson et al (14)

The points P_1, P_2 and P_3 refer to parts of the displacement-time graph equivalent to fig. 1.3.

The arrow heads show time increasing. With no relative velocity (section A of the curve) μ rose to the high, static value. Sliding then started and the friction dropped (section B) with increasing velocity, as predicted. When the sliding velocity decreased, however, the system exhibited hysteresis. That is, the

the curve did not retrace itself and the friction remained low (section C).

Using more modern equipment, Brockley and Ko (15) obtained the function μ $(\dot{x} - V_o)$ in the following manner: They measured displacement with strain gauges, acceleration with an accelerometer and velocity with a magnet and coil velocity transducer. They then fed the voltages from these into a simple analogue computer connected to the X and Y plates of a storage oscilloscope. The analogue computer was patched to do the arithmetic required to solve equation 5 for μ. The resulting voltage was connected to the Y plates. The voltage representing $\dot{x} - V_o$ was fed to the X plates. The results are shown in fig. 1.7a.

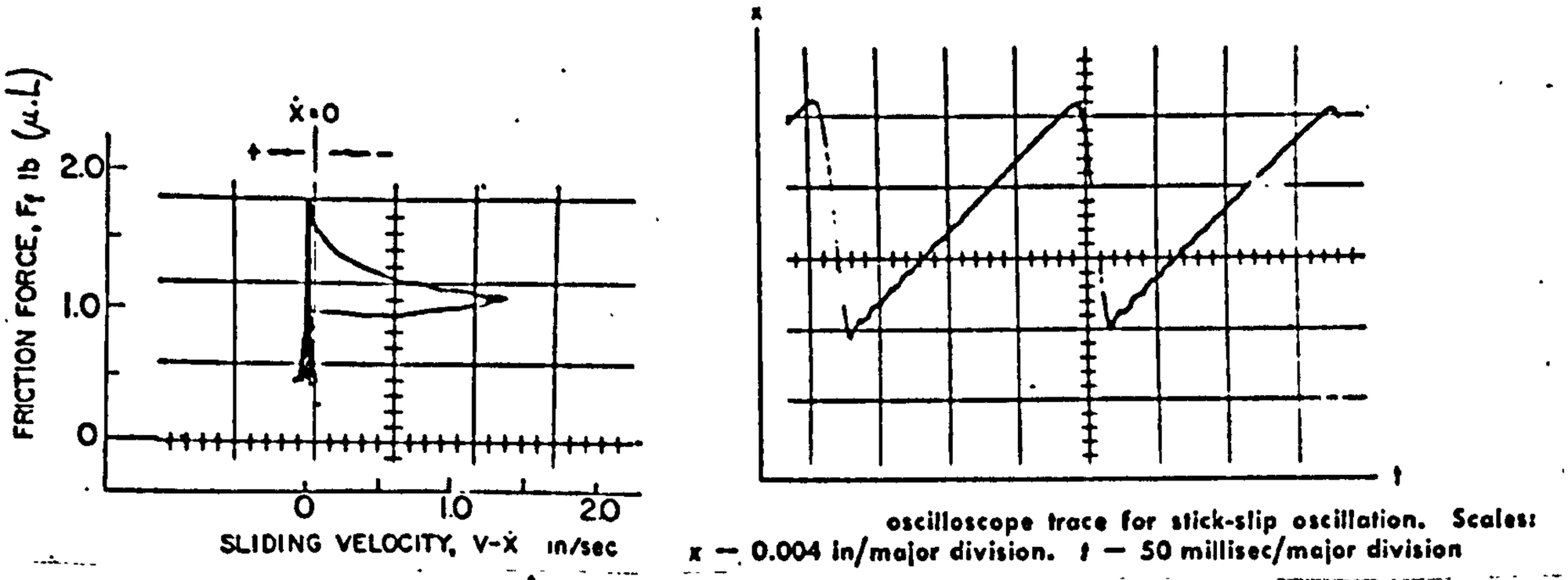

a: μ vs. $V_o - \dot{x}$ b: x vs. t

Fig. 1.7 Brockley and Ko's determination of the function μ $(\dot{x} - V_o)$

As can be seen, the same hysteresis as that shown in fig. 1.6 is present. The actual stick-slip is shown in fig. 1.7b (cf. figs. 1.3, 1.4).

Antoniou (9) solved equation 5 from stick-slip data using a reversal of the geometrical phase-plane method of Linhard (16), adapted for a digital computer.

The advantage of all these methods is that they require only one stick-slip cycle to give a complete plot of the function μ $(\dot{x} - V_o)$.

In another paper (17), Brockley and Ko consider a rather different form of stick-slip from that so far described, which they call quasi-harmonic. This is not stick-slip in the literal sense as the surfaces never stick. Their graph of x vs. t is shown in fig. 1.8a. As can be seen, the motion is substantially sinusoidal.

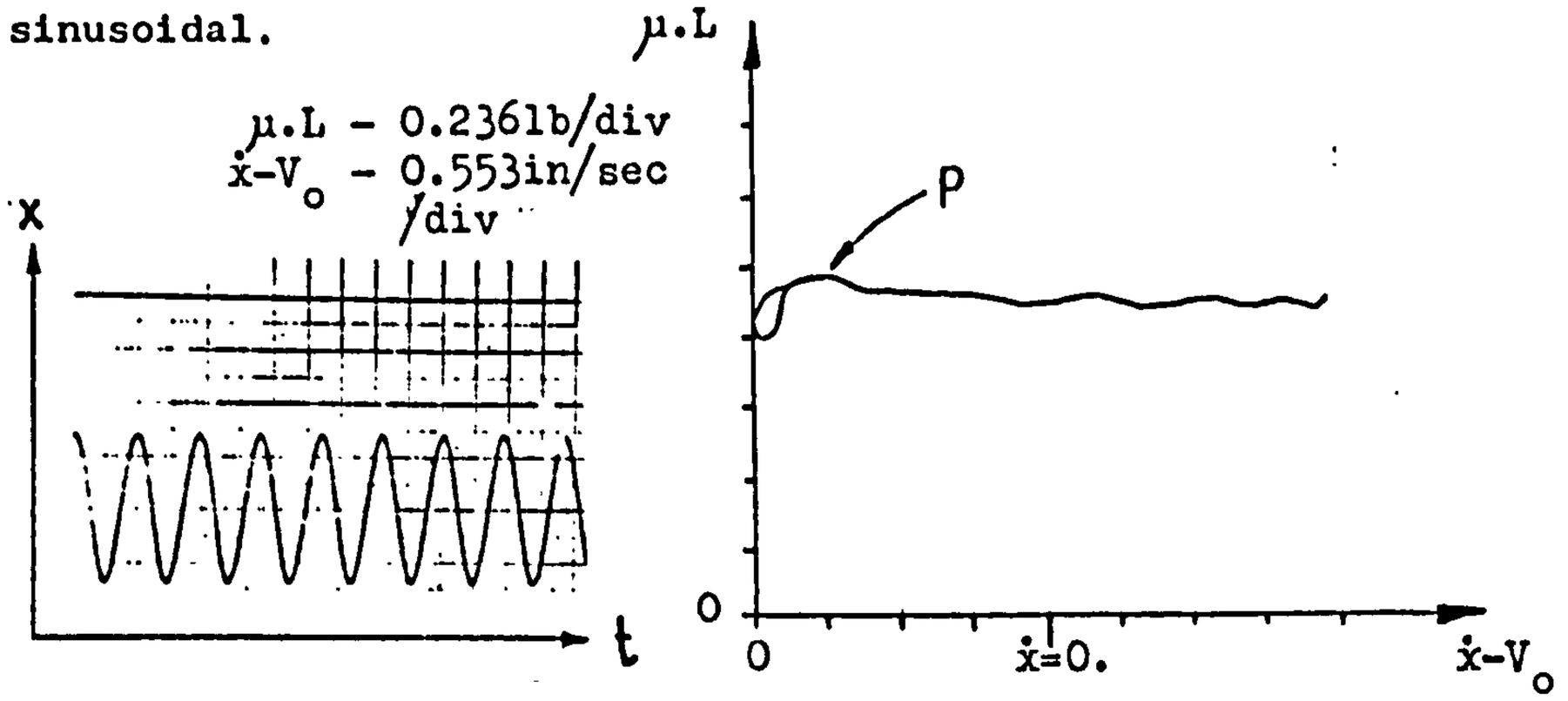

a: x vs. t b: $\mu (\dot{x} - V_o)$

Fig. 1.8 Quasi-harmonic stick-slip from Brockley and Ko (17)

The function $\mu (\dot{x} - V_o)$ that they obtained for this type of vibration is shown in fig. 1.8b, and they conclude that the hump, P, is necessary for this type of vibration. Note that the curve is not hysteresial. The tendency to this type of stick-slip increases as V_o increases.

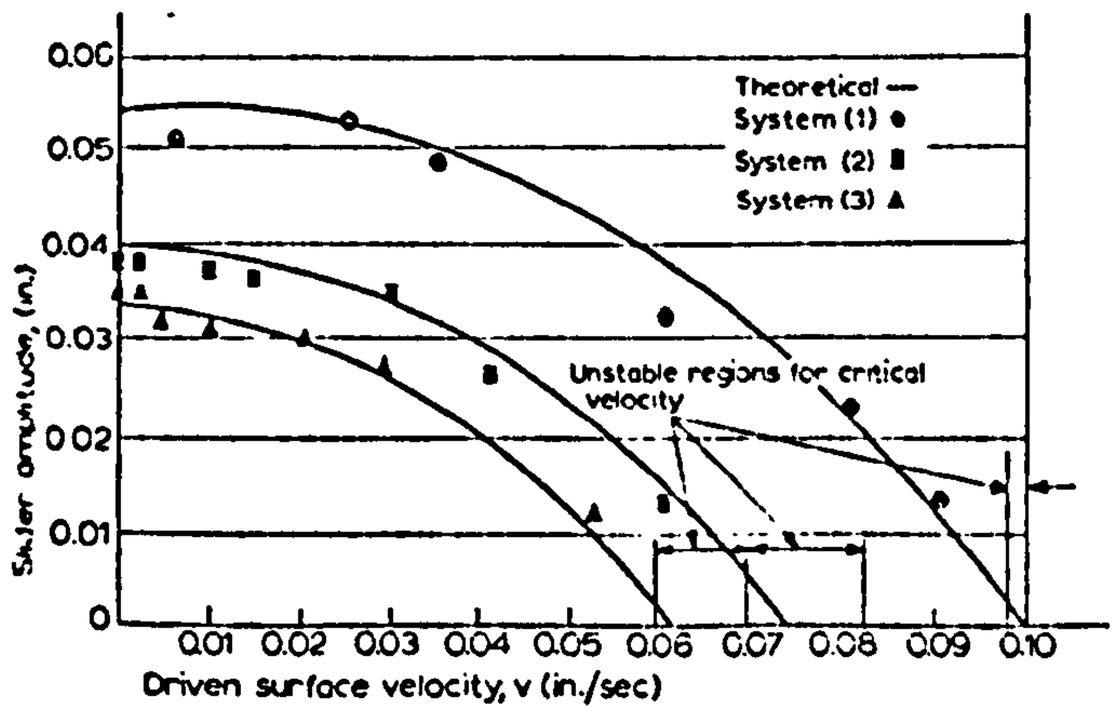

Fig. 1.9 Critical value of V_o from Brockley, Cameron and Potter (18)

Brockley, Cameron and Potter (18) show that the amplitude of vibration in stick-slip systems reduces with increasing V_o

until V_o reaches a value above which stick-slip vanishes altogether (fig. 1.9). They call this the critical velocity and do a theoretical analysis to show how this behaviour relates to the external damping, if any, and the friction-velocity curve. Banerjee (19) published a computer analysis of this phenomenon which agrees broadly with Brockley et al.

Cockenham and Cole (20) did an analogue computer simulation of stick-slip using simple μ $(\dot{x} - V_o)$ assumptions to determine the degree of external viscous damping required to eliminate stick-slip. As viscous damping has a force vs. velocity relationship with a positive gradient, and stick-slip friction has a negative one, the former may be used to counteract the latter.

1.3 The effect of stick time - Adhesion

Rabinowicz (21) gives a graph of static friction against the time that the surfaces had been together, using results taken from Dokos (22) (fig. 1.10).

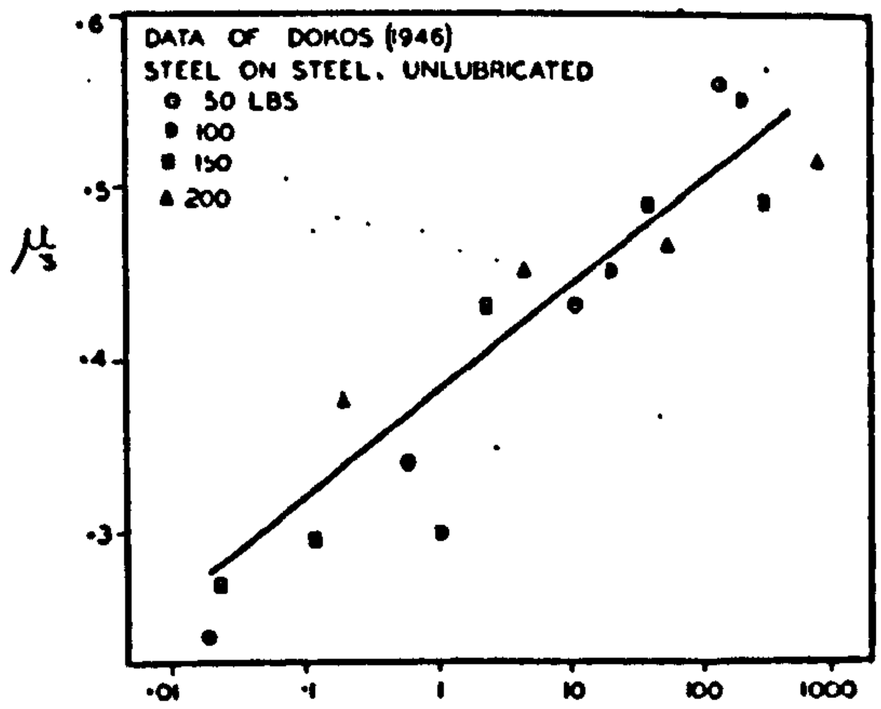

Fig. 1.10 μ_s vs. stick time from Dokos (22)

As can be seen, the longer the surfaces remained together the greater the static friction was between them. This has also been investigated by Bowden and Tabor (23).

It is generally considered that this phenomenon is the result of adhesion between the surfaces. The surface asperities

are assumed to creep plastically to a greater degree of conformity over a period of time and possibly some welded junctions are formed between them. See, for example, Tabor (24) and Syrop (25).

Green and Brockley (26) consider that, in many cases, it is the rate of application of shearing force, $\dot{F}$, to a frictional contact that decides the static friction (fig. 1.11).

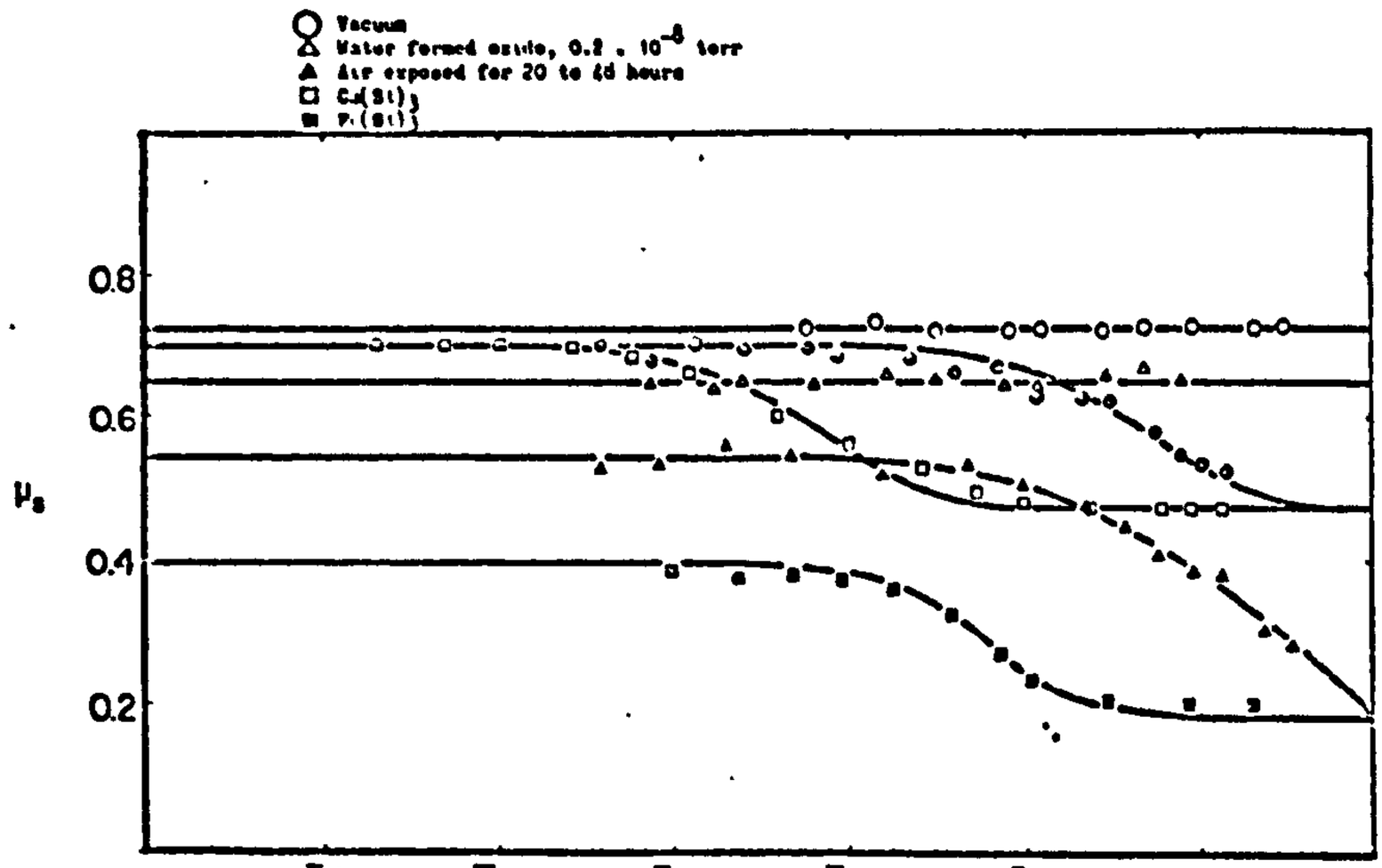

Fig. 1.11 The variation of μ_s with rate of application of shearing force, from Green and Brockley (26)

As can be seen, the static friction drops with increasing $\dot{F}$, except under clean, vacuum conditions. The authors conclude that this behaviour is caused by the adsorption of hydrocarbons etc. from the air onto the cleaned surfaces to form a non-Newtonian viscous layer.

1.4 Perpendicular movement between the sliding surfaces

Tolstoi (27) showed that when surfaces slide they also move in a direction normal to their sliding motion. He gives a graph (fig. 1.12) of this normal movement during the slip portion of stick-slip, which he measured by means of interferometry.

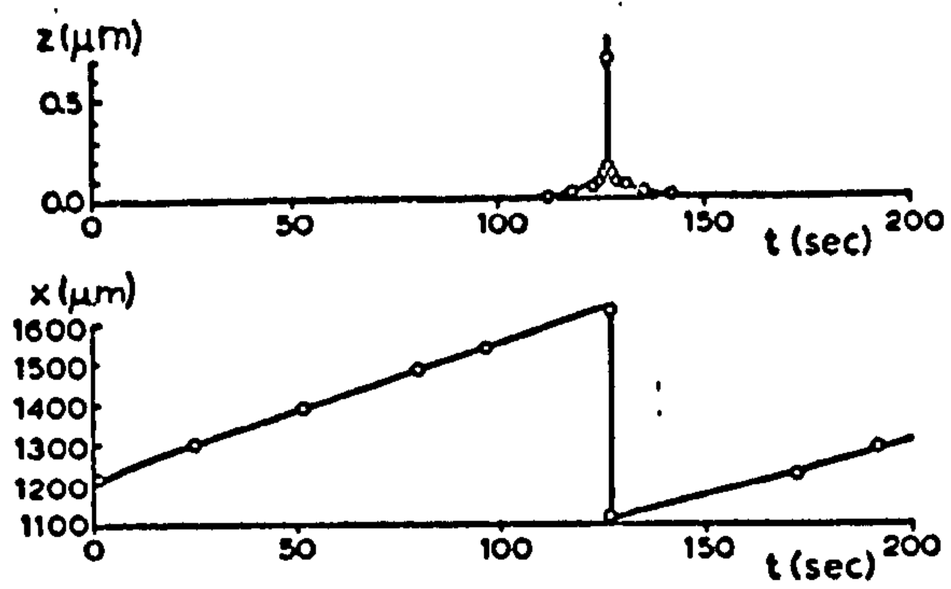

Fig. 1.12 Normal movement during stick-slip from Tolstoi (27)

Tolstoi claimed that this normal movement is caused by asperity interaction, which would tend to produce a separating, as well as a frictional, force (fig. 1.13).

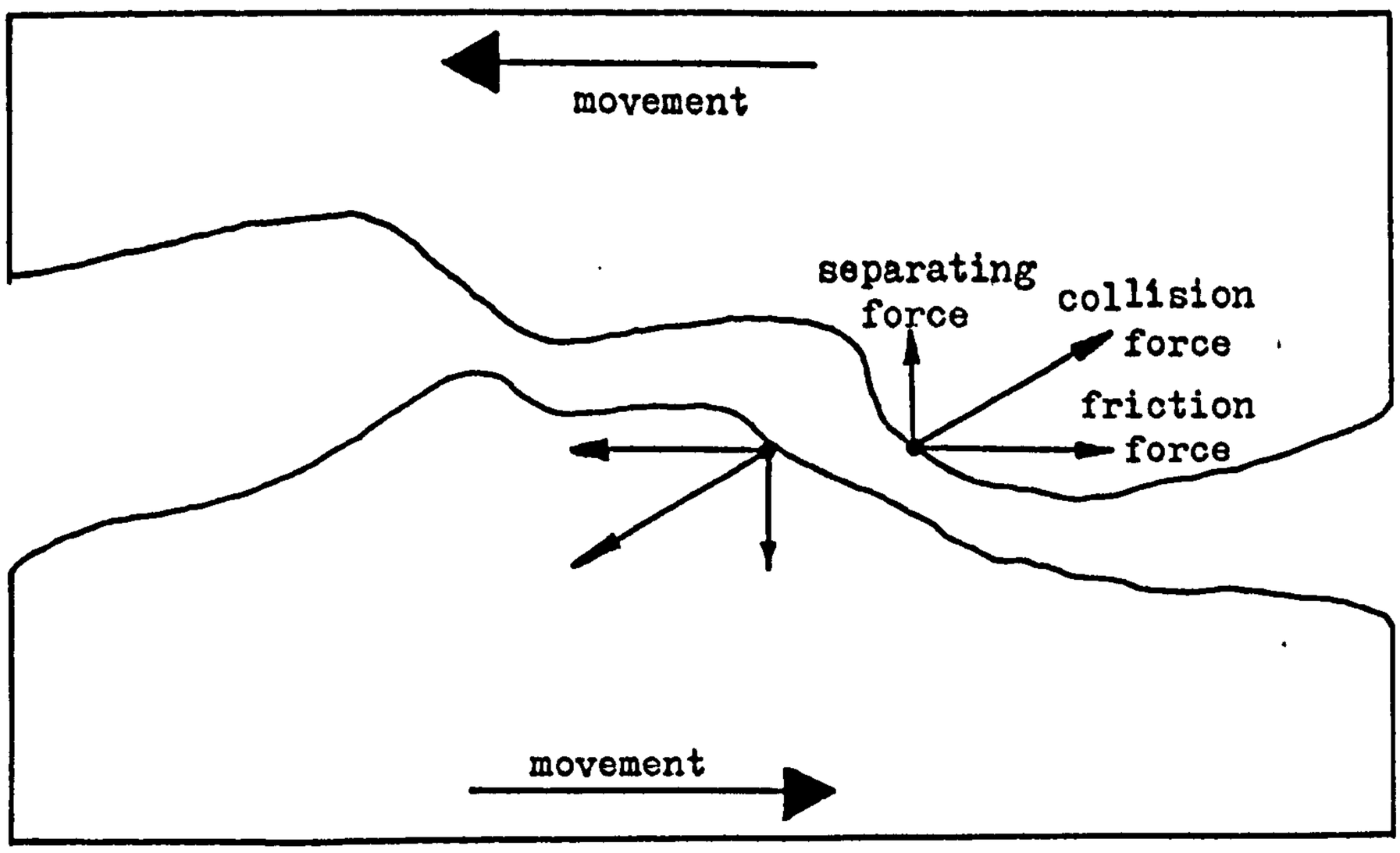

Fig. 1.13 Normal force from asperity collisions

Elder and Eiss (28) conducted experiments where they gradually increased the normal stiffness in sliding, thus impeding this normal movement. The effect of this on the stick-slip produced is shown in fig. 1.14.

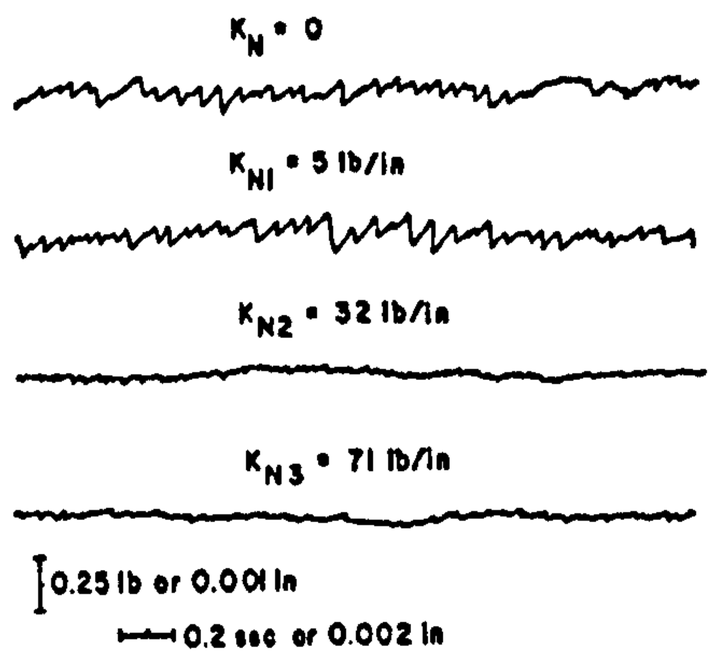

Variation of stick-slip amplitude with normal stiffness for a 300 μ in. surface.

Fig. 1.14 The effect of normal stiffness on stick-slip from Elder and Eiss (28)

As can be seen, the larger the normal stiffness, the lower the stick-slip. Antoniou (9) points out that, if surfaces move apart as they slide relative to each other, then friction should drop as asperity contact is reduced. This goes some way towards explaining the negative slope on the friction-velocity characteristic (B, fig. 1.6).

The necessity for a finite stick time to obtain high static friction coefficients (section 1.4) gives a partial explanation of the appearance of hysteresis in the friction-velocity curve (C, fig. 1.6). Relative motion might tend to reduce any adhesion between the sliding surfaces.

1.5 Surface roughness measurement

If sliding surfaces were perfectly plane, friction would not exist. It is the minute irregularities in a surface that, in colliding, welding, shearing and ploughing cause the friction force.

Most rough surfaces are random, both in the heights and shapes of their asperities. Consequently, they are usually treated statistically.

A general introduction to the study of rough surfaces may be found in Leather (29), and a wide ranging review of literature was given by Thomas and King (30).

The most common measuring instrument used in the study of rough surfaces is the stylus profilometer or Talysurf* machine. This works on the same principle as a gramophone cartridge. A fine diamond stylus is drawn at a constant, slow rate across the surface to be studied. The movement of the stylus as it traverses the surface asperities is measured by means of a linear variable displacement transducer (LVDT, see Appendix 2, p.156) which produces a voltage proportional to the movement. This voltage is then fed to a pen plotter to produce a profile of the surface (fig. 1.15).

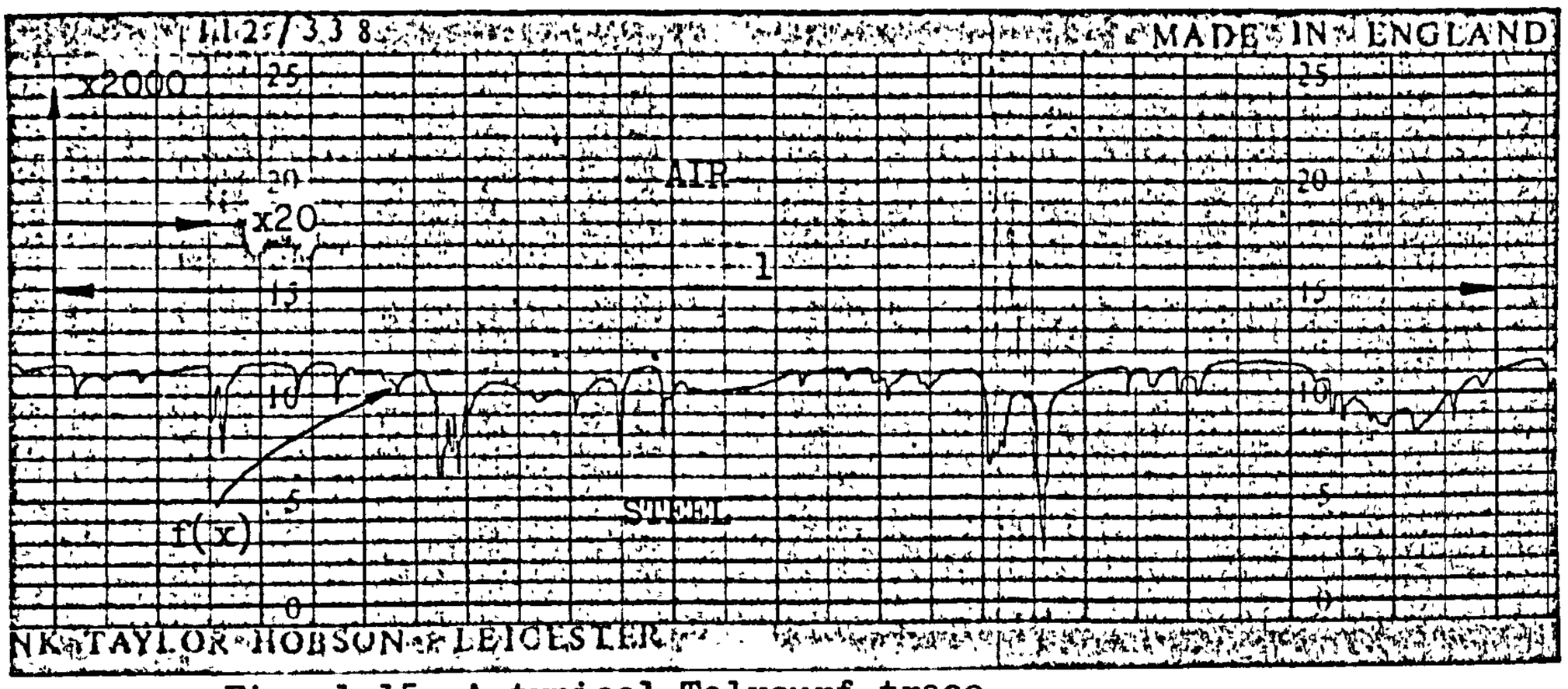

Fig. 1.15 A typical Talysurf trace

The magnification factors, as are shown on the diagram, are generally different, the vertical magnification being much greater than the horizontal. This can lead to some misconceptions. Because of their differential magnifications, the slopes of the

*This is the trade name of a stylus profilometer made by Rank-Taylor-Hobson Limited, but, like the word Hoover, it has passed into use as a generic term.

asperities in fig. 1.15 seem to be of the order of 60^{o}-70^{o}, whereas, in reality, they would probably not be greater than about 4^{o}.

In addition to being fed to the plotter, the signal also drives an electronic circuit to calculate the centre line average (CLA) of the waveform. This is defined as:-

$$\sigma_{CLA} = \frac{1}{l}\int_{o}^{l} |f(x)|\, dx \quad \ldots\ldots\ldots\ldots (6)$$

where l is the length of the sample and f(x) is the profile. The CLA value of the surface in fig. 1.15 is 2.3 μm.

Profilometers are generally equipped with variable low-pass filters to remove large wavelengths that are not proper roughness variations, but are changes in bulk geometry. The shortest wavelength that can be resolved is set by the tip radius of the stylus. In the case of the Talysurf, this is 4 μm in the direction of sliding. For reasons of strength, however, the stylus is chisel shaped. It is wider across the direction of sliding than the 4 μm implied by the above radius. This means that some profile errors can be caused by the profilometer stylus riding over the shoulders of asperities (fig. 1.16).

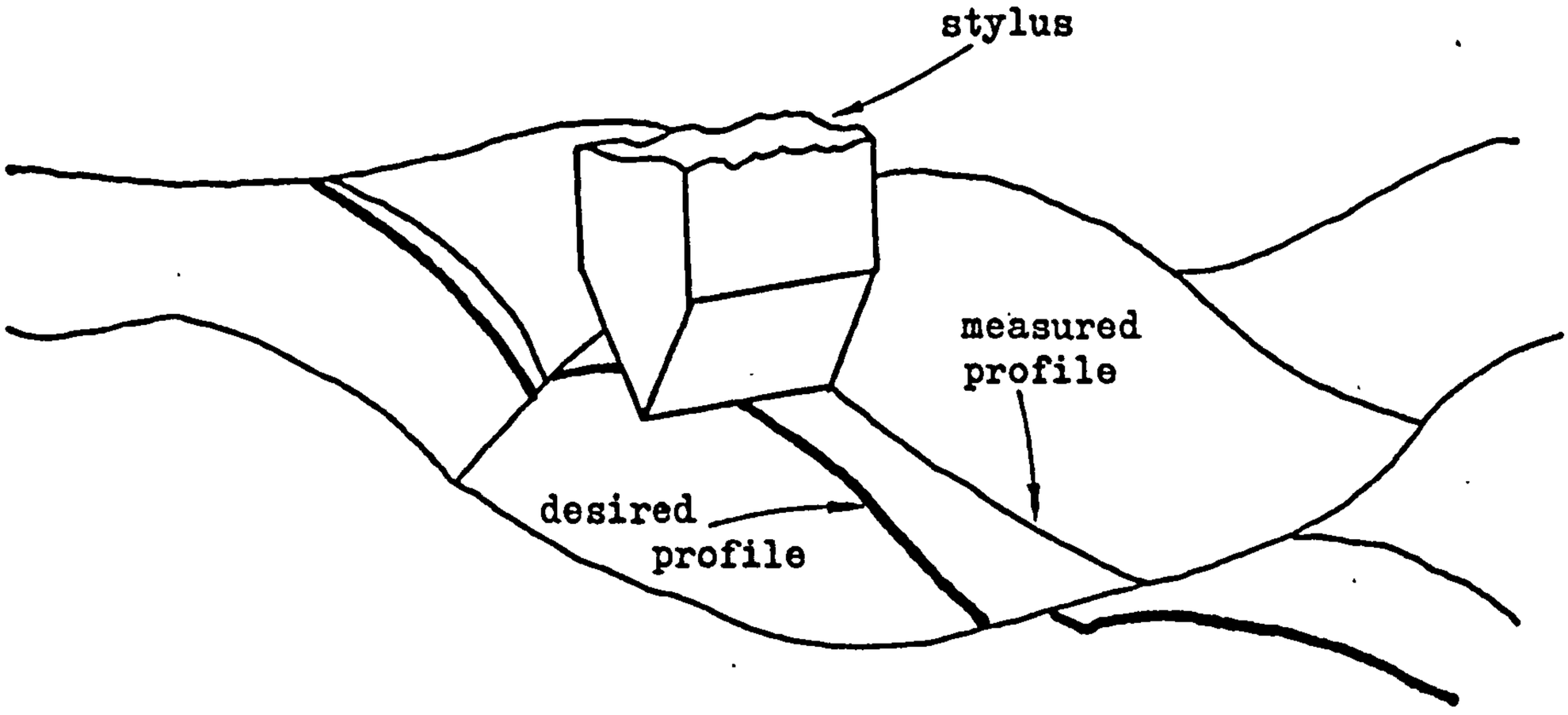

Fig. 1.16 Stylus profile errors

Other methods of studying surfaces have been used. The scanning electron microscope can be employed to produce a picture of the asperities on a surface. Taper sections and shallow-angled shadowing can be used to differentially magnify surface asperities to facilitate their study. Recently, laser scattering (31) from rough surfaces has been used in asperity analysis. This works on a similar principle to the hologram, which is a two-dimensional Fourier transform of a three-dimensional object, produced by laser interferometry. Transforms of rough surfaces can be obtained in a similar manner.

1.6 The contact between two rough surfaces

Consider what happens when two rough surfaces are forced together by some load, L (fig. 1.17).

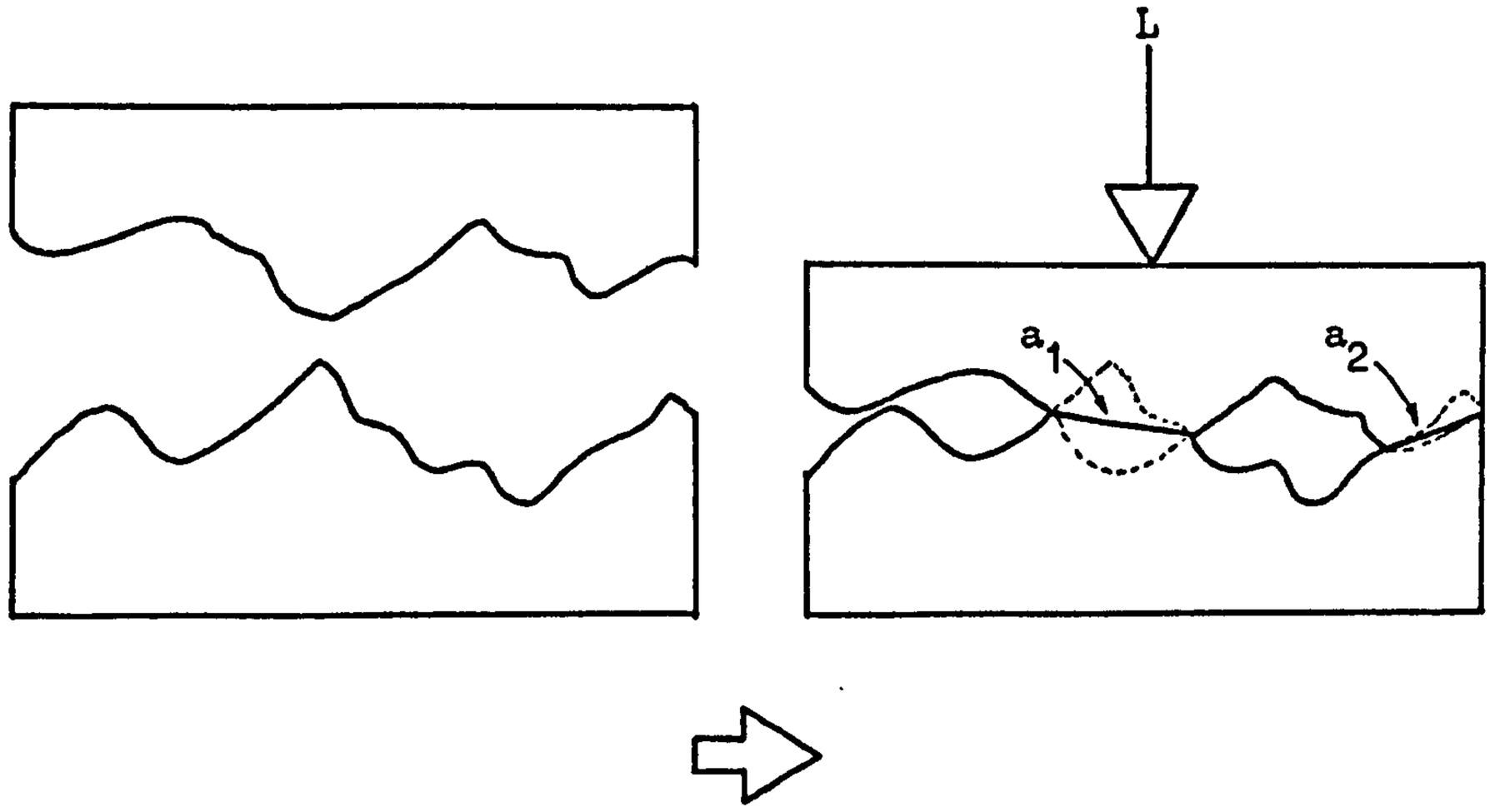

Fig. 1.17 Squashing rough surfaces together

The asperities that come into contact will deform, either elastically or plastically, and the real area of contact, A, will be the sum of all the microcontacts between the individual asperities, a_1, a_2, etc.:-

$$A = \sum \left(a_1 + a_2 + a_3 \ldots\ldots \right) \qquad \ldots\ldots\ldots (7)$$

As L increases, A will increase, as those asperities already in contact deform further and more come into contact.

A is therefore a function of L and is generally small compared to the apparent area of contact. Bowden and Tabor (23) attempted to measure the real area of contact by measuring changes in its electrical resistance. Dyson and Hirst (32) squeezed together a piece of ground steel and an optically flat piece of glass and used a phase contrast technique to show up the areas of contact (fig. 1.18).

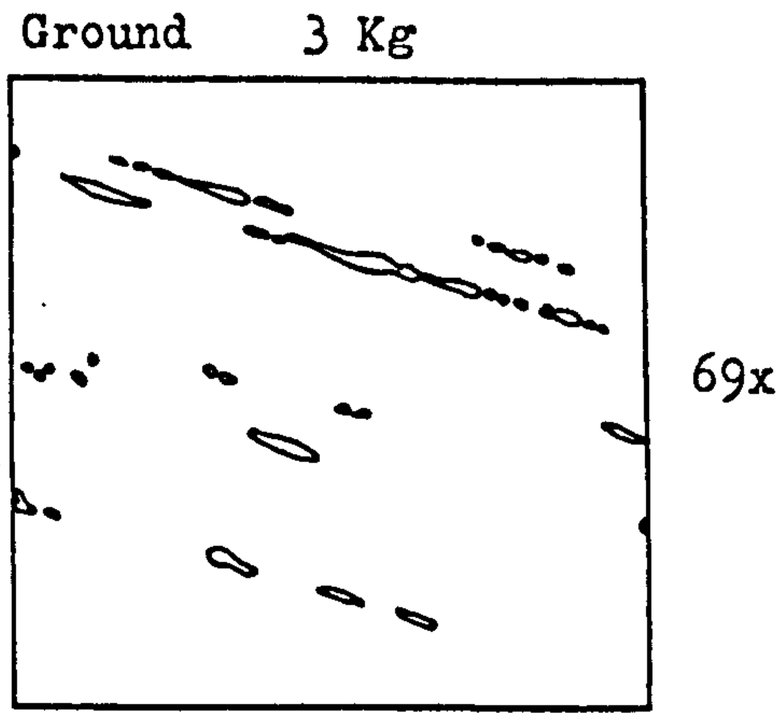

Fig. 1.18 The contact between ground steel and glass, from Dyson and Hirst (32)

Similar work has been done by Uppal, Probert and Thomas (33). Archard (34) showed that, with fairly flat asperities, deformation would be elastic and the real area of contact would be proportional to load. Greenwood (35) considered plastic deformation of surface asperities and showed that the average size of a microcontact was almost independent of load.

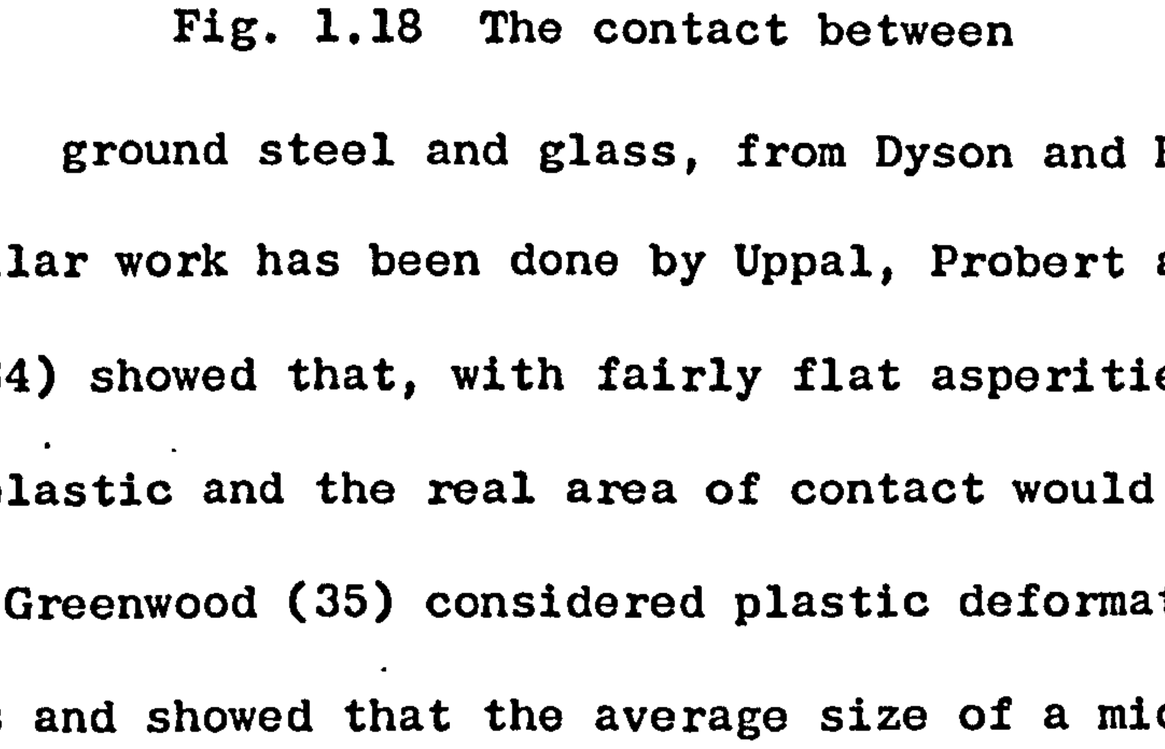

Fig. 1.19 Plastic deformation of asperities from Pullen et al. (36)

Pullen and Williamson (36) took successive, relocated profiles of a rough surface after it had been subjected to increasing load against a harder flat surface. Their results are shown in fig. 1.19. As can be seen, the shape of the profile where no contact has occurred does not change. The contact simply seems to truncate the tops of the asperities. Pullen et al. suggest that the displaced material volume is evenly distributed throughout the bulk, thus raising the whole profile slightly. The idea of asperity truncation in contact, vindicated by these results, is very useful in the modelling of contacts,especially in computer programmes, and will be returned to later in this thesis.

If the deformation of the asperities is plastic (35) (36) (37), the stress tending to separate each asperity is the yield stress and is independent of the asperity deformation. This means that the surfaces will move together until the force obtained by multiplying the real area of contact by the yield stress of the material is just able to support the applied load. Again, the value of A is directly proportional to L, or L to some power (depending on the bulk conformity of the surfaces). This, of course, ignores any work hardening that may take place.

If the shear strength of the contacts is a constant, the friction force, F, will be:-

$$F = A.p_s \quad \ldots\ldots\ldots (8)$$

If, in addition, A is proportional to L, A will be given by:-

$$A = \frac{L}{p_c} \quad \ldots\ldots\ldots\ldots (9)$$

where p_c is the compression strength.

So, from (8):-

$$F = \frac{L}{p_c} p_s \quad \ldots\ldots\ldots\ldots (10)$$

The coefficient of friction will also be constant and will be given by:-

$$\mu = \frac{F}{L} = \frac{p_s}{p_c} \quad \ldots\ldots (11)$$

where p_s is the shear strength and p_c is the compression yield

strength of the contact.

Courtney-Pratt and Eisner (37) demonstrated that, when a contact was subjected to shear stress, plastic flow occurred and the area of contact grew. This phenomenon is known as junction growth.

Tabor (38) considered the effect of contaminating films, such as oxides and lubricant additives, on this junction growth. His model showed that perfectly clean surfaces in vacuo would eventually weld together completely under the action of shear, producing an effective friction coefficient of infinity (a finite shear force would be required to move the specimens under no load). However, with a shear film separating the surfaces of approximately 0.95 times the strength of the parent material, μ dropped to unity. Further reduction in film shear strength to about 0.2 times the bulk value gave values of μ of about 0.1. Despite simplifying assumptions, this theory matches experimental results quite well.

1.7 Characterisation of rough surfaces

In addition to the CLA value of a surface, its RMS value can also be obtained:-

$$\sigma_{RMS} = \sqrt{\frac{1}{l}\int_0^l \left[f(x)\right]^2 dx} \quad \ldots\ldots\ldots (12)$$

The relation between the CLA and RMS values for a given surface depends on the surface structure. For most surfaces, the RMS values are 10%-30% higher than the CLA values.

Some workers (e.g. Thomas (39)) have connected the output voltage from a Talysurf via an analogue-to-digital converter (ADC) to a digital computer, which is used to sample the profile at regular, repeated intervals to obtain a digital record of the profile.

Greenwood and Williamson (40) and Greenwood and Trip (41) used such a digital technique to investigate the nature of the contact between rough surfaces. They also show that the height distribution of many rough surfaces is very close to gaussian. Williamson (42) used a digital technique to examine mean radius of asperity curvature and other variables of surfaces.

Digital techniques also facilitate the calculation of another useful statistical characteristic of a rough surface, its auto-correlation function (ACF). This is defined as:-

$$C(\beta) = \frac{1}{l} \int_0^l f(x).f(x+\beta).dx \quad \ldots\ldots\ldots \quad (13)$$

It is the product of a waveform with itself displaced, with the degree of displacement as the independent variable. The ACF is very useful in showing up periodicities in the waveforms of rough surfaces. Fig. 1.20 shows the ACF of a fine-turned surface (from Leather (29)).

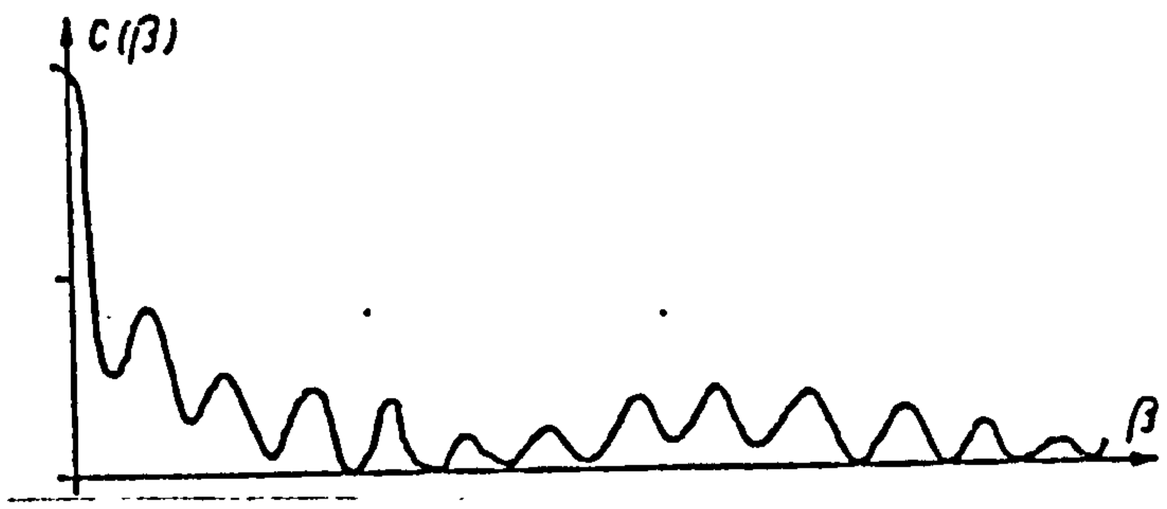

Fig. 1.20 Auto-correlation function of a fine-turned surface from Leather (29)

As the periodic part of the waveform goes in and out of phase with itself as β changes, the product $f(x).f(x+\beta)$ displays a similar periodicity.

Whitehouse and Archard (43) propose an exponentially decaying ACF for a random rough surface. This imposes an upper limit on the finer wavelengths in the surface, but it allowed them to assign a new variable, the correlation distance β^*, to a rough surface. This is defined thus:-

$$C(\beta) = e^{-\frac{\beta}{\beta^*}} \quad \ldots\ldots\ldots (14)$$

Hirst and Hollander (44) take the two lengths σ_{RMS} and β^* and give an expression for plasticity index, ψ :-

$$\psi = 0.6 \frac{E'}{H} \frac{\sigma_{RMS}}{\beta^*} \ldots\ldots (15)$$

where H is the hardness of the material, and

$$E' = \frac{E}{1 - \nu^2} \quad \ldots\ldots\ldots (16)$$

where E is the Young's modulus and ν is Poisson's ratio for the material of the surface. The value of ψ determines the likelihood of plastic flow and damage in a contact between rough surfaces. Hirst and Hollander conducted experiments on surfaces with various values of σ_{RMS} and β^* and, from the results, drew conclusions about safe and unsafe operating conditions (fig. 1.21).

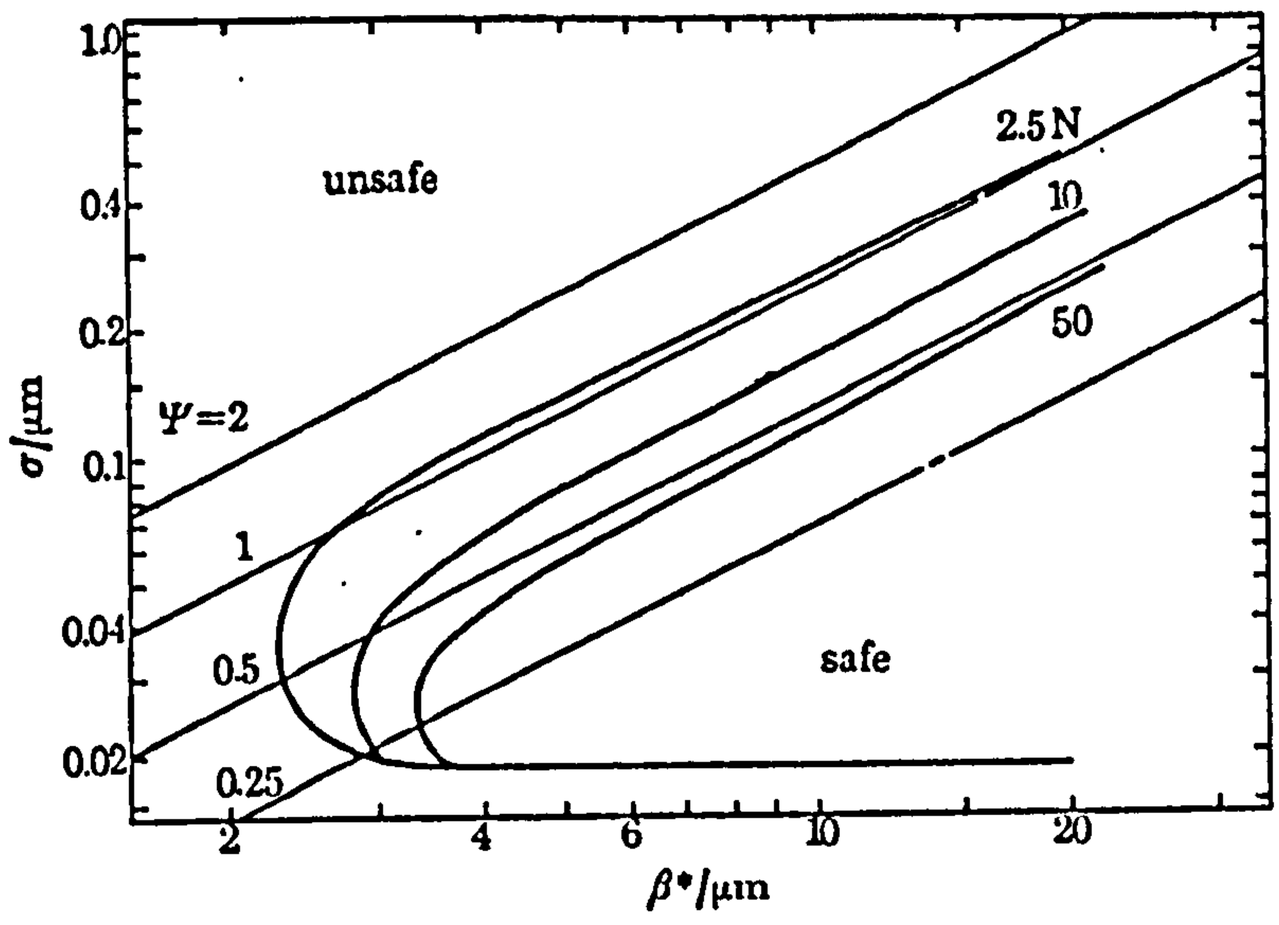

σ–β^* map for abraded surfaces. ——, lines of constant ψ; ——, boundary between safe and unsafe regions.

Fig. 1.21 Safe and unsafe combinations of σ_{RMS} and β^* from Hirst and Hollander (44)

Sayles (45) and Sayles and Thomas (46) (47) have taken multiple parallel passes with an automatic Talysurf/computer system to produce surface maps (fig. 1.22).

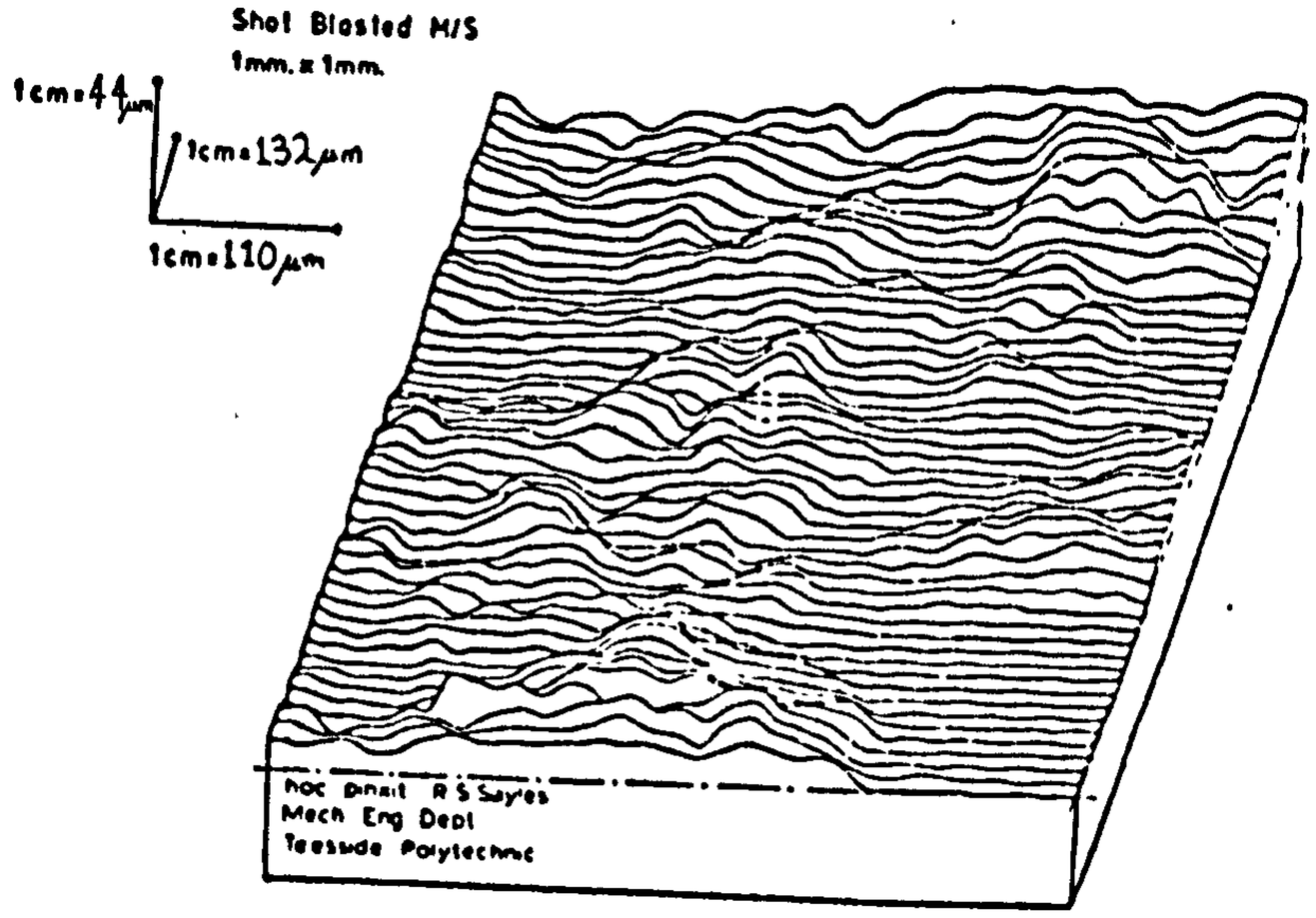

Fig. 1.22 Surface map of shotblasted mild-steel, from Sayles and Thomas (46)

They then took two such maps and forced them together, using a computer model that assumed the overlapping material simply disappeared (fig. 1.23).

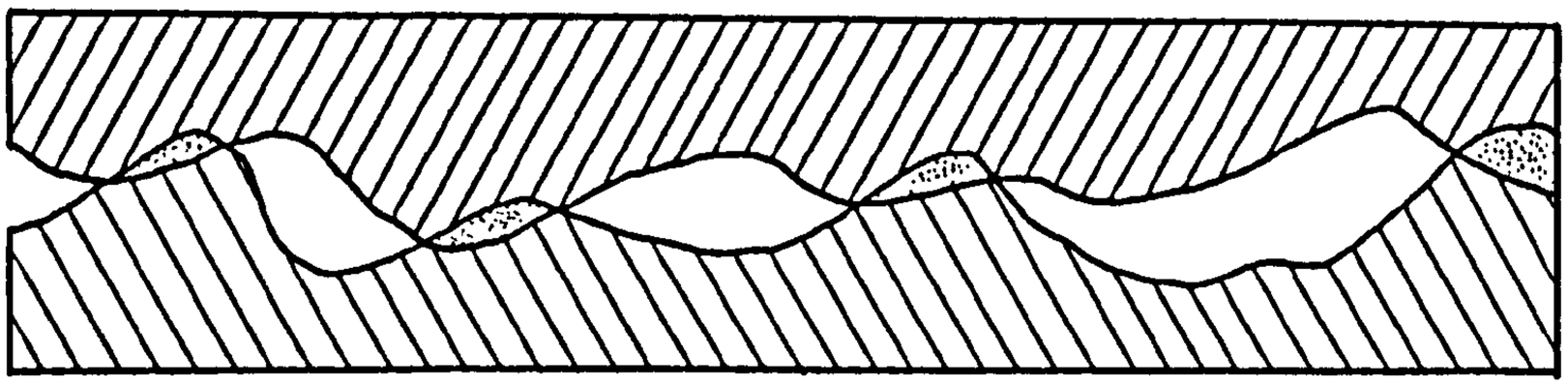

Fig. 1.23 The overlap between two surface profiles moved together

A picture of the contact pattern was produced. The assumption of disappearing overlapping material is fairly realistic for small real areas of contact (and the real area of contact between rough surfaces is small under usual loads). (See Pullen et al. (36) and p.29) It must be remembered that the actual slopes of the asperities, as mentioned previously, are only 4^{o} or so (fig. 1.24), so the overlap is quite thin for reasonable real contact areas.

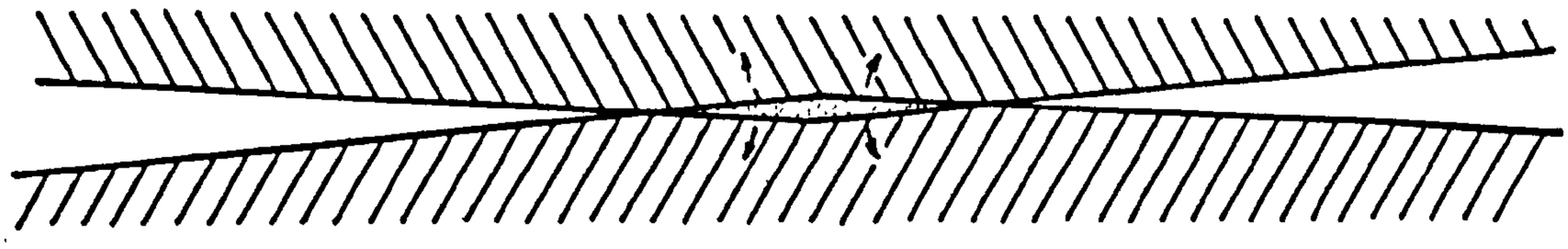

Fig. 1.24 Overlap with realistic asperity angles

The material moves plastically down into the bulk of the solid (arrows, fig 1.24) and does not raise the whole profile a great deal (36) (48).

1.8 Surface roughness and stick-slip

Barwell (49) has produced a review of work done on measurement of rough surfaces and their general frictional characteristics.

Antoniou (9) attempted to measure the vertical movements of Tolstoi (27) and relate them mathematically to stick-slip characteristics. Not a great deal of work has been done, however, upon the effect of roughness on this vertical movement, and, as Elder and Eiss (28) have demonstrated, the phenomenon is very important to the stick-slip characteristics of a sliding system. This is despite the fact that the vertical movement must be caused by the irregularities in the surface (two completely flat planes cannot move apart under the action of parallel motion, even by hydrodynamic forces).

The reason for this lack of attention is that the vertical movement is very difficult to measure. Tolstoi (27) finds its amplitude to be 10^{-3} times the amplitude of the associated stick-slip, so the cross-talk problems in measuring it are very great. Once measured, it would have to be compared with the surface features on the wear track. Locating these would be difficult as well (50) (39).

Wear tracks formed during stick-slip have been studied by Takahashi, Yoshida and Okada (51) using a scanning electron microscope. They observed a piling up of material where the surfaces (diamond on steel) stuck. The contact stresses in their experiments were very high and consequently a great deal of plastic flow took place.

Gregory (52) checked for the transfer of material from one rough surface to another during sliding by making one of the sliding surfaces radioactive and then exposing a photographic film over the other after the experiment. Rabinowicz (8) mentions the use of this technique in stick-slip experiments and concludes that concentrations of transferred material occur where the surfaces have stuck for some time.

CHAPTER TWO

A DESCRIPTION OF THE EXPERIMENTAL APPARATUS AND PROCEDURE

2.1 The Bowden-Leben machine

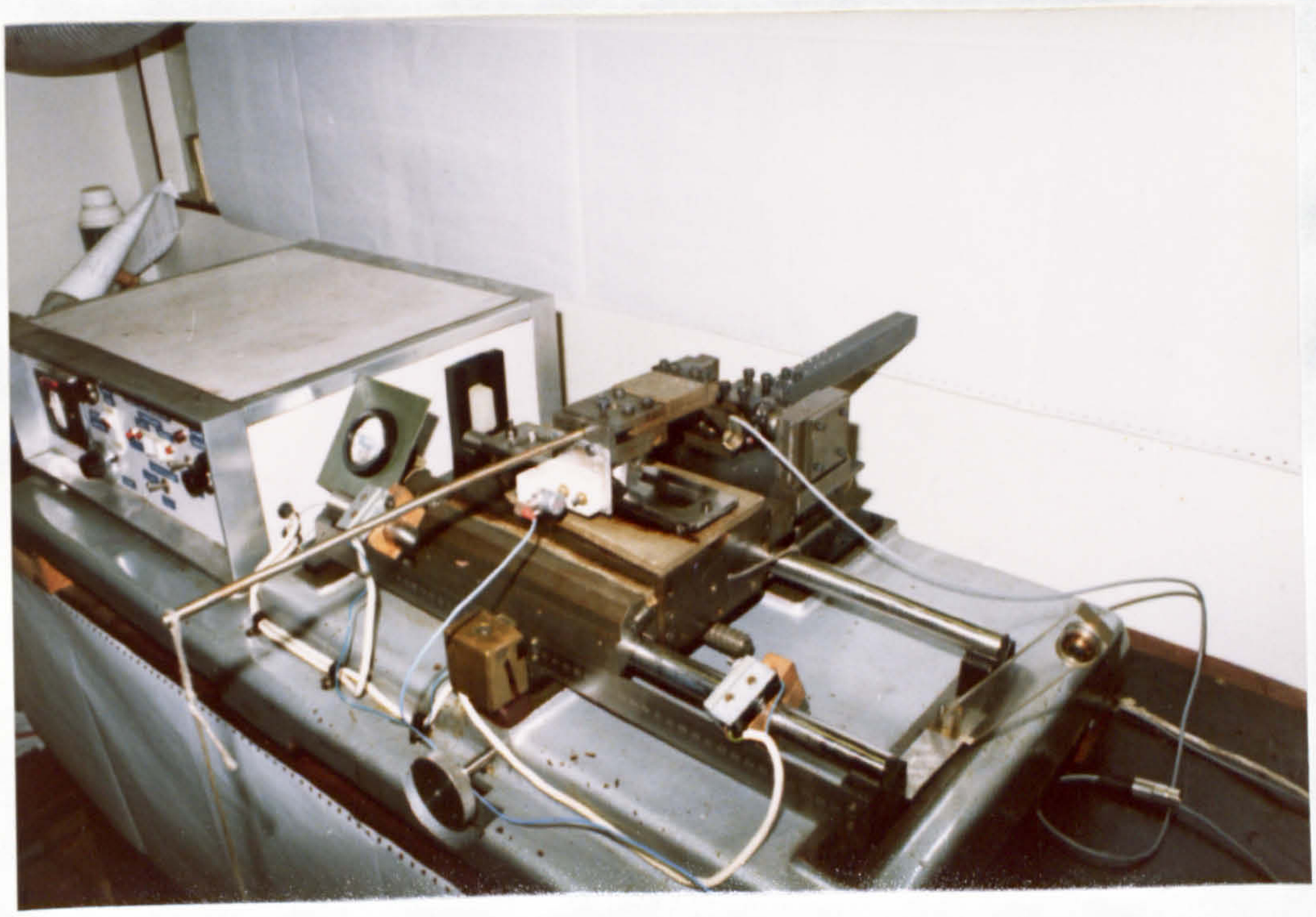

Fig. 2.1 The Bowden-Leben machine

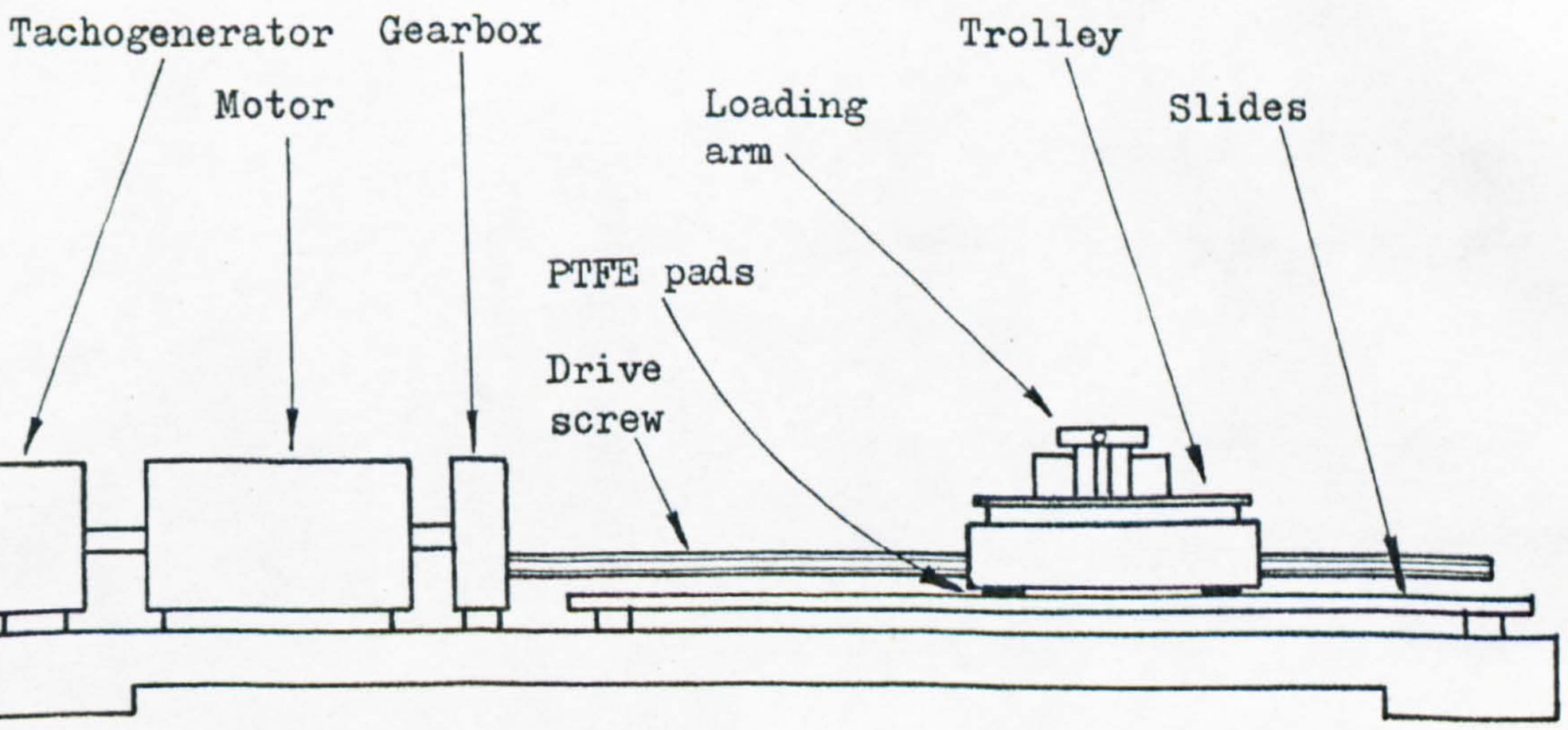

Fig. 2.2 Schematic

The apparatus used for the experimental investigation was an electrically driven Bowden-Leben machine (1) (figs. 2.1 and 2.2) which is accurately modelled by fig. 1.1.

This machine comprised a D.C. electric motor driving a screw via a precision reduction gearbox. The speed of the motor was monitored by a tachogenerator. The output of this was fed to electronic control circuitry providing the current for the motor, forming a negative feedback loop giving constant speed control over about a 1000:1 range.

The screw was connected to a trolley by means of a recirculating ball nut. The trolley was mounted on cylindrical slides with PTFE bearing pads. As the screw was rotated by the motor, the nut drove the trolley slowly along the slides. The range of speeds was 0.01 mm/s to 10 mm/s. This range could be expanded by changing the gear wheels in the gearbox.

A shallow, stainless steel trough was mounted on top of the trolley to contain the lower sliding specimen. This specimen was held in the trough by means of a packing piece made from scrap stainless steel. The largest specimen that could be accommodated was 6" x 1" x $\frac{1}{4}$".

2.2 The loading arm

The upper sliding specimen was fastened in a stainless steel chuck mounted on a loading arm (figs. 2.3 and 2.4). This loading arm was designed by Dr A. N. Syrop (25) and the author.

The loading arm consisted of a cantilever spring with strain gauges mounted on it to measure its deflection. There was an arrangement for clamping the cantilever at various points along its length in order to vary its stiffness.

The whole loading arm was free to rotate in a vertical plane

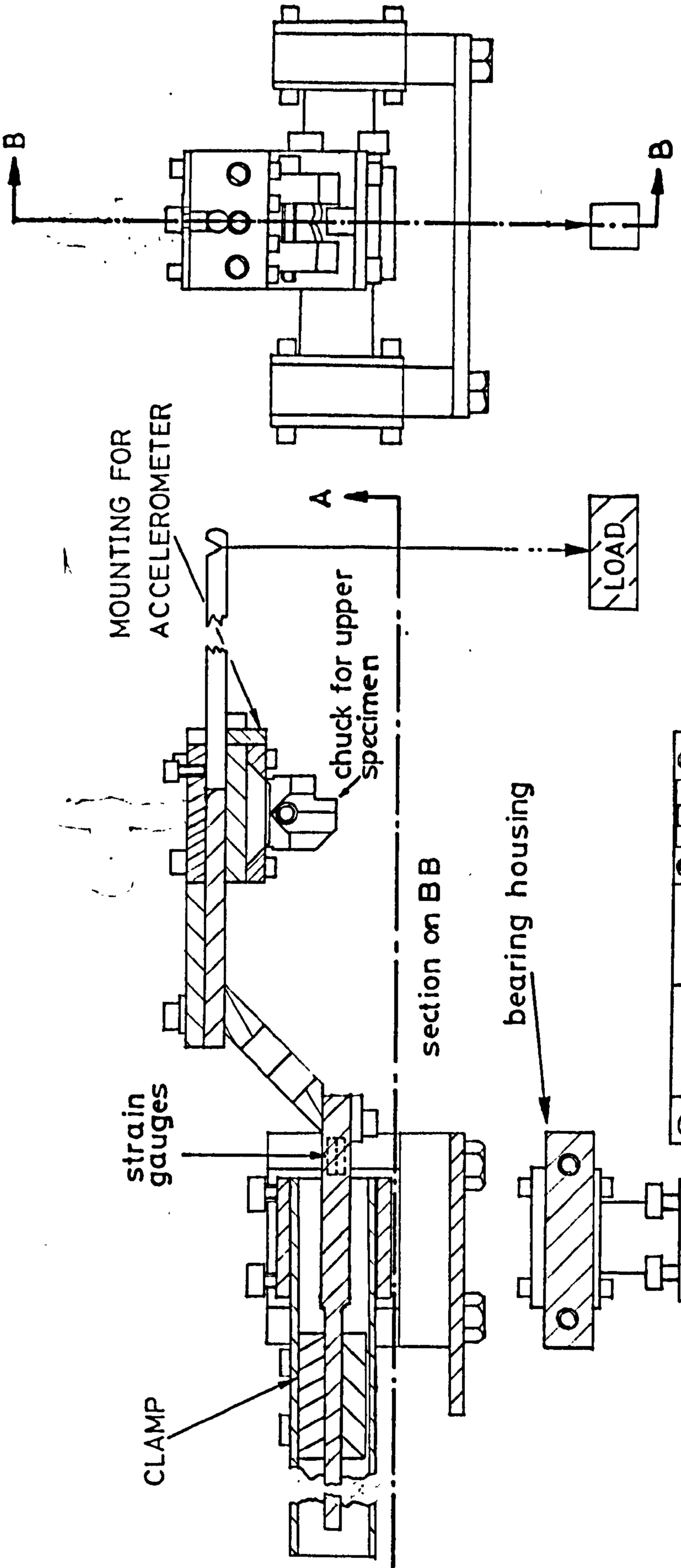

Fig. 2.3 THE LOADING ARM

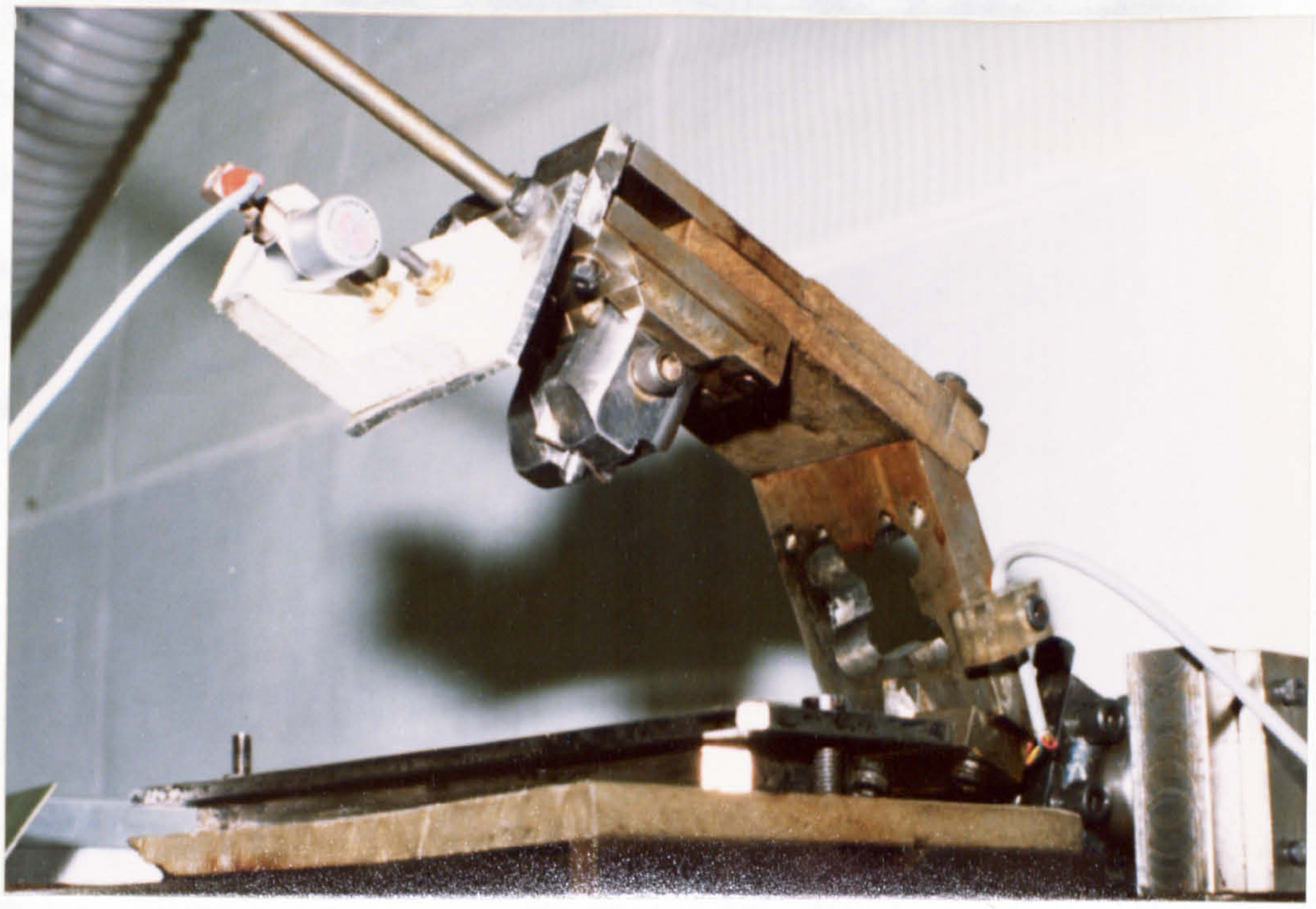

Fig. 2.4 The head of the loading arm, the chuck, the accelerometer and the specimen trough

(cf. figs. 2.4 and 2.1) so that the specimen in the clamp could be loaded against the specimen in the trough. The load was applied by means of weights on the end of a piece of thread tied to the free end of the loading arm. This thread was about a meter long and its purpose was to ensure that the loading weights were horizontally decoupled from the loading arm, thus not affecting its inertia. To vary this inertia, weights could also be clamped directly onto the arm itself.

The point of contact between the specimens was co-linear with the axis of the cantilever. This was to minimise torsion in the cantilever.

The whole loading arm could be moved backwards and forwards (perpendicular to the direction of sliding) and clamped so that several wear tracks could be made on the same lower specimen.

2.3 The measuring and recording system

The strain gauges on the cantilever were used to measure the displacement of the top slider (x in equation 5). They were wired in

a bridge (fig. 2.5). They had a nominal resistance of 120Ω and were rated at 25 mA. This meant that the power supply had to provide 50 mA at 6V. The circuit diagram of the supply used is given in appendix 2, p.155.

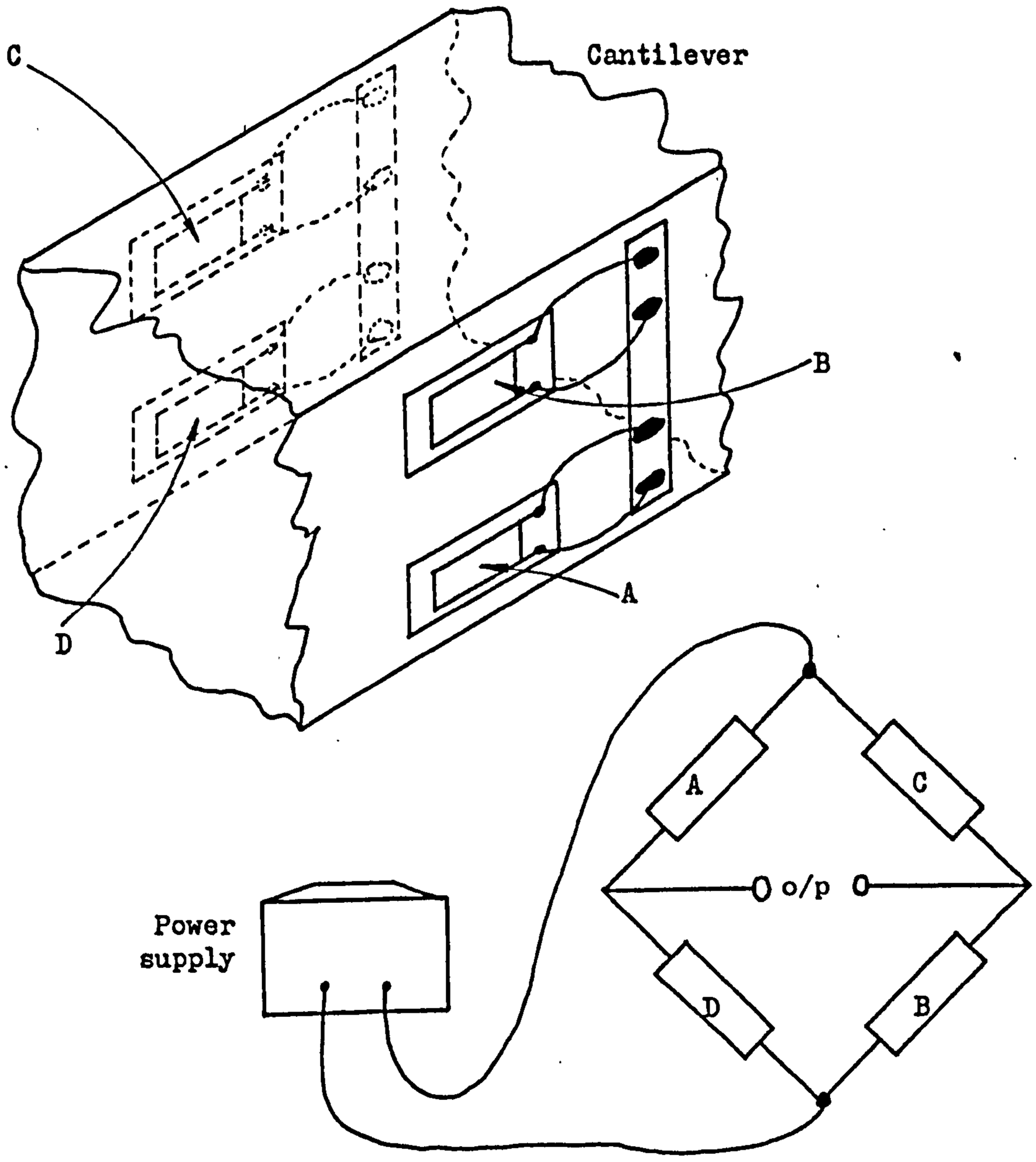

Fig. 2.5 Strain gauge circuit

The advantage of the bridge connection shown was that it was sensitive to horizontal bending but not to compression, tension, torsion or vertical bending.

The output from the bridge was recorded on an ultra-violet recorder. This device had the advantage that it produced a continuous record and had a fairly high frequency response (up to a few hundred Hz).

The accelerations during stick-slip ($\ddot{x}$ in equation 5) were measured by means of an accelerometer attached to the arm. As this device was piezo-electric, it required an amplifier with a very high input impedance in order to give faithful readings. Such amplifiers are called charge amplifiers as they draw a very small current (fractions of a pA) from whatever is connected to their input. One was constructed (circuit diagram appendix 2, p.155) for use with the accelerometer. The output of the charge amplifier was connected to a second channel on the U.V. recorder. The whole arrangement is shown in fig. 2.6.

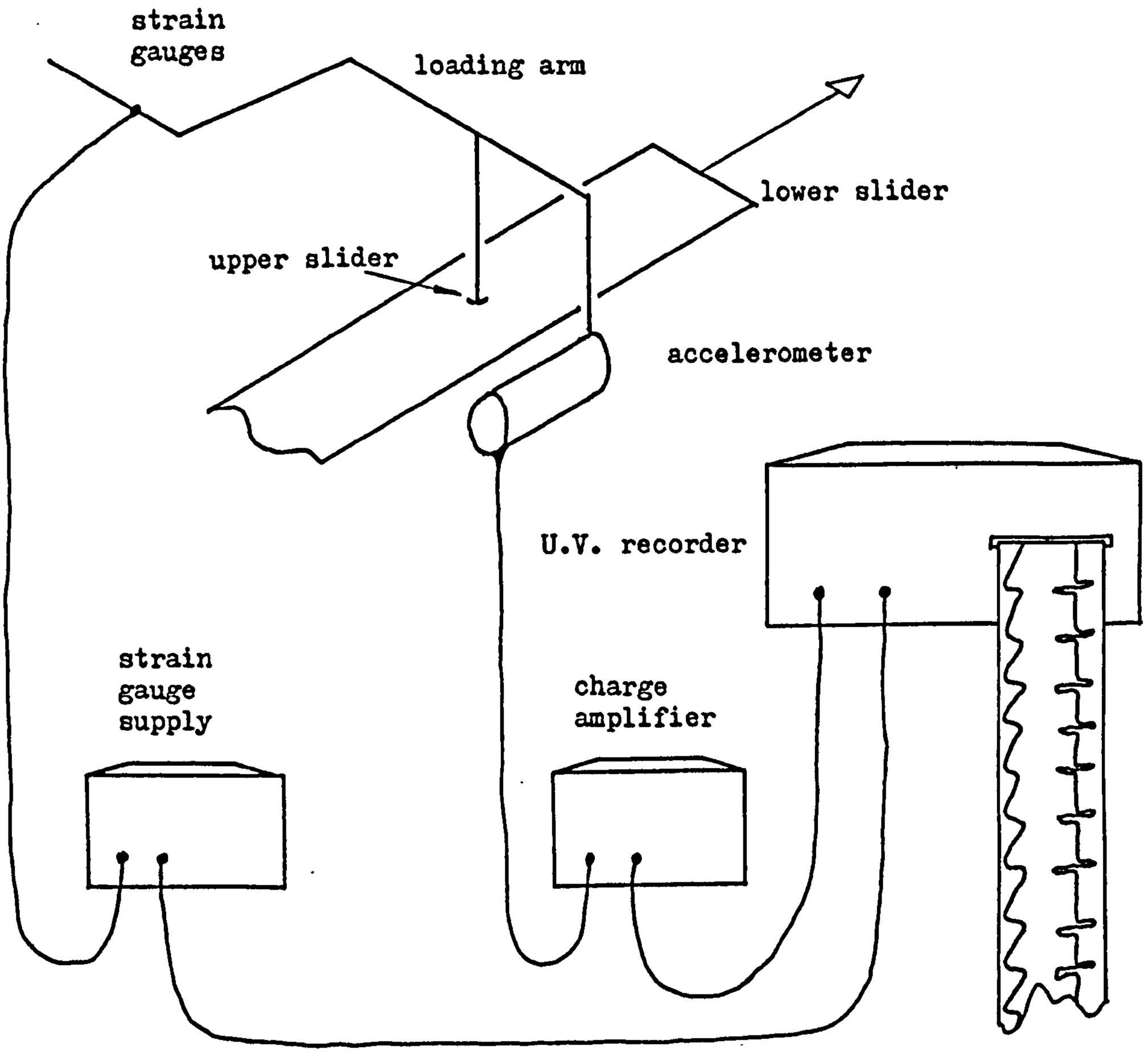

Fig. 2.6 Electrical measurements on the experimental rig

2.4 Calibration

Before experimentation could begin, it was necessary to calibrate the strain gauges and the accelerometer/charge amplifier and to measure the constants k and M in equation 5.

To calibrate the strain gauges and to measure k, the arm was pulled sideways by weights on a thread running over a pulley (fig. 2.7). The pulley ran on a ball-race to minimise friction.

Fig. 2.7 Calibrating the loading arm

A linear variable displacement transducer (LVDT) was also connected to the arm and its output was monitored on a voltmeter. An explanation of the workings of an LVDT is given in appendix 2, p.156 .

The apparatus was switched on and allowed to warm up for ten minutes. The paper drive on the recorder was turned on for a few seconds with no weight on the thread to give a zero reading. The LVDT was adjusted to read 0 volts.

Weights were then added in 100 or 200 gram intervals. After each weight had been added, the U.V. paper drive was turned on for a few seconds and the voltage from the LVDT was recorded.

The resulting staircase on the recorder paper was measured with a rule and the results are recorded in table 2.1

TABLE 2.1

LVDT o/p (Volts)	Load (g)	U.V. Deflection (mm)	Actual Deflection (mm)
0.18	100	2.0	5.64×10^{-2}
0.27	200	2.5	8.46×10^{-2}
0.52	300	4.5	1.63×10^{-1}
0.94	500	8.5	2.96×10^{-1}
1.34	700	12.0	4.20×10^{-1}
1.82	1000	18.0	5.70×10^{-1}

The figures for the actual deflection of the loading arm are calculated from the LVDT voltages. The LVDT produced an output of 3.192 volts/mm.

Graphs were plotted of U.V. recorder galvanometer deflection against actual deflection and of load against actual deflection (fig. 2.8).

The gradient of the first line was the scaling factor that had to be applied to the recorder output of x vs. t. The gradient of the second was k (see equation 5).

A powerful audio oscillator and an electromagnetic vibrator were used, in conjunction with the LVDT, to calibrate the accelerometer/charge amplifier combination.

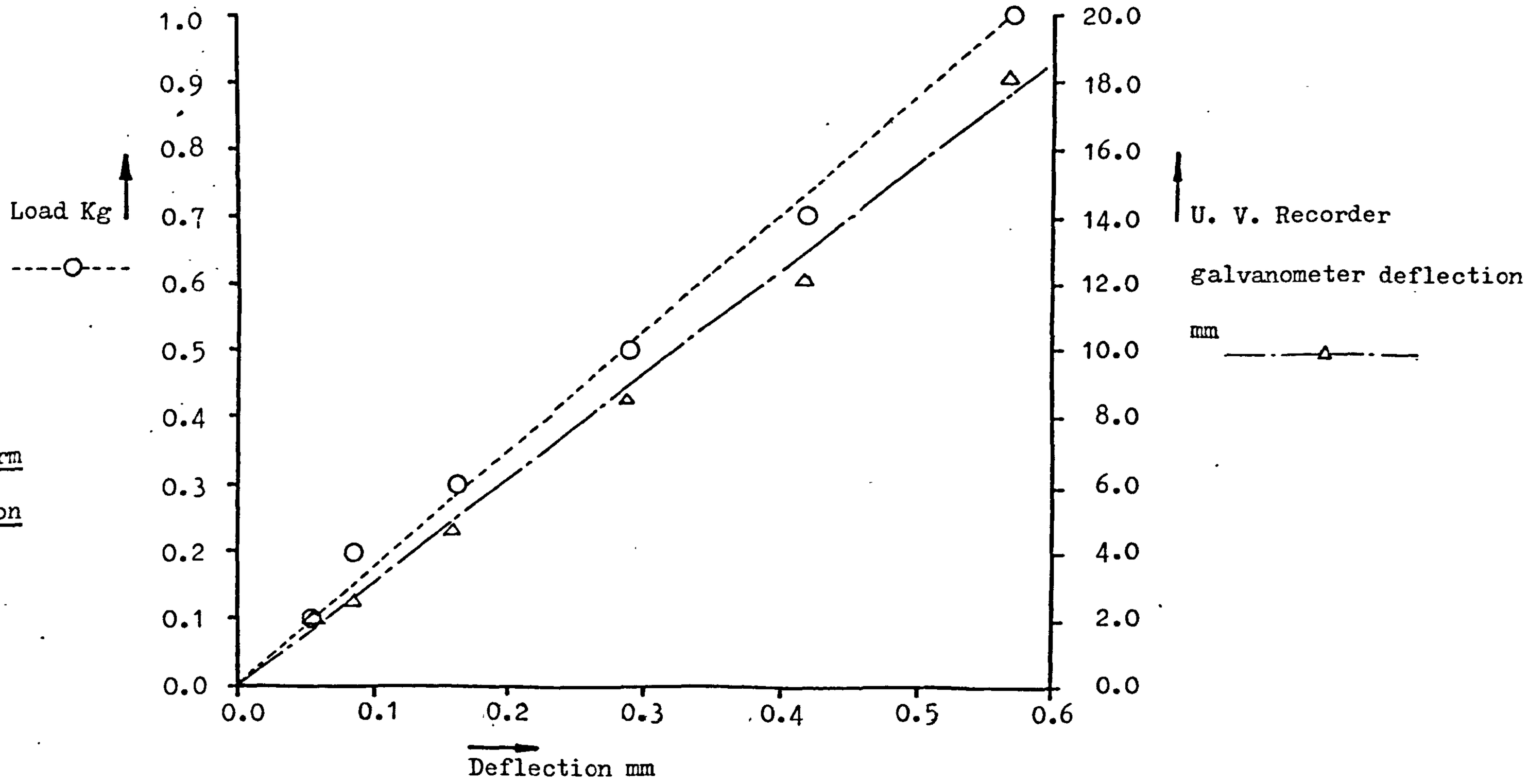

Fig. 2.8

Loading arm calibration

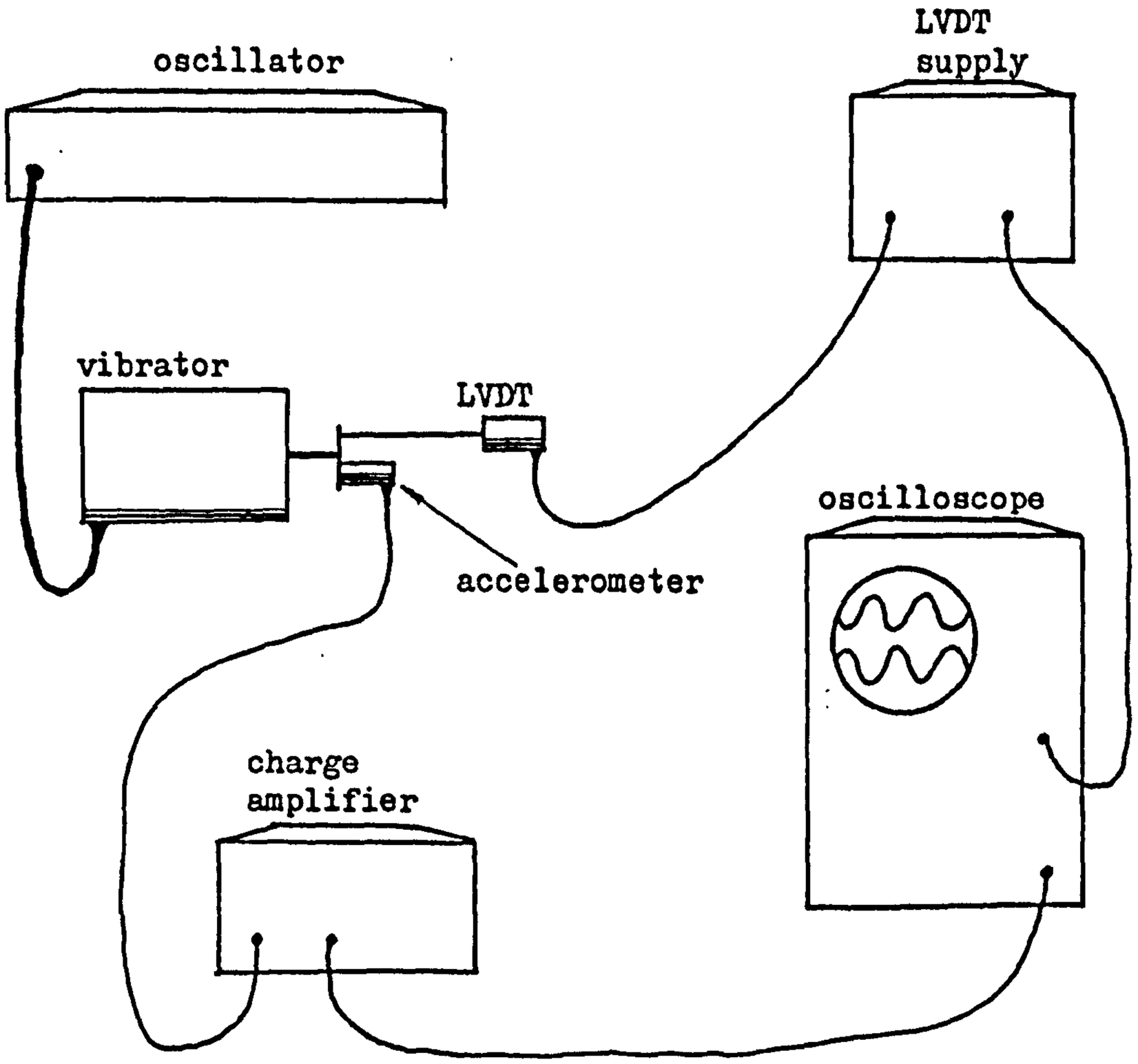

Fig. 2.9 Accelerometer/charge amplifier calibration

The oscillator was used to drive the vibrator at a variety of frequencies. Both the accelerometer and the LVDT were connected to the output of the vibrator and the signals from both were displayed on a double beam oscilloscope (fig. 2.9).

The peak-to-peak voltages of each signal were then tabulated against frequency (table 2.2).

If the displacement was of the form

$$x = a \sin \omega t \quad \ldots\ldots\ldots \quad (17)$$

The acceleration is

$$\frac{d^2x}{dt^2} = -a\omega^2 \sin \omega t \quad \ldots\ldots \quad (18)$$

x peak-to-peak would be 2a

$\frac{d^2x}{dt^2}$ peak-to-peak would be $2a\omega^2$

TABLE 2.2					
Frequency		LVDT o/p	Accelerometer/charge amplifier o/p	Displacement	Actual Acceleration
Hz	rads/s	mV p-p	mV p-p	mm p-p	mms^{-2} p-p
10	62.8	3000	6	0.940	3710
15	94.3	2600	18	0.815	7239
25	157.0	1600	50	0.503	12398
50	314.2	360	60	0.113	11141
75	471.2	150	90	0.047	10426
100	628.3	90	80	0.028	11042

As can be seen, the tabulated values of acceleration vs. voltage (table 2.3) are frequency dependent.

TABLE 2.3	
Frequency	(Accelerometer/charge amplifier o/p)/(Actual acceleration)
Hz	$(mV)/(mms^{-2})$
10	1.617×10^{-3}
15	2.487×10^{-3}
25	4.033×10^{-3}
50	5.386×10^{-3}
75	8.632×10^{-3}
100	7.245×10^{-3}

A graph of these values is given in fig. 2.10. As can be seen, the sensitivity drops off at low frequencies, despite the high input impedence of the charge amplifier. The mean of the values above 50 Hz is 7.087×10^{-3} mV/mms^{-2} and the standard deviation is 1.33×10^{-3} mV/mms^{-2}. It was decided to use these values as the acceleration/deceleration cycle of most of the stick-slip studied took about 0.02 of a second or less.

The speed of the trolley (V_0 in equation 5) for various settings of the motor controller was established by means of a

Fig. 2.10

Accelerometer calibration

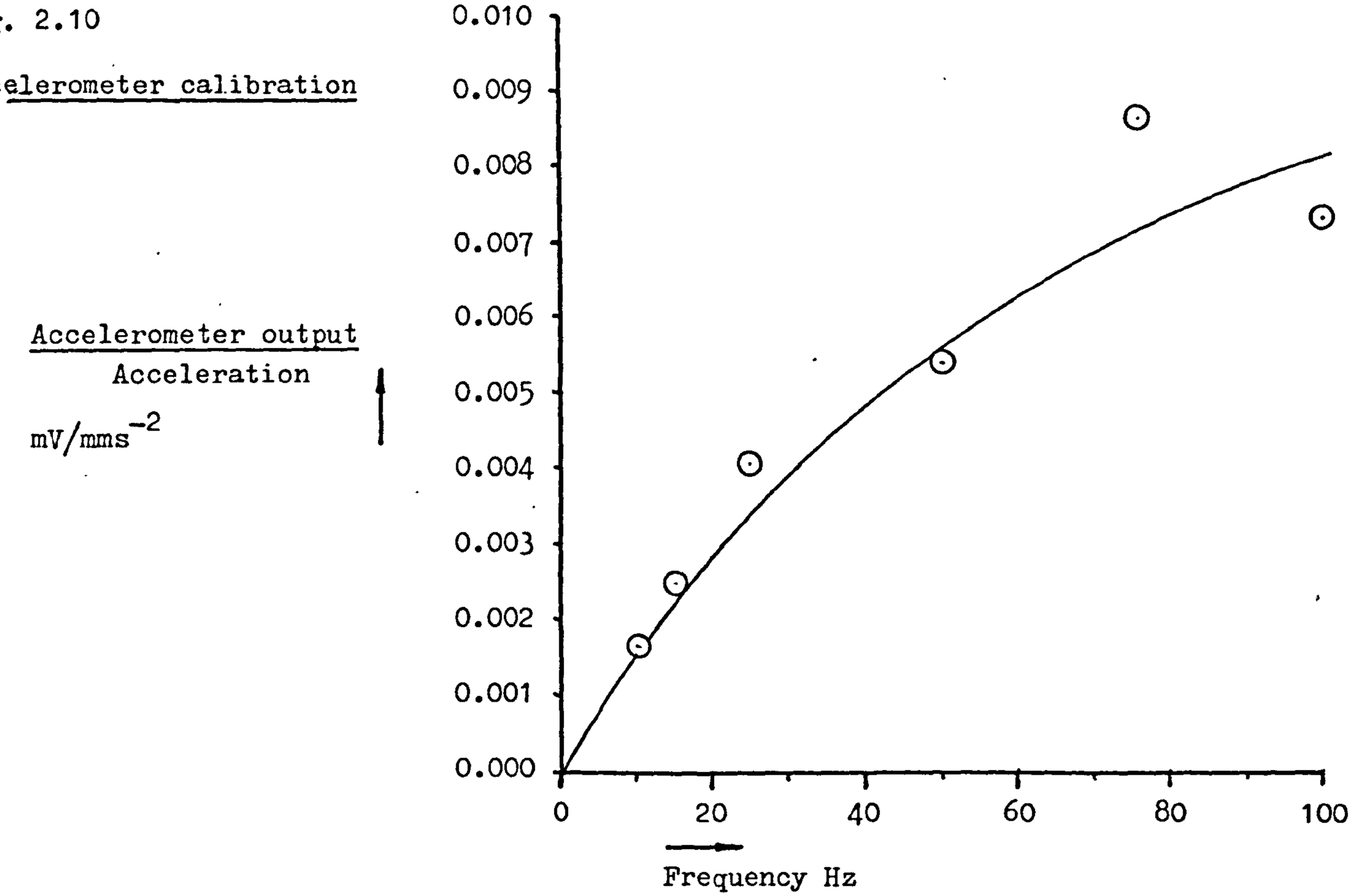

dial gauge and a stop watch.

It was also necessary to obtain a figure for M in equation 5. The desired figure would be some combination of the mass and moment of inertia of the chuck assembly and the cantilever that could not be determined by simple weighing. However, the resonant frequency for small oscillations of a spring and mass system is given by the equation:-

$$f = \frac{1}{2\pi}\sqrt{\frac{k}{M}} \quad \ldots\ldots\ldots (19)$$

k was known. f was found by gently tapping the chuck assembly with the rubbing surfaces separated and turning on the U.V. recorder paper drive for a few seconds, the number of oscillations in that time giving a value for f. M could thus be calculated.

2.5 Experimental preparation

The lower sliding surface used in the tests was stainless steel (EN58b) ground and then abraded with 400-grade emery paper (25).

The upper sliding component was a peg of EN58b machined to a frustum of a cone (fig. 2.11), the area of the flat being 1 mm^2 (see Chapter Five). This was again abraded with 400-grade emery paper.

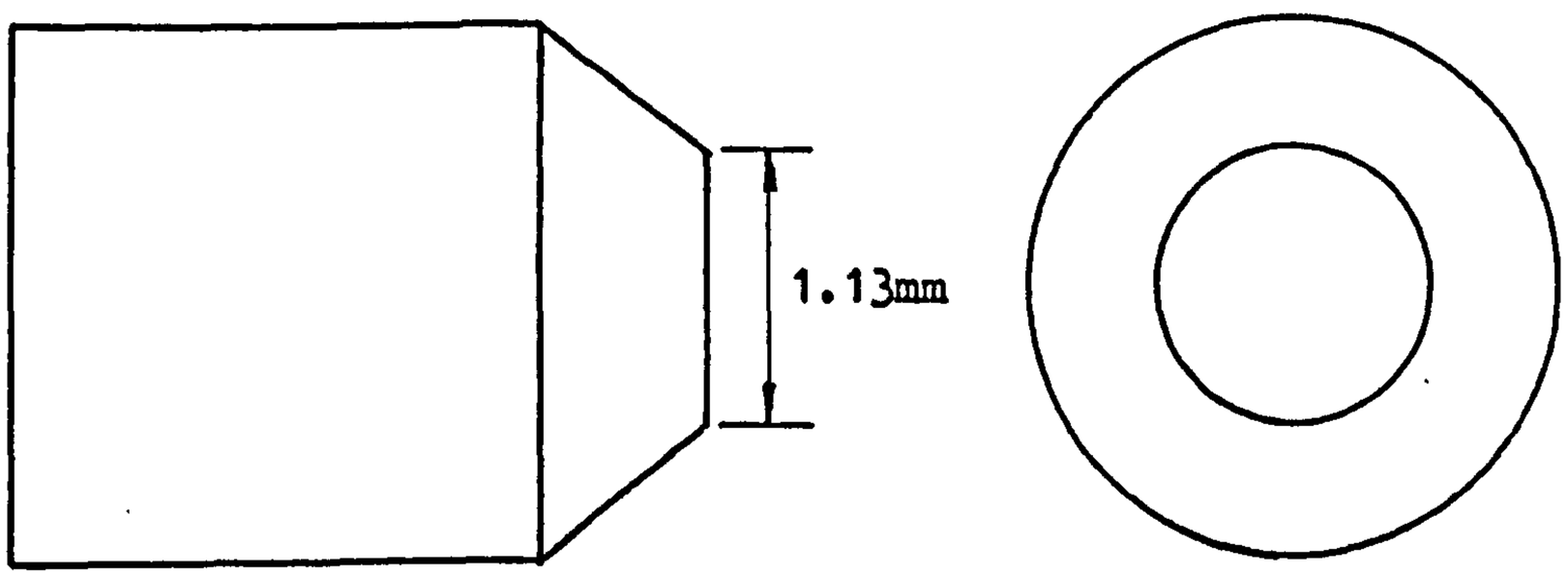

Fig. 2.11 The peg slider

Both the sliding components were cleaned and de-greased in refluxing toluene for about an hour prior to any experiment.

2.6 Typical experimental procedure

All the electronic equipment in the apparatus was switched on at least ten minutes before the start of an experiment to ensure that it reached thermal equilibrium, so minimising drift.

After cleaning, as previously described, the lower and upper specimens were placed in the trough and clamped in the loading arm chuck respectively. In the latter case, some care was taken to clamp the peg with its face as parallel as possible to the lower surface.

The weight was attached to the end of the thread on the loading arm to give the desired load and the arm was gently lowered until the two surfaces came into contact. The motor controller was adjusted to give the desired trolley speed. The U.V. recorder paper drive was turned on, followed by the Bowden-Leben motor. A typical recorder trace resulting from such a procedure in fig. 2.12.

As can be seen, there is some 50 Hz mains interference on the traces. This was despite careful screening of all the electronic apparatus. This problem could be overcome to a certain extent by considering the envelope of the 50 Hz oscillation to be the desired curve.

2.7 Curve digitisation

The experimental traces had to be digitised as the first stage of solving equation 5 by computer. A DMAC digitising table was available and was used for this purpose.

The table was connected to a standard card-punching machine. The desired values of X and Y were punched in I4 format; this meant that ten values of X and Y could be recorded on one eighty-column card. The digitising area of the table was 1 m square. With four-figure accuracy (0 - 9999) this gave a resolution of 0.1 mm, which

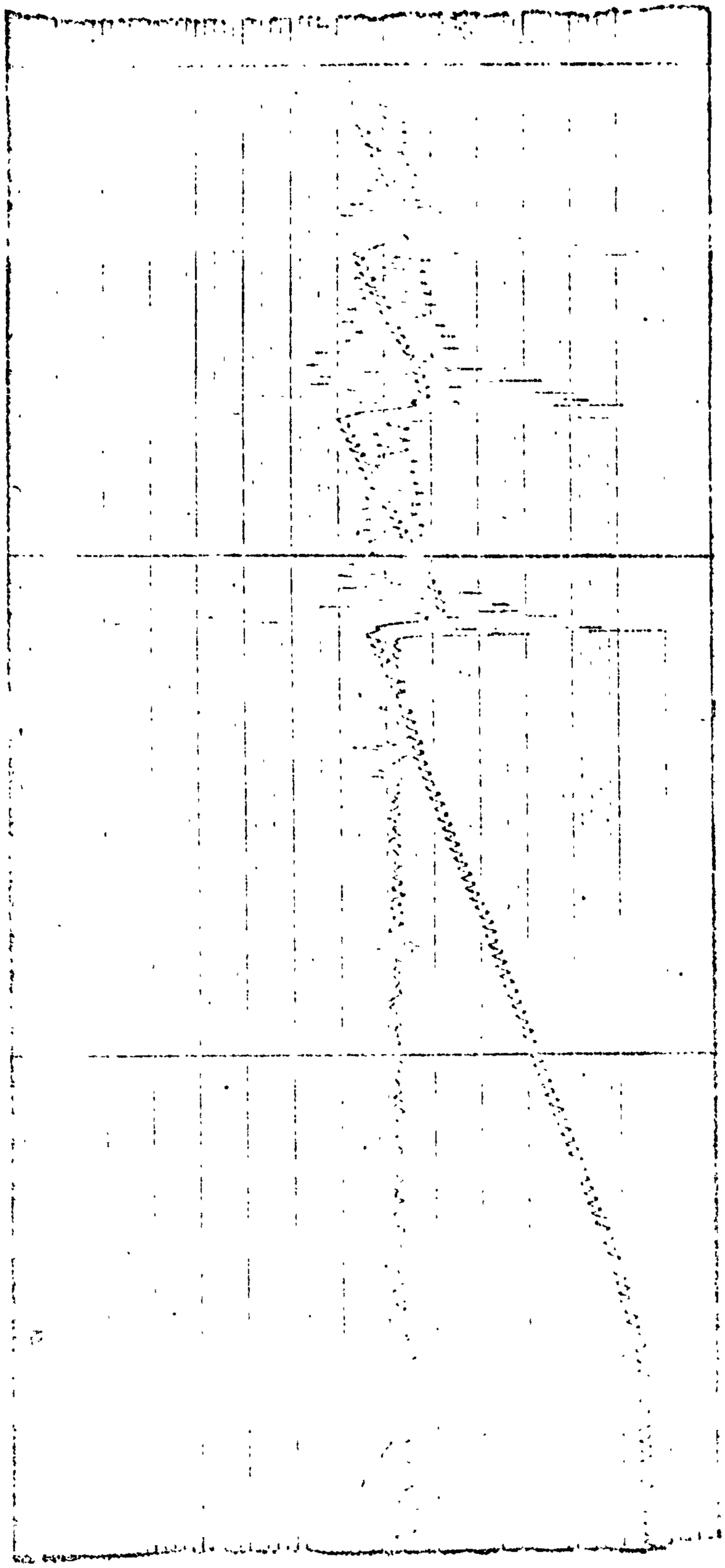

Fig. 2.12 Typical U.V. recorder output

was less than the thickness of the line produced by the U.V. recorder.

The recorder output to be digitised was taped to the table after being moved so that the Y values of two points (a and b, fig. 2.13) on the trace, as displayed on the digitiser, were the same.

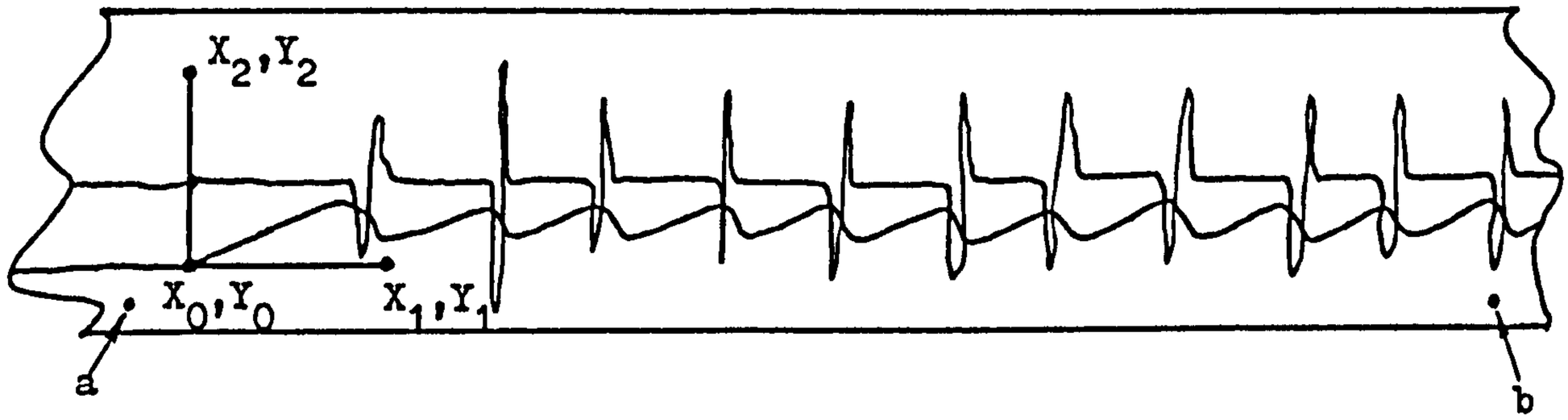

Fig. 2.13 Digitisation of experimental data

This ensured that the trace was parallel to the digitising table datum.

Two orthogonal lines 100 mm long were drawn from the origin of the trace, X_o, Y_o, to the points X_1, Y_1 and X_2, Y_2.

These points were digitised first to give a scale to the traces. The digitiser was then moved slowly along the curves, the points during the slip portion of the curve being particularly closely spaced as this was the most important section of the data. A listing of the data from a typical trace is given in table 2.4.

The first card was punched with an identifier consisting of the month and day that the experiment was performed and a number indicating which of that day's experiments the data represented. For example, 2/5*10 would be the tenth experiment conducted on the fifth of February. Values of V_o, k and the resonant frequency, f, of the system (to determine the true value of M, see p.48) made up the second data card, along with scaling factors, controlling flags etc.

The processing of these data is described in the next chapter.

```
24/5*12
1,5.208,22.,1.75,3...004,12.38,0.,5.208
32492238425122353242324O
3250223833762235338021733386217734062265341822303428224634422211345021703456215 4
34702290347922753484224634892194350821943518223435292266353622443544220535842060
35672014358018113591242135962488360628043614255136272346363422423640218036502100
36552020366418193871183636772055369124763701212437132061372118493731289537442902
37562586376223663763218037782108379220463801198038101647382021853632277138382537
38502301385321613858209038652006387523053866217138912250389821073905210539132227
39242348393323113941234039502203396621443974223639802211398723844002224040132091
40232253402921724038234640491903406819644072276040842051411713494153291141811874
41961902421018294244198742842034430720504316194043371481434422644358217143931462
44062617445520644480199144872042451823284540156245571914456626294582248746112660
46421644465124634664213346762390468717074705196347272137475929024789211148142057
48301845484219504654245446682502487922504881191849021839491420664924223249532818
49712910498523805001207550261986503915295050188050571762506827235084266150962043
51072905511728005150163751602383517424455190174452111629522024805230206152362751
52582906526829055282215252871945529519745308217553212019533319055346226753562100
53781923538119145390203954022152541122320000000054212246543222 79-003
N
32461805424816043248260 9
32511613329516543340170833941790344718663498194035532010359820463654208436992110
37582084380921153855215239142208396222424010227540572303408523134101230441242256
41392177415720604167201141831994420919734216197242231975423619924265201443182077
43392101435520984368209044152107447221264521213945702152462821344674216147212178
47442162477821134793211448252131487321644916218049452163486721354986211450292133
50452150506421545079214151342116514621255181214252232144525720985283206553322090
53902140541721405432212200000000544211054582105-002
0.0317
```

Table 2.4 Typical data

CHAPTER THREE

THE COMPUTER PROCESSING OF EXPERIMENTAL DATA

3.1 Objectives

Equation 5, derived in Chapter One, was:-

$$\mu (\dot{x} - V_o) = \frac{kx + M\ddot{x}}{L} \quad \ldots\ldots\ldots (5)$$

It was pointed out that the characteristics of the function $\mu (\dot{x} - V_o)$ determine the nature of stick-slip in a sliding system. Equation 5 can be solved for this function. L was known. M, k and V_o could be measured as has been previously described. x and $\ddot{x}$ were recorded on the U.V. recorder. This leaves the function, μ, and the velocity of the slider, $\dot{x}$, as unknowns. $\dot{x}$ might be found by differentiating x or integrating $\ddot{x}$, enabling equation 5 to be solved numerically for μ. Ideally, $\mu (\dot{x} - V_o)$ would be displayed as a graph against $\dot{x} - V_o$.

3.2 The computer system

The computer available for use by the author (the Imperial College CDC6400/CYBER174) had an interactive graphics facility with an option of microfilm hardcopy. A programme stored permanently on disc could be run interactively on a special VDU capable of displaying, in addition to normal alphanumeric data, graphs or pictures generated by subroutines in the programme, or by standard library subroutines called from the programme. One library subroutine, when called by the user, would take the graphical information displayed on the

screen and transmit it along a land line to the microfilm plotter at the University of London Computer Centre. The microfilm hard-copy thus produced forms the basis of all the computer graphics in this thesis, with the exception of the frontispiece, which was drawn on the Kingmatic plotter at Imperial College.

3.3 Data input

The solution of equation 5 requires values of V_o, k, M, x and $\ddot{x}$ to be in consistent units. The order of the amplitude of most of the stick-slip studied was about 1 mm. Consequently, the millimeter was chosen as a convenient length standard; so x was in mm, $\ddot{x}$ was in mms^{-2}, V_o in mms^{-1}, M in kg and k in Nmm^{-1}.

First of all it was necessary to convert the digitised results into actual values in mm (x) and mms^{-2} ($\ddot{x}$). Another problem also had to be overcome. As the two curves were digitised consecutively, the values of the abcissae (time) on each curve did not necessarily coincide with those on the other. This meant that interpolation had to be performed on one curve to ensure its values of t coincided with those on the other. It was decided to retain the values of t on the acceleration curve and to use these to interpolate on the displacement curve. This course was chosen as the displacement curve had more gentle gradients and gradient changes than the acceleration curve (see results - Chapter Four) and consequently interpolation upon it was more likely to be accurate.

It was decided to incorporate the conversion of the digitised data into actual values of x and $\ddot{x}$ and the interpolation into a data preparation programme separate from the main programme for the solution of equation 5. A flow diagram of this data preparation programme is given in appendix 1, p.134 .

3.4 The derivation of $\dot{x}$

As is mentioned in section 3.1, all the variables in equation 5 were known except $\dot{x}$ and the desired answer, $\mu (\dot{x} - V_o)$. After reading in the experimental data the first computation required was the derivation of $\dot{x}$ as a function of time, either by the integration of $\ddot{x}$ or by the differentiation of x.

There are advantages and disadvantages to both of these methods. Consequently, the programme was written so that either method could be chosen.

3.4a) Integration

To integrate the $\ddot{x}$ curve, the programme fitted a parabola to each point on the $\ddot{x}$ curve and summed the area under it (fig. 3.1).

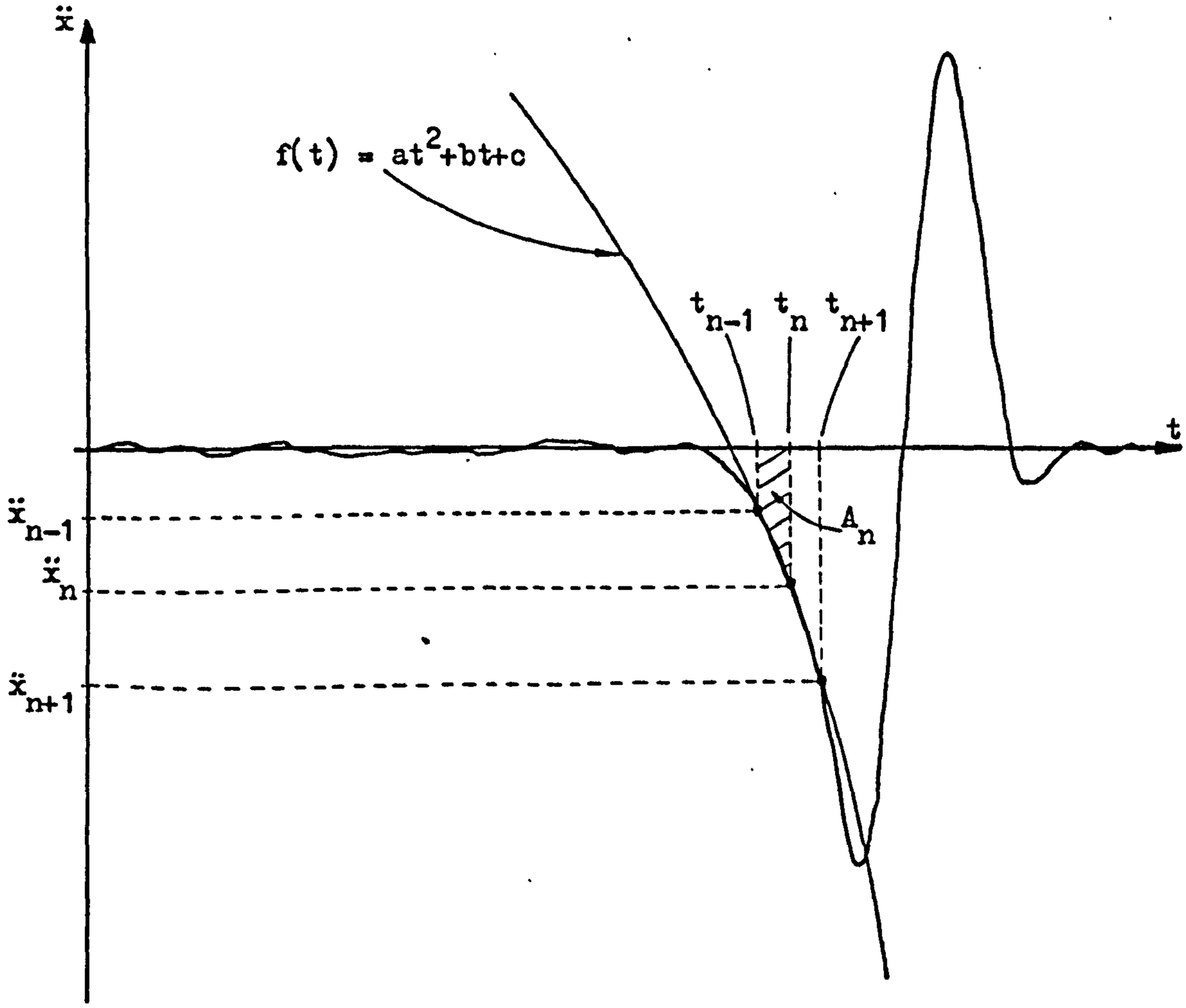

Fig. 3.1 Parabola fitting on $\ddot{x}$ curve

The parabola fitted was of the form:-

$$f(t) = at^2 + bt + c \quad \ldots\ldots\ldots \quad (20)$$

(See appendix 1 for a listing of the fitting subroutine.)

The area under the parabola between t_{n-1} and t_n being:-

$$A_n = \frac{a\left[(t_n)^3 - (t_{n-1})^3\right]}{3} + \frac{b\left[(t_n)^2 - (t_{n-1})^2\right]}{2} + c\left[(t_n) - (t_{n-1})\right] \ldots\ (21)$$

As n was incremented from 1 to the value at the end of the $\ddot{x}$ curve, the running total of A approximated well to the area under the curve.

The first value of $\dot{x}$ had to be known and added onto the integral as a boundary condition. This value of $\dot{x}$ would normally be the trolley velocity, V_o, as the digitisation started at the beginning of the curves, where the two sliding surfaces had no relative motion.

The advantage of the integration method of finding $\dot{x}$ was that it was insensitive to small, random digitising errors in $\ddot{x}$, as these did not make a great deal of difference to the area under the curve.

The disadvantage of this method was that it was very sensitive to systematic errors in $\ddot{x}$, i.e. an offset. When a small offset was present on the integrand, a ramp was superimposed upon the integral. This problem was overcome to a certain extent by starting and ending the digitising on a portion of the curve where the slider was stuck. At these points the slider had a velocity of V_o. The integration subroutine subtracted the final from the initial values of $\dot{x}$. This difference represented the area under the $\ddot{x}$ curve contributed by the erroneous offset (fig. 3.2).

This difference was then divided by the total time of the data sample, T, to give the value of the offset. This value was subtracted from the $\ddot{x}$ curve and the curve was re-integrated, the error being thus corrected (55).

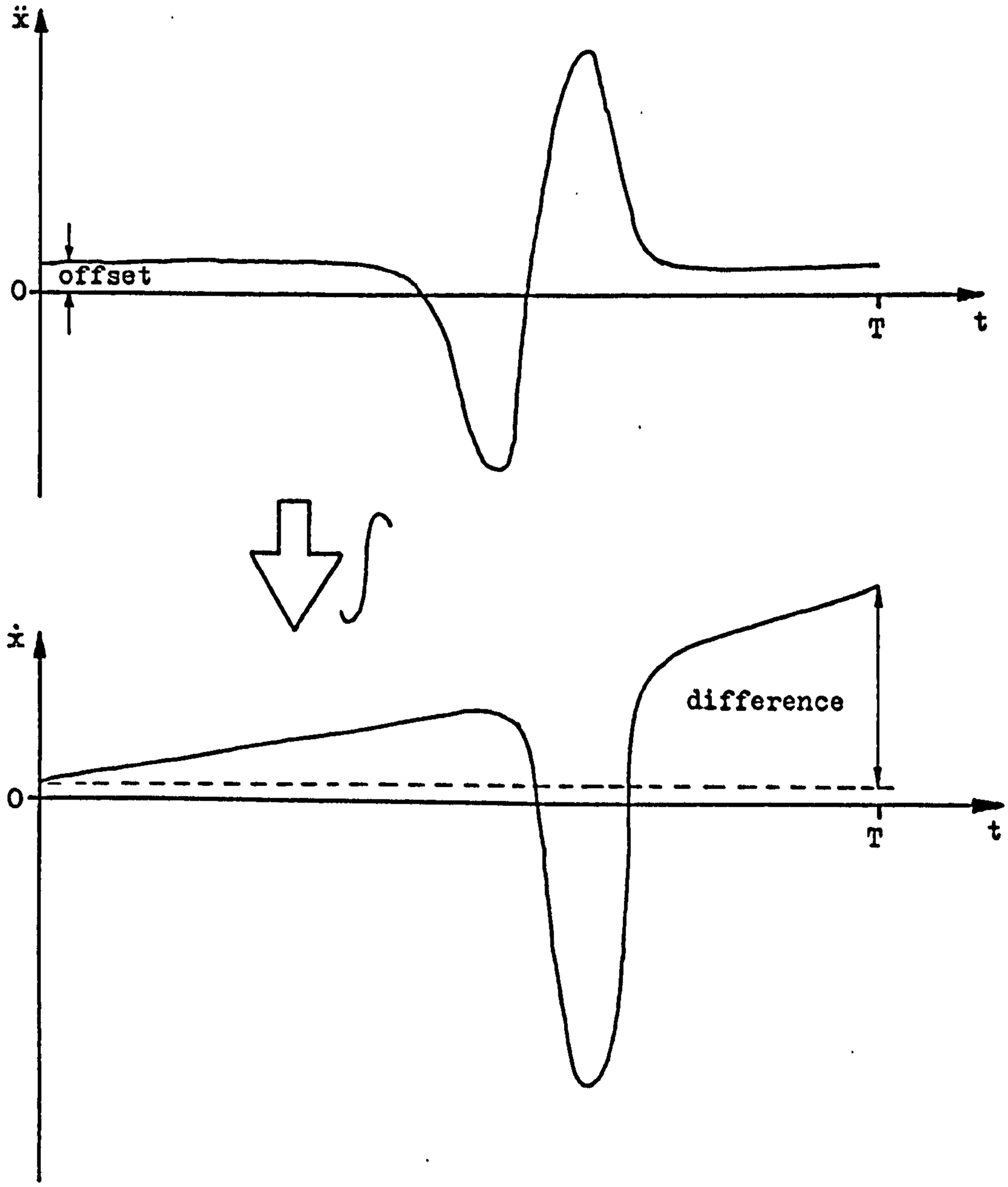

Fig. 3.2 The effect of an offest on the $\ddot{x}$ curve

3.4b) Differentiation

To differentiate the x curve a parabola was fitted to consecutive points as before (fig. 3.3).

The gradient of the parabola was:-

$$\dot{x}_n = \left(\frac{dx}{dt}\right)_n = 2a\left[t_n\right] + b \quad \ldots\ldots\ldots \quad (22)$$

The advantage of this method is that, unlike integration, it is not sensitive to systematic errors. The disadvantage is that random errors are transmitted to the $\dot{x}$ curve (fig. 3.4).

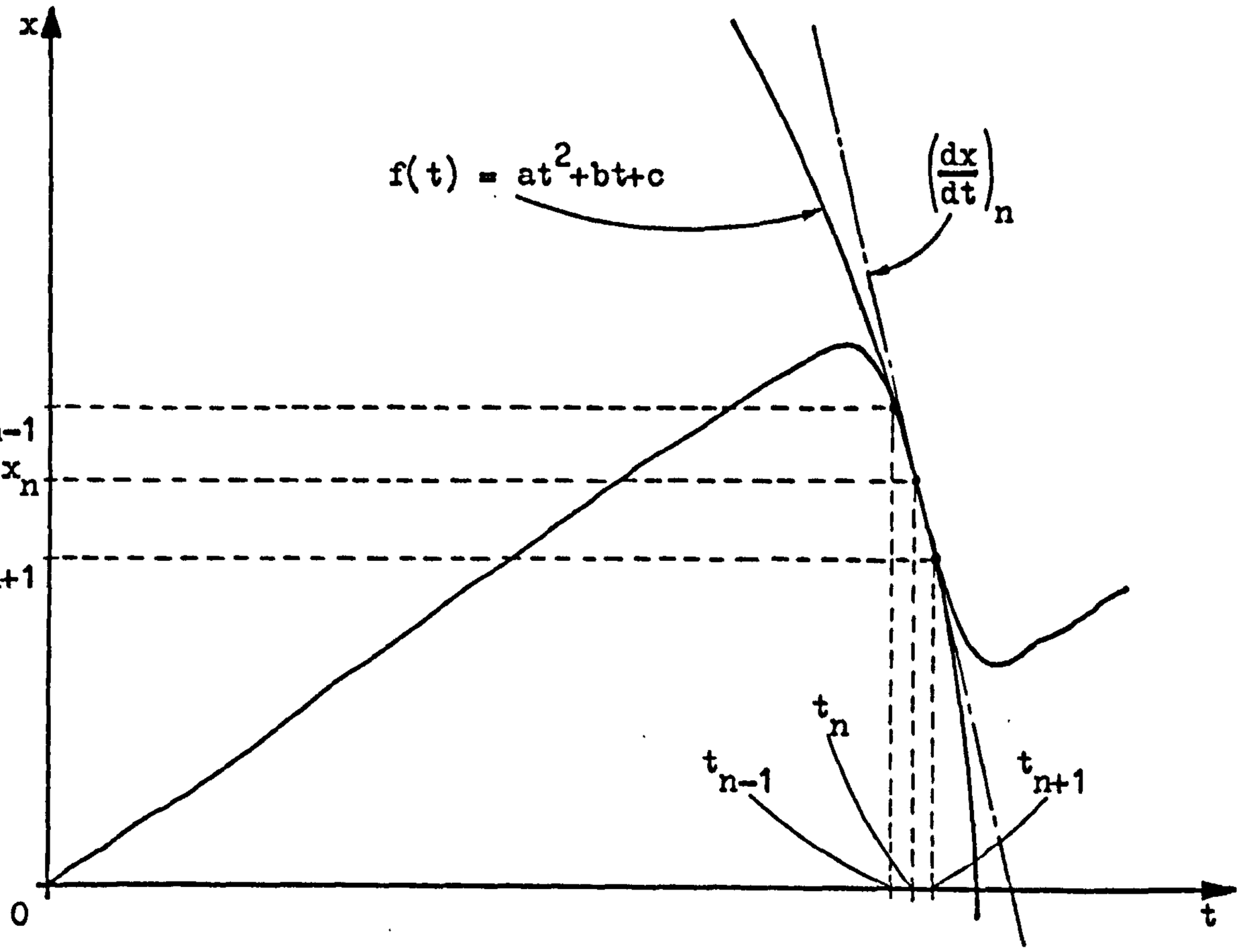

Fig. 3.3 Fitting a parabola to the x curve

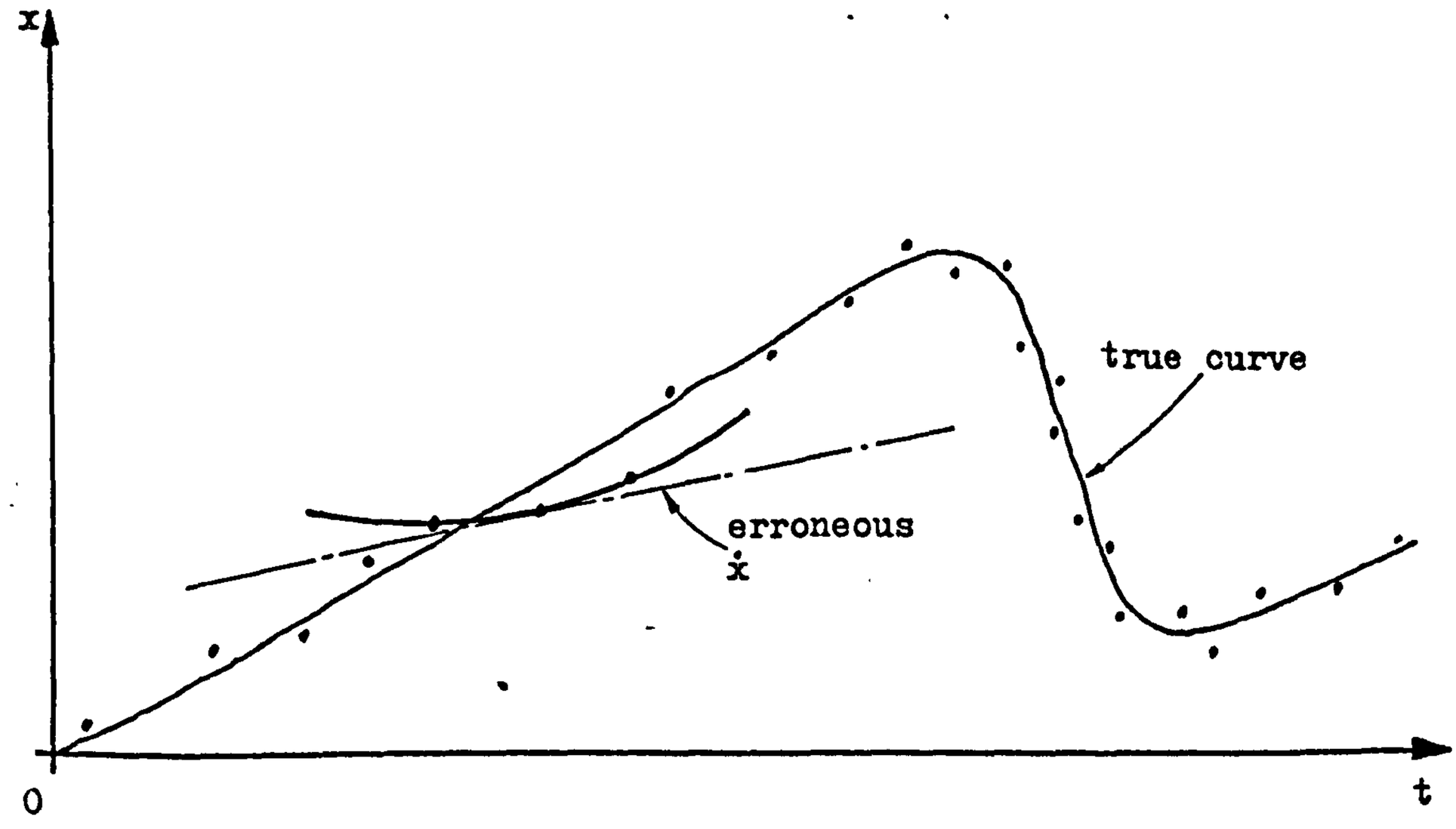

Fig. 3.4 The effect of digitising errors on the x curve

This problem always occurs when a signal with scatter is differentiated.

3.4c) Comparison of the two methods

Figures 3.5 and 3.6 show typical displacement vs. time and acceleration vs. time graphs for stick-slip. Figure 3.7 shows the result of integrating fig. 3.6 by the method previously described and fig. 3.8 shows the result of differentiating fig. 3.5.

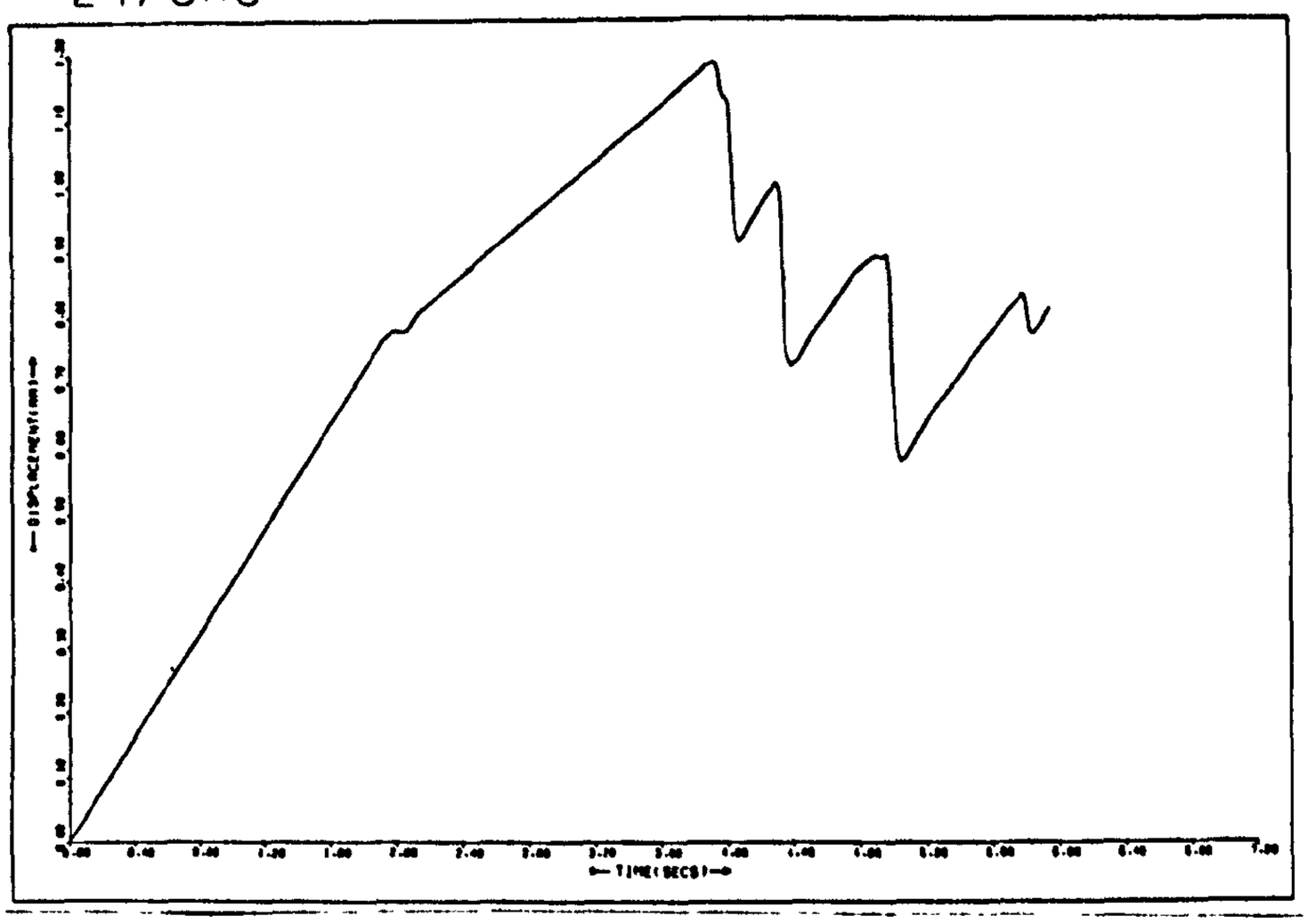

Fig. 3.5 Displacement vs. time

Fig. 3.6 Acceleration vs. time

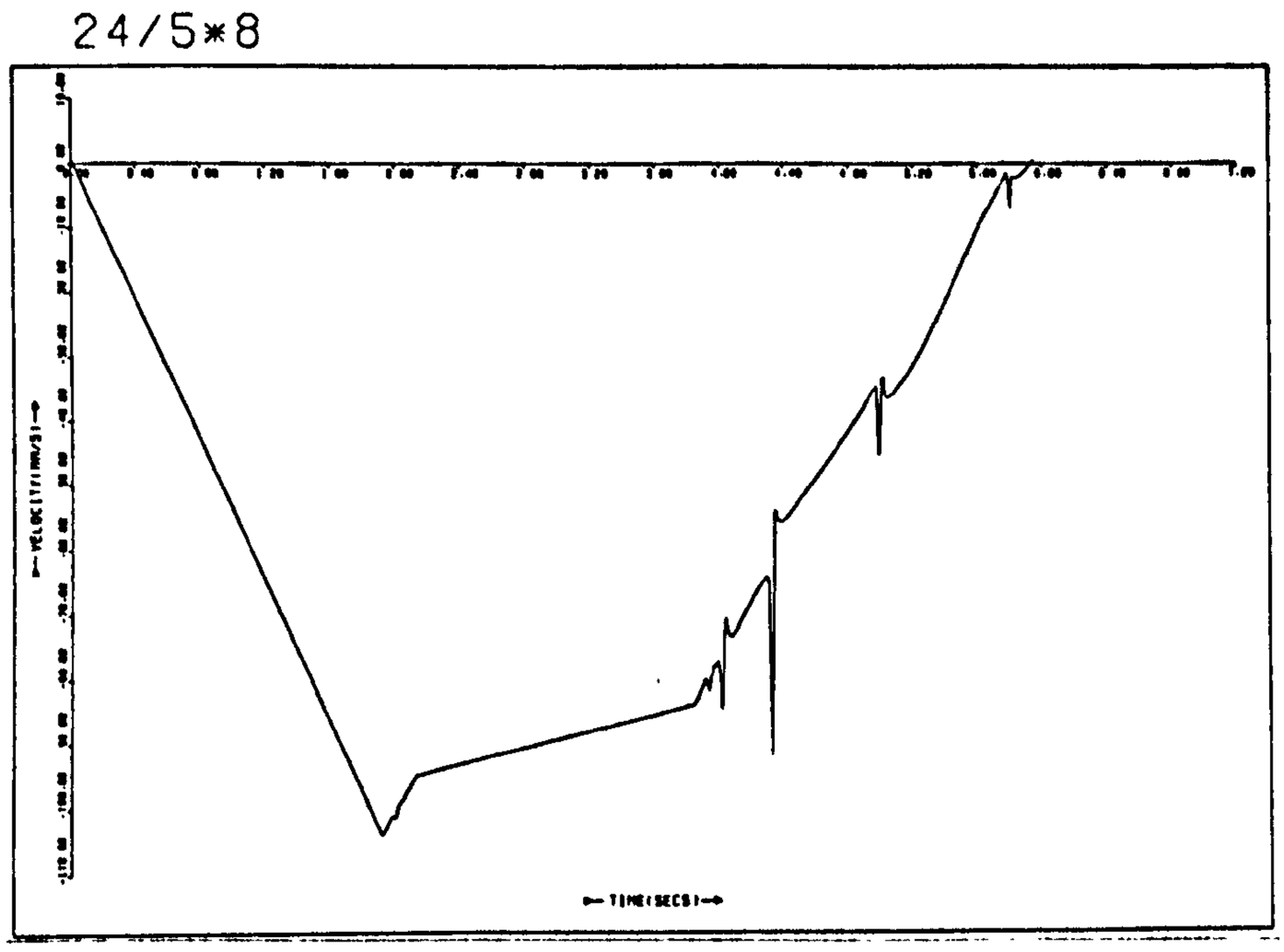

Fig. 3.7 Integration of fig. 3.6

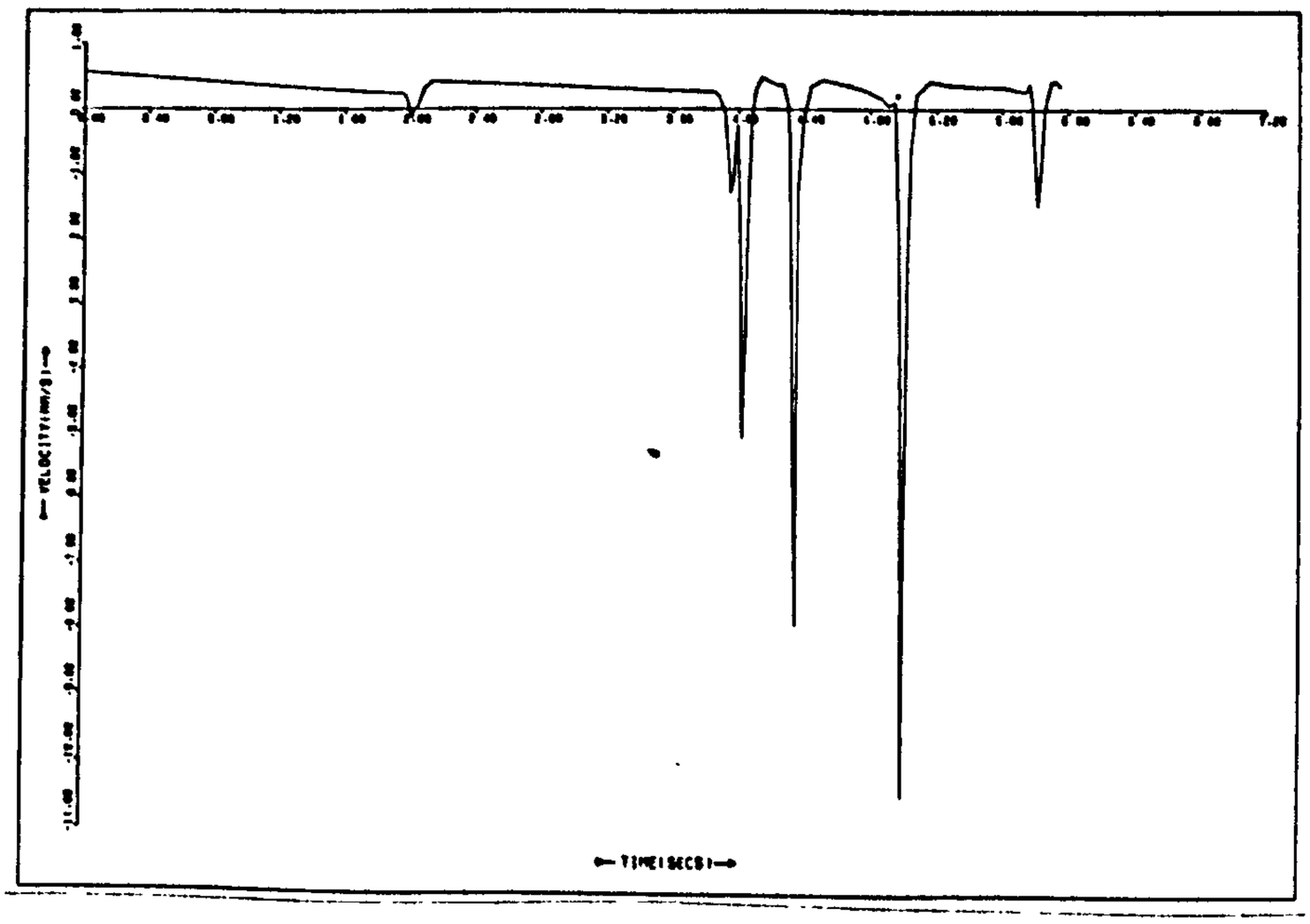

Fig. 3.8 Differentiation of fig. 3.5

As can be seen, despite the fact that the integrated curve starts and ends at the same value of $\dot{x}$, a large error is superimposed upon it. Consequently, it was decided that differentiation was the best method of obtaining the function $\dot{x}$ vs. t and this method was used to produce all the results shown in Chapter Four.

3.5 The solution of equation 5

Equation 5 was:-

$$\mu\,(\dot{x} - V_o) = \frac{M\ddot{x} + kx}{L} \quad \ldots\ldots\ldots\ (5)$$

The computer solved this equation for μ as a function of time. It had previously calculated $\dot{x}$ vs. t and could therefore plot a graph of μ against $\dot{x} - V_o$. The programme also plotted graphs of $\ddot{x}$, $\dot{x}$ and x against t as it progressed through the analysis. A full listing and flow diagram of the programme are given in appendix 1.

CHAPTER FOUR

EXPERIMENTAL RESULTS

4.1 A typical experimental result

Figure 4.1 a, b and c give typical curves for displacement, velocity and acceleration during two cycles of stick-slip. When these were analysed by the programme described in Chapter Three and Appendix One, the friction-velocity curve shown in fig. 4.1d was found.

As can be seen, these results produced the same looped characteristic as those of Sampson et al. (14) and Brockley and Ko (15). The two cycles follow similar paths. The friction rose to a high, static value of about 0.23 and, as relative motion started, it dropped gradually, reaching a value of about 0.18 at the maximum relative velocity of 8 mms^{-1}. As the slider decelerated, friction continued to fall, reaching a value of about 0.1 just as relative motion ceased and the system stuck again.

4.2 Varying the input speed

Figures 4.2, 4.3 and 4.4 show the effect of increasing the lower slider velocity (V_o in equation 5) to 0.7 mms^{-1}, 1.0 mms^{-1} and 2.0 mms^{-1} respectively in the experiment described above. The number of cycles used depended upon the size of the chart that could be placed on the digitising table (see Chapter Two) and the paper speed used for recording the results on the U.V. recorder.

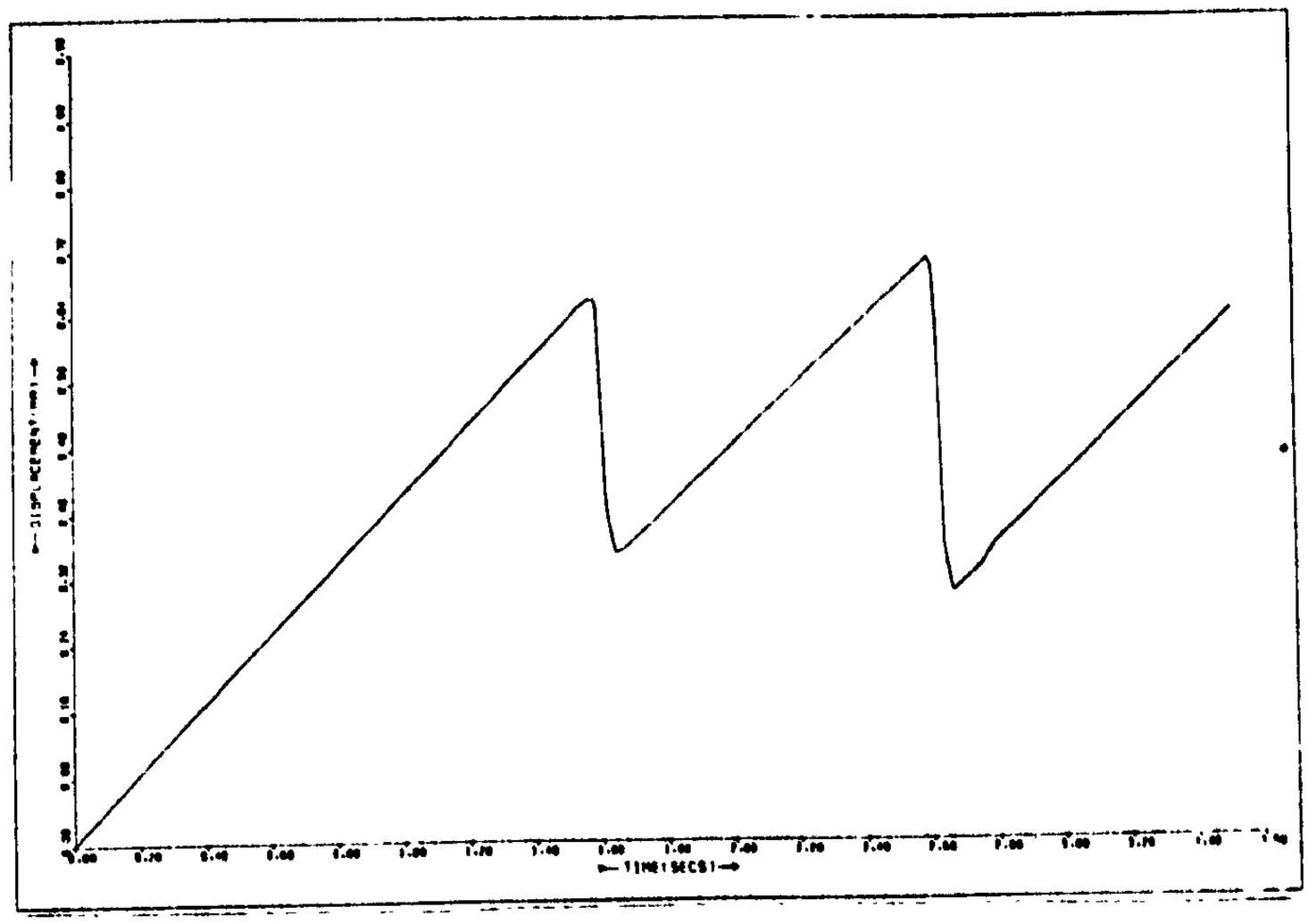

Fig. 4.1a

x vs. t

V_o = 0.5 mm/s

L = 3 Kg

k = 17.1 N/mm

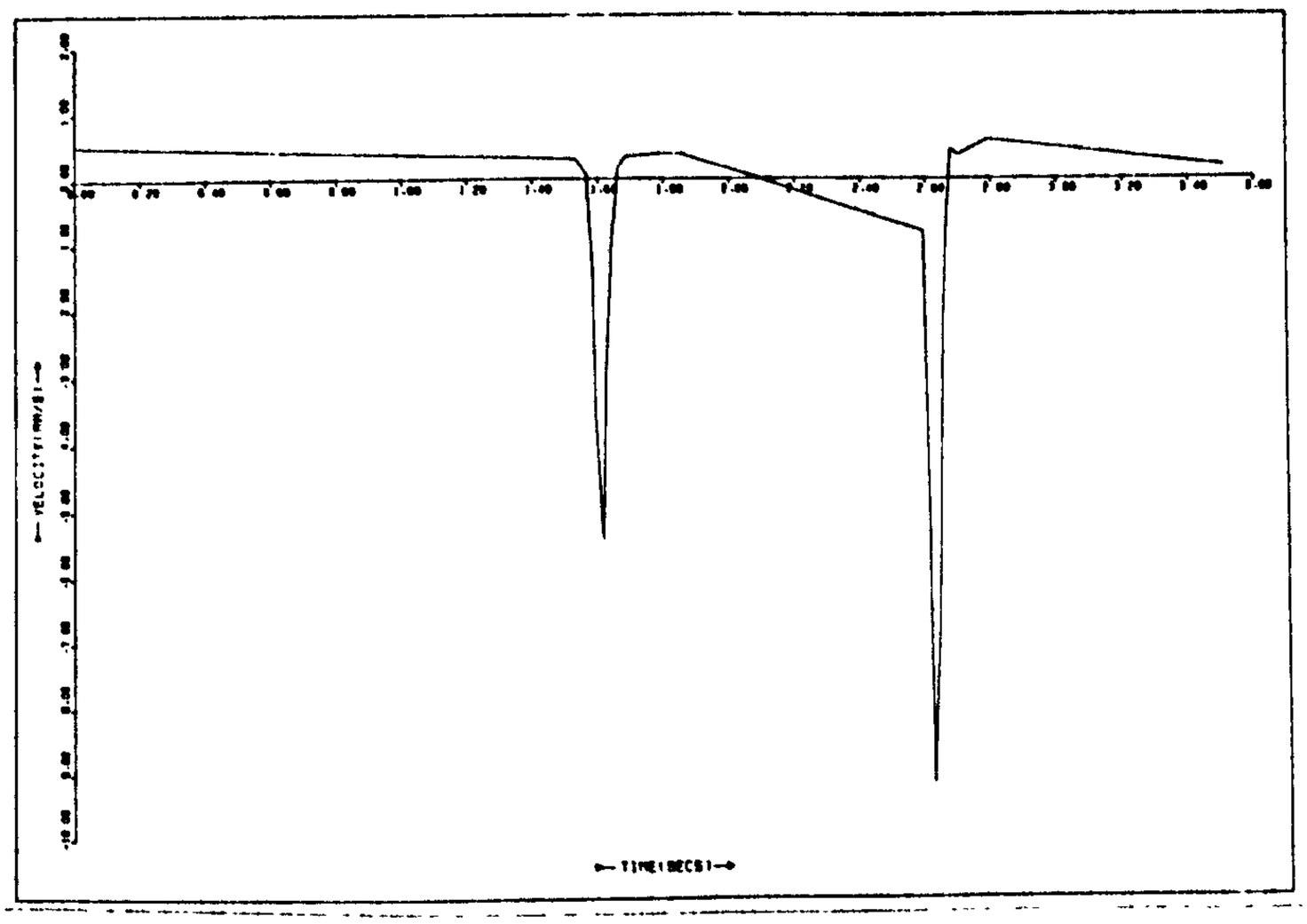

Fig. 4.1b

$\dot{x}$ vs. t

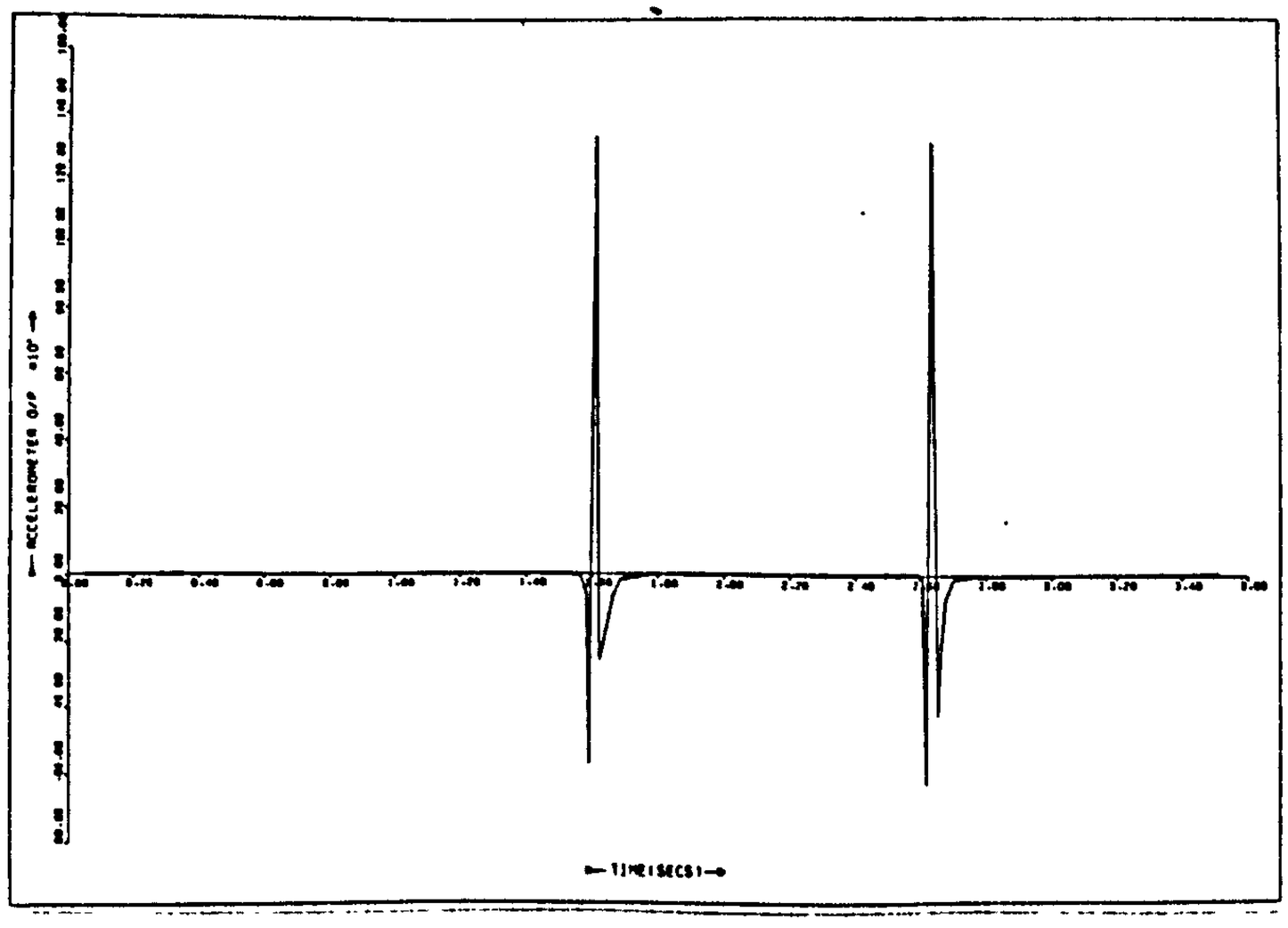

Fig 4.1c

$\ddot{x}$ vs. t

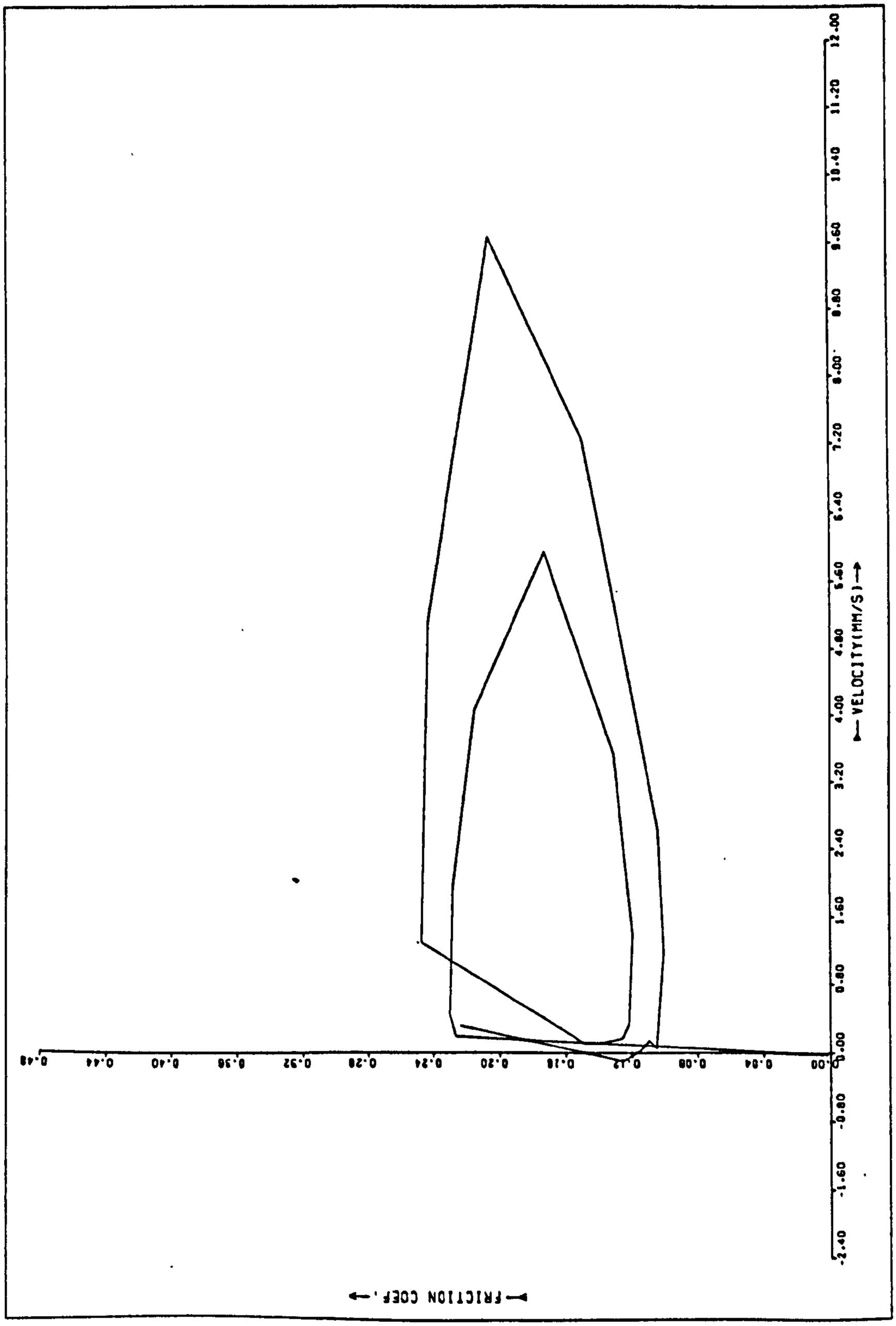

Fig. 4.1d μ vs. $\dot{x} - V_o$

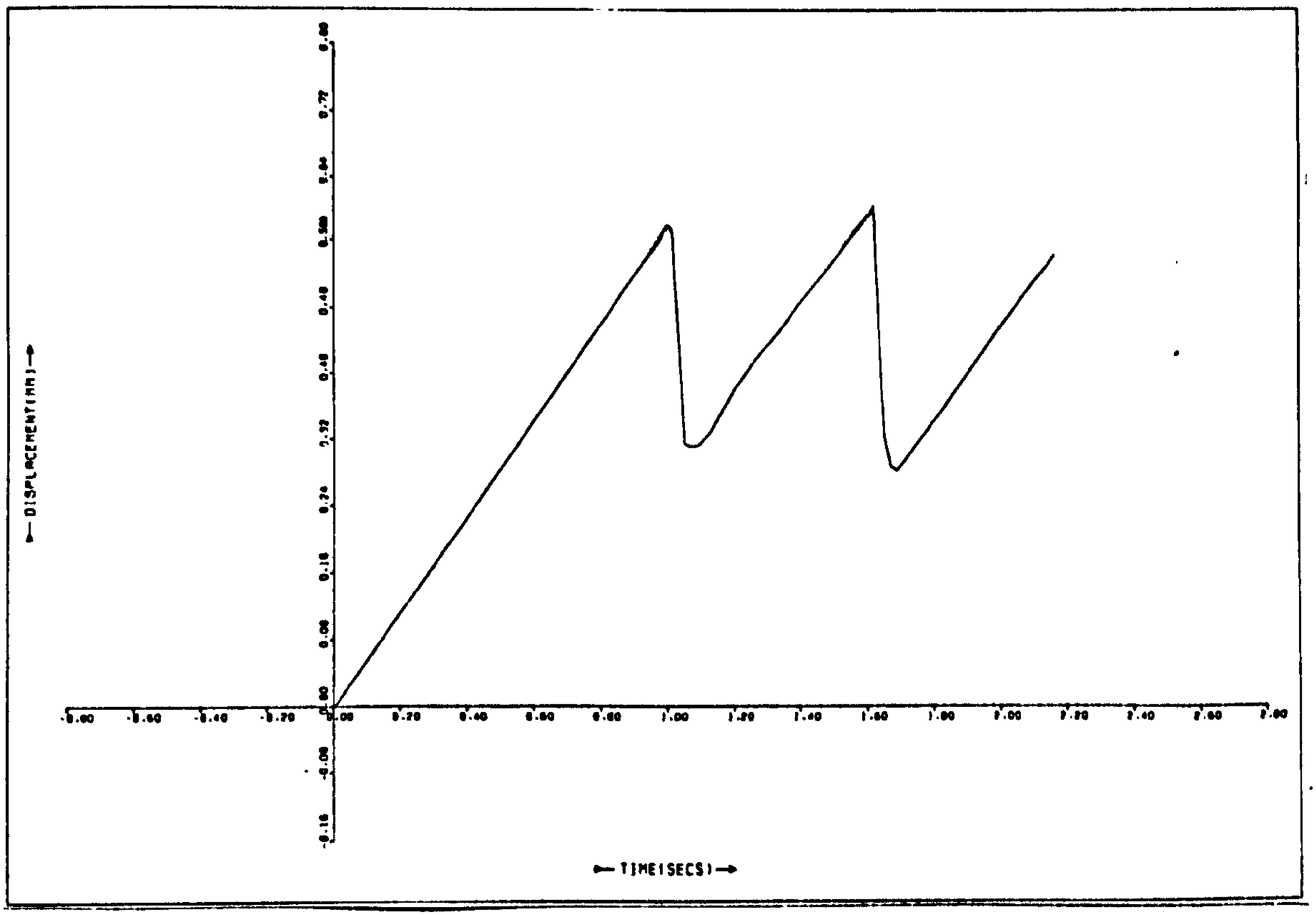

Fig. 4.2a x vs. t

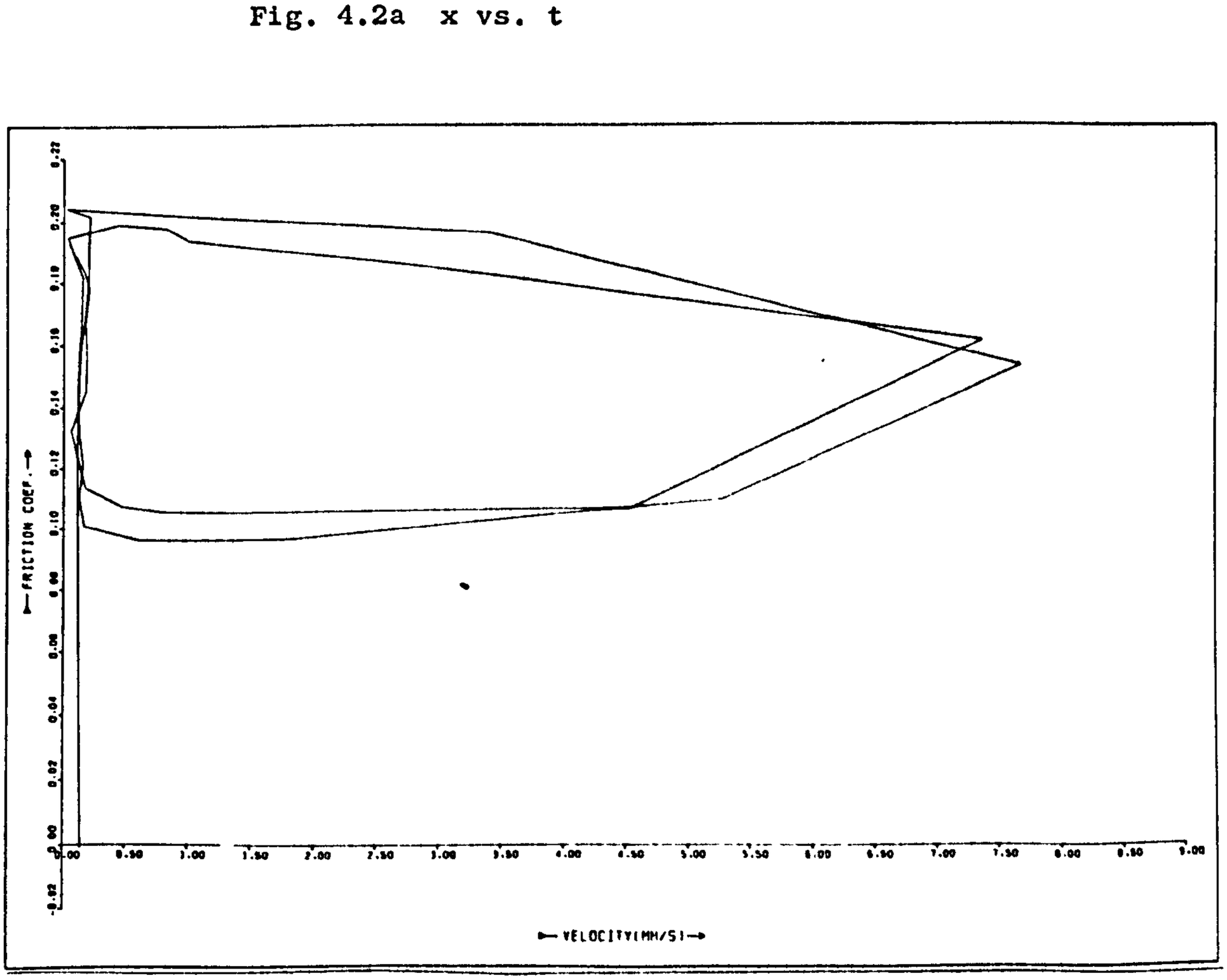

Fig. 4.2b μ vs. $(\dot{x} - V_o)$

V_o = 0.7 mm/s L = 3 Kg k = 17.1 N/mm

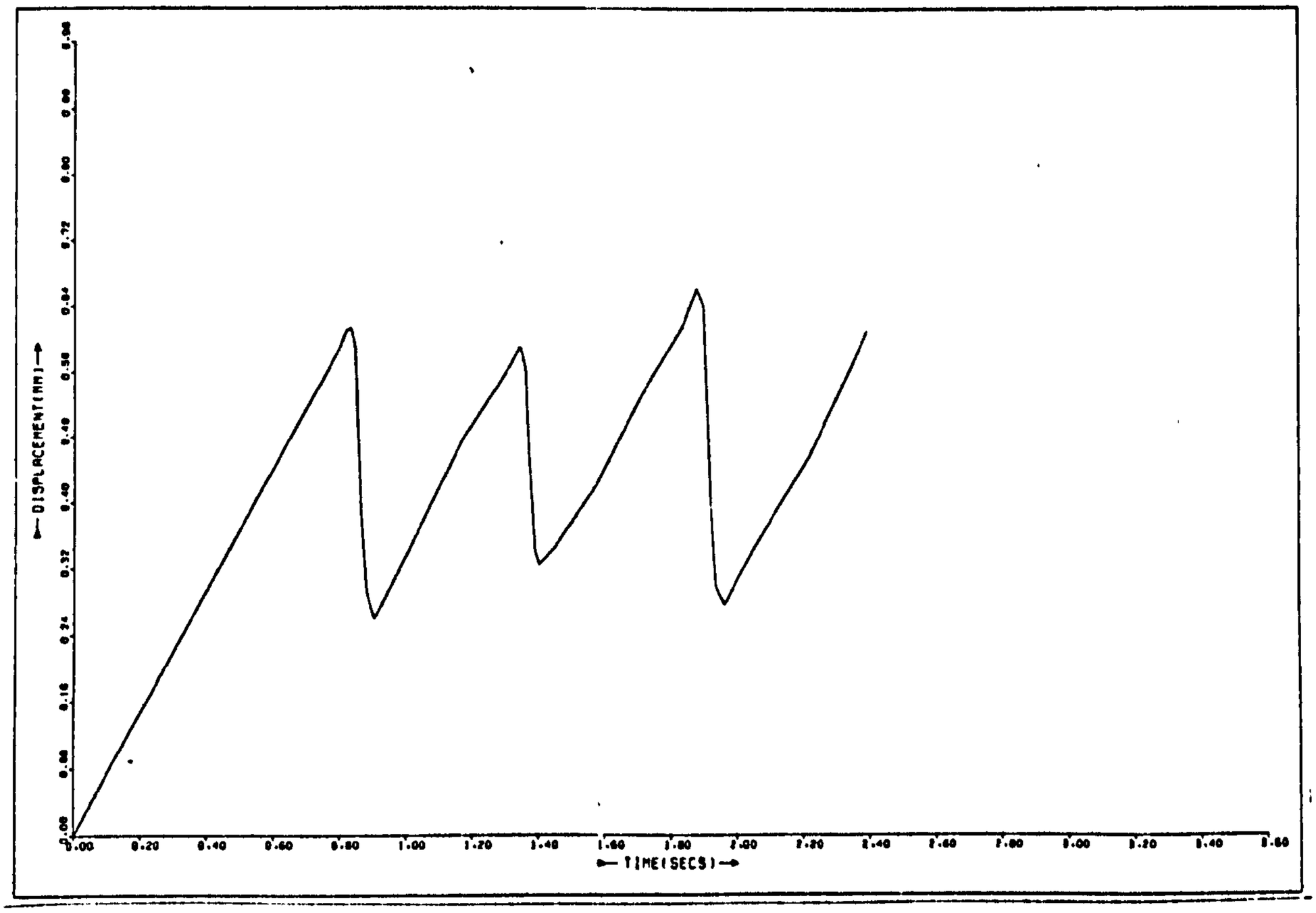

Fig. 4.3a x vs. t

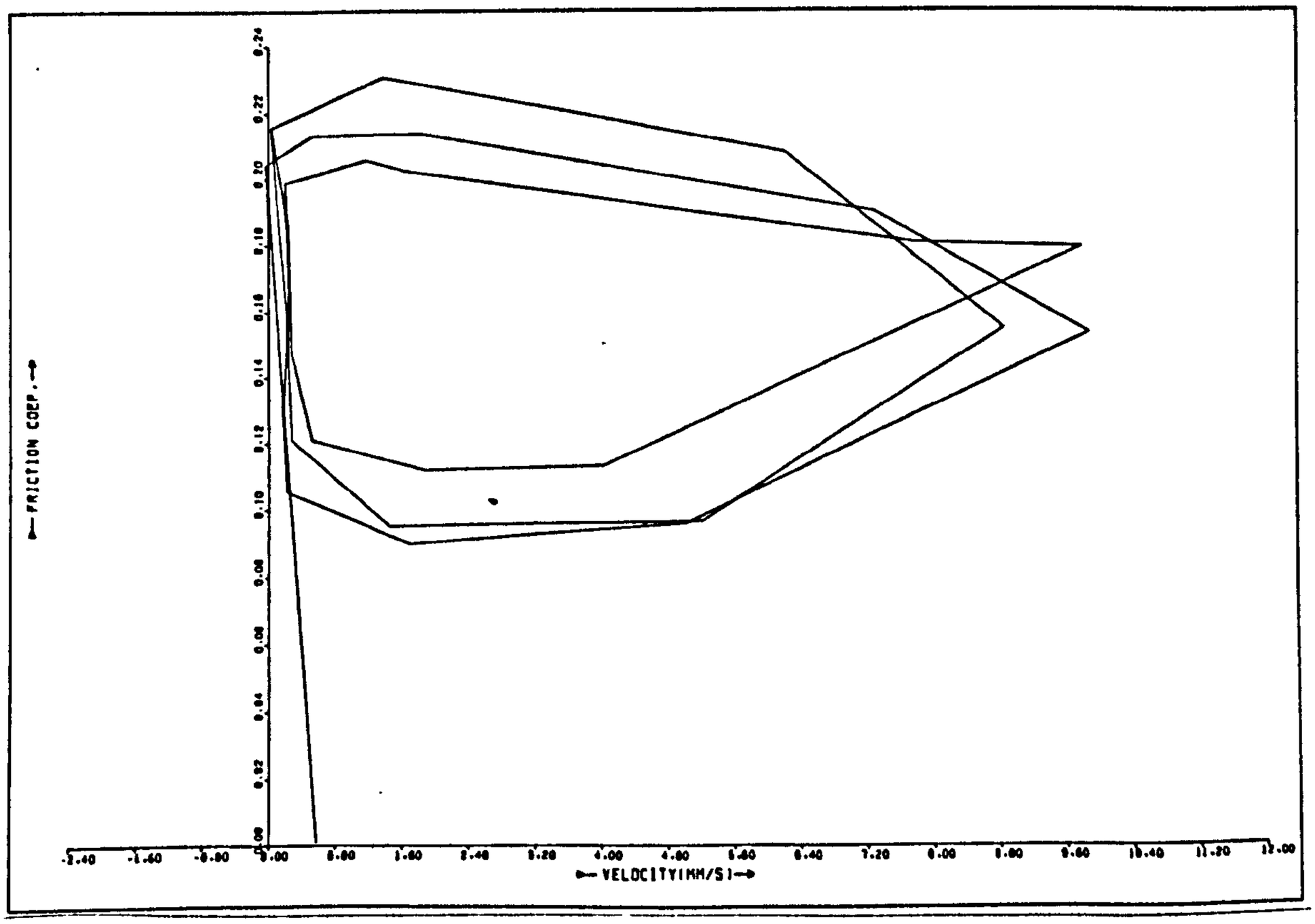

Fig. 4.3b μ vs. $(\dot{x} - V_o)$

V_o = 1.0 mm/s L = 3 Kg k = 17.1 N/mm

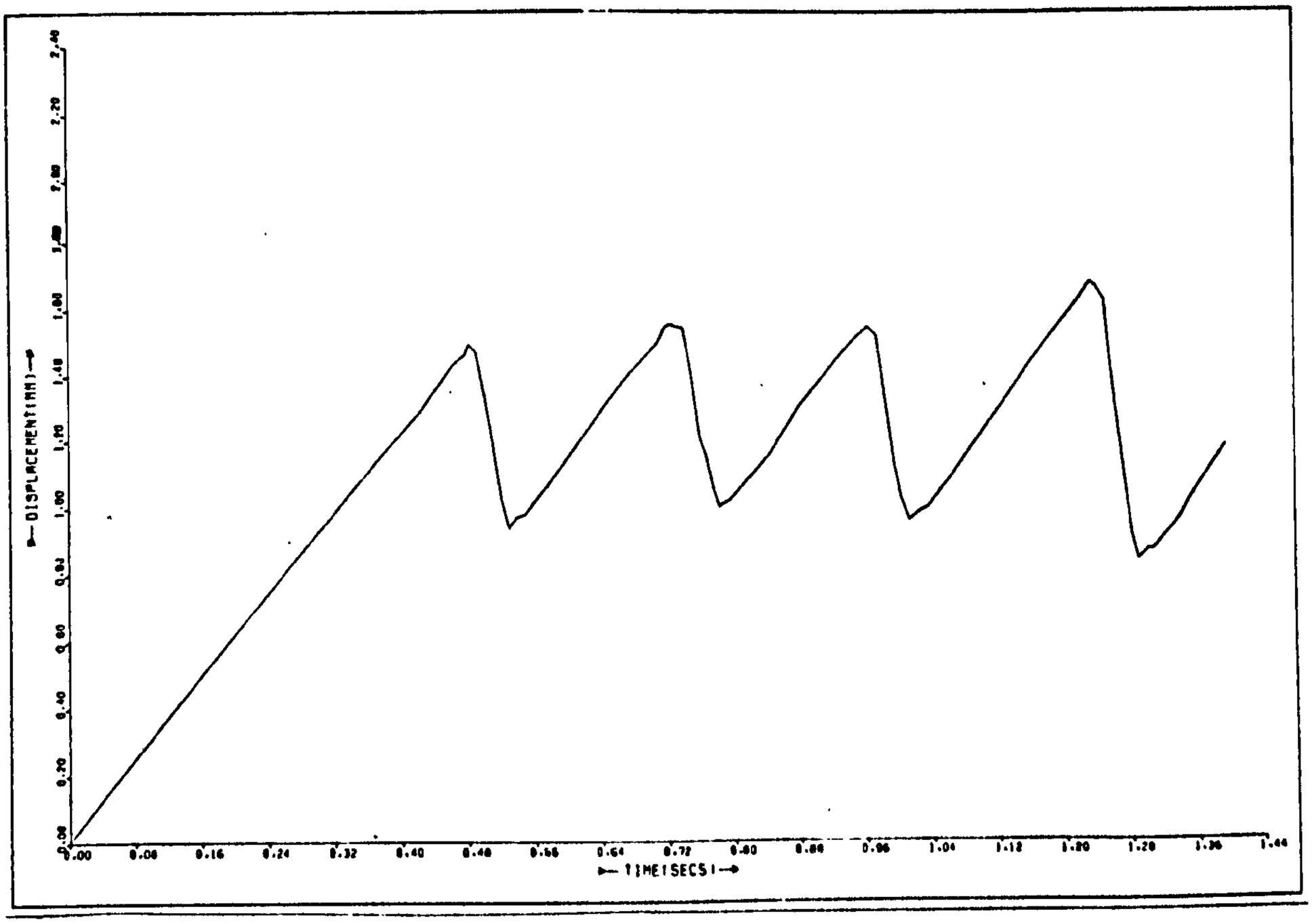

Fig. 4.4a x vs. t

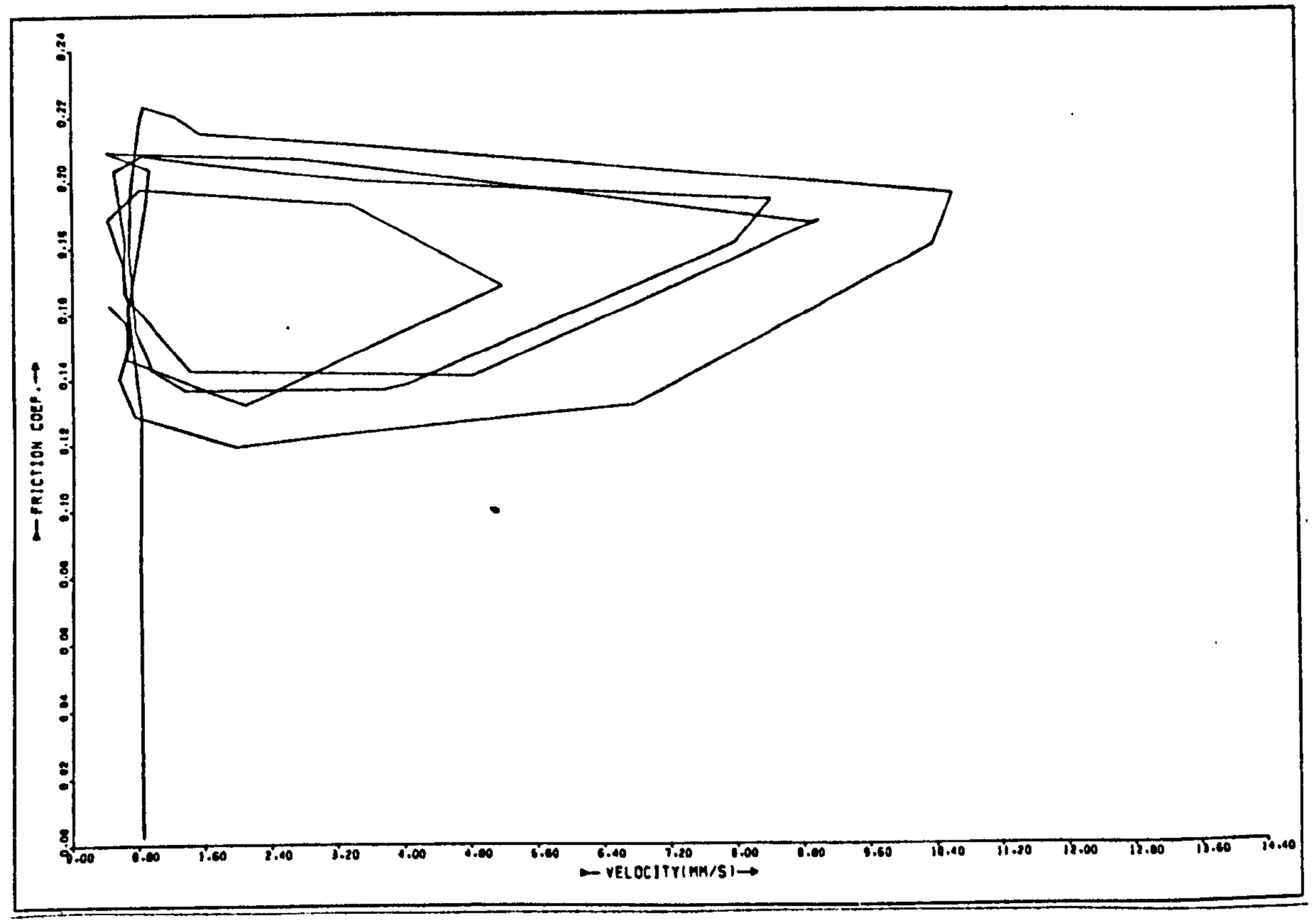

Fig. 4.4b μ vs. $(\dot{x} - V_o)$

V_o = 2.0 mm/s L = 3 Kg k = 17.1 N/mm

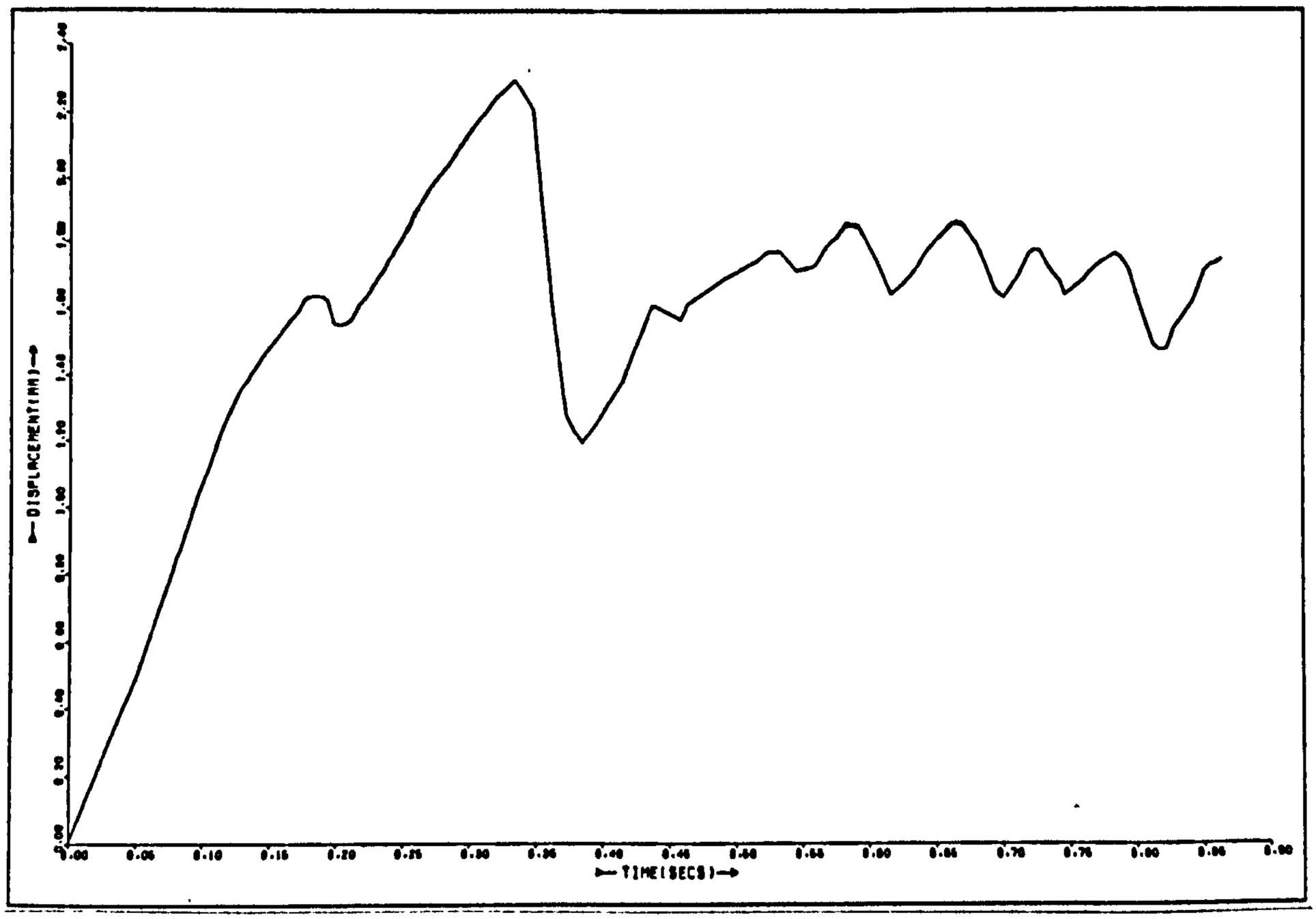

Fig. 4.5a x vs. t

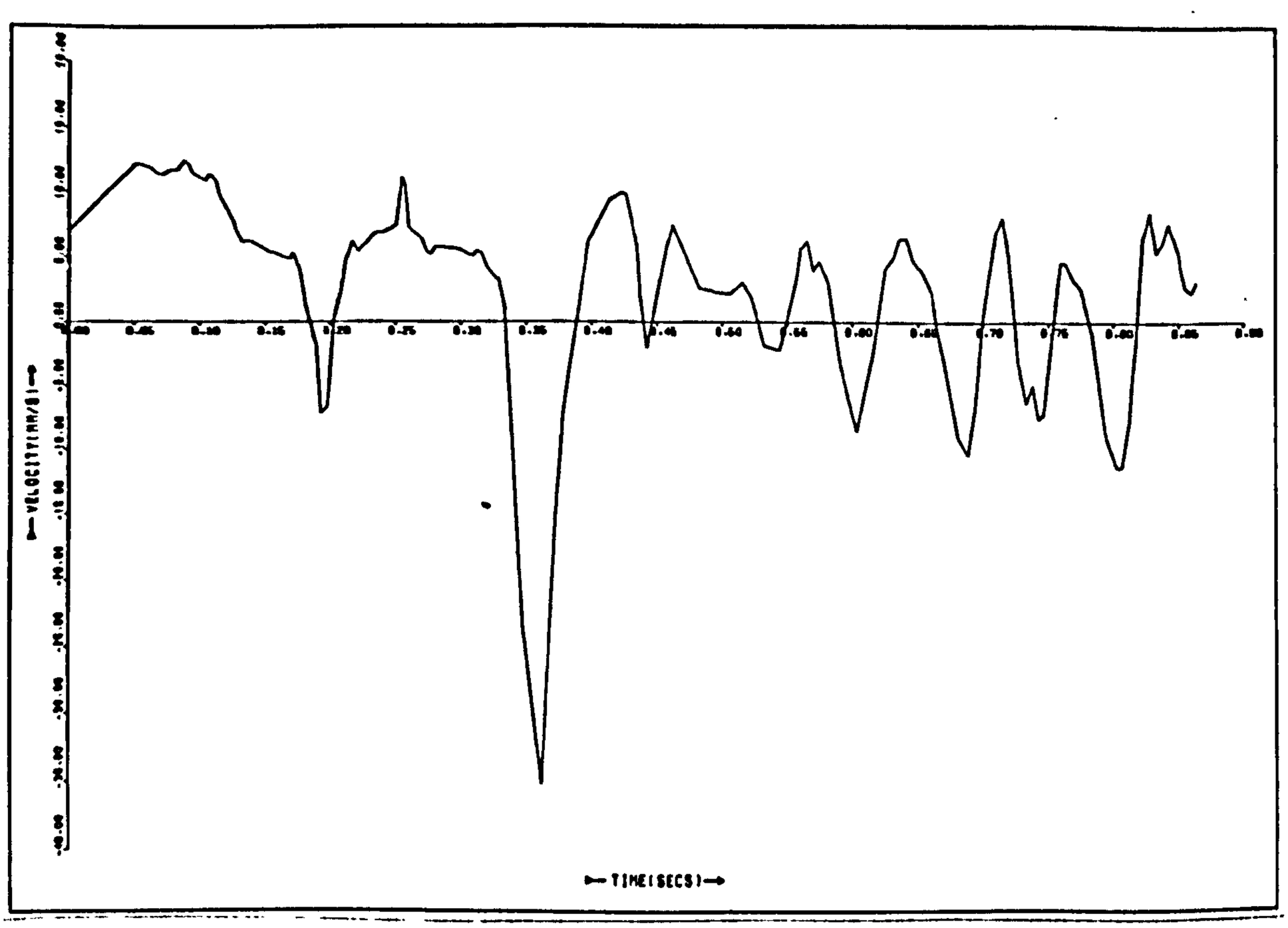

Fig. 4.5b $\dot{x}$ vs. t

V_o = 5.2 mm/s L = 3 Kg k = 17.1 N/mm

In all cases, the friction-velocity characteristics are substantially similar. Note that the high friction, just prior to sliding, in the slowest case (fig. 4.1b), is slightly higher than the others. This could well be due to the effect of stick time (see, for example, Rabinowicz (21)) as discussed in Chapter One, section 1.3. Note also that the shape of the oscillation at the peak and especially the trough is more rounded in the fastest case (fig. 4.4a) than the others, and is just starting to become quasi-harmonic (fig. 1.8, Brockley (17)).

The amplitude is also smaller than in the other cases, lending support to the idea of critical velocity (Brockley (18), and Banergee (19)). Figure 4.5 shows the results for a high value of V_o (5.2 mms^{-1}). After the first cycle, the motion becomes similar to the quasi-harmonic oscillation of Brockley. This can probably be more easily seen on fig. 4.5b, the $\dot{x}$ vs. t trace. The motion is rather irregular. This may be caused by the occurrance of some momentary adhesion in the sliding contact (Brockley's results were for blotting paper sliding on steel. Adhesion would not be expected between these materials.).

4.3 Varying the stiffness

Figure 4.6a shows the stick-slip that resulted from an experiment conducted under conditions similar to those of fig. 4.1, except that the stiffness of the cantilever was halved.

As would be expected, the peak value of displacement is greater than previously and the velocities and accelerations are not as great; furthermore, the amplitude has decreased. There are two possible explanations for this. One follows from the fact that the relative sliding velocities involved were less than in fig. 4.1a. Consequently, the kinetic energy of the top slider at the point

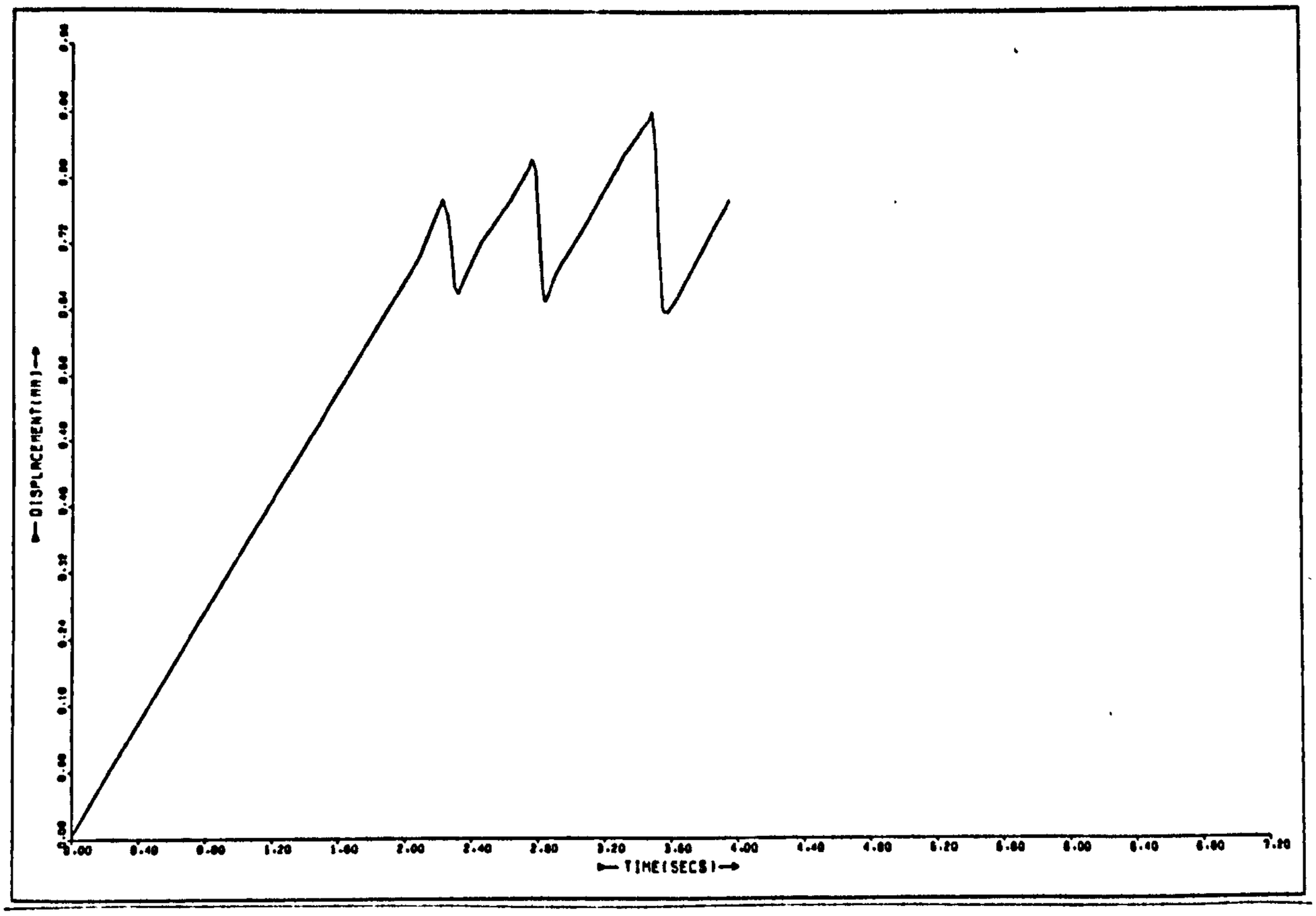

Fig. 4.6a x vs. t

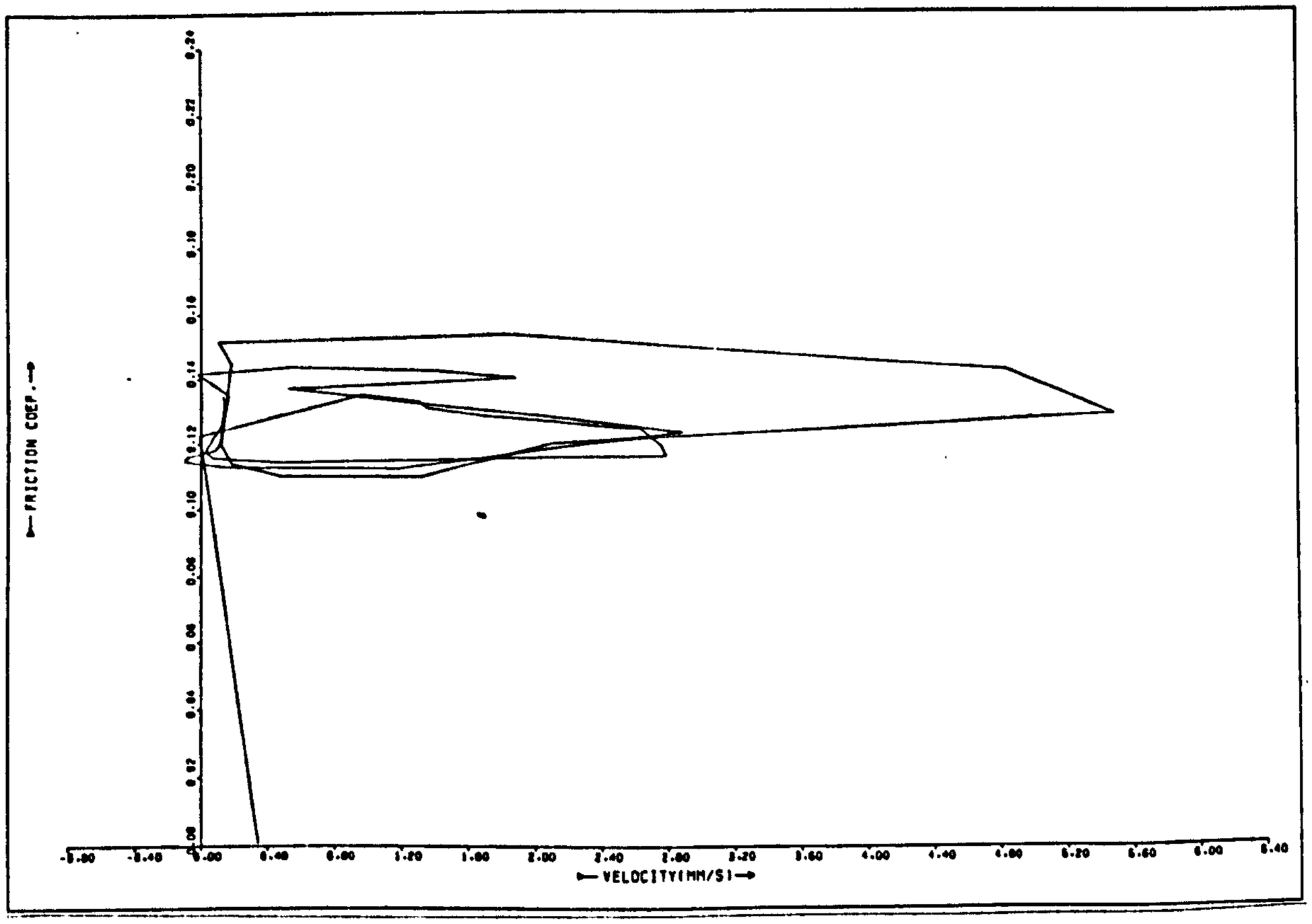

Fig. 4.6b μ vs. $(\dot{x} - V_o)$

V_o = 0.5 mm/s L = 3 Kg k = 9 N/mm

where deceleration started (P_2, fig. 1.3) was also less and friction may have dissipated all the energy more quickly. The other possibility is that, as the two sets of experiments were conducted one after the other on the same specimens, more material had condensed onto the surfaces in the second case, thus altering the friction-velocity curve (fig. 4.6b). As can be seen, the peak friction coefficient, just before sliding started, was about 0.14, whereas in fig. 4.1d it was about 0.23. This was despite the fact that the two surfaces had remained stuck for 0.7 seconds longer in fig. 4.6a than in fig. 4.1a, and it would be expected that longer stick times would give higher friction (Rabinowicz (21)). If a thicker, low shear, adsorbed film were present (Green and Brockley (26)), however, this behaviour would be likely.

Also, the friction-velocity curve in the second case (fig. 4.6b), though looped in a similar manner to figure 4.1d (but with rather more scatter), shows much less of a drop in friction with sliding. This is consistent with the presence of a shear film with ordinary viscous characteristics (i.e. force increasing with shear rate) interfering with the expected friction-velocity characteristic (force decreasing with shear rate).

Figures 4.7, 4.8 and 4.9 show the effect of increasing lower slider velocity, V_o, to 0.7 mms^{-1}, 1.0 mms^{-1} and 2.0 mms^{-1} respectively. Note that, as before, the stick-slip becomes more rounded at higher values of V_o (fig. 4.9a). The amplitude increases before decreasing as expected from the previous results and from Brockley (26). This might have been caused by the adsorbed film's being wiped off as the experiment progressed. The peak friction (figs. 4.7b, 4.8b and 4.9b), before the start of sliding, also rises then falls.

The friction-velocity curves all have the same form, the

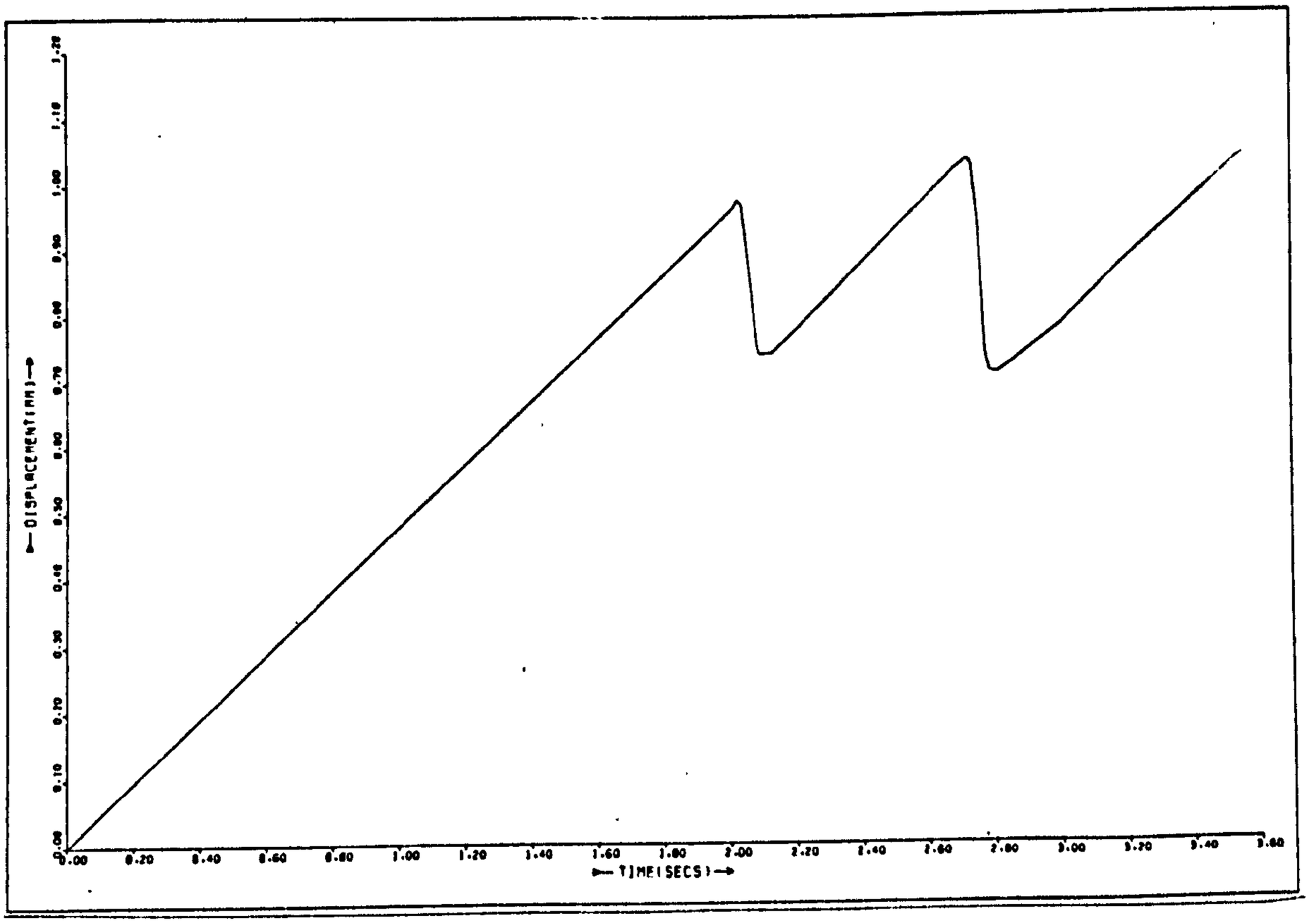

Fig. 4.7a x vs. t

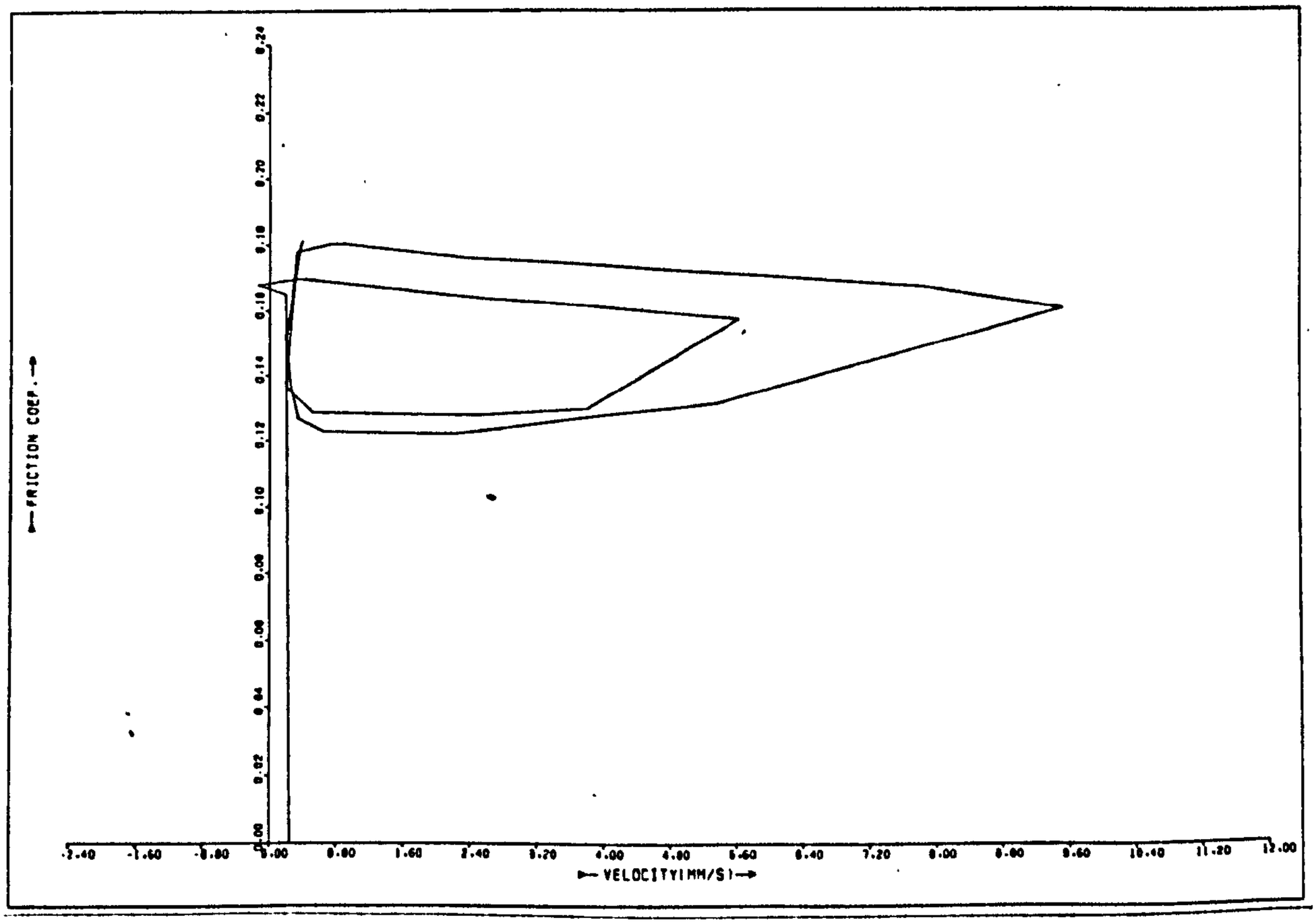

Fig. 4.7b μ vs. $(\dot{x} - V_o)$

V_o = 0.7 mm/s L = 3 Kg k = 9 N/mm

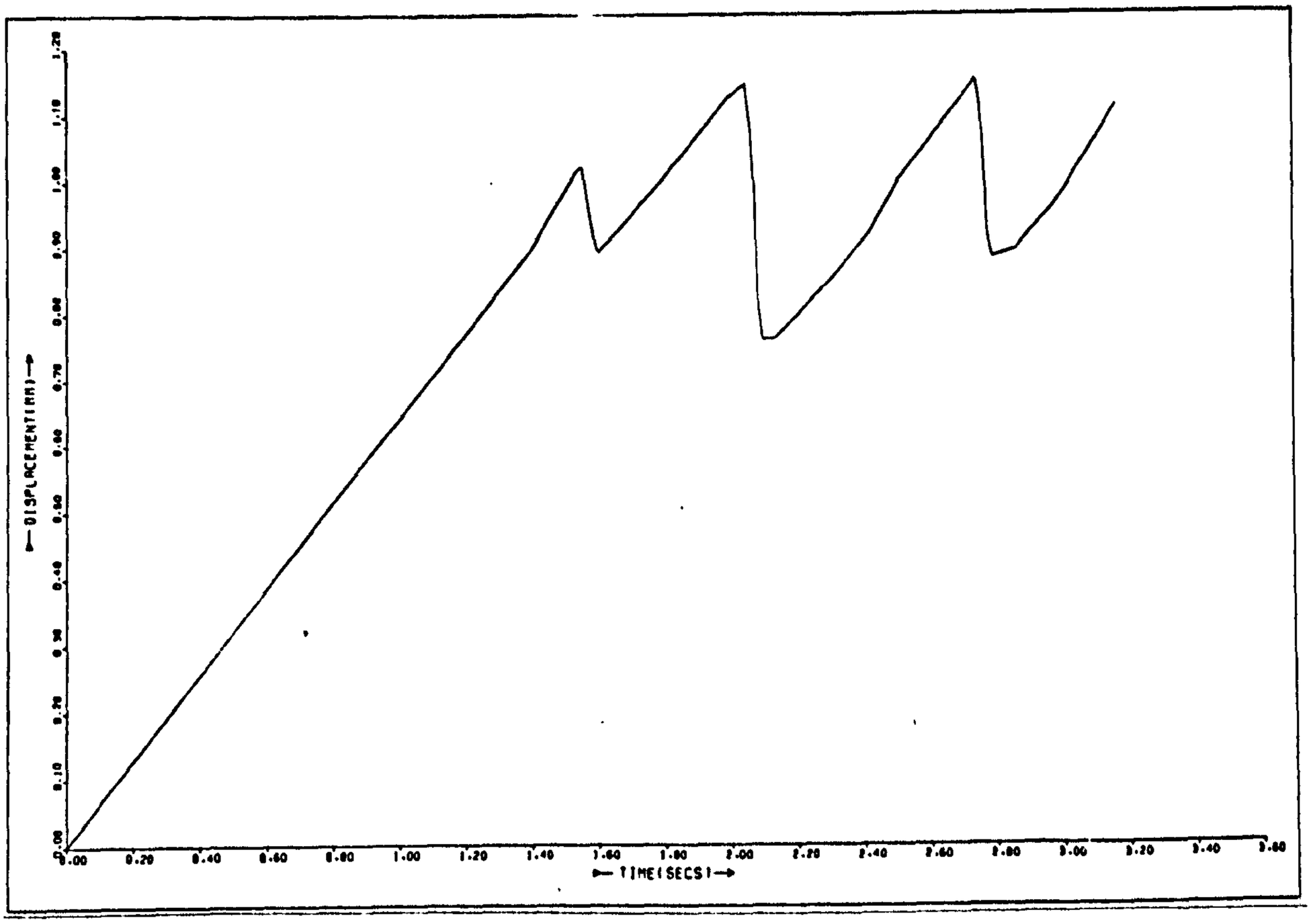

Fig. 4.8a x vs. t

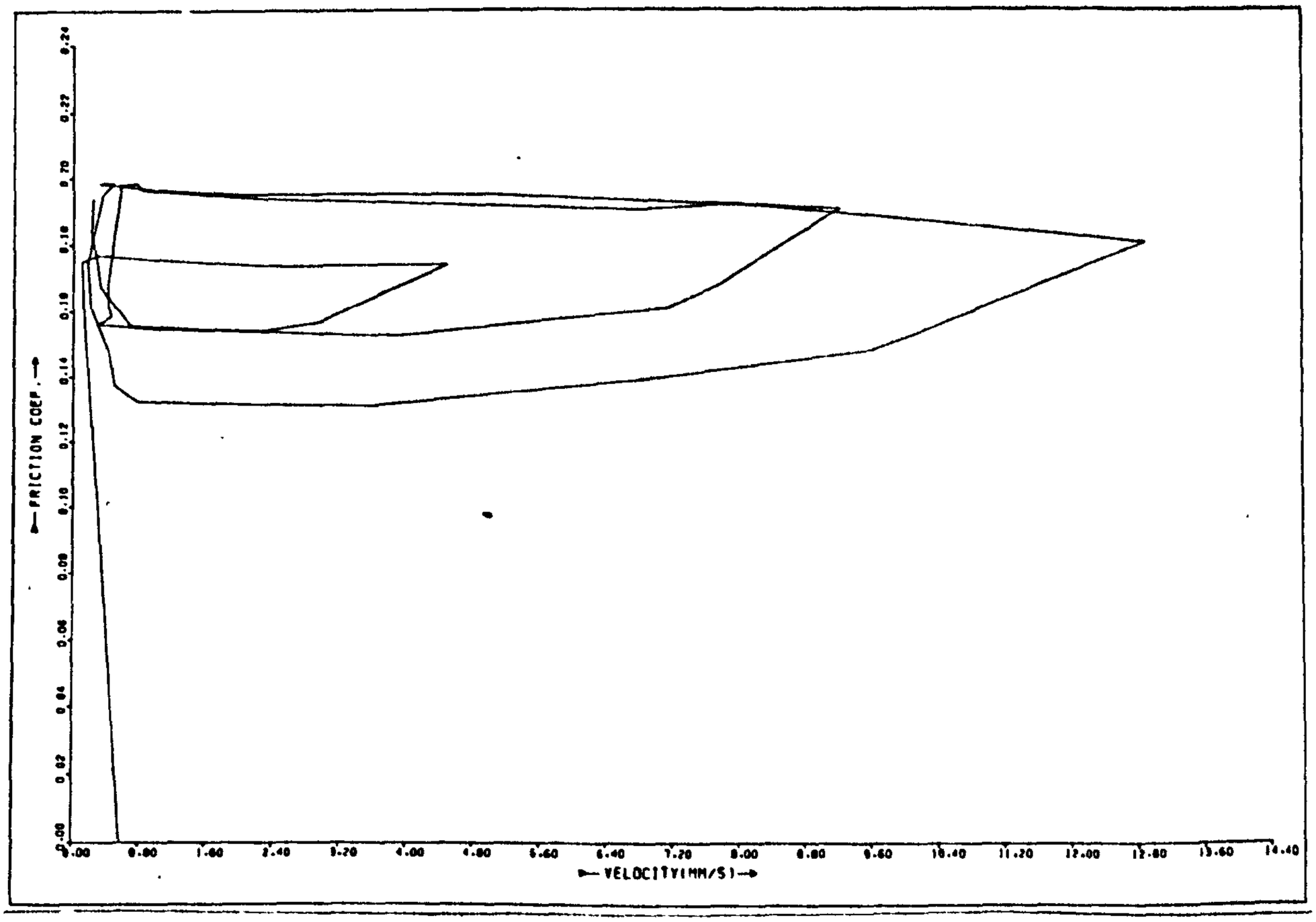

Fig 4.8b μ vs. $(\dot{x} - V_o)$

V_o = 1.0 mm/s L = 3 Kg k = 9 N/mm

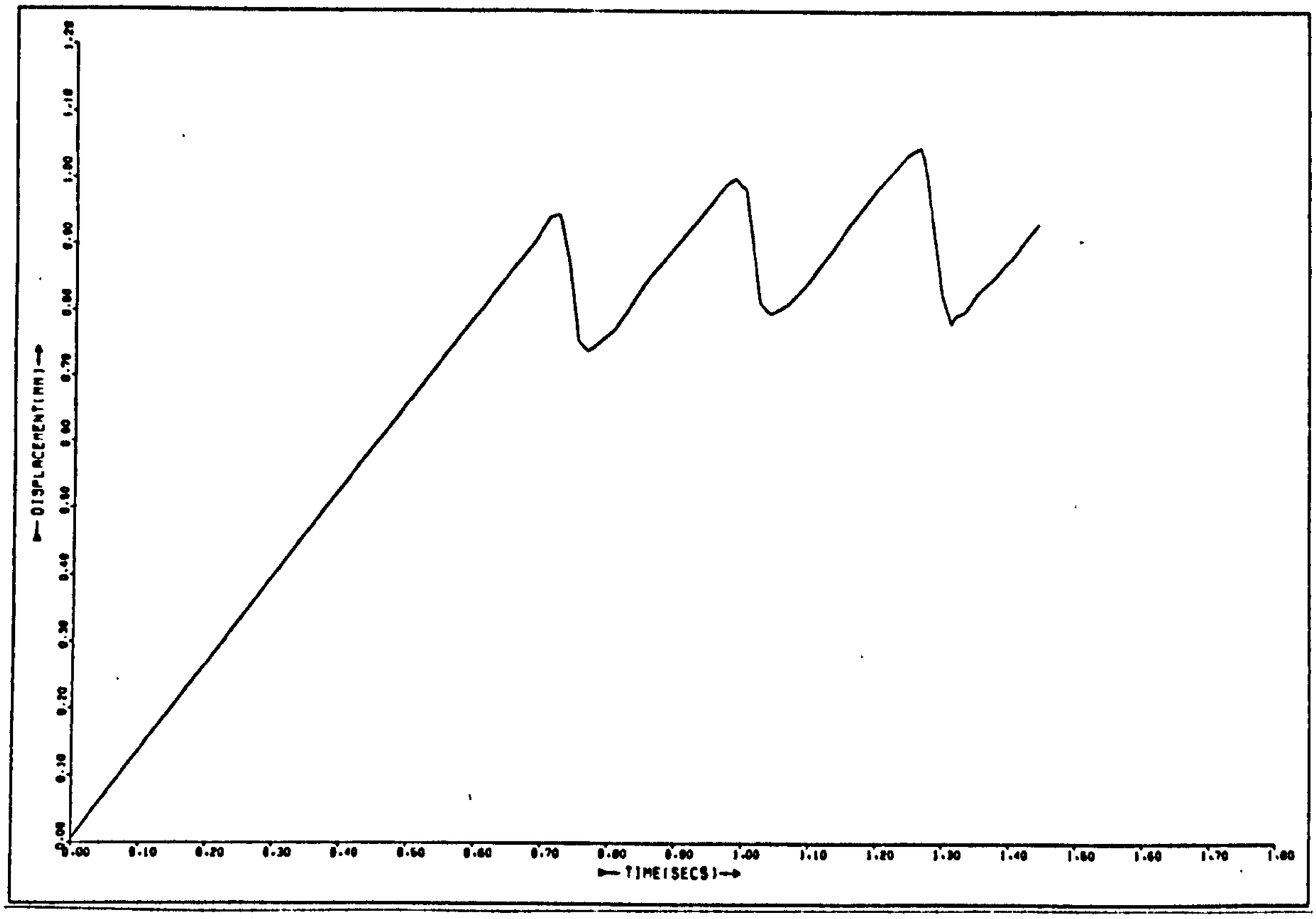

Fig. 4.9a x vs. t

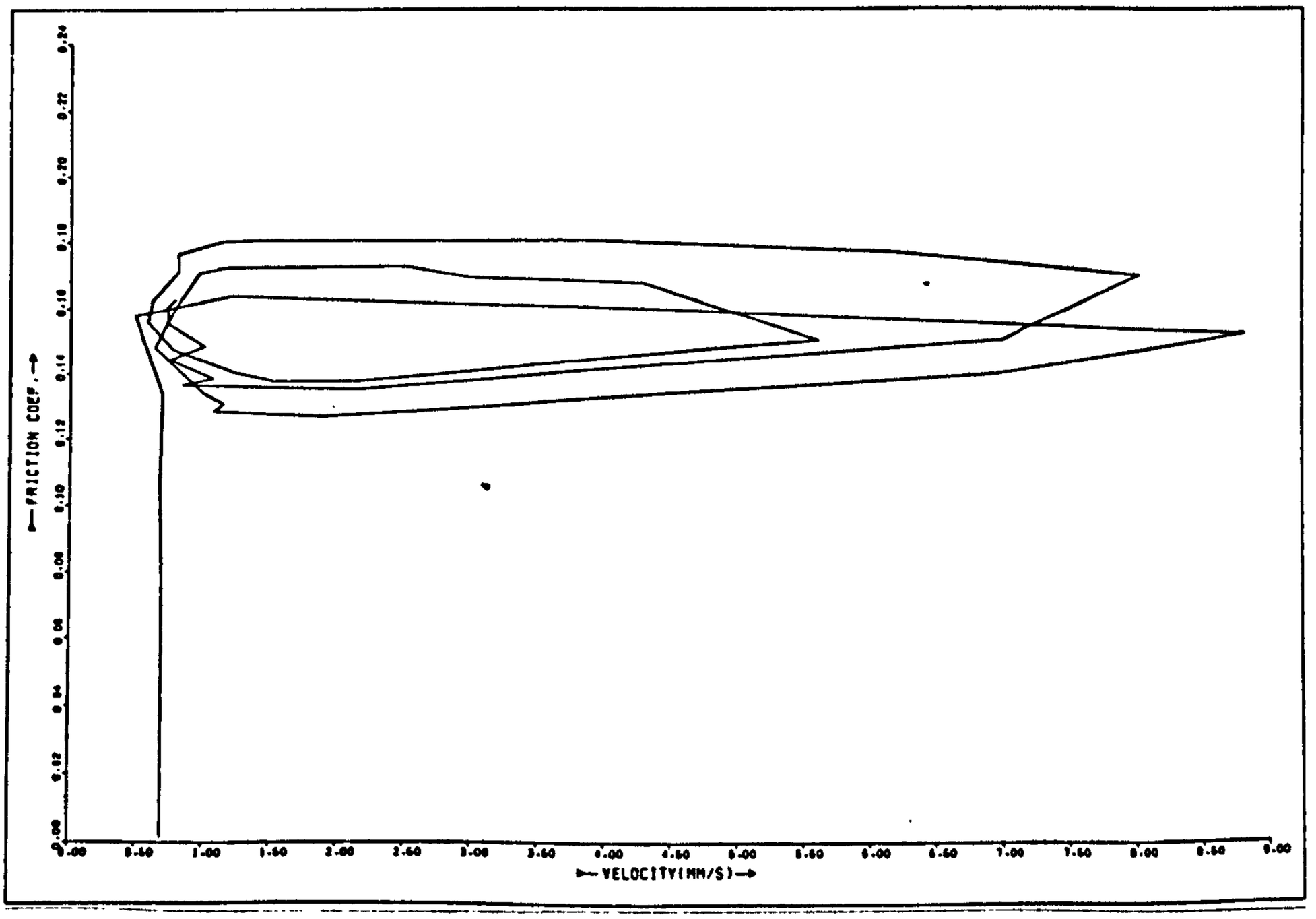

Fig. 4.9b μ vs. $(\dot{x} - V_o)$

V_o = 2.0 mm/s L = 3 Kg k = 9 N/mm

friction rising to a high, static value and then falling with increasing relative velocity and continuing to fall with decreasing relative velocity, beginning to rise again only at very low relative velocities just before sticking.

4.4 Varying the load

All the above experiments were conducted with a horizontally decoupled load of 3 kg forcing the specimens together. Figures 4.10, 4.11, 4.12 and 4.13 show the results of experiments conducted under similar conditions to those in figures 4.1, 4.2, 4.3 and 4.4 respectively, except that the load was doubled to 6 kg.

As might be expected, the peak displacements have just about doubled. The frequency has halved. Again, this is predictable as the spring has to stretch twice as far when the surfaces are stuck to generate a force sufficient to overcome the greater friction force.

The friction-velocity curves (figs. 4.9b, 4.10b, 4.11b and 4.12b) again show the looped characteristic and the actual values of friction along them correspond quite well to the earlier graphs (figs. 4.1d, 4.2b, 4.3b and 4.4b). There is a digitising error on fig. 4.10a that has caused the negative velocity spike on the friction-velocity characteristic (fig. 4.10b). The rest of the curve will be unaffected by this small error. Note particularly the cycles in figs. 4.10b and 4.11b which have only attained a peak velocity of about 8 mms^{-1}, and compare these with figs. 4.1d and 4.3b respectively.

The effect of high load with low stiffness is shown in figs. 4.13, 4.14, 4.15 and 4.16. These correspond to values of V_o of 0.5, 0.7, 1.0 and 2.0 mms^{-1} respectively.

As before, the displacements are about double those under

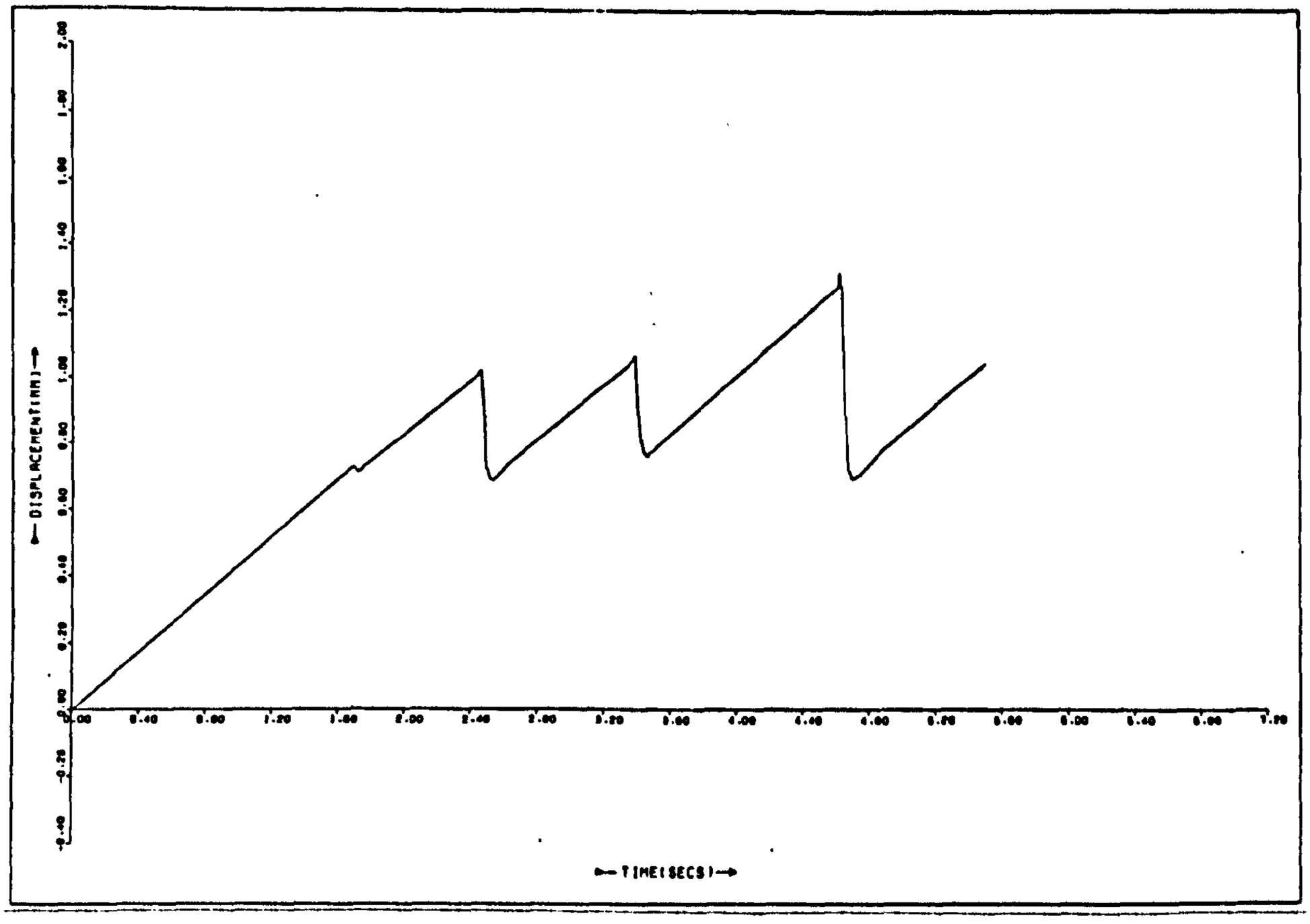

Fig. 4.10a x vs. t

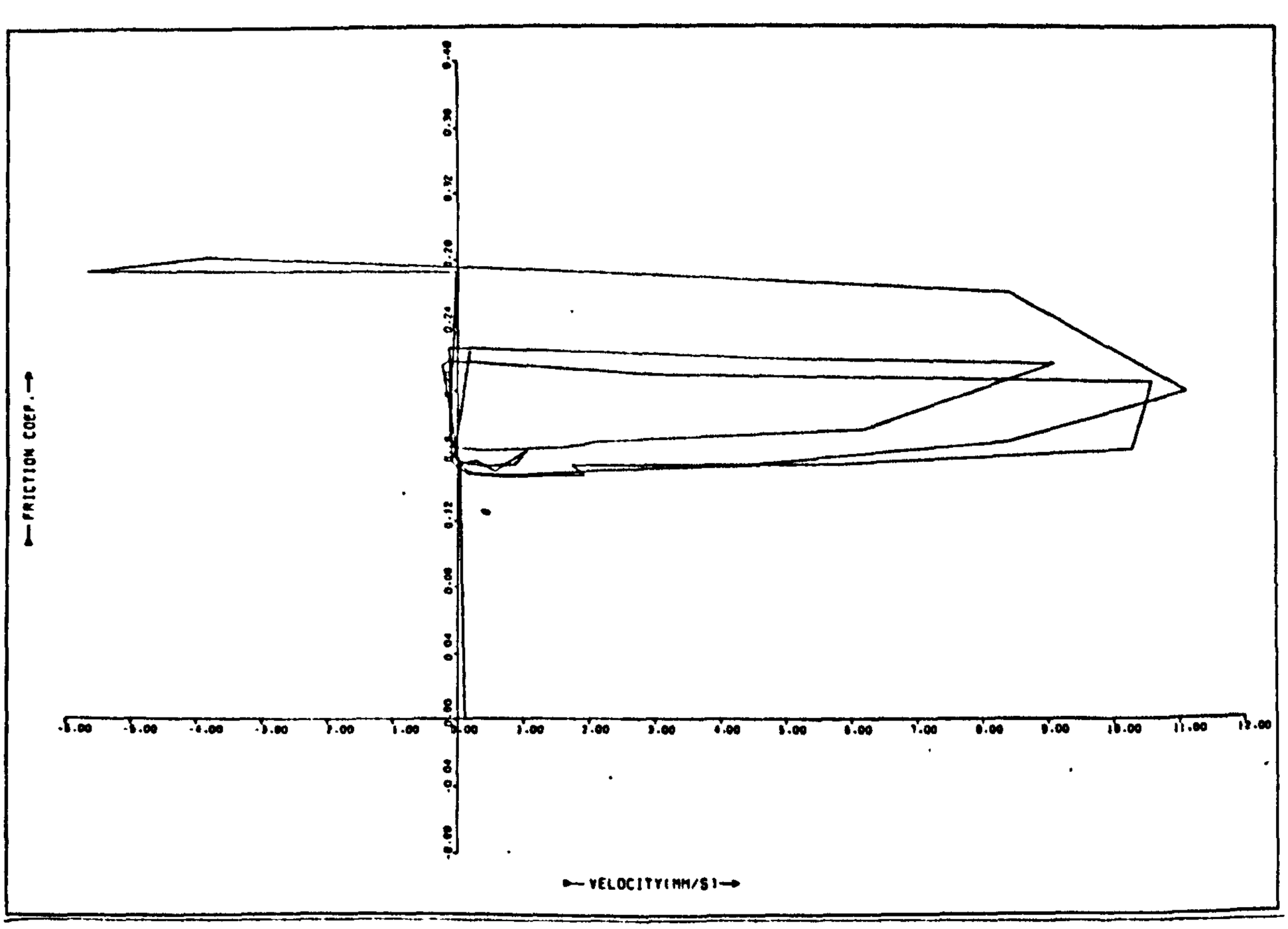

Fig. 4.10b μ vs. $(\dot{x} - V_o)$

V_o = 0.5 mm/s L = 6 Kg k = 17.1 N/mm

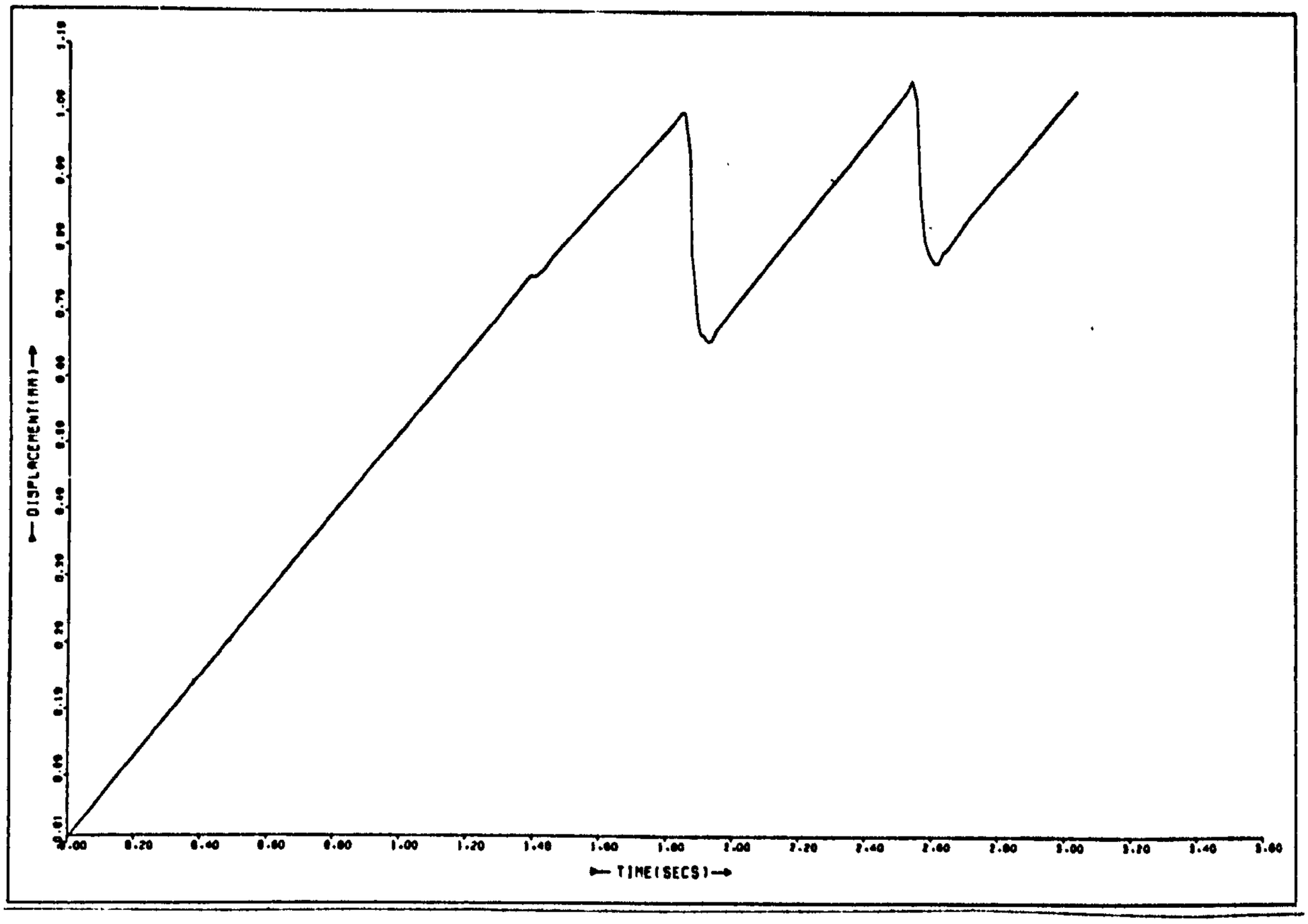

Fig. 4.11a x vs. t

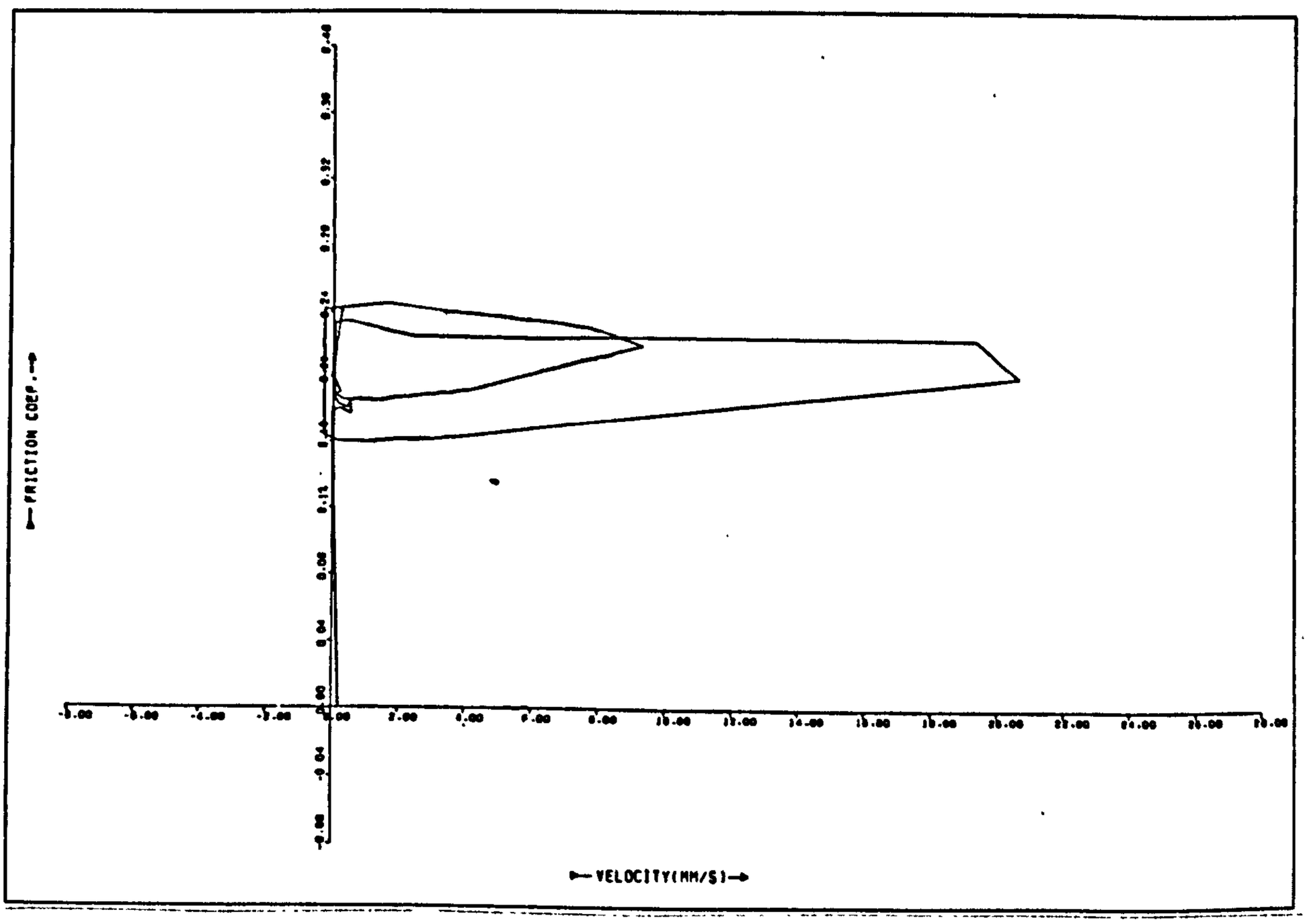

Fig. 4.11b μ vs. $(\dot{x} - V_o)$

V_o = 0.7 mm/s L = 6 Kg = k = 17.1 N/mm

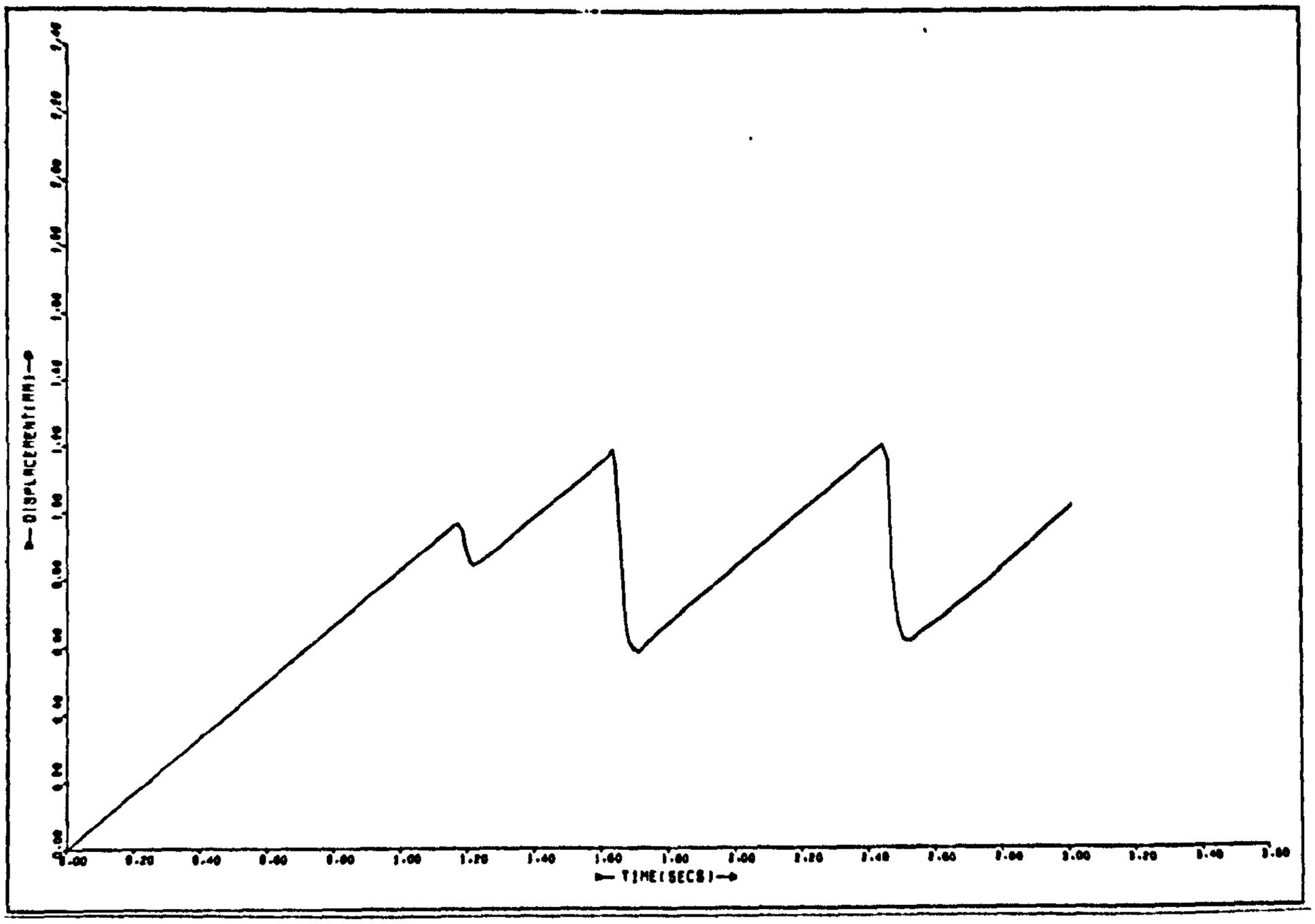

Fig. 4.12a x vs. t

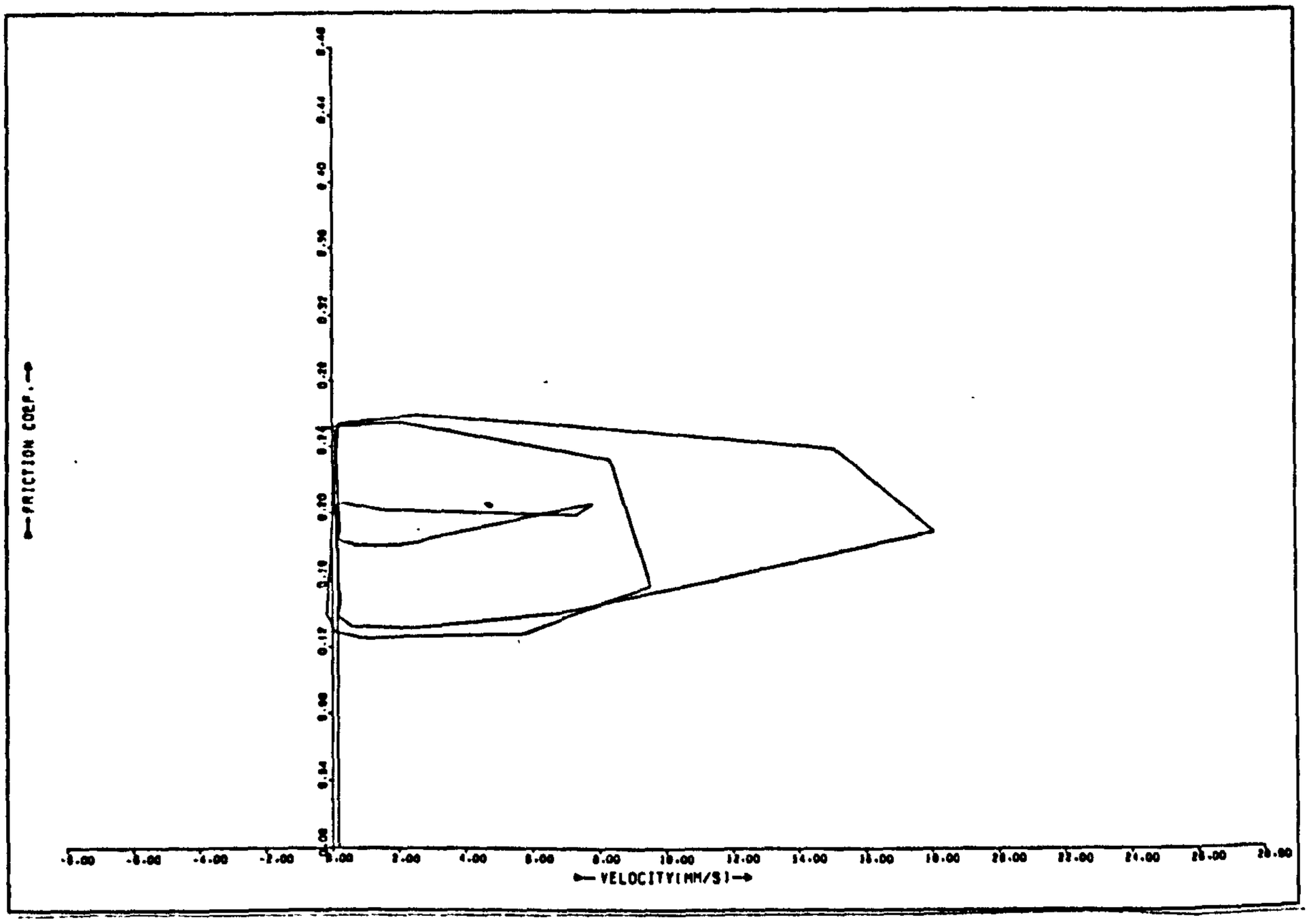

Fig. 4.12b μ vs. $(\dot{x} - V_o)$

V_o = 1.0 mm/s L = 6 Kg k = 17.1 N/mm

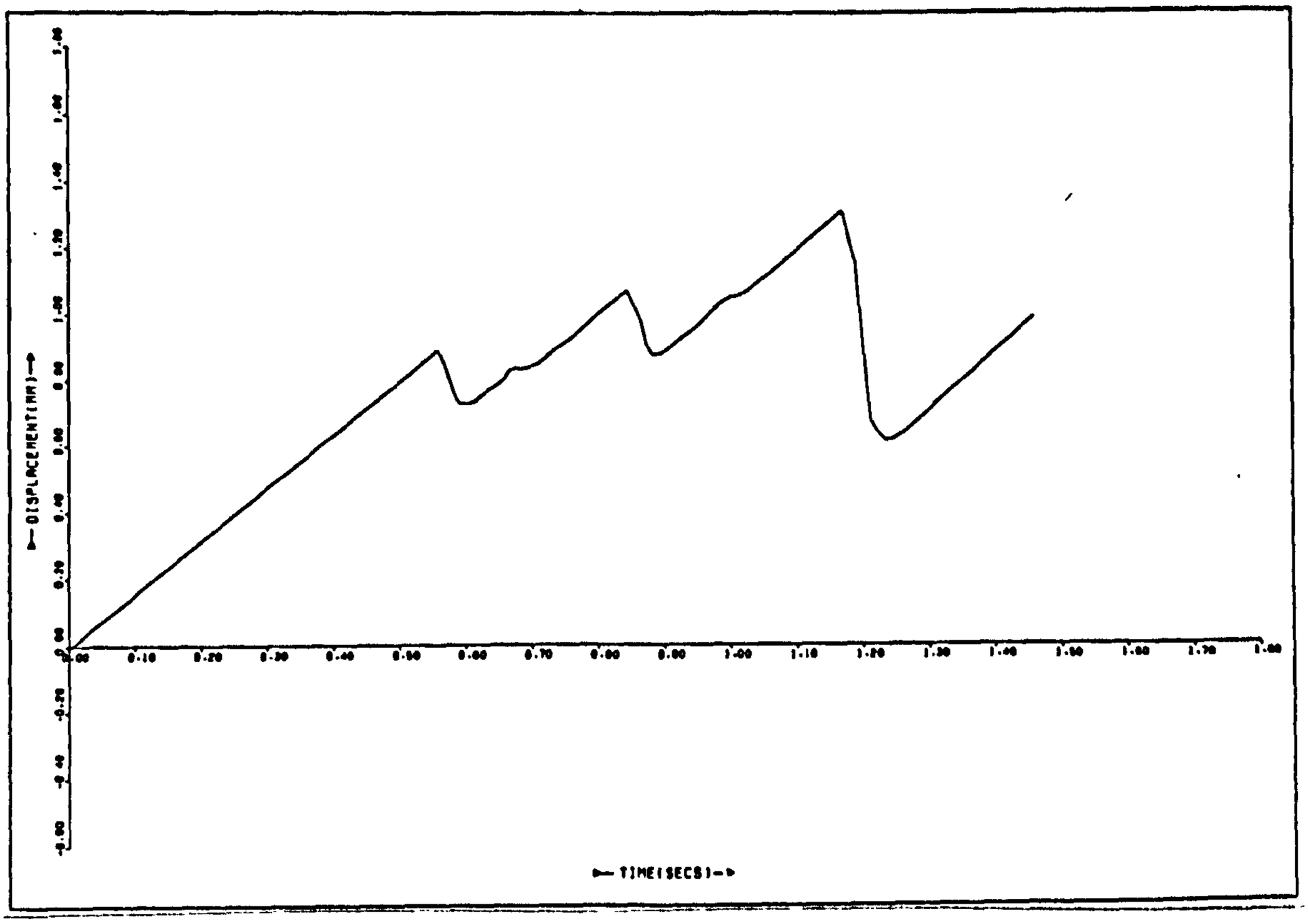

Fig. 4.13a x vs. t

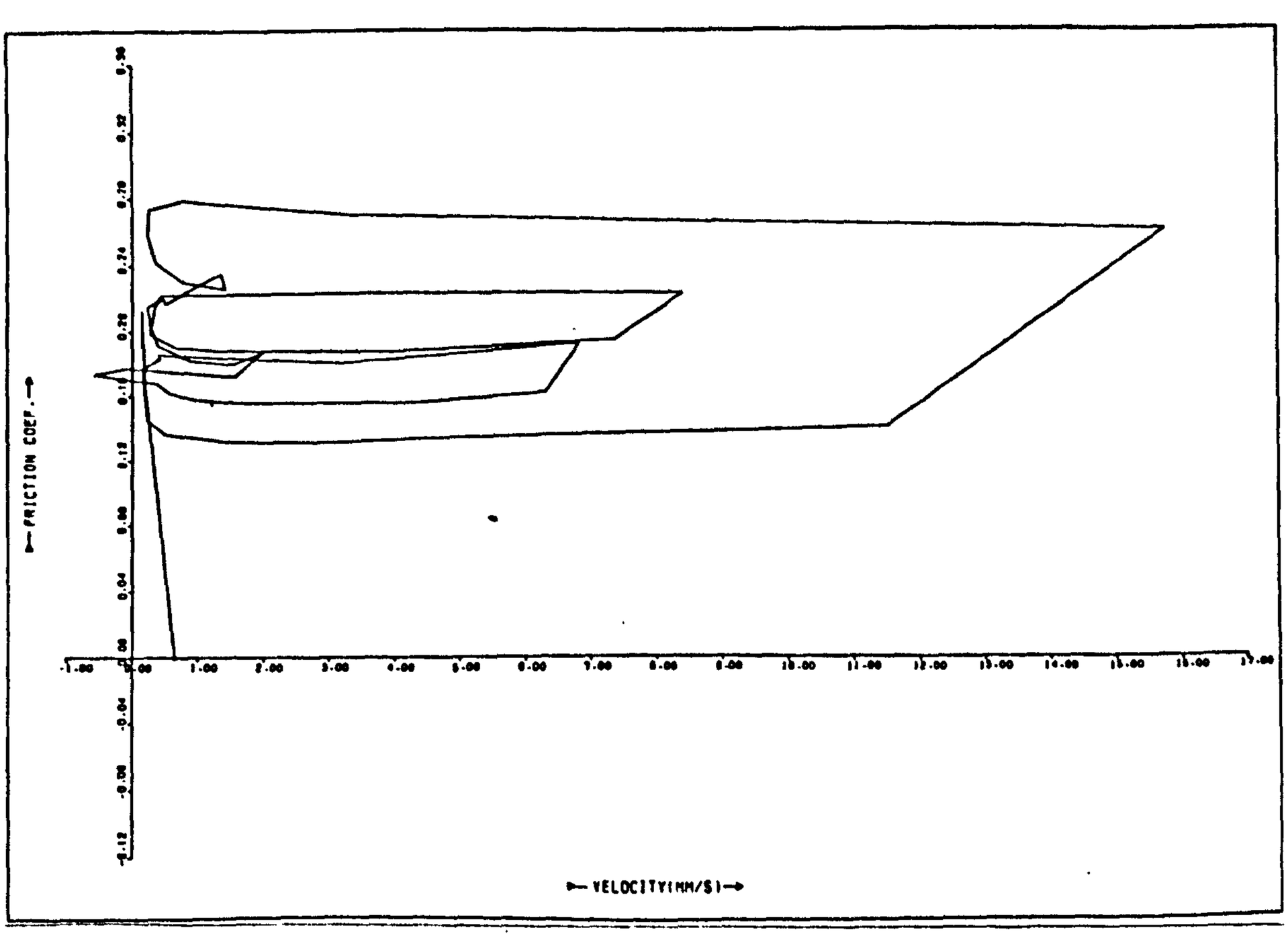

Fig. 4.13b μ vs. $(\dot{x} - V_o)$

V_o = 2.0 mm/s L = 6 Kg k = 17.1 N/mm

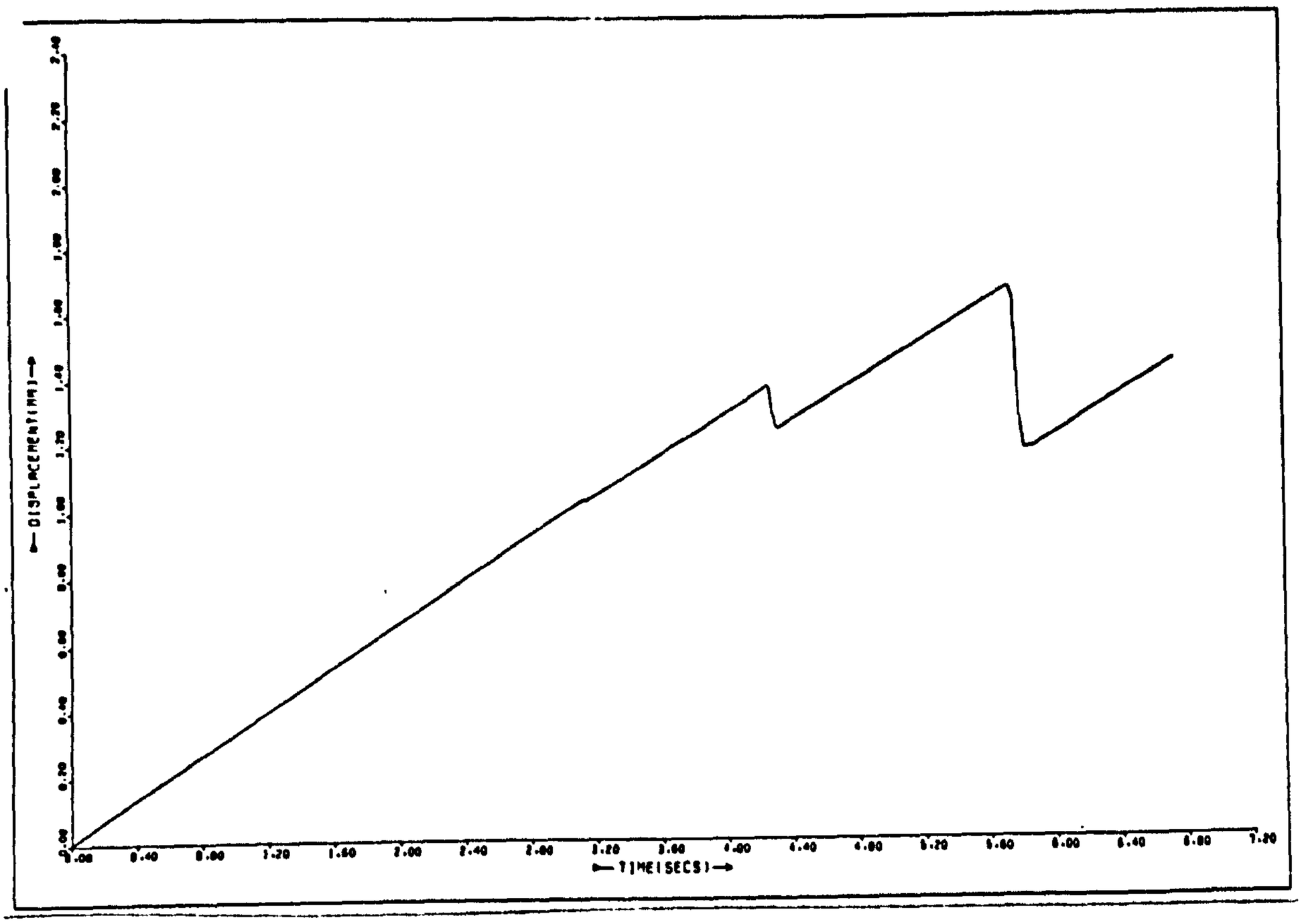

Fig. 4.14a x vs. t

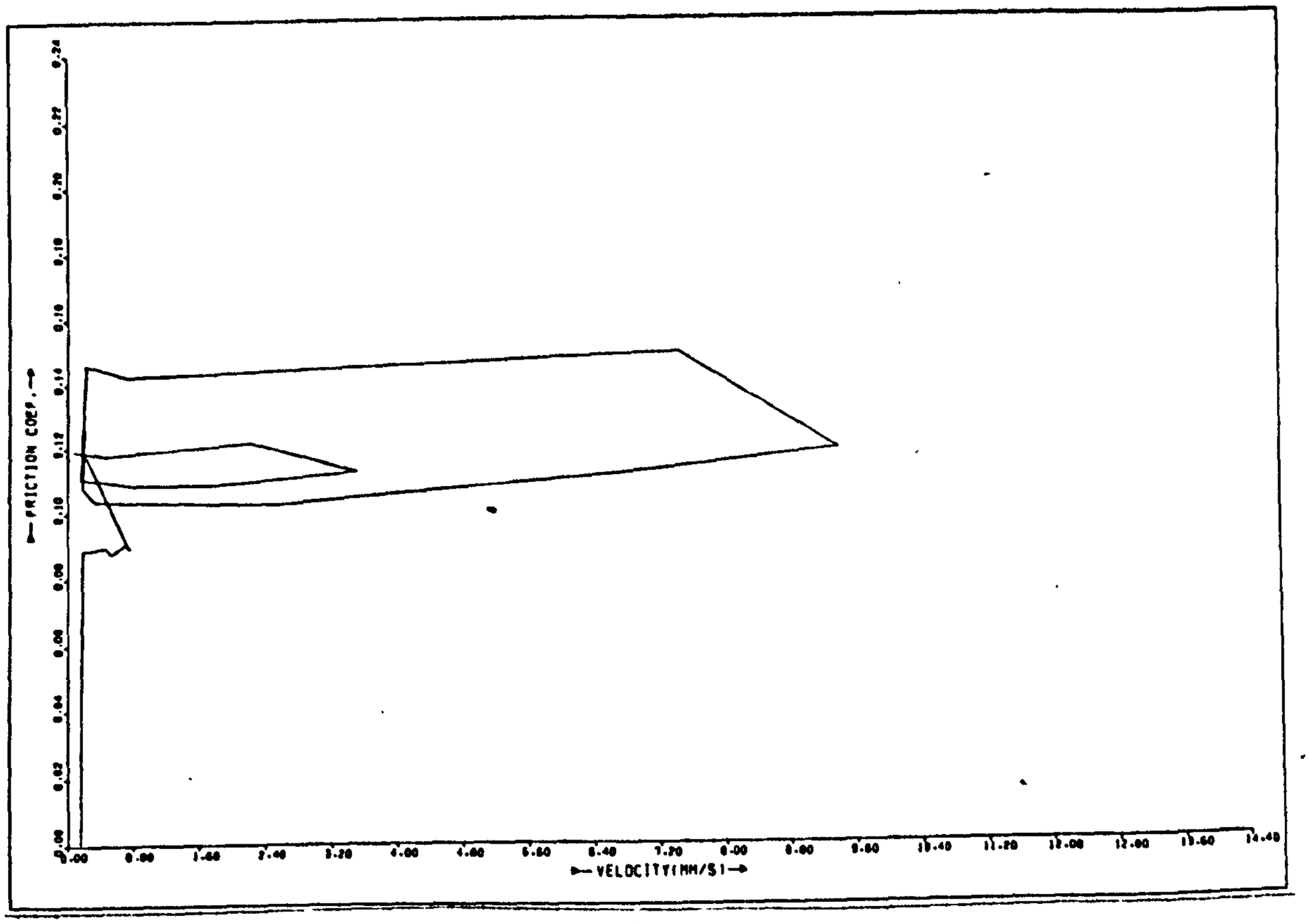

Fig. 4.14b μ vs. $(\dot{x} - V_o)$

V_o = 0.5 mm/s L = 6 Kg k = 9 N/mm

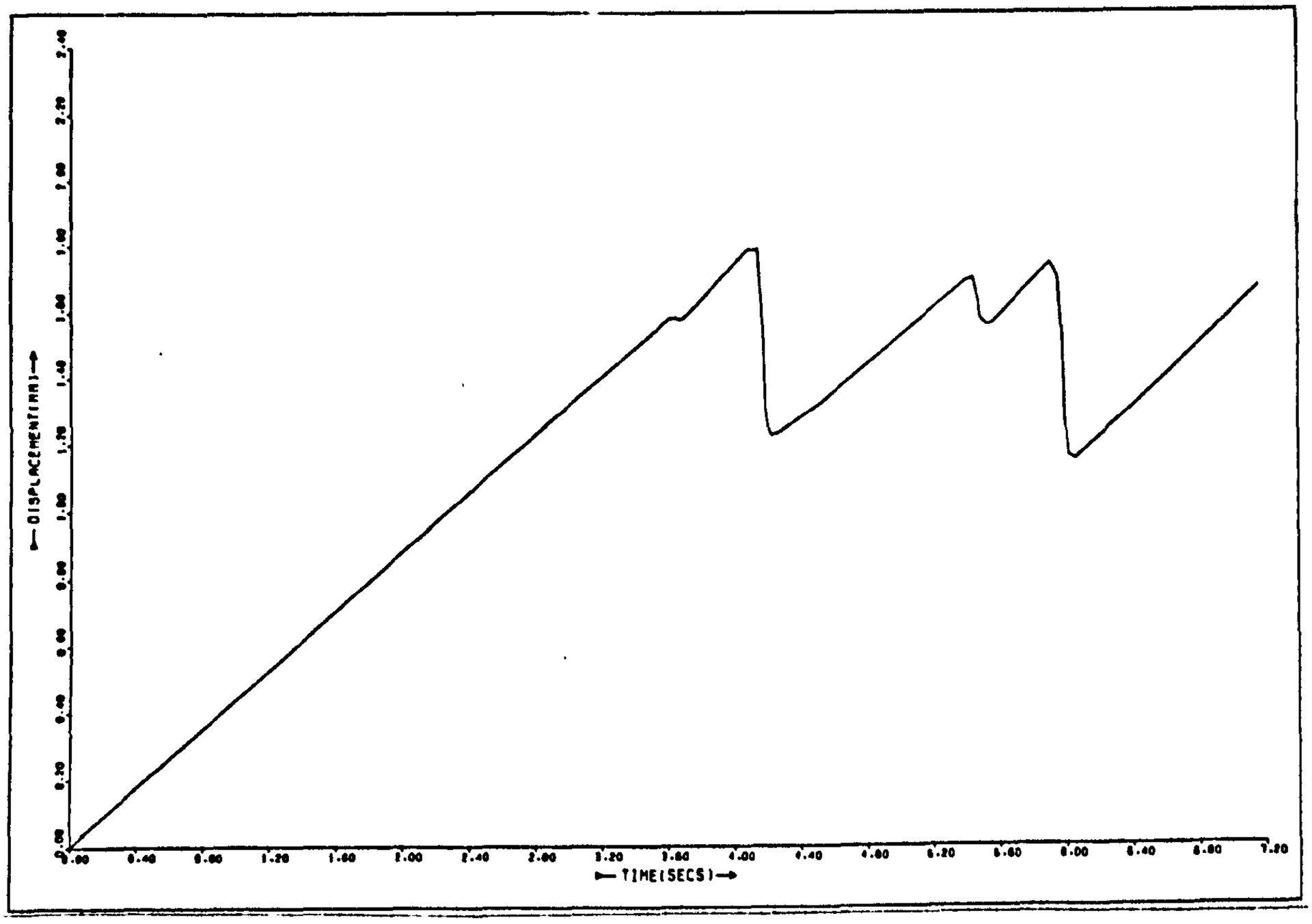

Fig. 4.15a x vs. t

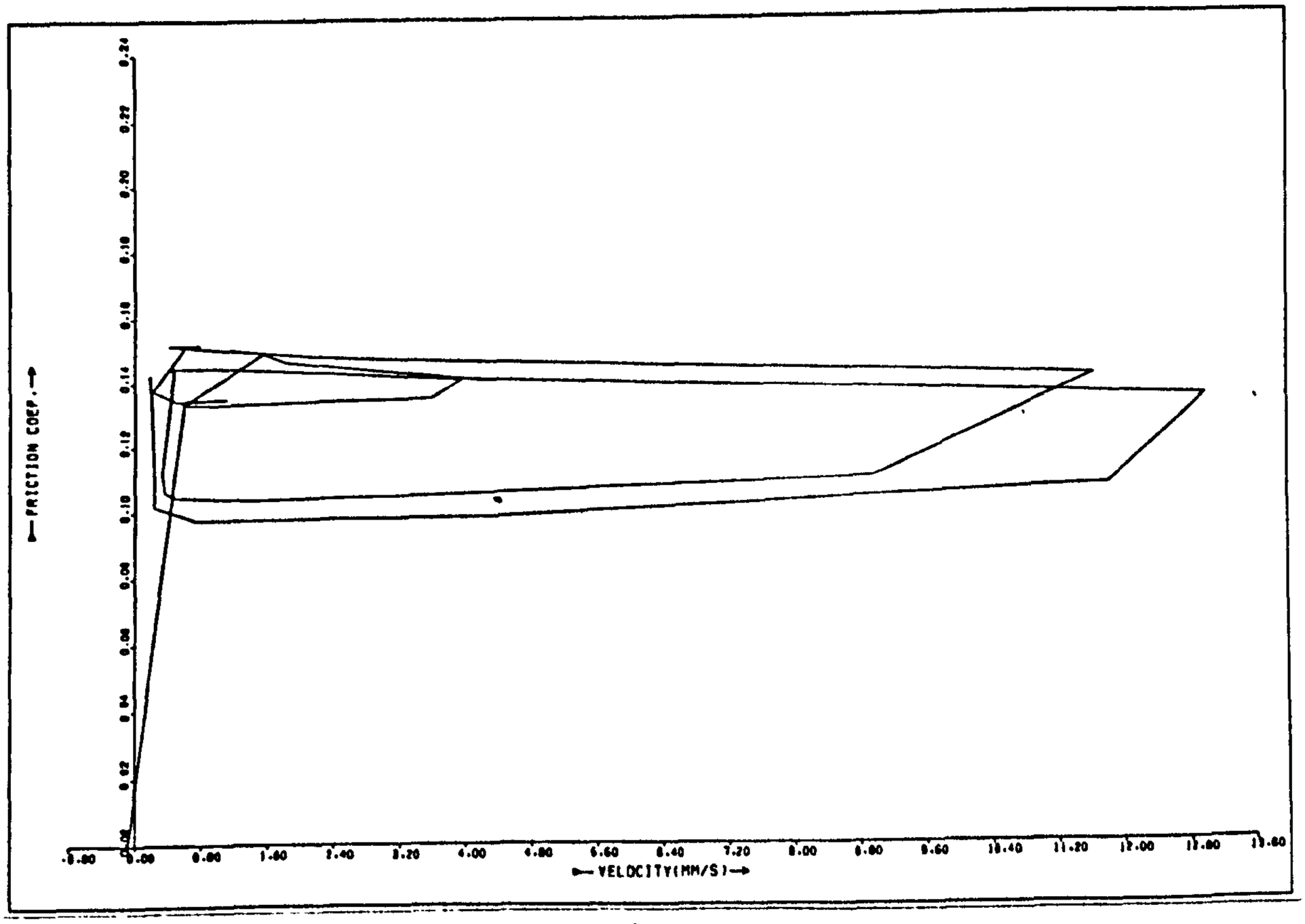

Fig. 4.15b μ vs. $(\dot{x} - V_o)$

V_o = 0.7 mm/s L = 6 Kg k = 9 N/mm

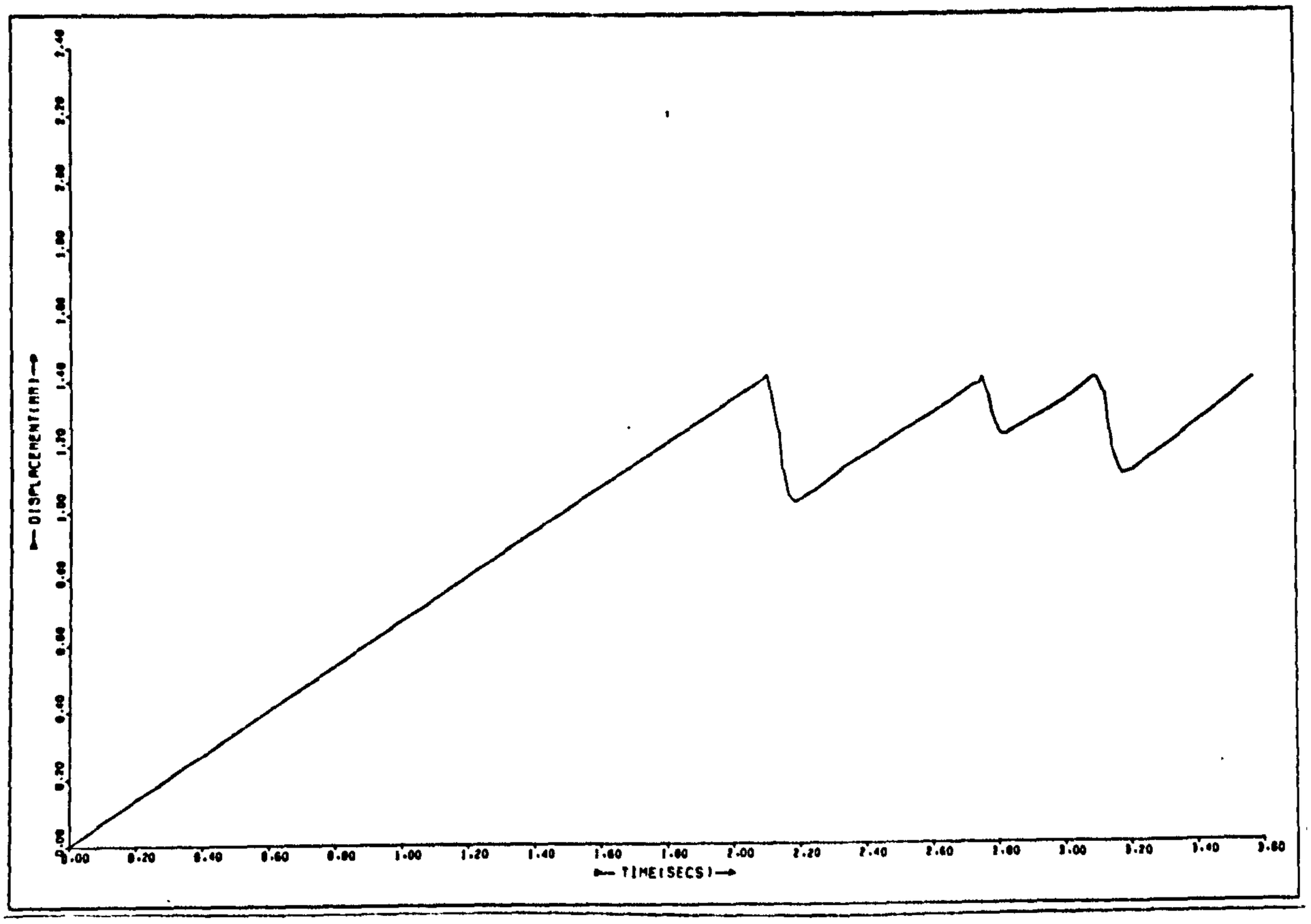

Fig. 4.16a x vs. t

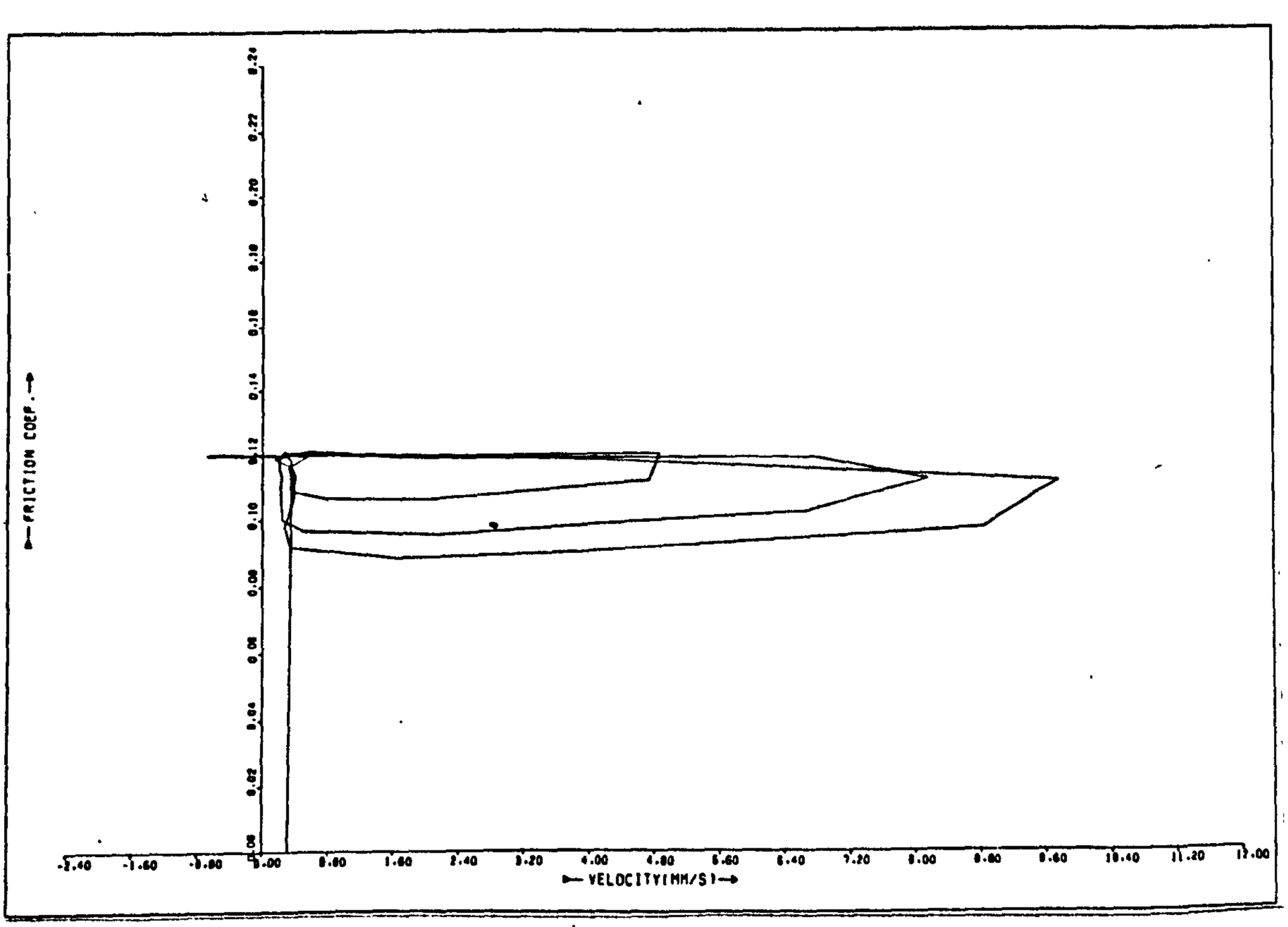

Fig. 4.16b μ vs. $(\dot{x} - V_o)$

V_o = 1.0 mm/s L = 6 Kg k = 9 N/mm

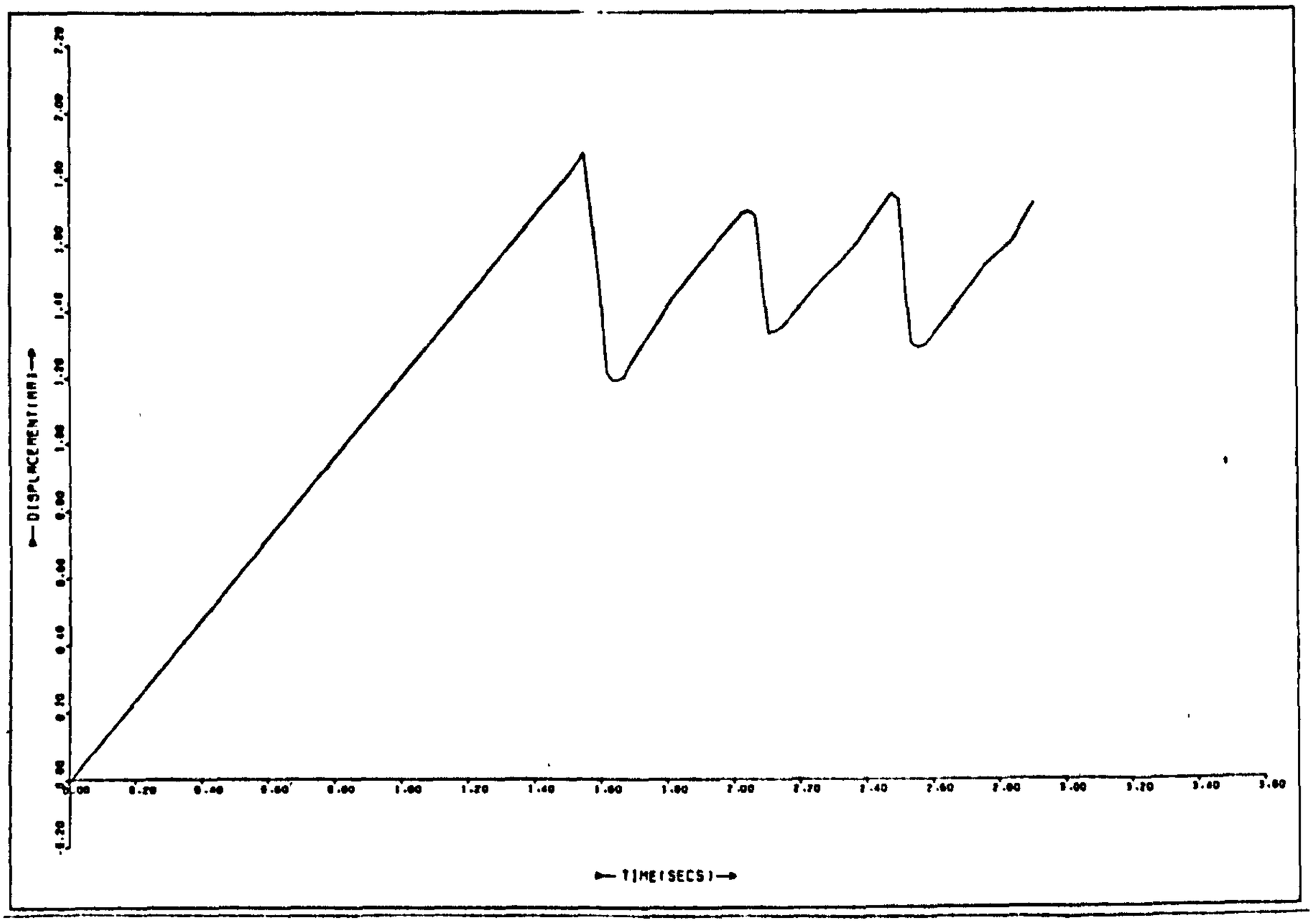

Fig. 4.17a x vs. t

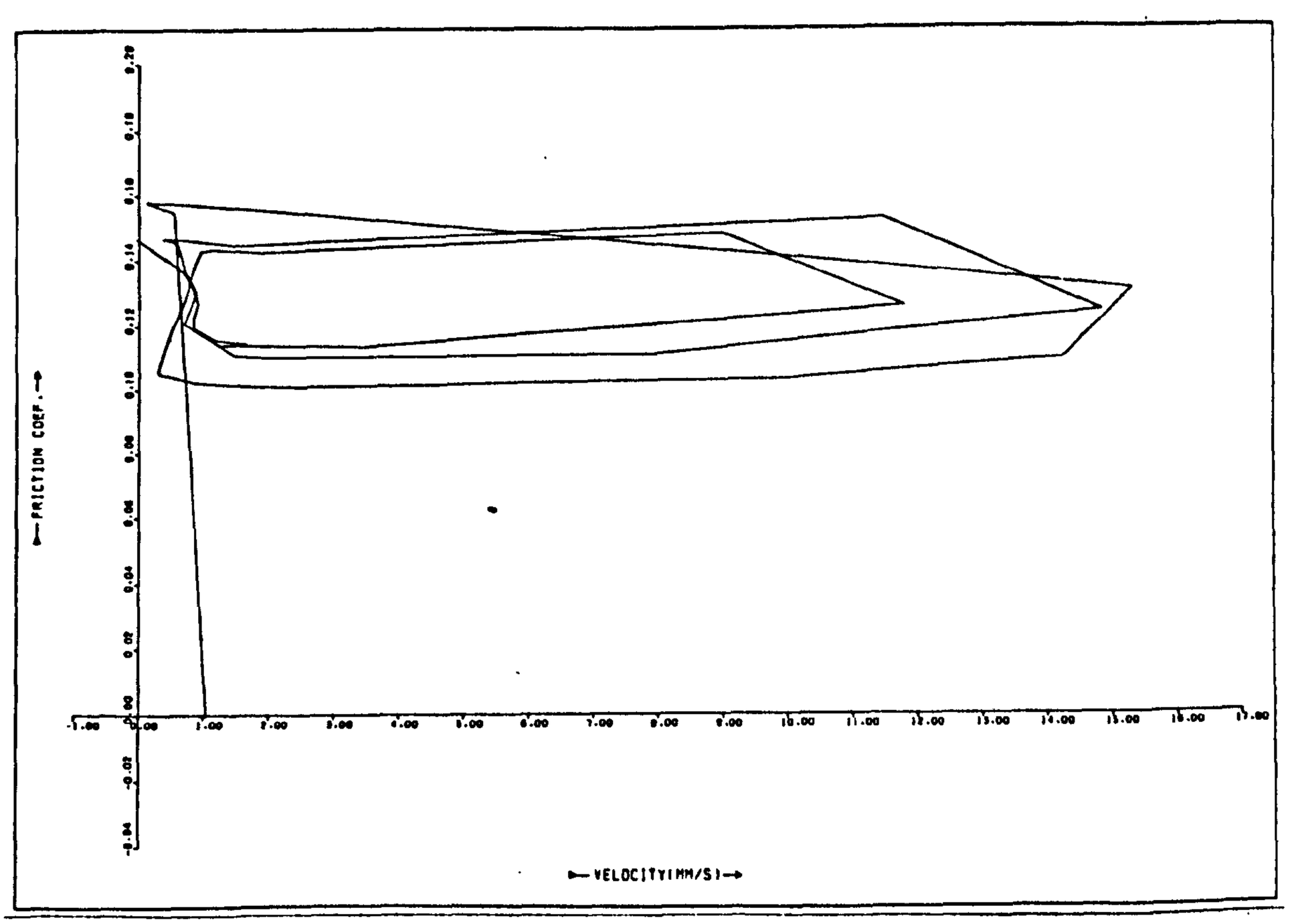

Fig. 4.17b μ vs. $(\dot{x} - V_o)$

V_o = 2.0 mm/s L = 6 Kg k = 9 N/mm

low load (figs. 4.5a, 4.6a, 4.7a and 4.8a), and the displacement curves become progressively more rounded and reduced in amplitude as the velocity, V_o, increases. The friction-velocity curves show the looped characteristic seen before.

Again, the peak friction seems lower in the low-stiffness cases than in the higher ones and, as before, the high-stiffness runs were done immediately after cleaning and the low-stiffness runs were done after ten or twenty minutes' exposure to the atmosphere. To see if this was an effect of the time after cleaning, the order was reversed, low-stiffness runs being done immediately after cleaning and high-stiffness runs being done after exposure to the atmosphere. The results are shown in figs. 4.18 and 4.19 (low stiffness, V_o = 0.7 and 1.0 mms^{-1}) and 4.20 and 4.21 (high stiffness, V_o = 0.7 and 1.0 mms^{-1}).

As can be seen, the overall friction is higher than before, and the stick-slip is less regular. This could be caused by differences in atmospheric humidity or some other uncontrollable variable (Antoniou (9) found that an r.h. of over 70% could stop stick-slip completely in some circumstances). The friction at low stiffnesses is still lower, however, than that at high stiffnesses. At low stiffness the rate of application of shear force, $\dot{F}$, is smaller than at high stiffness (see Green and Brockley (26), and in Chapter One), so this behaviour is consistent with their findings.

If this explanation is correct, it means that the hydrocarbon layer on the surfaces, condensed from the atmosphere, must build up quite fast. As all the experiments were, of necessity, conducted in a laboratory where a great number of oils and lubricant additives were handled, some at elevated temperatures, the ambient air probably contained a large amount of the vapour of such substances.

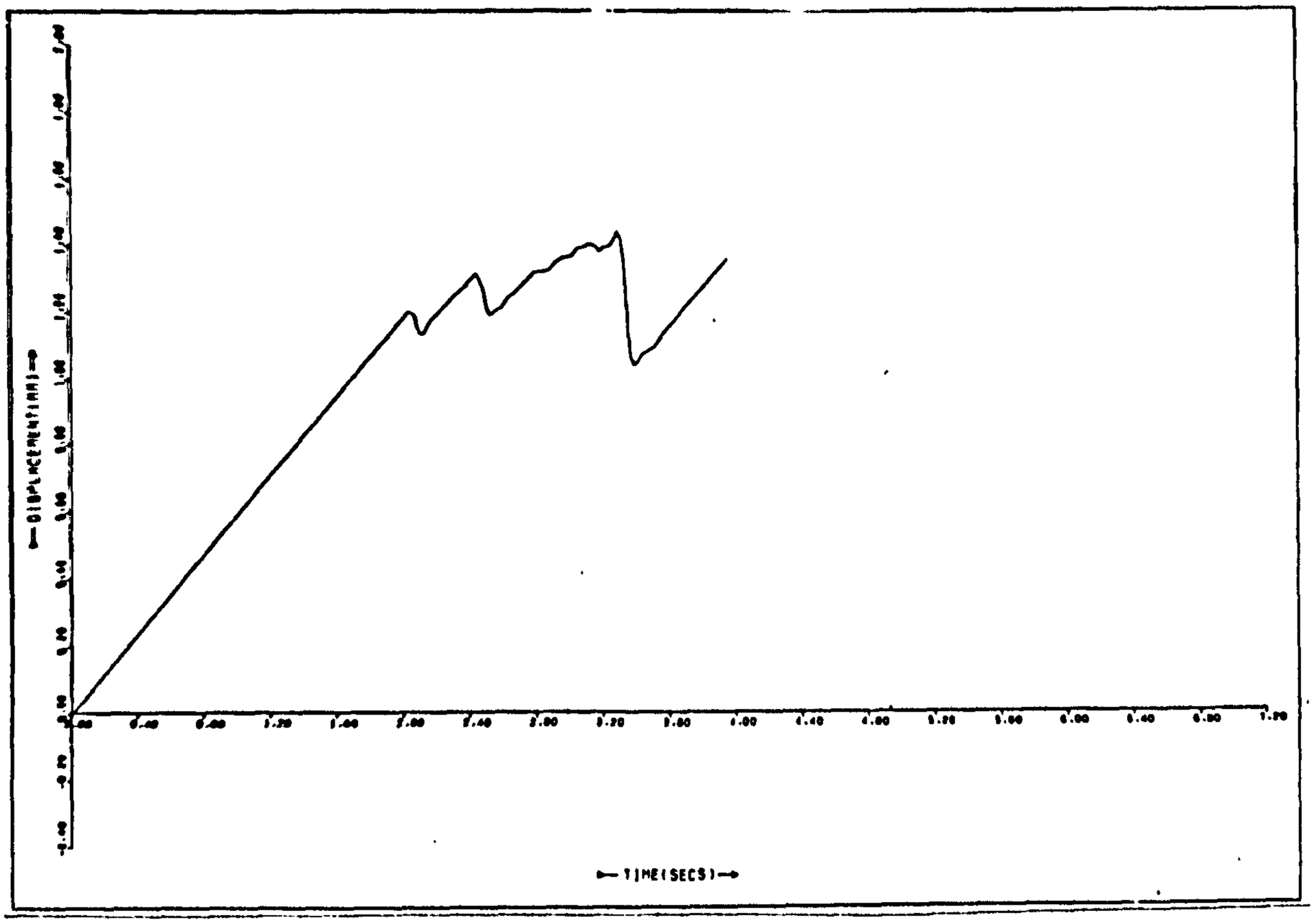

Fig. 4.18a x vs. t

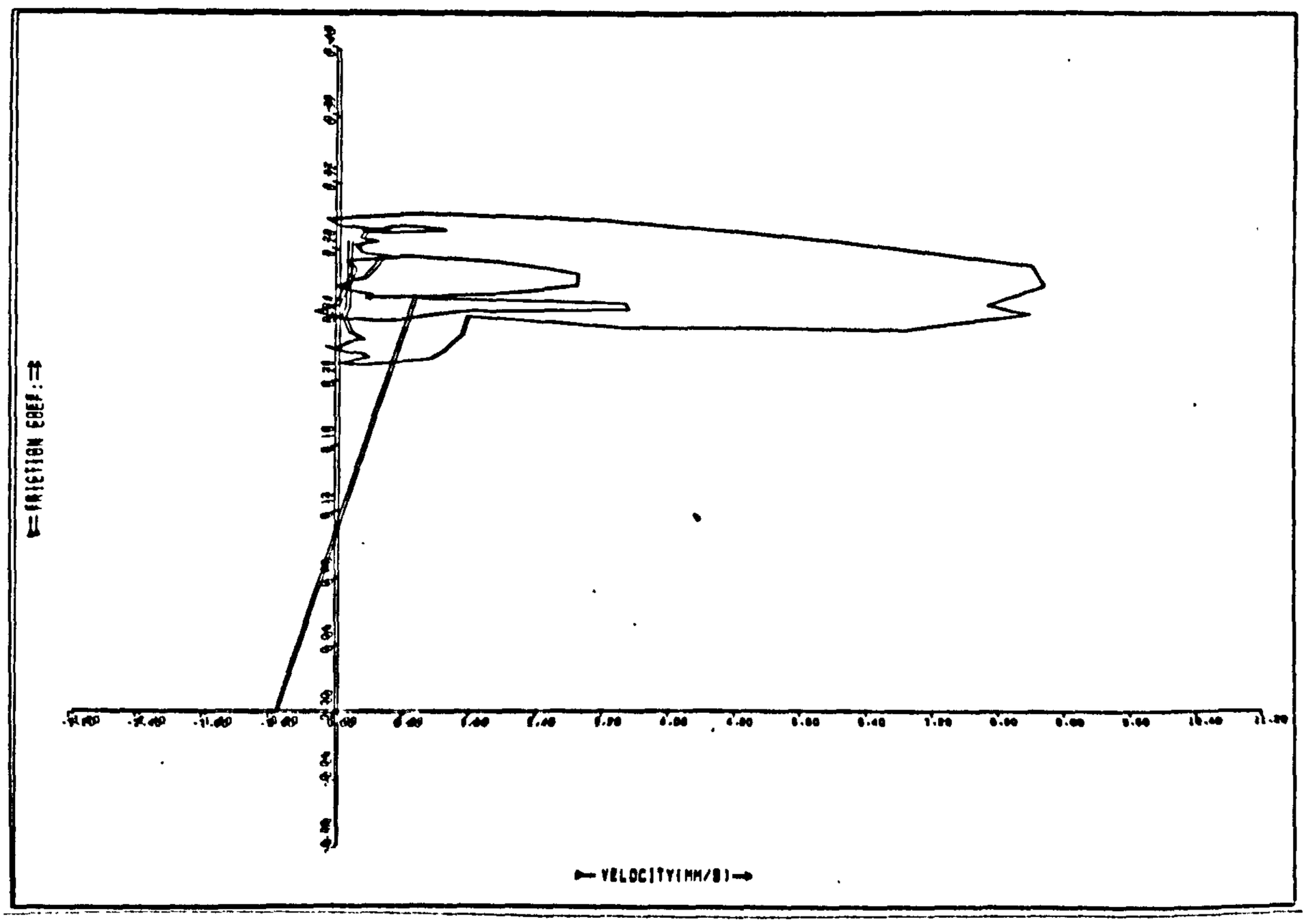

Fig. 4.18b μ vs. $(\dot{x} - V_o)$

V_o = 0.7 mm/s L = 3 Kg k = 9 N/mm

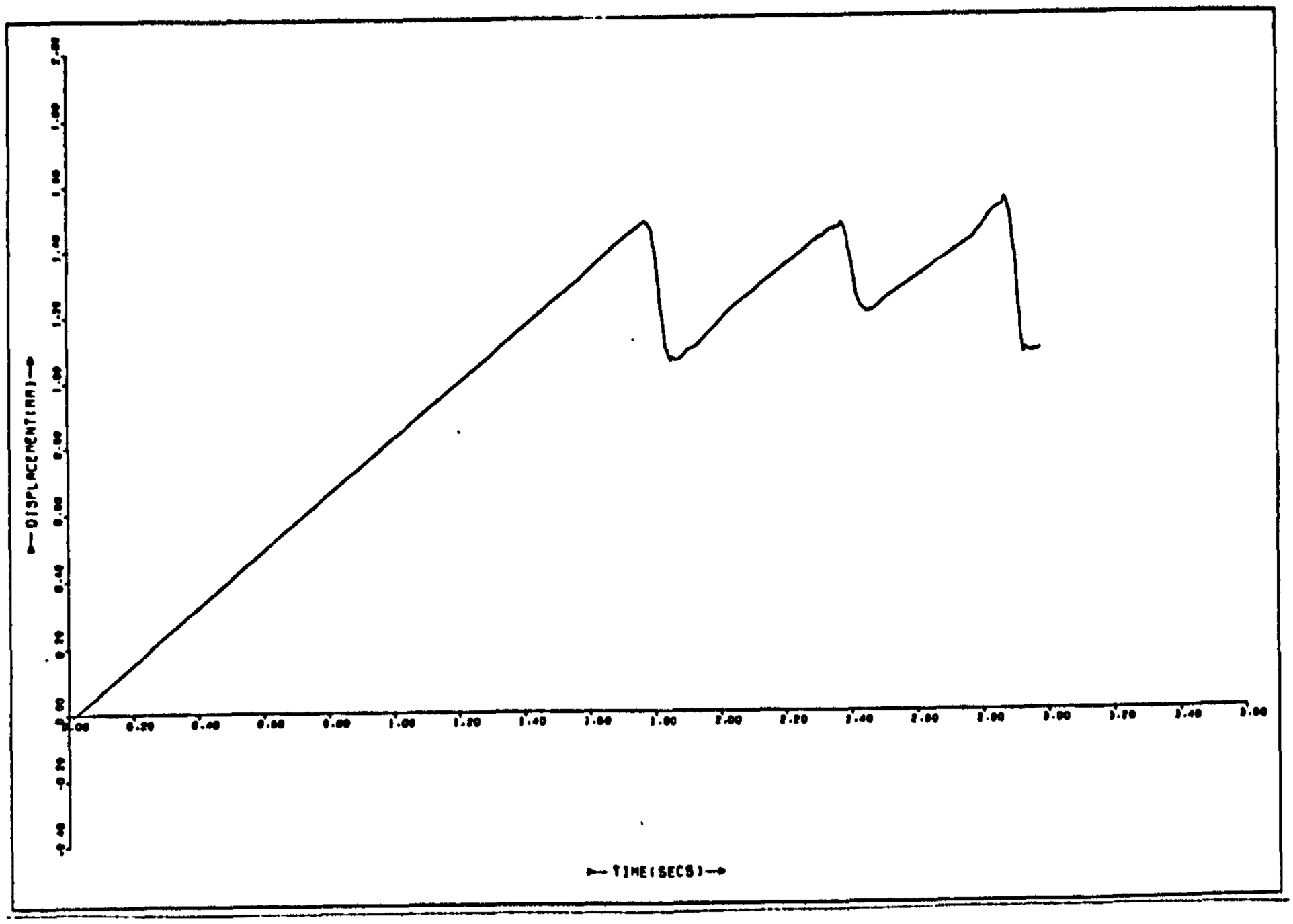

Fig. 4. 19a x vs. t

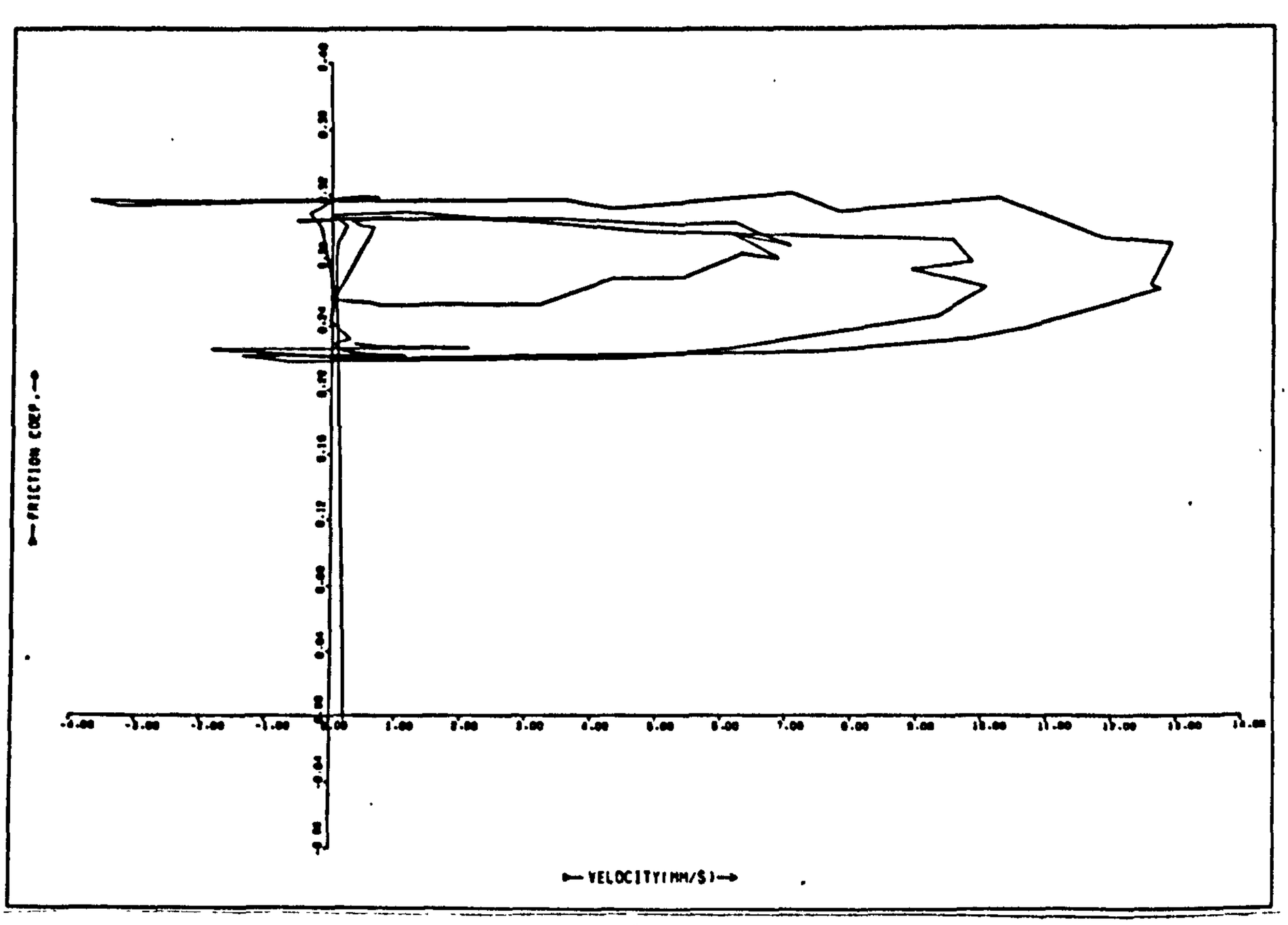

Fig. 4.19b μ vs. $(\dot{x} - V_o)$

V_o = 1.0 mm/s L = 3 Kg k = 9 N/mm

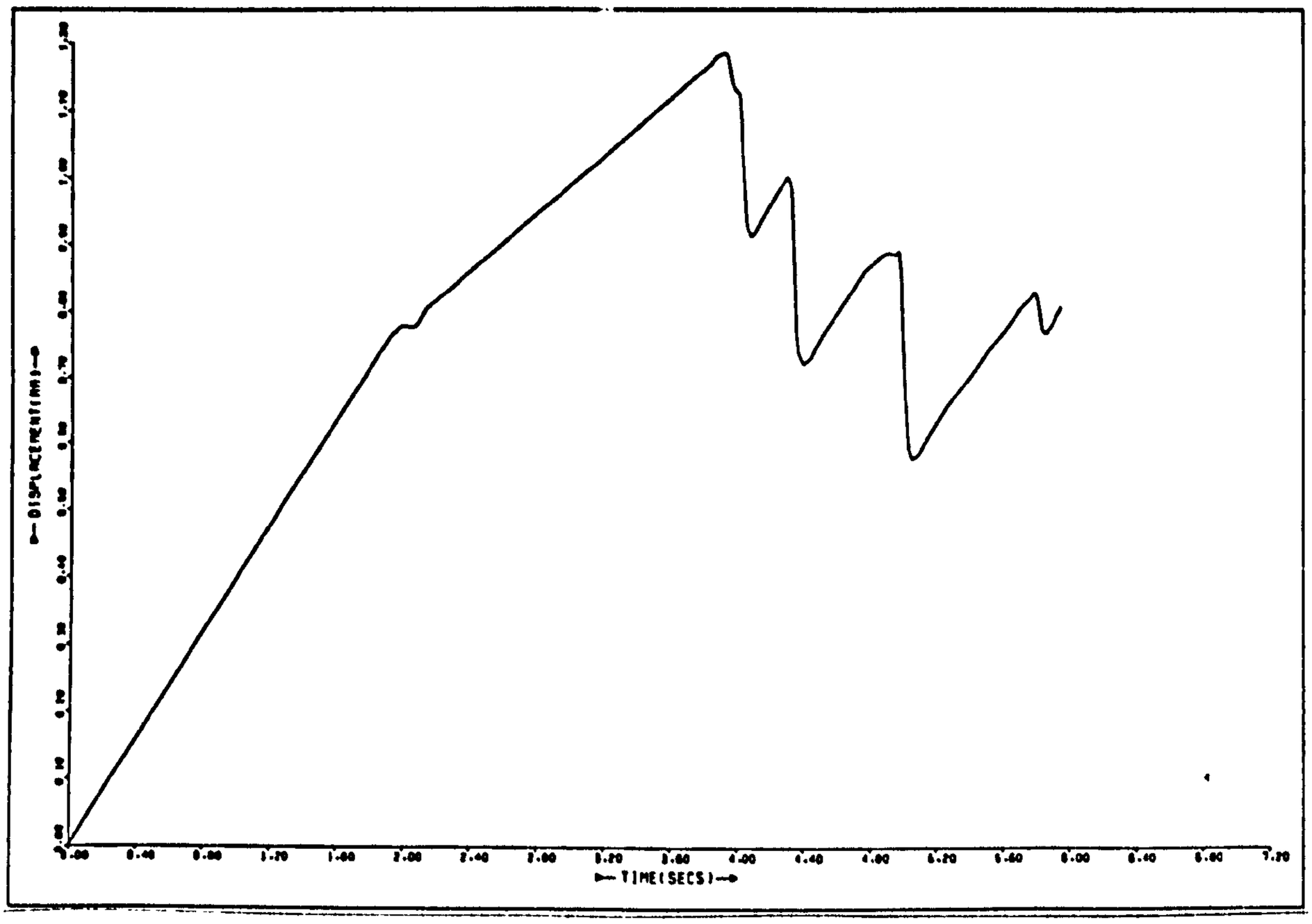

Fig. 4.20a x vs. t

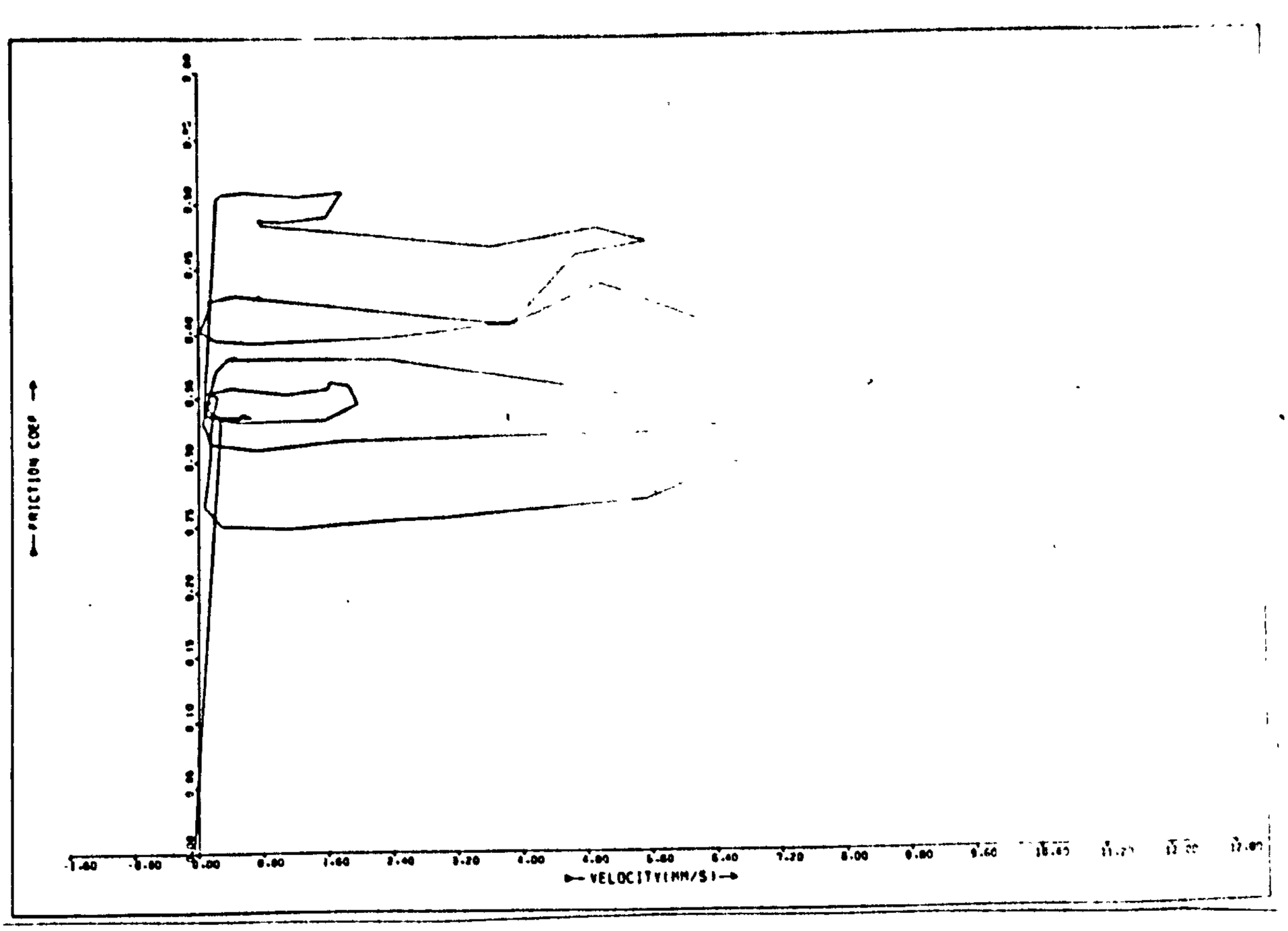

Fig. 4.20b μ vs. $(\dot{x} - V_o)$

V_o = 0.5 mm/s L = 3 Kg k = 17.1 N/mm

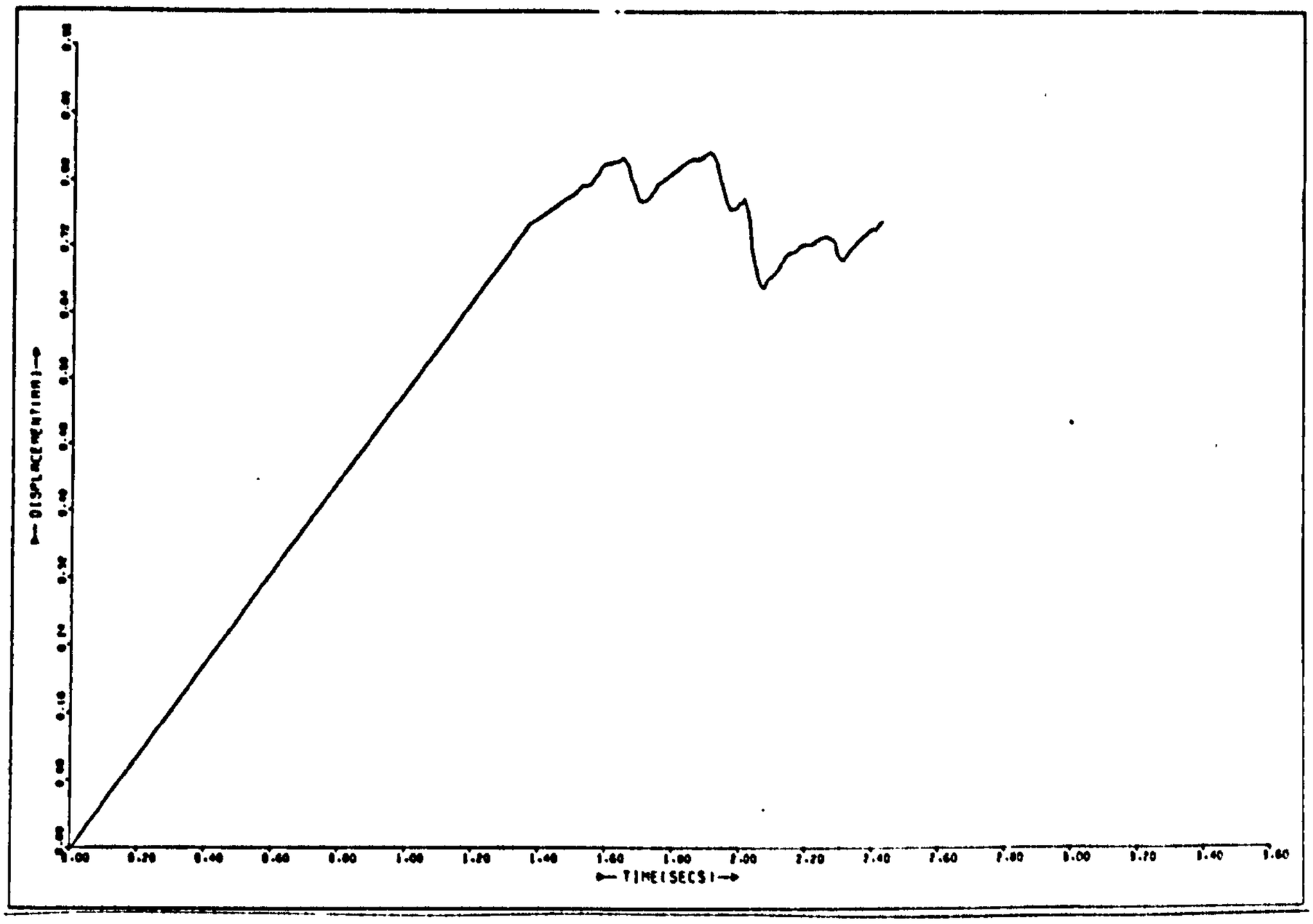

Fig. 4.21a x vs. t

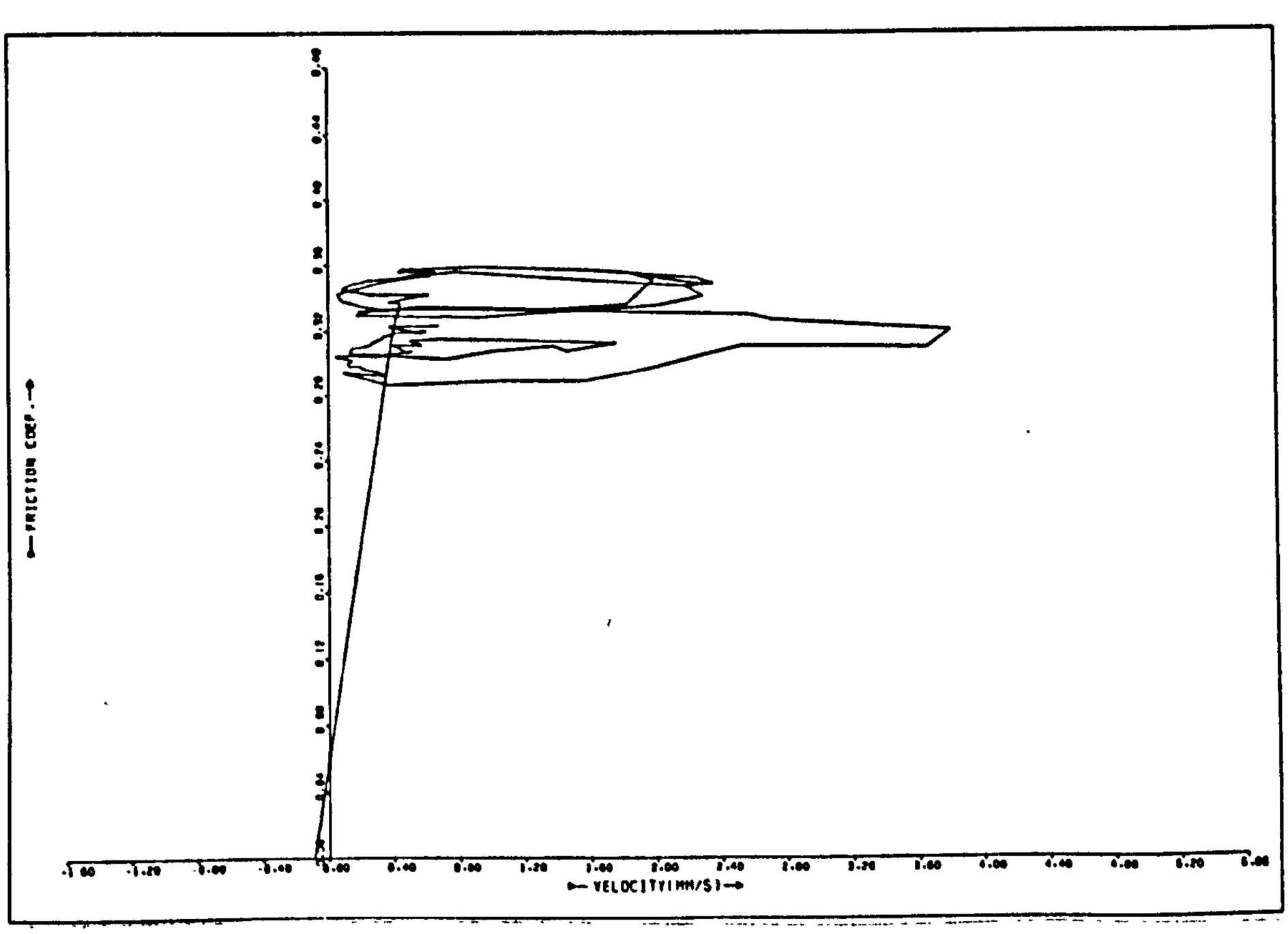

Fig. 4.21b μ vs. $(\dot{x} - V_o)$

V_o = 0.7 mm/s L = 3 Kg k = 17.1 N/mm

4.5 Discussion

The variation of friction with velocity in all the above tests shows the same looped characteristic seen by Brockley and Ko (15) and Sampson et al.

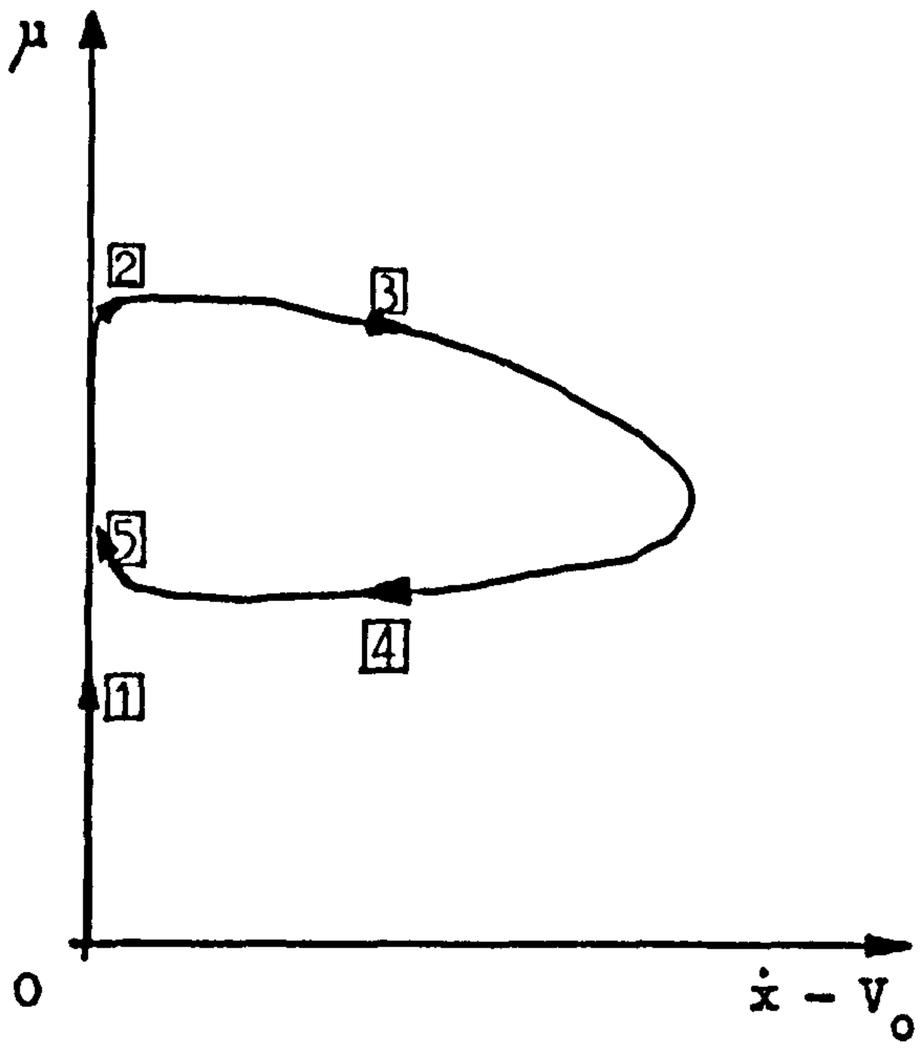

Fig. 4.22 μ vs. $\dot{x} - V_o$

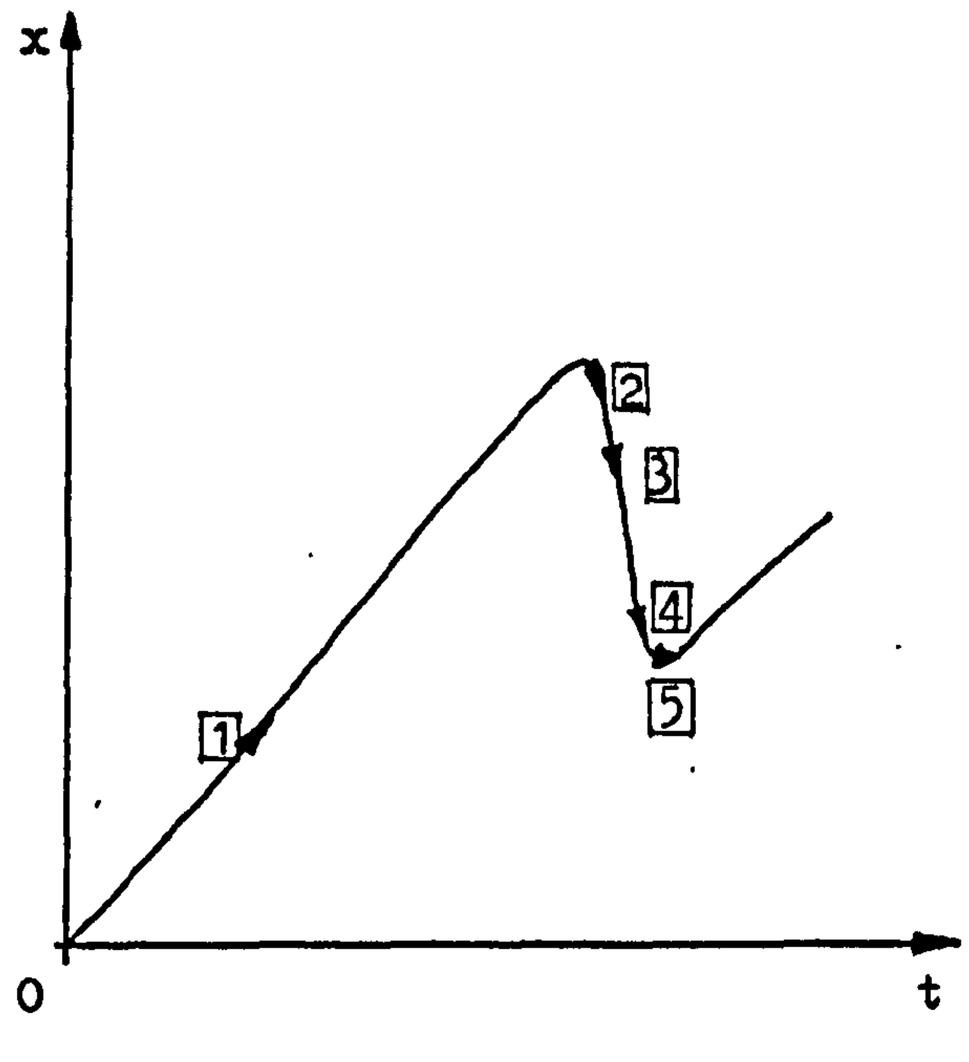

Fig. 4.23 Displacement vs. time

The friction rises to a high, static value (2 in fig. 4.22) and falls gradually as the relative sliding velocity grows (3 , in fig. 4.22). It continues to fall 4 as the relative sliding velocity decreases, instead of retracing the same path that occurred during acceleration. Figure 4.23 shows equivalent points to fig. 4.22 on the displacement vs. time graph.

What is the physical explanation for this behaviour? Consider, first of all, the fall in friction with increasing velocity. Tolstoi (27) has shown that surfaces separate with increasing relative velocity during stick-slip (fig. 1.12), and Elder and Eiss (28) (fig. 1.14) have shown that impeding this movement decreases, and can eliminate, stick-slip.

If two rough surfaces separate by some mechanism, the degree of asperity interaction, the real area of contact, and any viscous forces will all be reduced. Presumably this would cause the fric-

tion coefficient to fall. If the two surfaces were then to move back together as the relative sliding velocity decreased, the friction would retrace itself. This does not occur. If it is assumed that the actual mechanism of friction is the same during deceleration as acceleration (and there is no reason why it should not be so), then, ex hypothesi, the surfaces must retain, or possibly slightly increase, their acceleration acquired separation during deceleration, coming closer again only at very low relative velocities just prior to sticking (point [5] , fig. 4.22). Tolstoi's curves are not sufficiently detailed for this to show.

One possible reason for the surfaces' taking a finite time to fall together is simple inertia. Tolstoi gives an observed maximum separation of 0.5 μm. Accelerating under gravity it would take the surfaces about 3 ms to fall this far. The time of deceleration during the above experiments was always at least ten times this, so an additional factor is required.

One possibility is the time taken for the surfaces to squeeze out the intervening film of air or adsorbed hydrocarbons. A colleague of the author's, N. W. James, has written a computer programme to predict the behaviour of an elastic ball falling a small distance against a plate through a film of oil (56). This programme was run with air as the intervening medium and with two flats instead of a ball and a flat. The viscosity of air is so slight (1.78×10^{-5} Nsm^{-2}) that the equations were ill-conditioned and could not be propagated by using other than a very small time-step. This meant that it was not possible to solve the problem for more than the first few microseconds of fall without using an excessive amount of computer time. All problems of this nature produce a curve of separation, h, against time of the form shown in fig. 4.24.

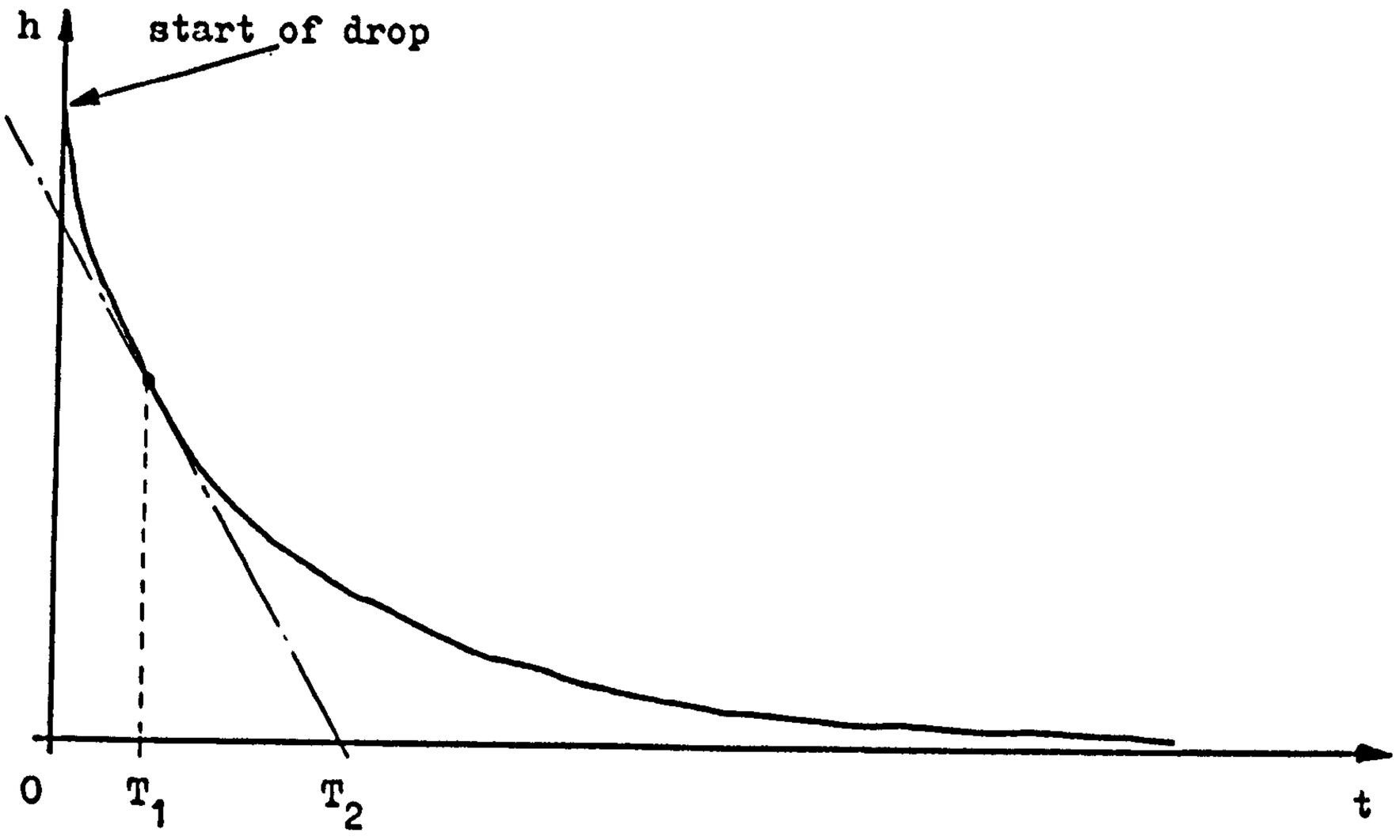

Fig. 4.24 The decay of a squeeze film

It was only possible to derive this curve up to T_1 (the dotted line). Extrapolating the gradient at this point (chain line) gives a very pessimistic figure of 20 ms for T_2, the time to actual contact. It must be realised that this does not allow for any effect of roughness, both on the diffusion of air out of the contact area (57) (58) and in supporting the falling top slider by increasing asperity contact. All these shortcomings mean that the figure of 20 ms must be regarded as a very approximate and conservative minimum. Despite this, it is of the same order of magnitude as the time taken for the surfaces to decelerate.

The presence of air and adsorbed hydrocarbon films (26)(59) also introduces another possible mechanism for the surfaces' separating, in addition to simple asperity interaction, as mentioned in Chapter One (fig. 1.13). This is the formation of microscopic, hydrodynamic films between gradually sloping asperities sliding towards one another (60) (fig. 4.25) that would tend to force the surfaces apart.

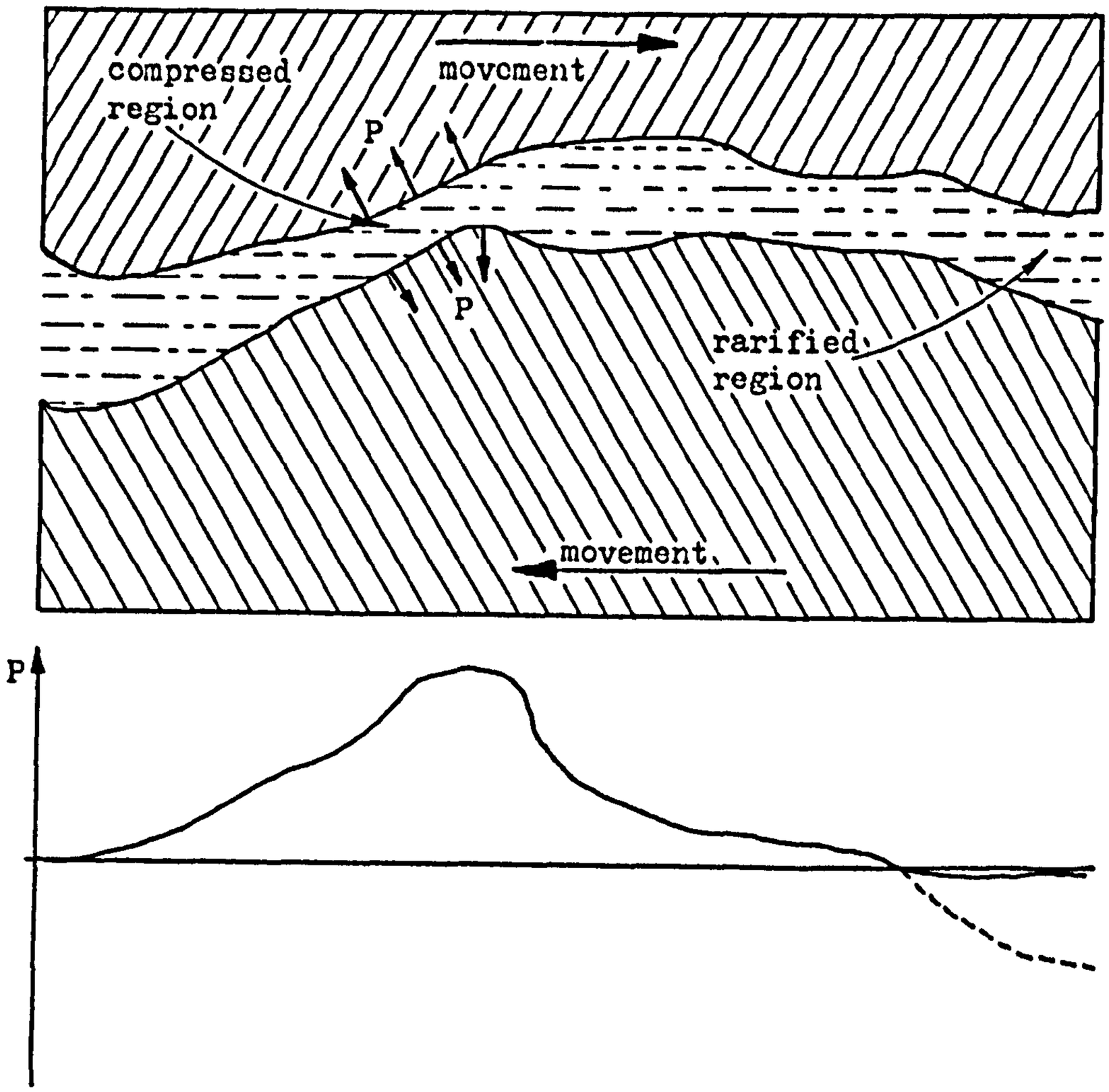

Fig. 4.25 Possible hydrodynamic film formation and pressure distribution between asperities

As in conventional hydrodynamic lubrication, the film would not be able to sustain a large negative pressure (dotted curve) in the region where the asperities were separating.

This model is also consistent with Brockley and Ko (17). If the sliding surfaces were always in relative motion during quasi-harmonic stick-slip, they would possibly always be separated, to a greater or lesser extent, and the μ ($\dot{x} - V_0$) curve would not show as much hysteresis (see fig. 1.8).

One way to test this theory (59) would be to conduct stick-slip experiments in a hermetically sealed container and to compare the results obtained when the container was filled with inert gas (to eliminate chemical effects) and when it was evacuated, though

even an inert gas might affect the spontaneous formation of contact welds between the clean surfaces. Facilities for conducting this type of experiment were not available.

Another possible explanation for the shope of the friction-velocity curve has been proposed by Brockley (59) (26). If an adsorbed film had thixotropic viscosity characteristics, the shear strength would be high at the end of the stick period when the film had been undisturbed for a time, and would fall with increasing relative velocity as the film was disturbed during slip. During deceleration the film would still be disturbed and so continue to exhibit a low viscosity, giving rise to the observed hysteresis. Once stuck again, the film would recover its high viscosity during the time of stick.

Brockley's theory and that of the author are not mutually exclusive. Both mechanisms could be acting together.

If the separated surfaces are considered to be supported by a squeeze film which prevents their coming together immediately the hydrodynamic and asperity separating forces are reduced, this squeeze film could be of adsorbed viscous material as well as just air.

It was decided to write a computer model of sliding rough surfaces to see what happened if they separated with increasing relative velocity. The results are presented in the next chapter.

CHAPTER FIVE

A COMPUTER MODEL OF SLIDING FRICTION †

5.1 Preliminary requirements

In order to investigate, by computer model, what happens when rough surfaces are rubbed together, it is first necessary to do two things:-

1) Produce maps of the surfaces
2) Determine what happens when they are forced together prior to sliding

As mentioned in Chapter One, Sayles and Thomas (45), (46) and (47) have done the former and have used the model of Pullen and Williamson (36) on the maps they produced to do the latter. It was decided to duplicate their work in order to attempt to extend it to sliding.

5.2 Surface mapping

R. A. Hill of the Imperial College Lubrication Laboratory has, with the assistance of the author, devised and built a surface mapping system based on a Talysurf machine and a Digital PDP8 mini-computer. A description of this system is given in Appendix Three.

The surface to be mapped was clamped securely to a microscope stage mounted under the Talysurf measuring head. The voltage produced by the Talysurf was fed to an A.D.C. connected to one of the PDP8's input ports. An accurate quartz crystal timer was

† See the Addendum, p159

also connected to the PDP8. In order to produce a map, a profile was taken on the Talysurf in the usual manner. The computer sampled the voltage produced, via the A.D.C., at regular intervals decided by the timer. It stored the results in its memory. When a complete profile was thus recorded, it was punched on paper tape by the computer. The microscope stage was then moved a small distance by means of its micrometer screw and another, parallel, profile was taken in the same manner. In this way a complete matrix of height values on a rectangular grid was built up of the area of the surface of interest.

The most time-consuming part of the whole process was the punching of the very large amount of information involved onto paper tape. It is recommended that any future mapping of this nature be stored on magnetic tape or disc. This would be much faster and considerably less prone to parity errors, punch misalignments, tears and similar problems always associated with paper tape.

The map used for this work took two days to prepare. It was taken from one of the flat, lower specimens of EN58b used for the experiments discussed in Chapter Four. The map was a 0.5 mm by 3 mm rectangle described by a 50 by 300 matrix of height values on a square grid with an element side length (Δx, Δy on fig. 5.1) of 10 μm. This grid was about two or three times bigger than the smallest possible resolution of the Talysurf machine, and was rather finer than that used by Sayles and Thomas.

The frontispiece of this thesis is a computer drawn contour map of this data. As can be clearly seen, the direction of grinding was parallel to the longer side. Subsidiary scratches can also be seen running at an angle of about 10^{o} to this side. The surface was abraded with 400-grade emery paper after grinding, this abrasion being done with a circular motion. It is possible that these

angled scratches are, in fact, arcs of large circles produced by the final pass of the emery paper.

The scratch running from about 5 mm up from the bottom, left-hand corner to about 75 mm from the top, right-hand corner is particularly marked and serves as a useful check on the relocation of the Talysurf at the beginning of each pass. The passes were parallel to the longer side of the map.

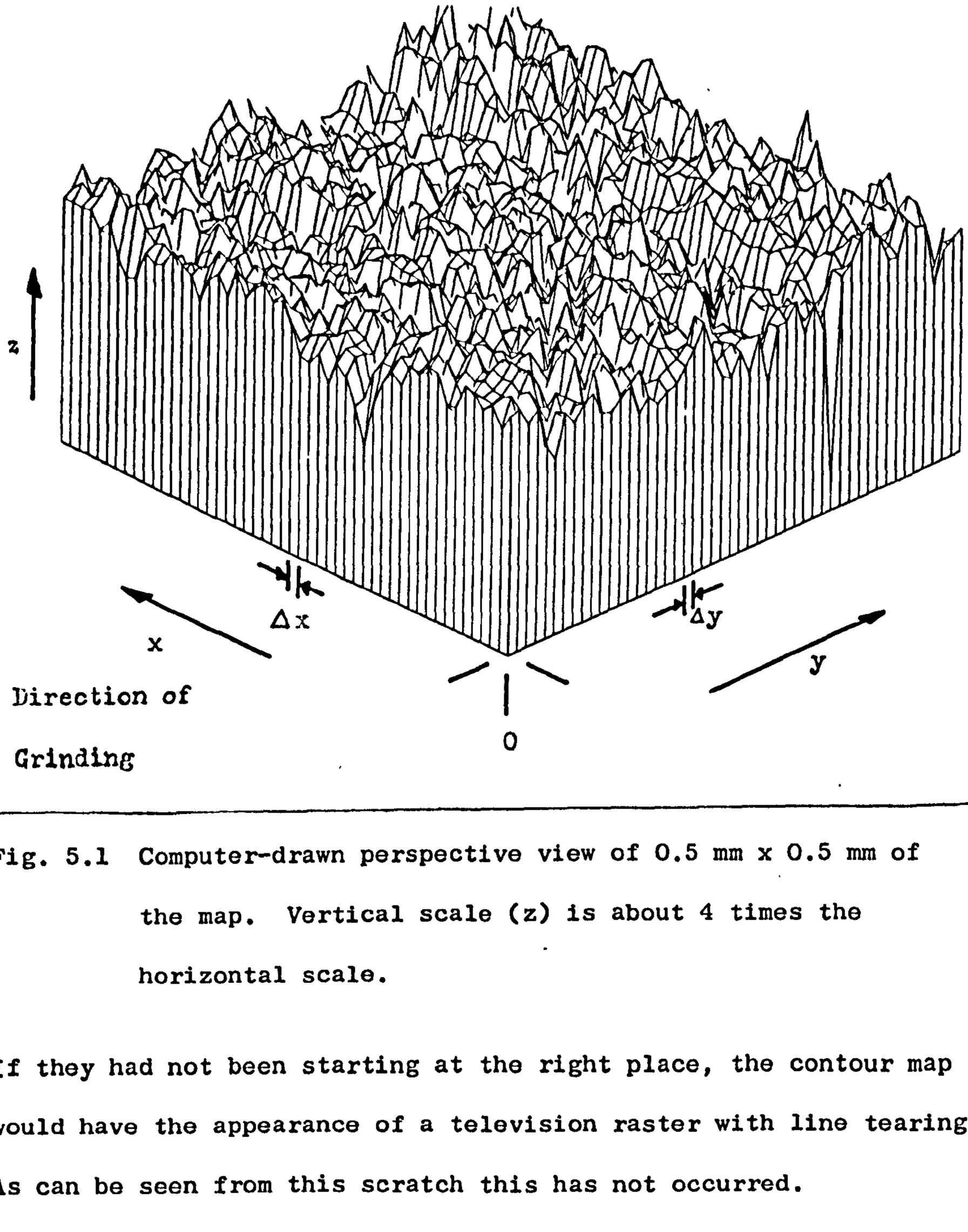

Fig. 5.1 Computer-drawn perspective view of 0.5 mm x 0.5 mm of the map. Vertical scale (z) is about 4 times the horizontal scale.

If they had not been starting at the right place, the contour map would have the appearance of a television raster with line tearing. As can be seen from this scratch this has not occurred.

Figure 5.1 is a perspective view of the left-hand 0.5 mm of the map.

5.3 Modelling the squeezing together of two surface maps

It was decided to make the simplifying assumption that all asperity deformations under load are plastic. This is realistic for newly abraded surfaces that have not run in (see, for example, Archard (34) and Pullen and Williamson (36)).

Pullen's work showed that contacting asperities were truncated at their points of contact and that the material displaced was evenly distributed throughout the rest of the solid, effectively raising the surface slightly (see fig. 1.19). For small, real areas of contact, the volume of material displaced is so small (see fig. 1.24) that this second finding may be ignored.

The Vicker's hardness of the EN58b specimen was measured and found to be 208 Nmm^{-2}†. The surface itself would, presumably, have been work-hardened by the grinding and abrading process and would therefore have a higher hardness. A figure of 280 Nmm^{-2} was estimated as an initial assumption (61). The lower load used for the experiments described in Chapter Four was 3 kg, i.e. about 30 N. If this is to be supported by plastically deformed asperities of yield strength 280 Nmm^{-2}, the real area of contact will have to be about 0.107 mm^2. This compares with an apparent area of contact of 1 mm^2 (the area of the frustum of the cone used in experiments, see fig. 2.11).

Owing to the tediousness of its production, the surface map was only 0.5 mm wide. To increase this to 1 mm, the computer was programmed to mirror it about a longer edge. It was thought that 15,000 height values constituted a big enough statistical sample for this duplication not to matter unduly.

The first millimeter of the resulting large map was inverted in the computer (fig. 5.2).

† This should be Kgf mm^{-2}. See p159

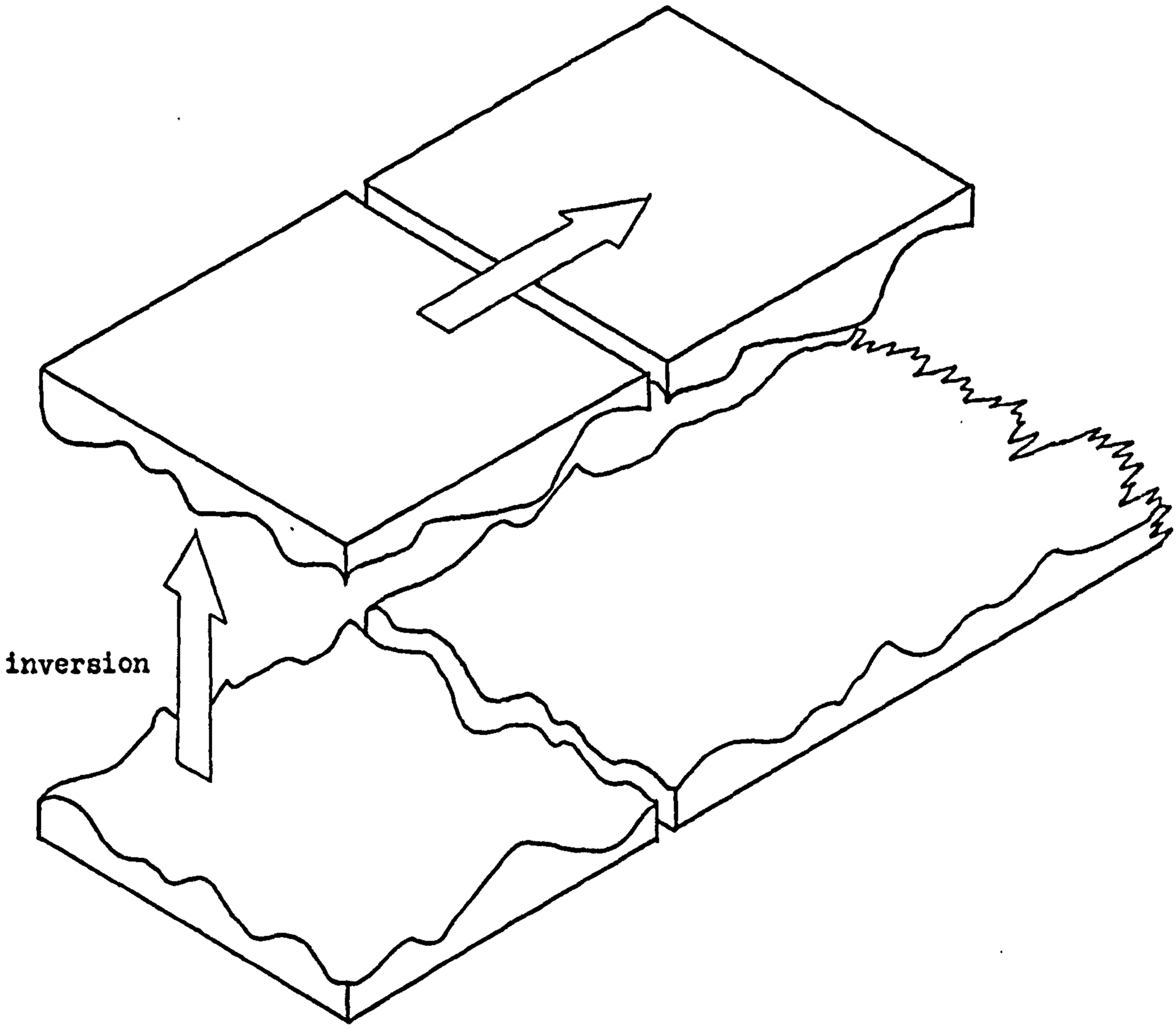

Fig. 5.2 Inversion of part of the map

z_1 is the depth value of the lowest peak of the inverted surfaces (fig. 5.3). The value z_1 was subtracted from the inverted surface to make all its height values positive. The height of the highest peak on the lower surface, z_2, was subtracted from all the highest values of the lower surface to make them all negative. Thus, none of the surface asperities could possibly be overlapping. Consequently, the computer set the value of the real area of contact,A, to zero.

The computer programme then contained a loop that subtracted a small value, Δz (set, for convenience, at $(z_1 - z_2)/1000$), from the top surface and scanned the arrays of the two surfaces looking for z values on the top surface that were lower than z values on the bottom surface. Whenever this condition occurred, the surfaces

were overlapping and A was incremented by an amount $\Delta x.\Delta y$, where Δx and Δy were the grid lengths in the x and y directions. Both were equal to 10 μm, so, at each overlap, A was incremented by 100 μm^2. When the arrays had been scanned, the value of A was multiplied by the plastic modulus of the material, p_c (set at 280 Nmm^{-2}) and the result was compared with the load under which the system was imagined to be operating, i.e. 30 N.

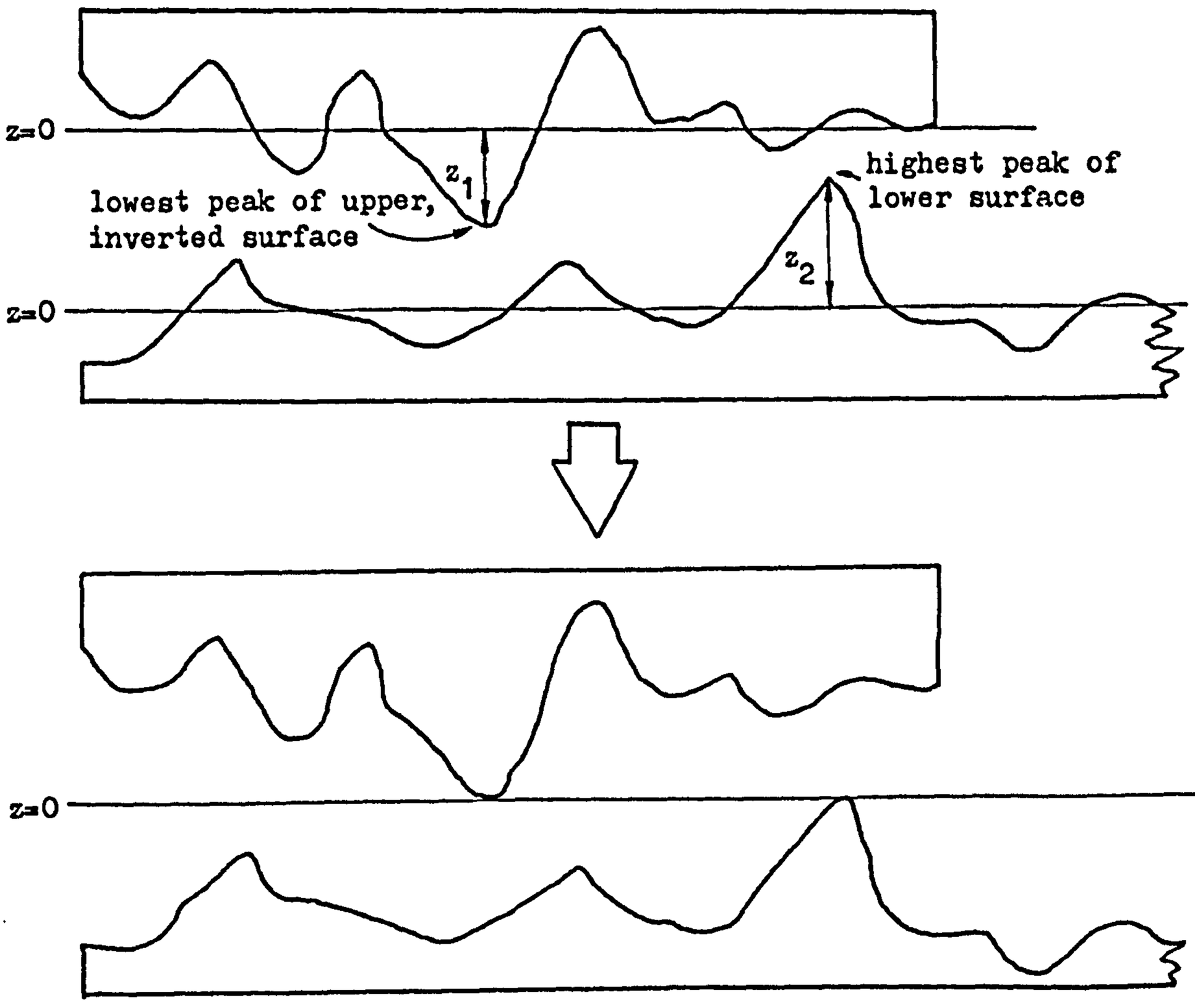

Fig. 5.3 Subtraction of z_1 from the upper surface and z_2 from the lower surface

The computer then plotted, on microfilm, a series of small squares at the appropriate values of x and y to represent the microcontact. The result of one of these plots is shown in fig. 5.4. If $A.p_c$ was less than the load, L, Δz was again subtracted

from the upper surface and the process was repeated until the point

$$A.p_c = L \quad \ldots\ldots\ldots\ldots (23)$$

was reached.

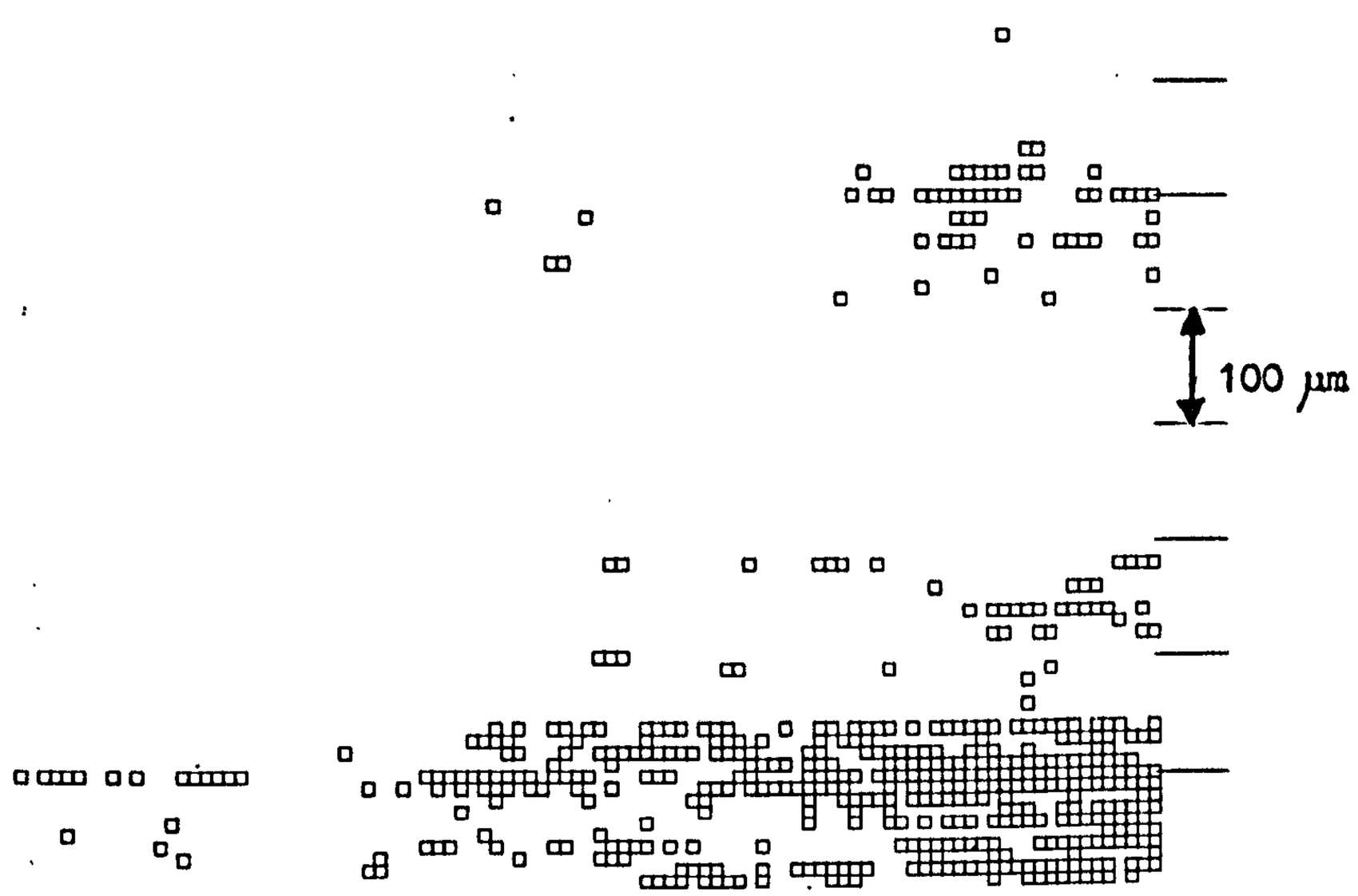

Fig. 5.4 The contact between the two surfaces

A problem is immediately apparent from fig. 5.4, viz: The surface was digitised with a slight tilt.

Fortunately, this was easily overcome by subtracting a least squares fit plane from the entire 0.5 mm by 3 mm map. A description of the analysis that was used for this is given in Appendix One.

When this had been done, the squashing programme was run again, and the result is shown in fig. 5.5. As can be seen, the error has been rectified.

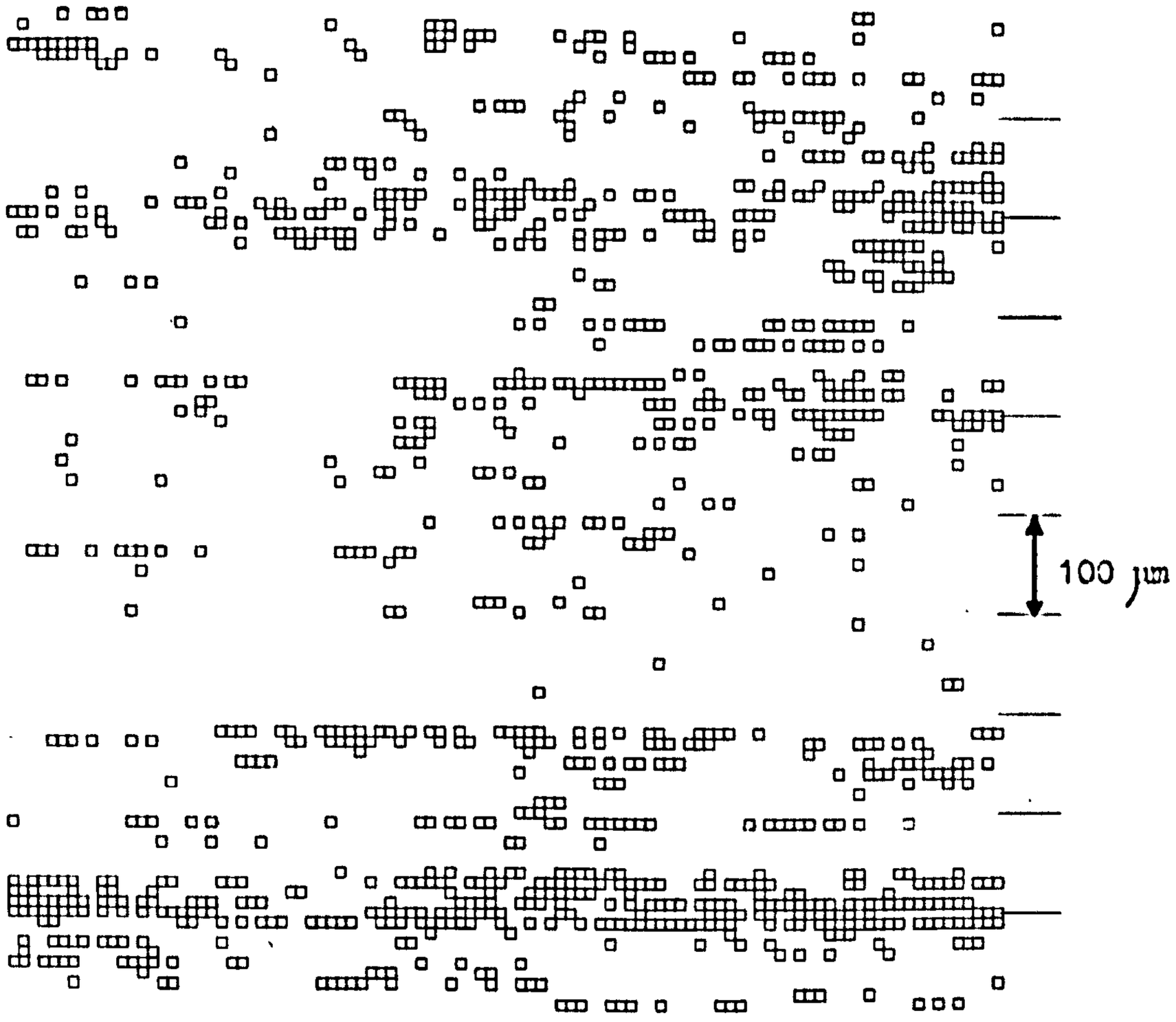

Fig. 5.5 The contact between the two surfaces after the subtraction of the least squares fit plane

The direction of grinding (x) shows up quite clearly. Figure 5.5 shows the contact pattern for the point where

$$A.p_c = L \qquad \text{for } p_c = 280 \text{ Nmm}^{-2} \text{ and } L = 30 \text{ N}$$

The University of London Computer Centre microfilm plotter had the facility for generating 16 mm sprocketed film. This meant that computer animations could be made. It was decided that it would be interesting and instructive to plot the contact patterns as the two surfaces were brought closer together onto 16 mm film to produce a moving picture of the growing contact. Fig. 5.6 shows some stills from the film. The top number on the right hand side

of the frames is the total of all the Δz's that have been subtracted, in mm, i.e. the distance through which the top surface has been lowered. The lower figure is the real contact area, A, at any instant, obtained as previously described.

Once A has become large, as it does towards the end of the film, neglecting the second finding of Pullen and Williamson (36) (that the displaced material is evenly distributed throughout the surfaces) becomes unreliable. The contact patterns are still realistic (see fig. 1.19) but the associated values of $\Sigma\Delta z$ must be considered questionable. The load values that these later contact areas represent, however, are very much higher than would normally be encountered in engineering design and in most friction experiments. Under them, the bulk of the material would certainly be undergoing gross plastic deformation.

The computing thus far described in this chapter forms the first part of the friction modelling programme described in Appendix One.

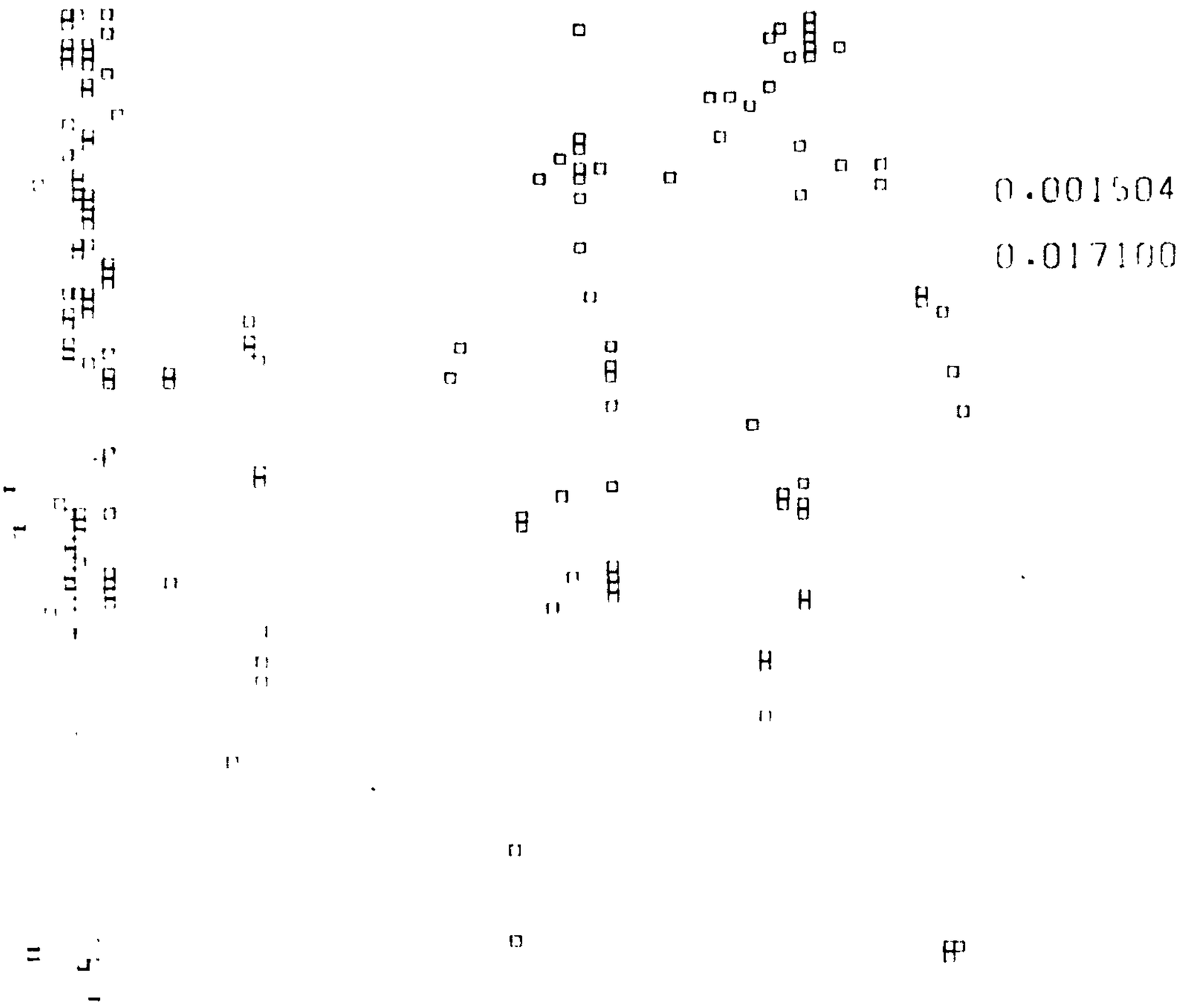

Fig. 5.6a

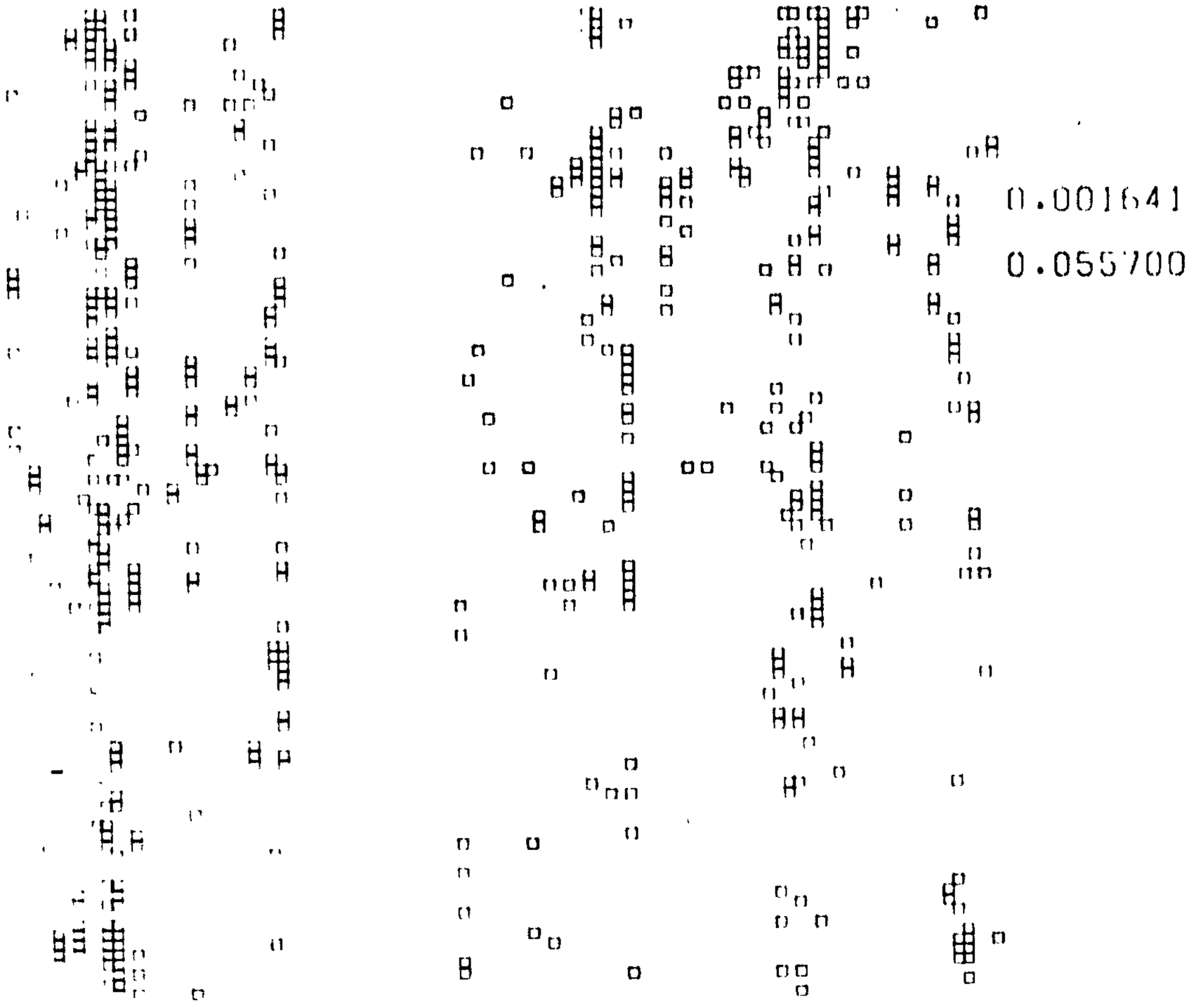

Fig. 5.6b

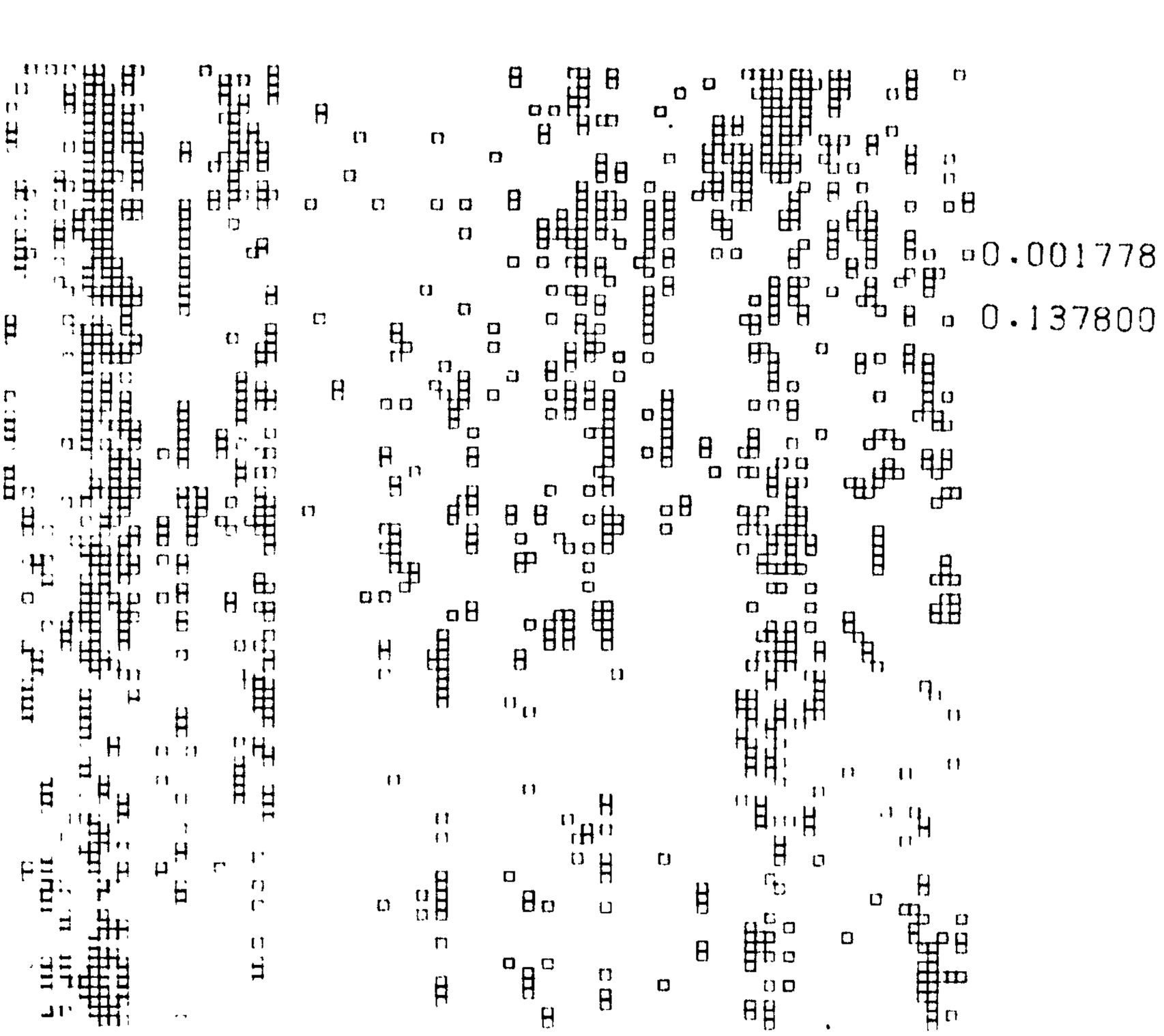

Fig. 5.6c

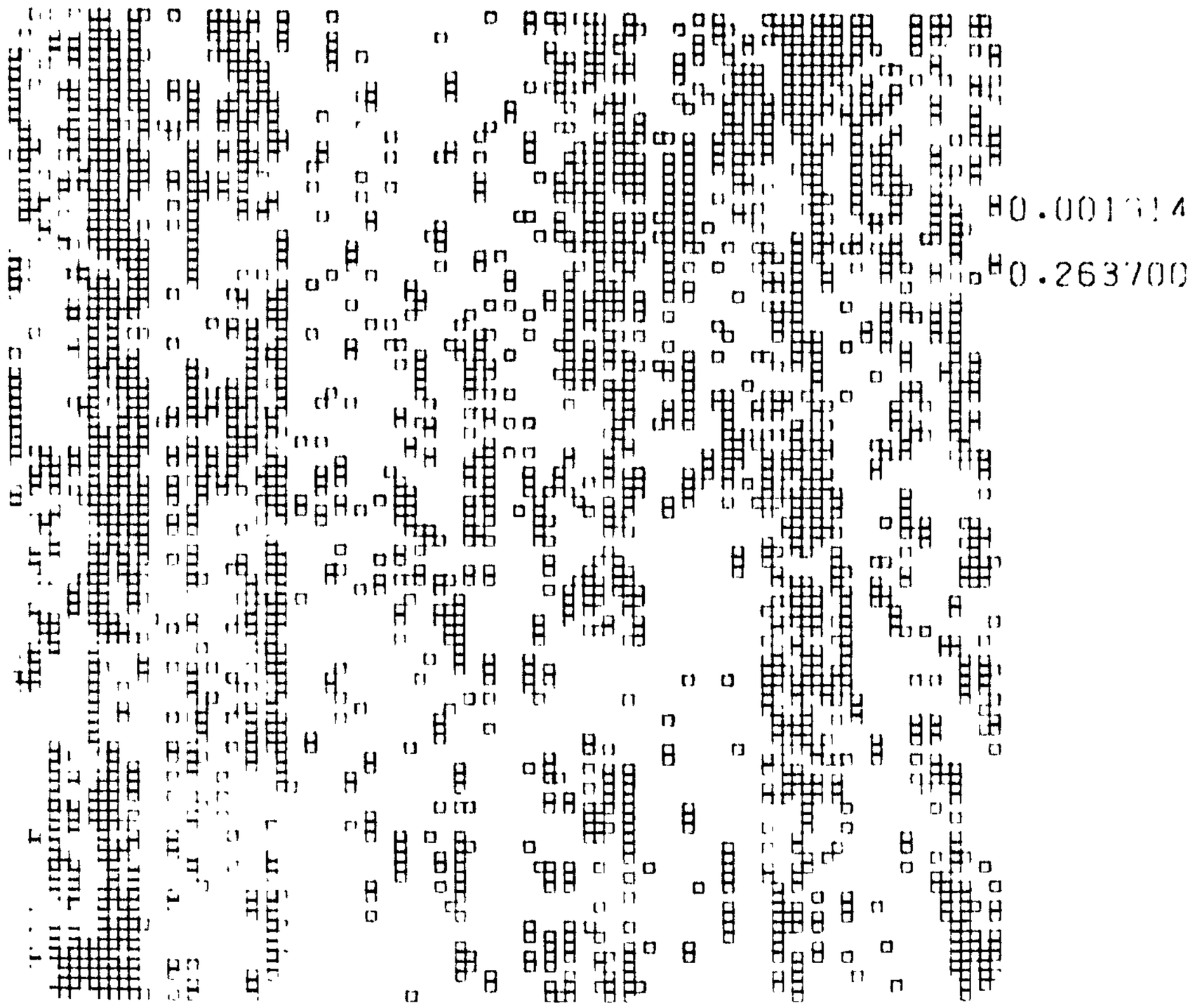

Fig. 5.6d

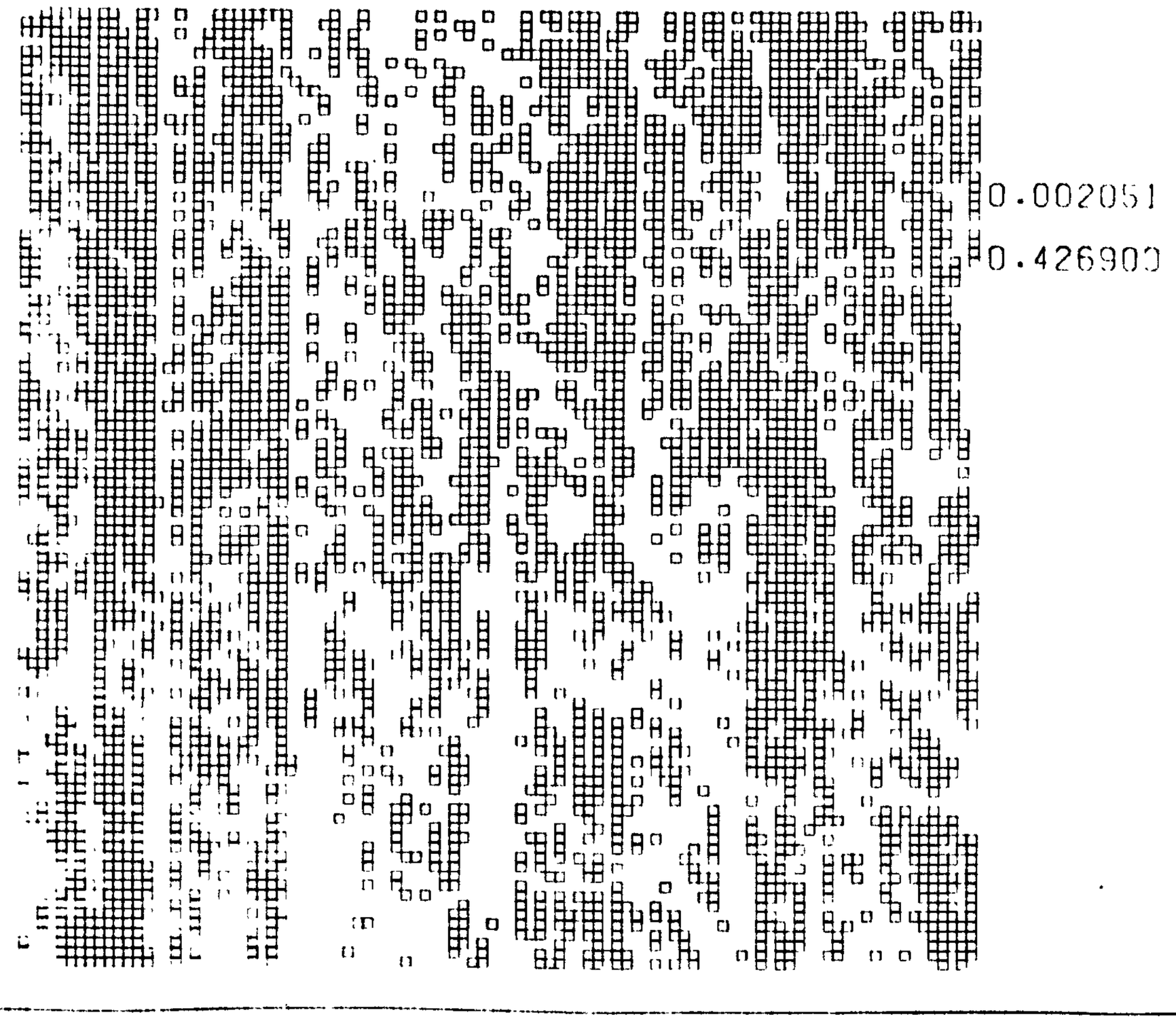

Fig. 5.6e

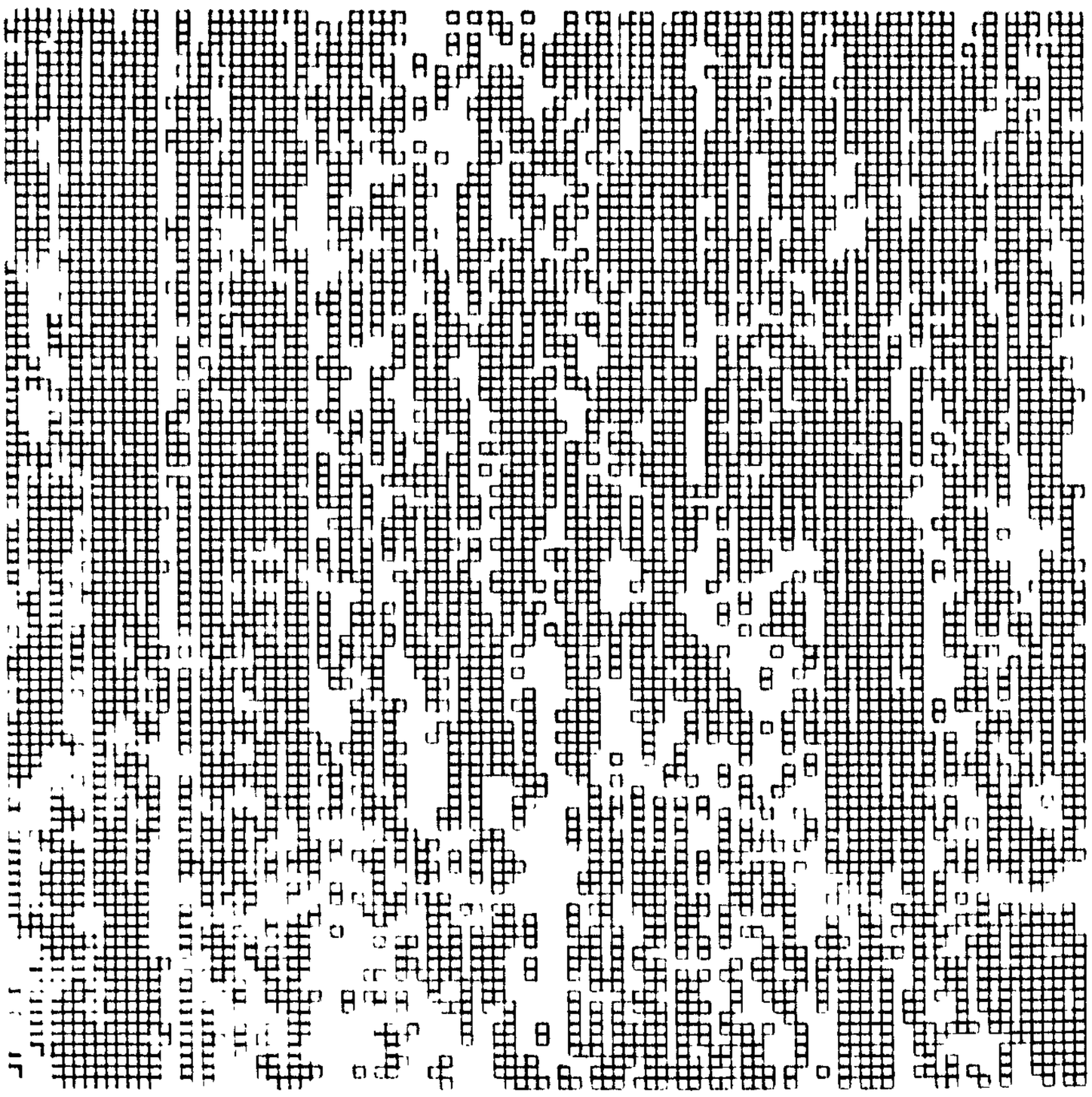

Fig. 5.6f

5.4 Sliding

Having modelled the contact of the surfaces under static load, the final step was to determine what would happen when sliding occurred between them. To do this, equation 5 (see Chapter One) had to be solved numerically by marching it forward in time. The simplest method of doing this is the Euler technique, which consists of taking the derivatives with respect to time in an equation, multiplying them by some small timestep, and adding the result to the values of the variables corresponding to the aforementioned derivatives. Thus, new values for these variables are found after the timestep has elapsed (fig. 5.7):

$$\left.\begin{aligned} \left(\frac{du}{dt}\right)_1 &= \tan\theta \\ \text{timestep} &= t_2 - t_1 \end{aligned}\right\} \quad \ldots\ldots\ldots\ldots (24)$$

From equation 24:

$$u_2 = u_1 + \left(\frac{du}{dt}\right)_1 \cdot (t_2 - t_1) \quad \ldots\ldots\ldots\ldots \quad (25)$$

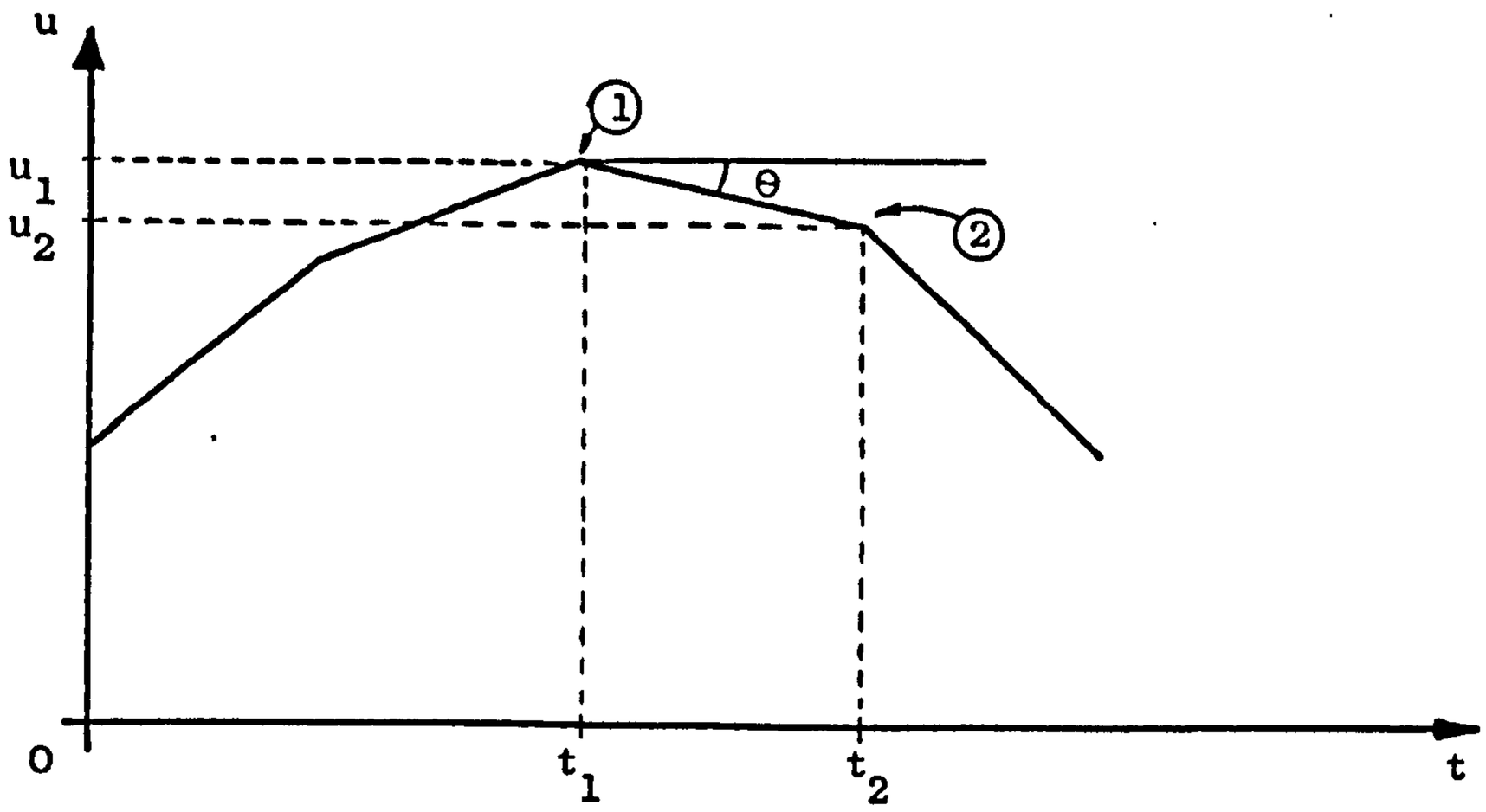

Fig. 5.7 The Euler marching technique for some variable u=u(t)

The accuracy of this technique obviously increases as the length of the timestep decreases until it is so small that the truncation errors in the calculations start to become significant. The time taken to compute a function by this method increases with decreasing timestep, so a compromise has to be reached.

Other, more sophisticated and accurate, methods of marching differential equations foreward in time exist, notably the Runge-Kutta rule and various predictor-corrector techniques. The price paid for this sophistication and increased accuracy is greater central processor time in the computer.

As the sliding model had to take account of the contact between the two maps by considering 20000 height values (10000 = 100 x 100 each surface) at each timestep it was decided, for reasons of economy, to use the fastest marching technique available, i.e. the Euler technique.

The equation of motion was:

$$\mu(\dot{x} - V_o) = \frac{M\ddot{x} + kx}{L} \quad \ldots\ldots\ldots\ldots \quad (5)$$

To march this equation forward to obtain x, $\dot{x}$ and $\ddot{x}$ as functions of time, the constants k, M, V_o and L had to be set and values of the variable μ ($\dot{x}$ - V_o) had to be computed.

In order to obtain values for μ, the simplest assumption was made, viz: The shear strength of the contact was a constant, p_s (see equation 8, p.29). Thus:-

$$\mu.L = p_s.A \quad \ldots\ldots\ldots \quad (26)$$

The computer programme could calculate A as previously described, so the problem could be solved.

It will be remembered that the model was to incorporate the fact that surfaces move apart when sliding. To do this, simple linear behaviour was assumed - the surface maps moving apart by some small distance proportional to their relative velocity, $\dot{x}$ - V_o (fig. 5.6, equation 27).

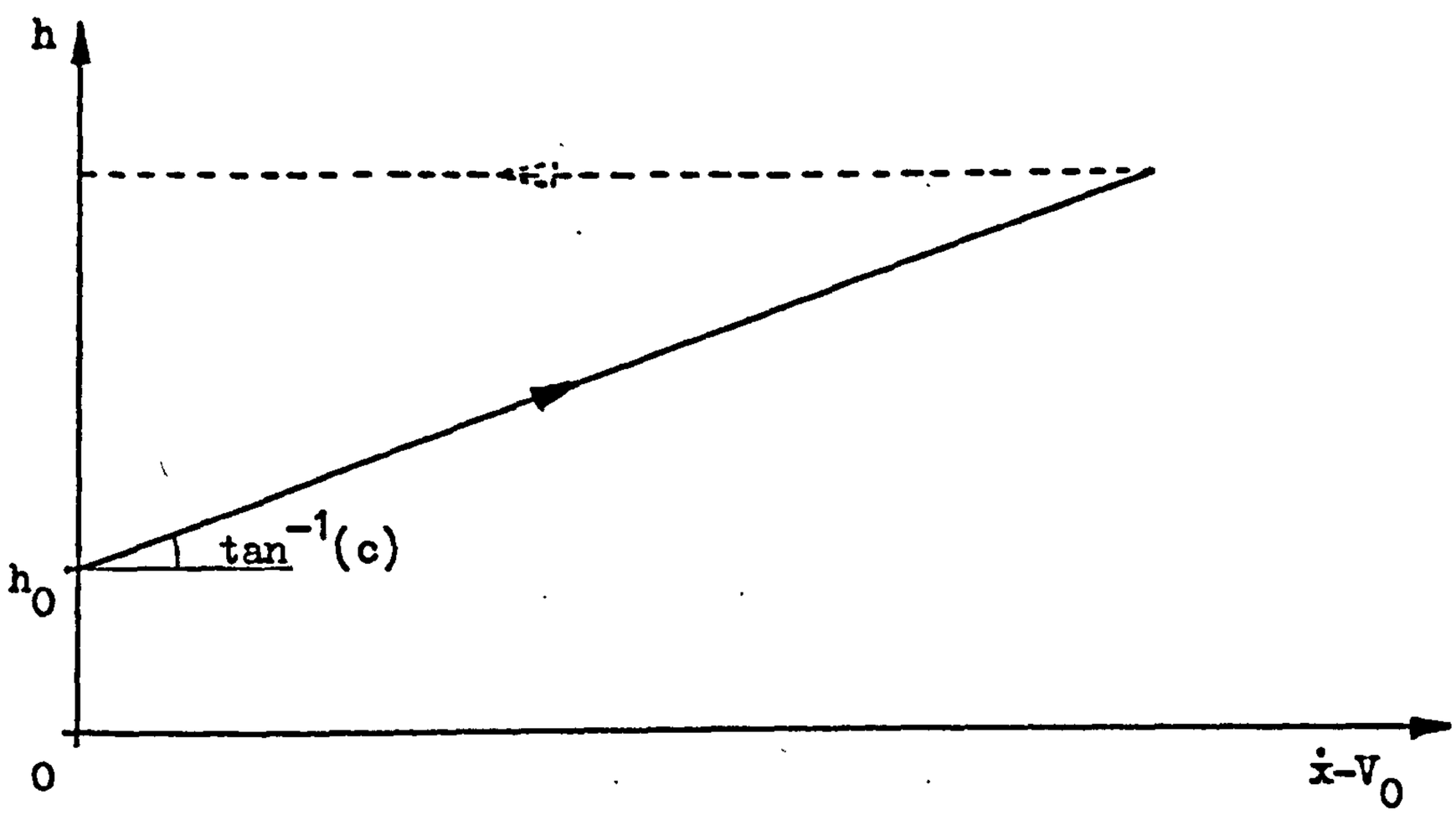

Fig. 5.8 The separation of the surfaces with relative velocity

$$h = h_o(1 + c.|\dot{x} - V_o|) \quad \ldots\ldots\ldots \quad (27)$$

The value, h_o, is the separation obtained under static loading. the programme was arranged so that it could be assumed that the surfaces stayed apart once they had separated (dotted line) until

they came to rest relative to each other, when they resumed the separation h_o(see Chapter Four). This assumption could be supressed, so that the separation of the surfaces was not decided by their past history, but just by their instantaneous relative velocity. The gradient of the separation characteristic, c (fig. 5.8), could be varied.

The contact pattern, and the resulting value of A and hence μ.L, was thus decided by two orthogonal displacements from the starting position:-

1) The amount of sliding that had occurred

2) The degree of separation of the surfaces

5.5 Results*

Figures 5.9, 5.10, 5.11, 5.12, 5.13 and 5.14 show the results (x vs. t) of setting c (equation 27) to 0.0, 0.001, 0.005, 0.01, 0.02 and 0.04 respectively. All other variables were kept constant, and it was assumed that the surfaces remained separated during deceleration. Table 5.1 gives the values of the variables.

TABLE 5.1

V_o = 0.2 mms^{-1}	p_c† = 280 Nmm^{-2}
L = 30 N	p_s† = 82.5 Nmm^{-2}
M = 0.6 kg	
k = 12.66 Nmm^{-1}	

With c = 0, the motion is rather erratic and, as c increases, the characteristic sawtooth of stick-slip emerges. In some cases, the relationship of the model to experiment is remarkable. For example, compare the slight movement labled P on fig. 5.12 with the similar feature on fig. 4.11a.

†These values are in error. See p159 and p168

*Resonant frequencies implied by these results are incorrect. See p159

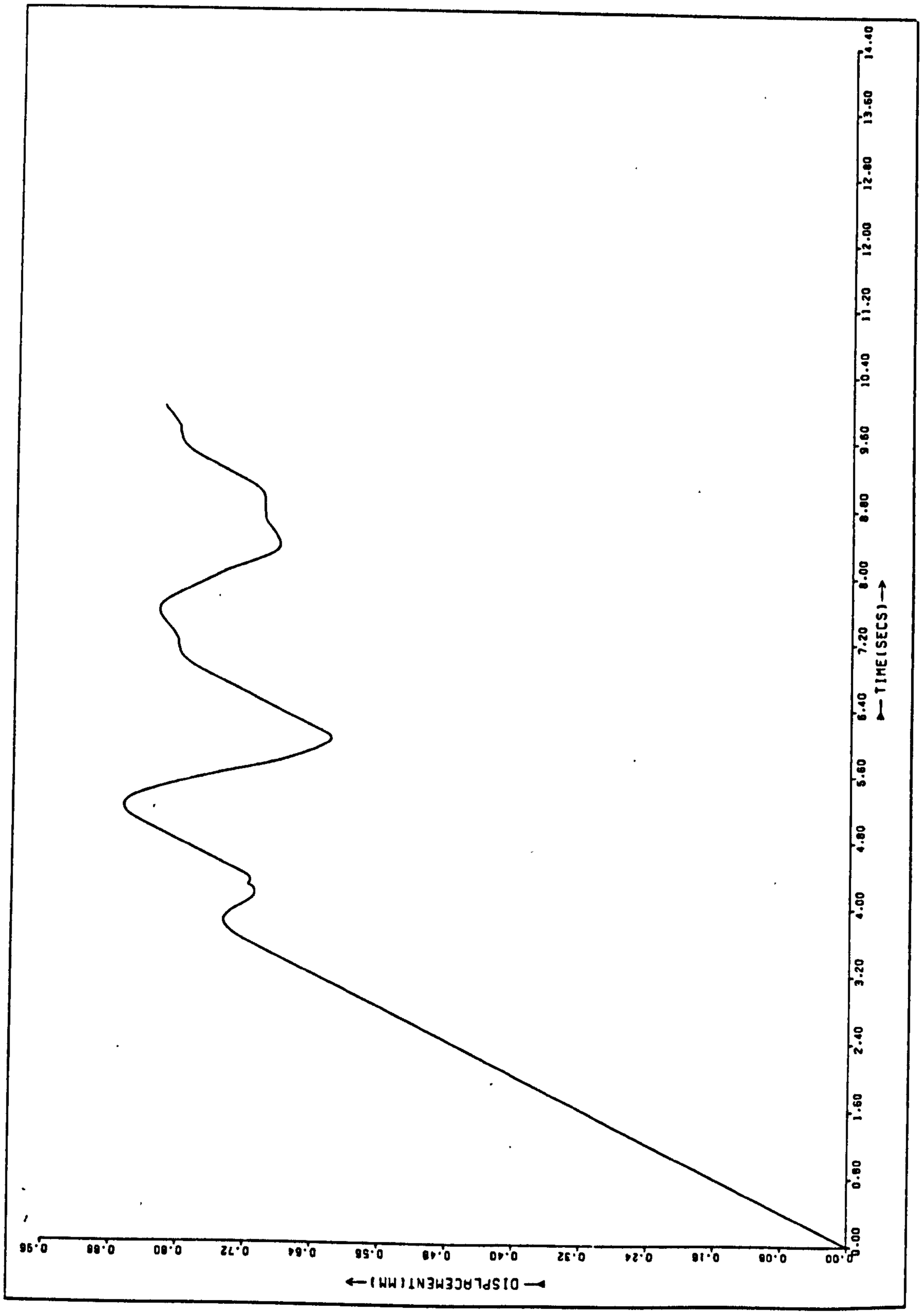

Fig. 5.9 x vs. t : C = 0

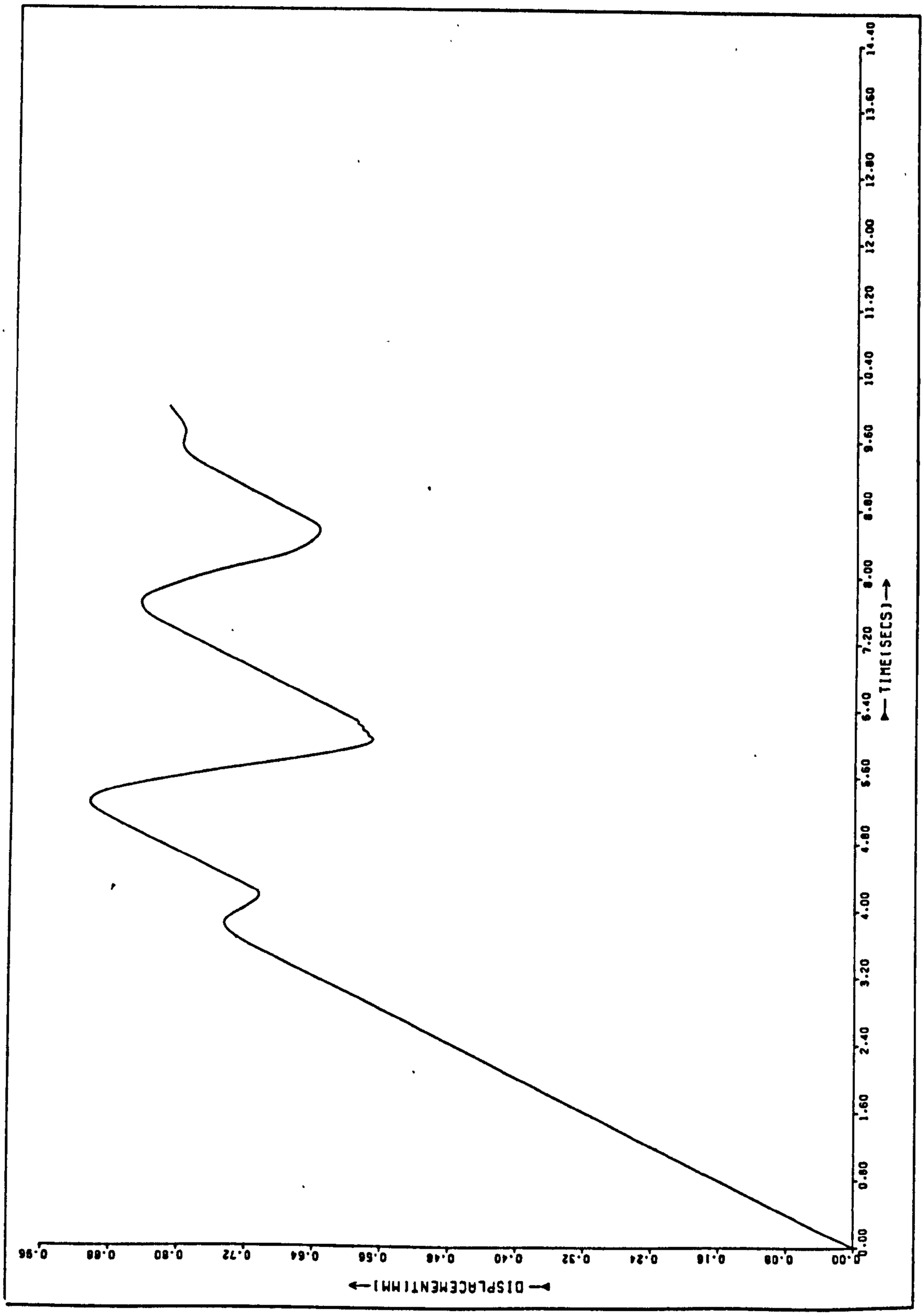

Fig. 5.10 x vs. t : C = 0.001

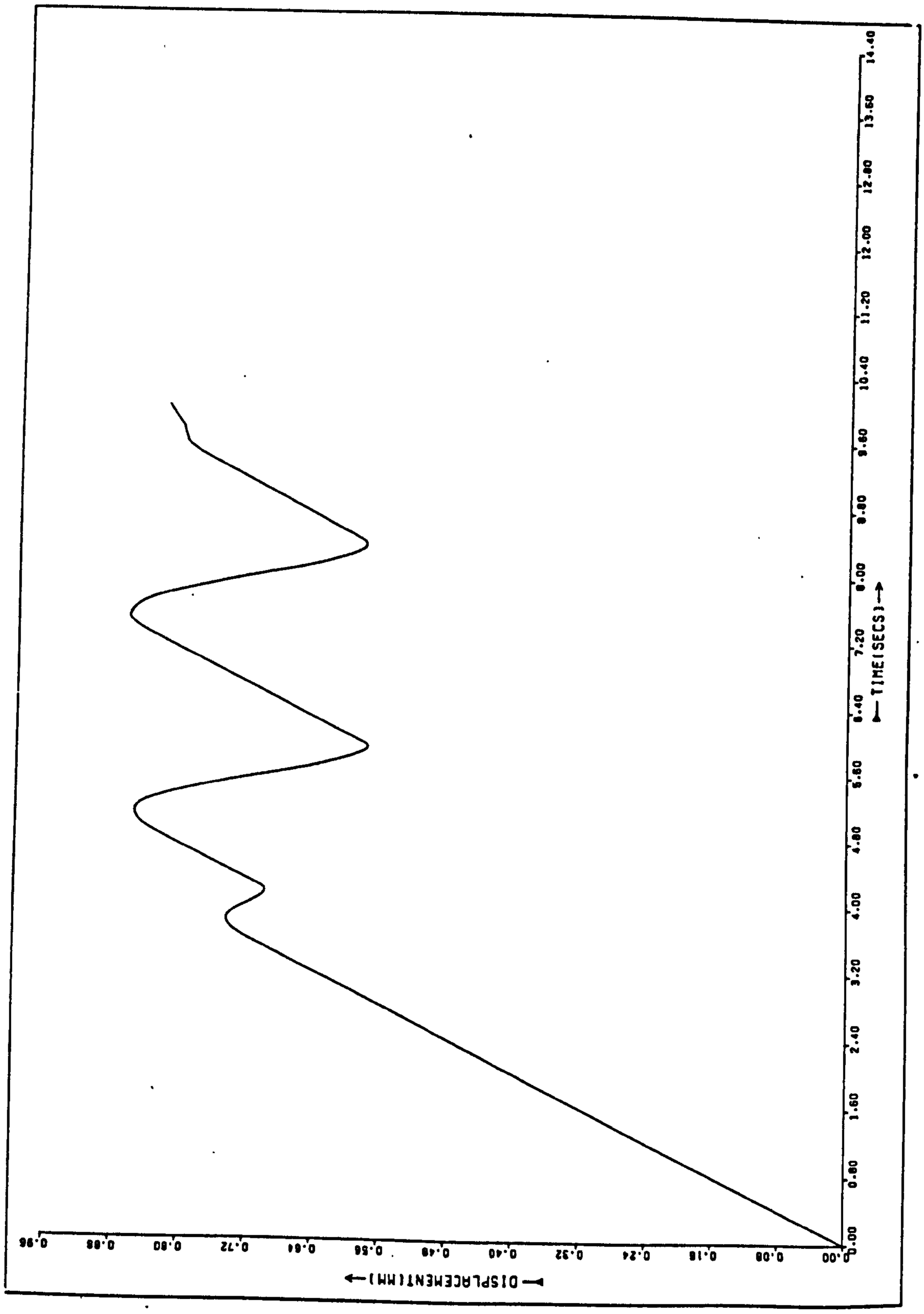

Fig. 5.11 x vs. t : C = 0.005

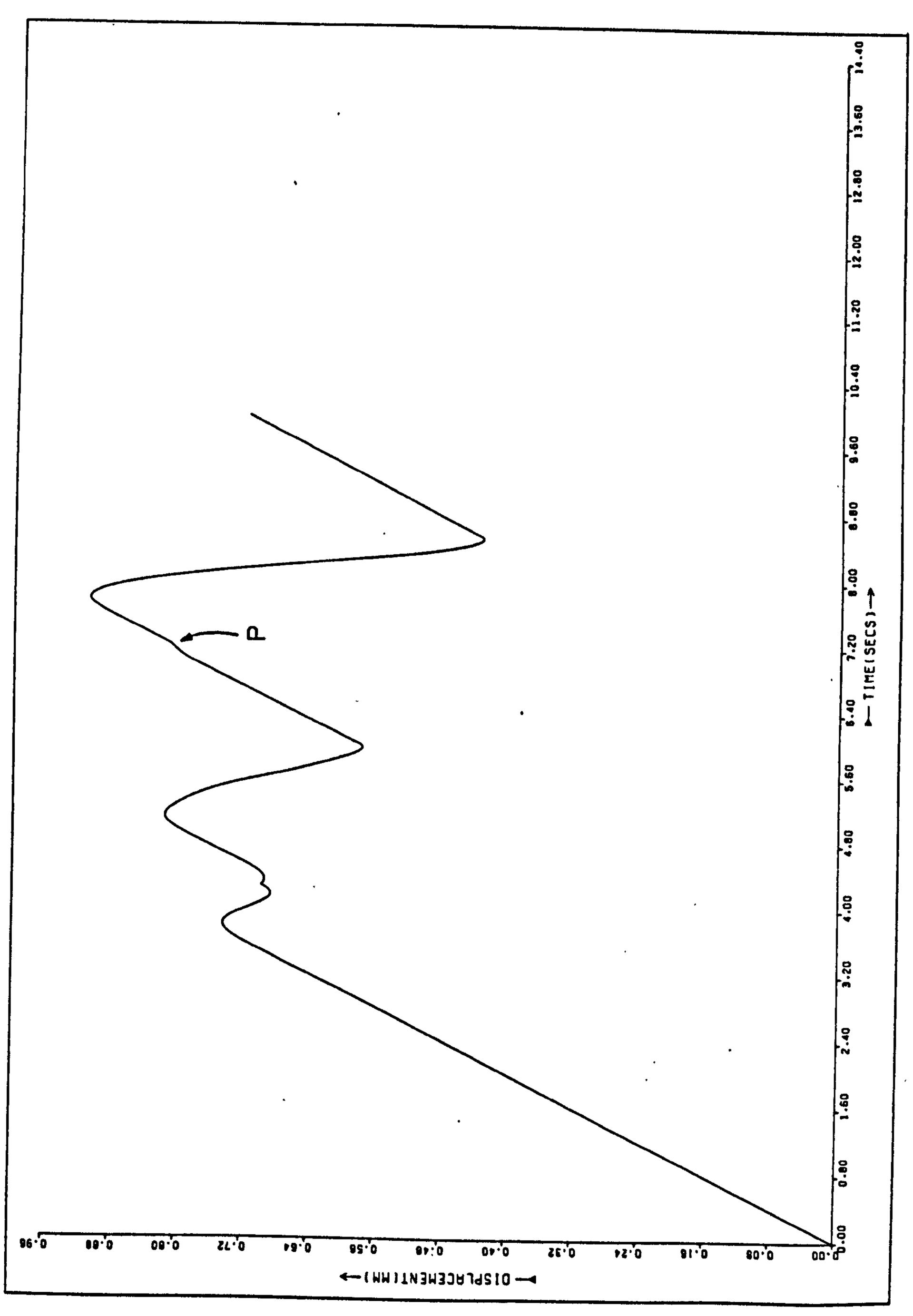

Fig. 5.12 x vs. t : C = 0.01

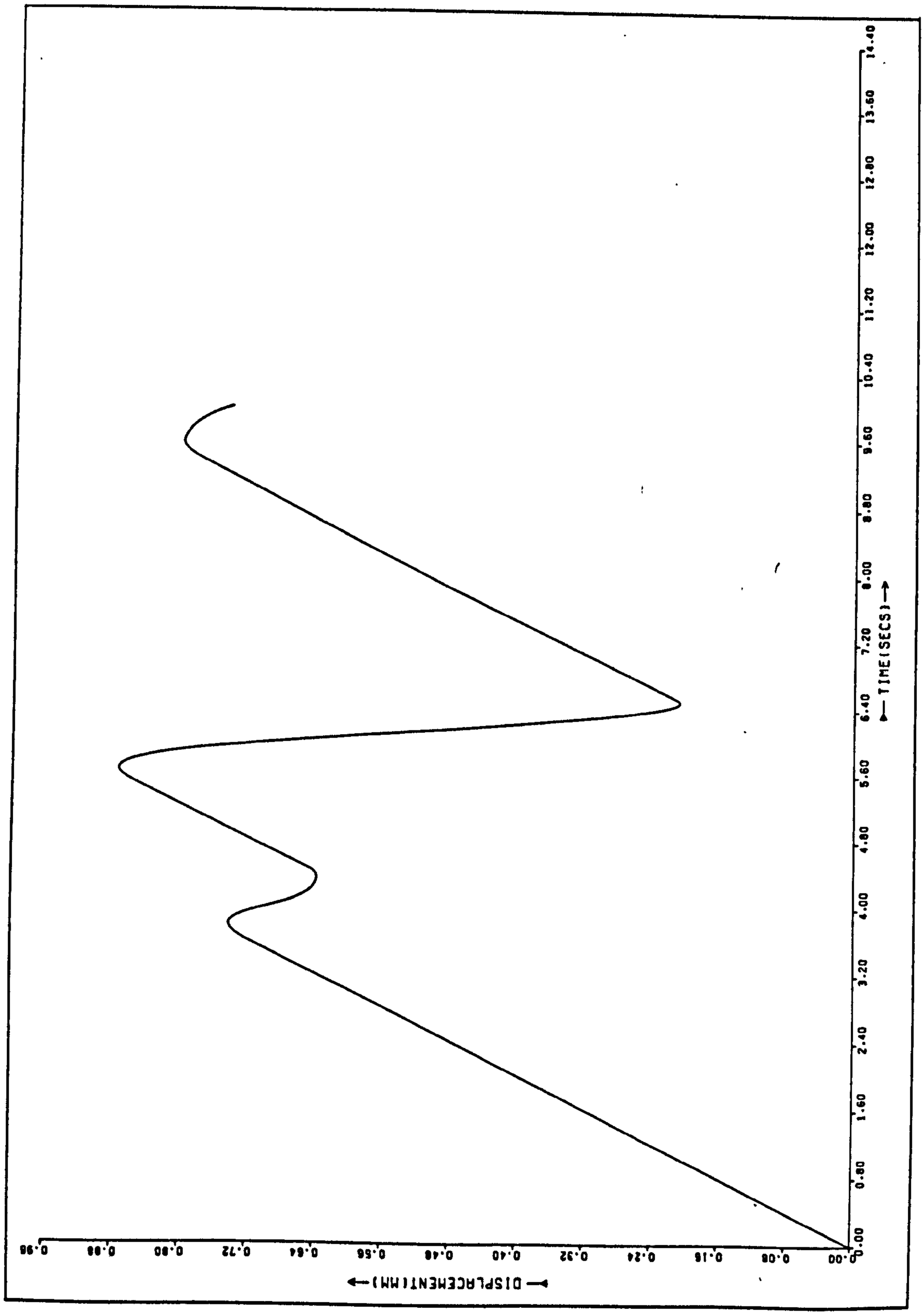

Fig. 5.13 x vs. t : C = 0.02

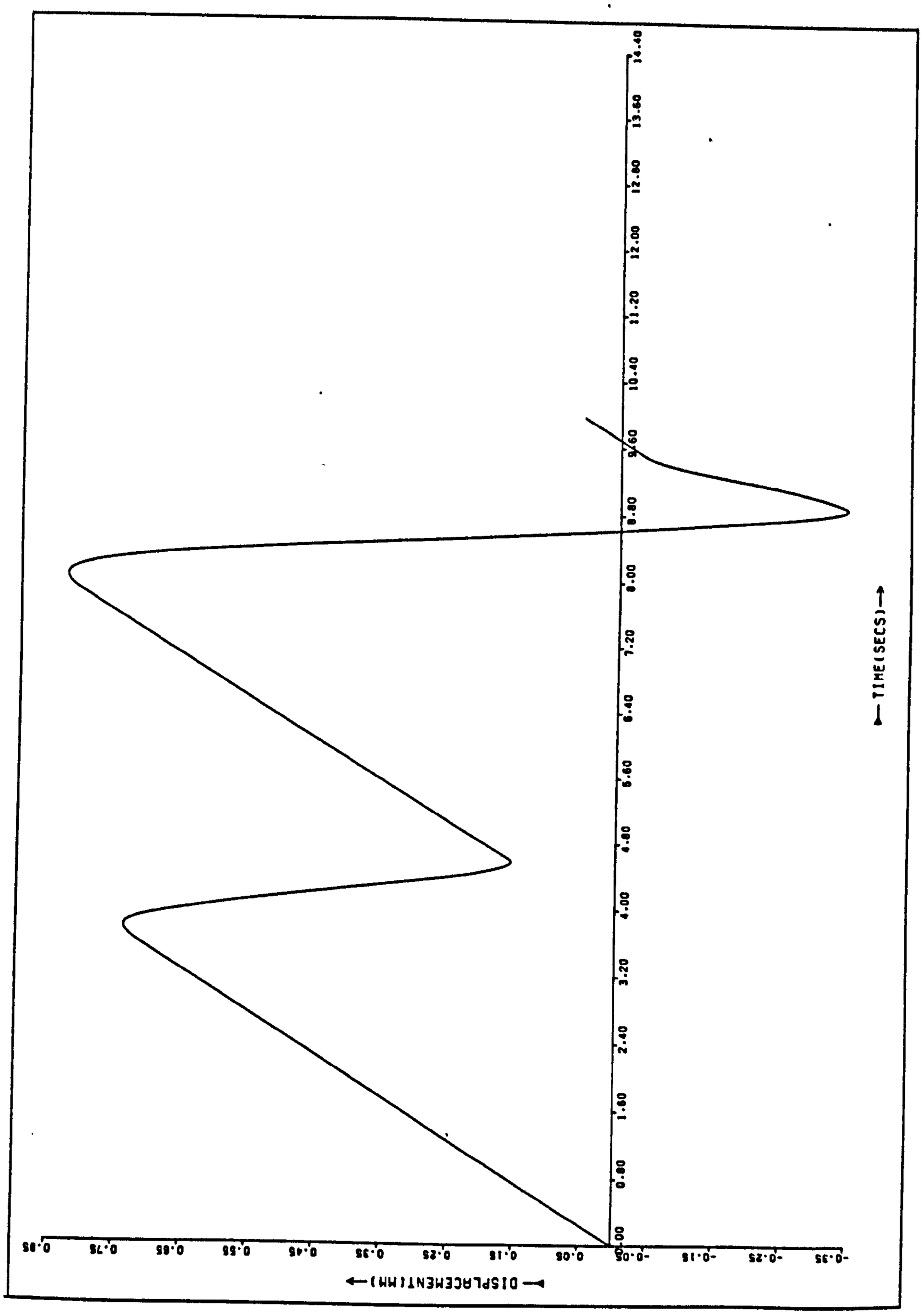

Fig. 5.14 x vs. t : C = 0.04

As c increases, the stick-slip amplitude increases, as would be expected, until it is almost equal to the total displacement. Indeed, on fig. 5.14, the system overshoots. Though this behaviour does not occur in any of the results in Chapter Four there is no reason why it should not, in some circumstances, occur in real stick-slip.

With c set at 0.01, and all the other variables the same as those in Table 5.1 above, V_o was varied. The results are shown in figures 5.15, 5.16 and 5.17 for V_o = 0.05, 0.1 and 0.5 mms^{-1} respectively.

As can be seen, the model is rather unstable at low values of V_o. This is probably because the small velocity below which the surfaces were assumed to be stuck (0.01 mms^{-1}, see Appendix One) was too finely set.

The motion tends towards the quasi-harmonic stick-slip of Brockley and Ko (17) at high speeds. This again is similar to the behaviour observed during experiments.

Figure 5.18 shows the friction-velocity curve obtained from the result shown in fig. 5.13. Compare the curve with the experimental results in Chapter Four and also with the results of Brockley (fig. 1.7) and Sampson et al. (fig. 1.6).

The variation of $\dot{x}$ with time corresponding to fig. 5.13 is shown in fig. 5.19. Figure 5.20 shows the corresponding graph of separation, h, against time. For ease of computation, h is, in fact, the degree by which the surfaces have been moved together from their no-contact position (see fig. 5.3). Consequently, it is seen to decrease as $\dot{x} - V_o$ increases. The effect of the assumption of sustained separation during deceleration can be clearly seen.

Figure 5.21 shows the stick-slip obtained when k was reduced to 6.3 Nmm^{-1} with V_o = 0.2 and c = 0.02 (cf. fig. 5.13). As can

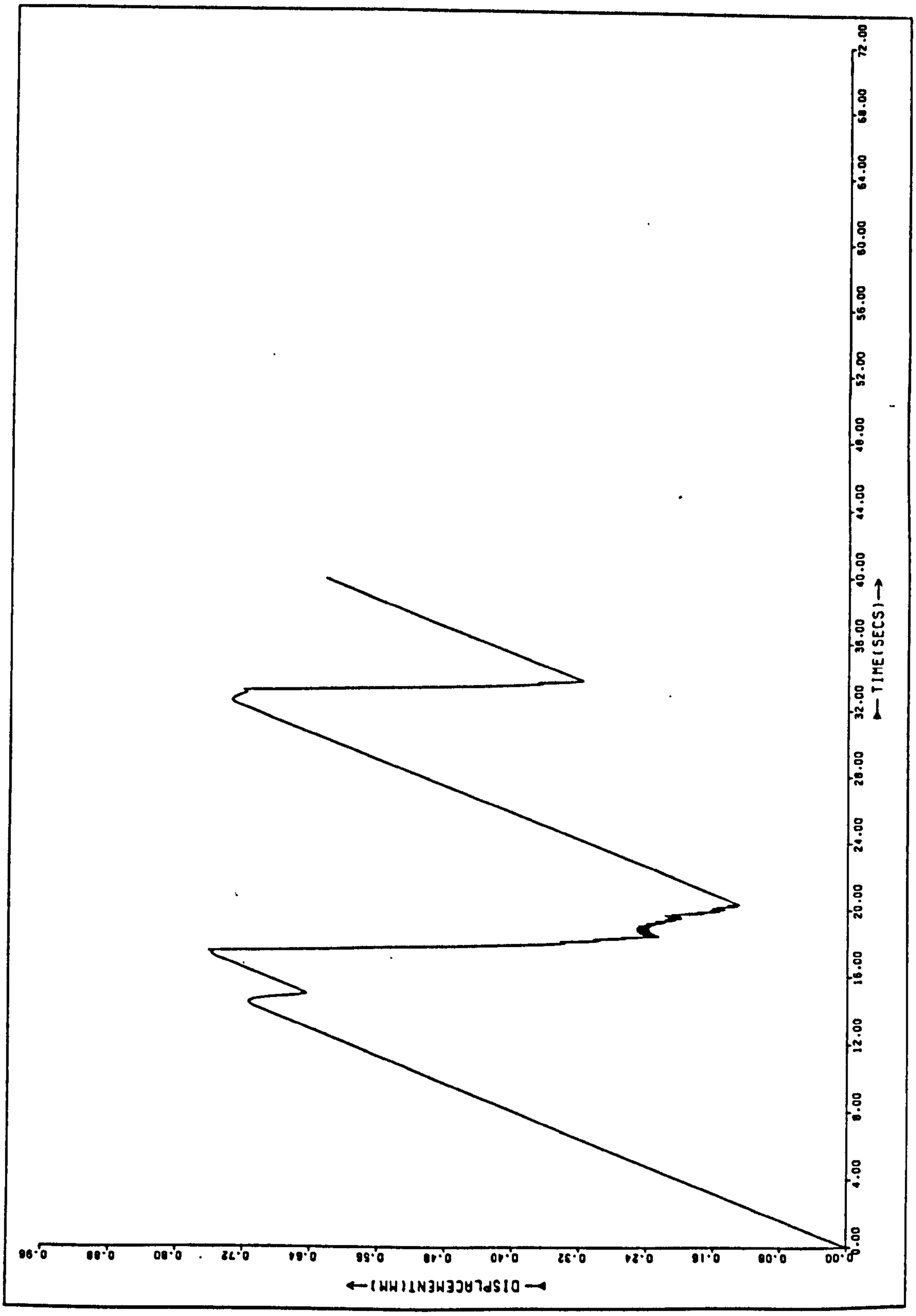

Fig. 5.15 x vs. t : V_o = 0.05 mm/s

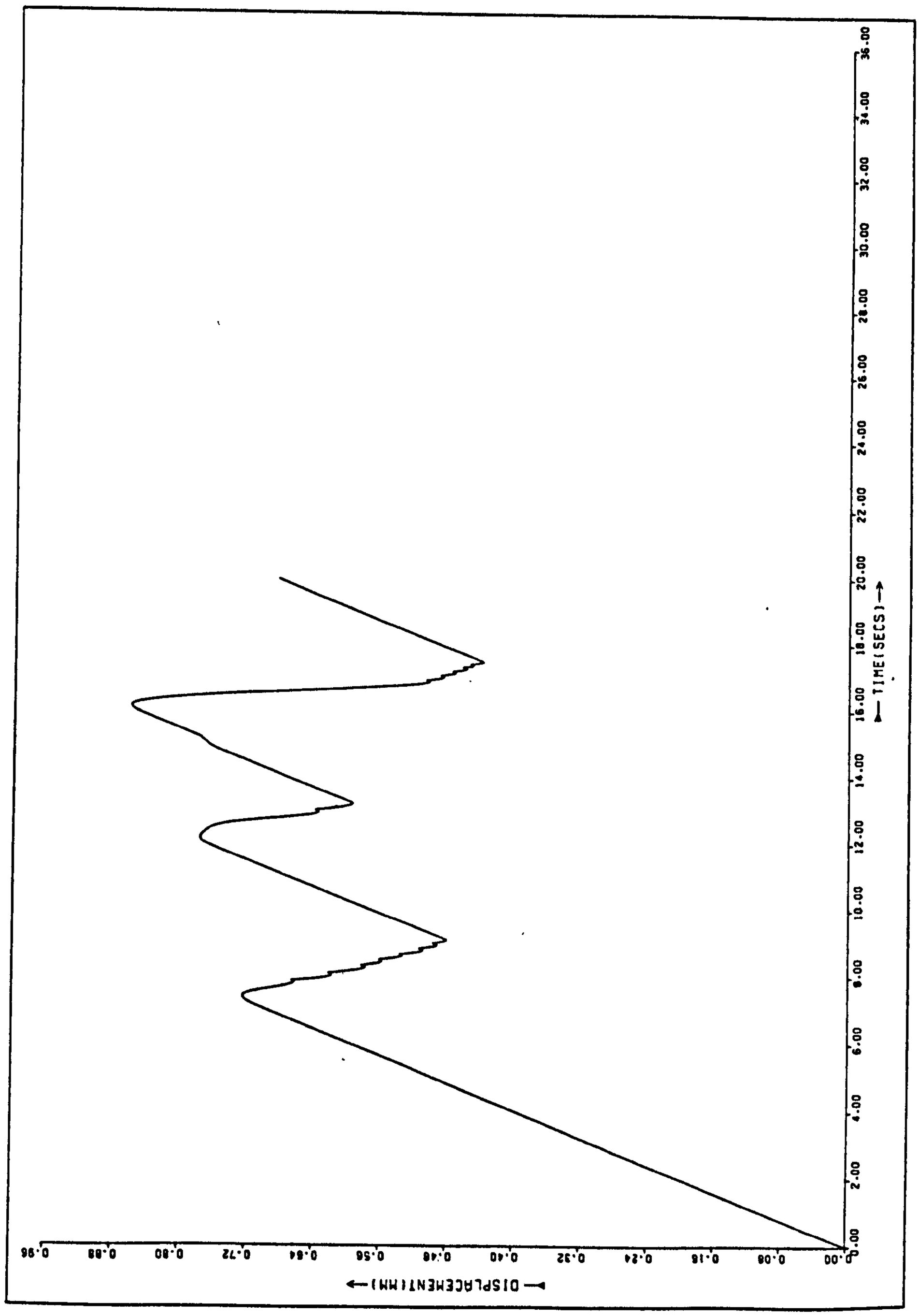

Fig. 5.16 x vs. t : V_o = 0.1 mm/s

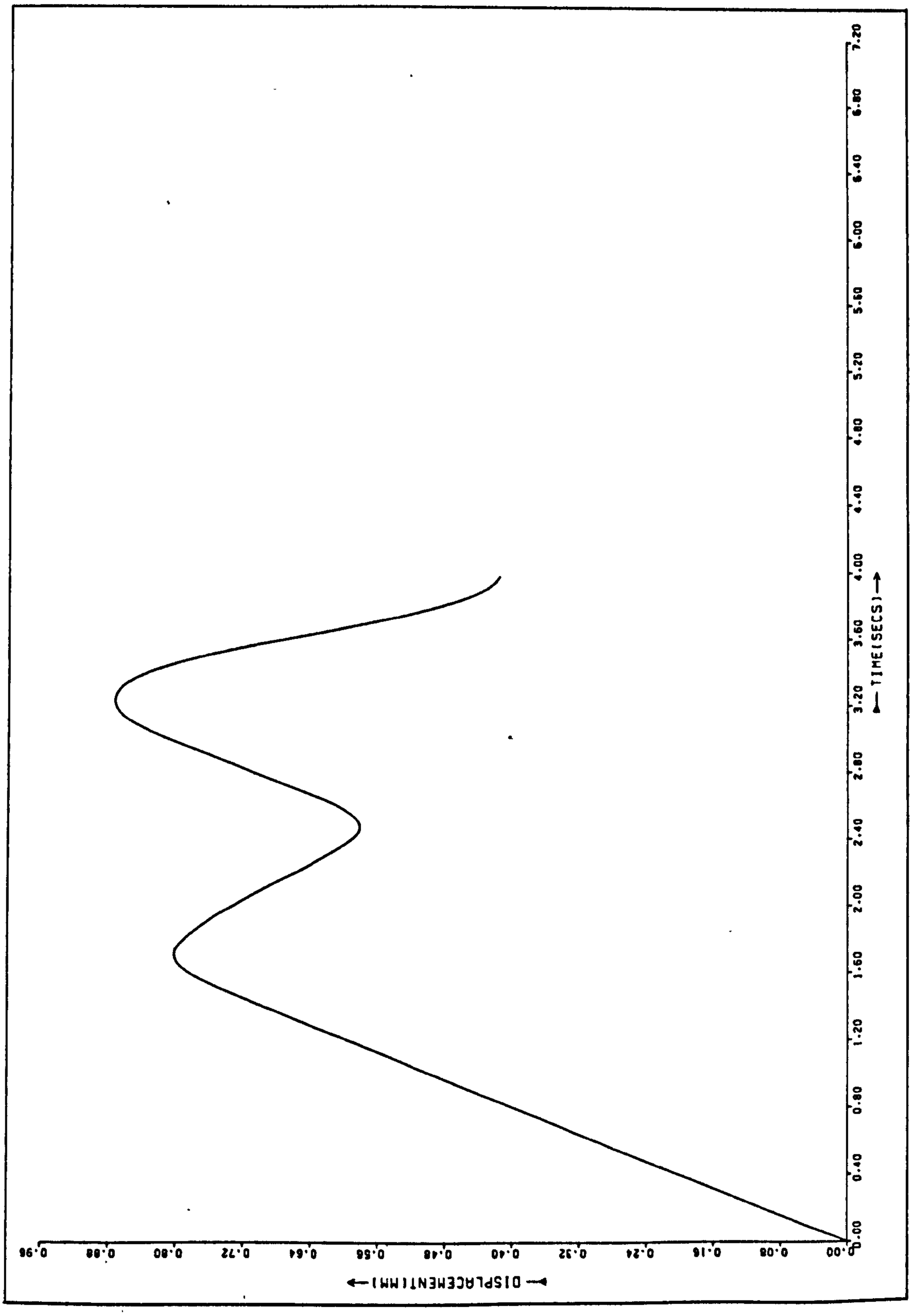

Fig. 5.17 x vs. t : V_o = 0.5 mm/s

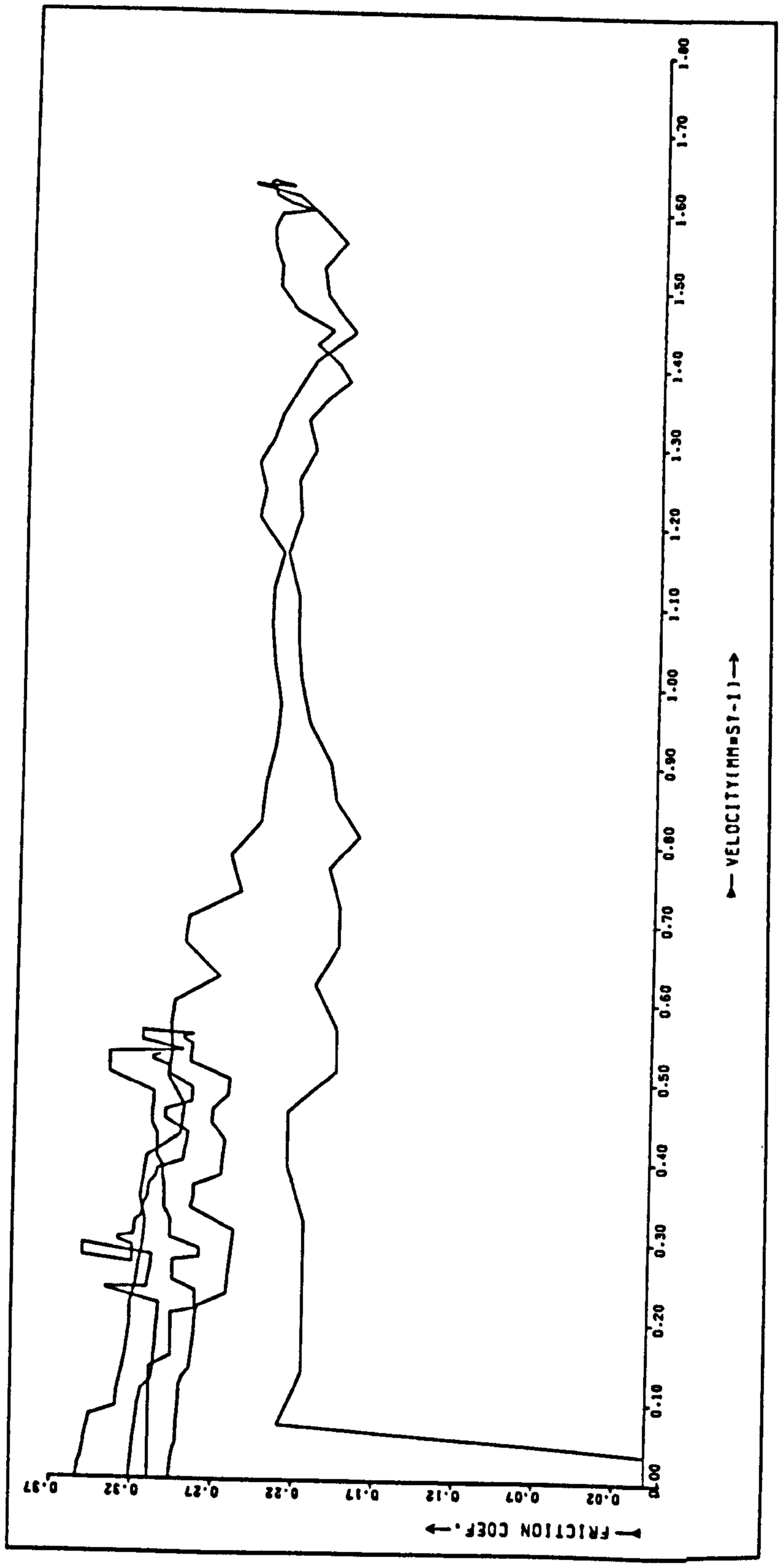

Fig. 5.18 μ vs. $(\dot{x} - V_o)$: Same conditions as Fig. 5.13

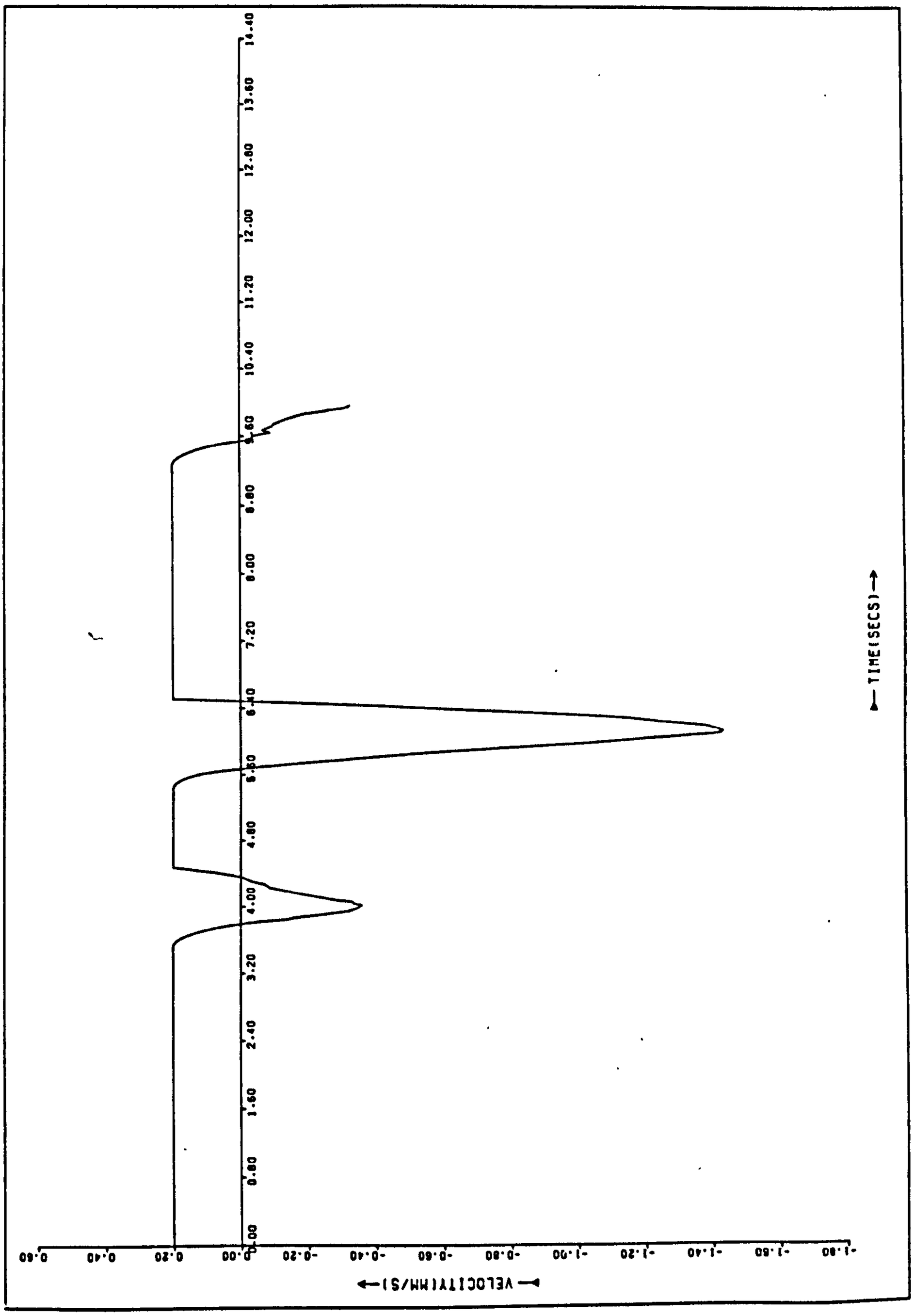

Fig. 5.19 $\dot{x}$ vs. t : Same conditions as Fig. 5.13

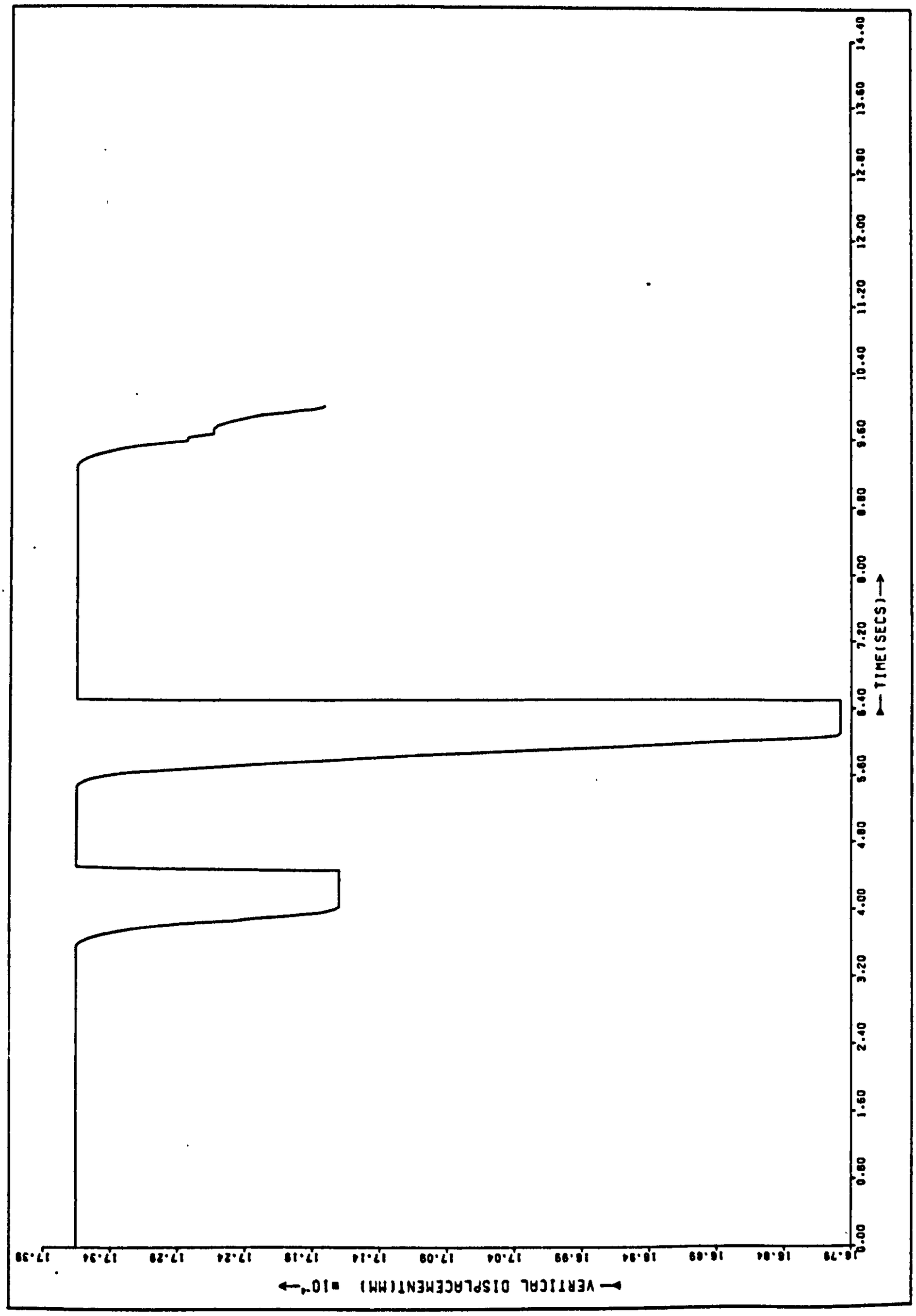

Fig. 5.20 h vs. t : Same conditions as Fig. 5.13

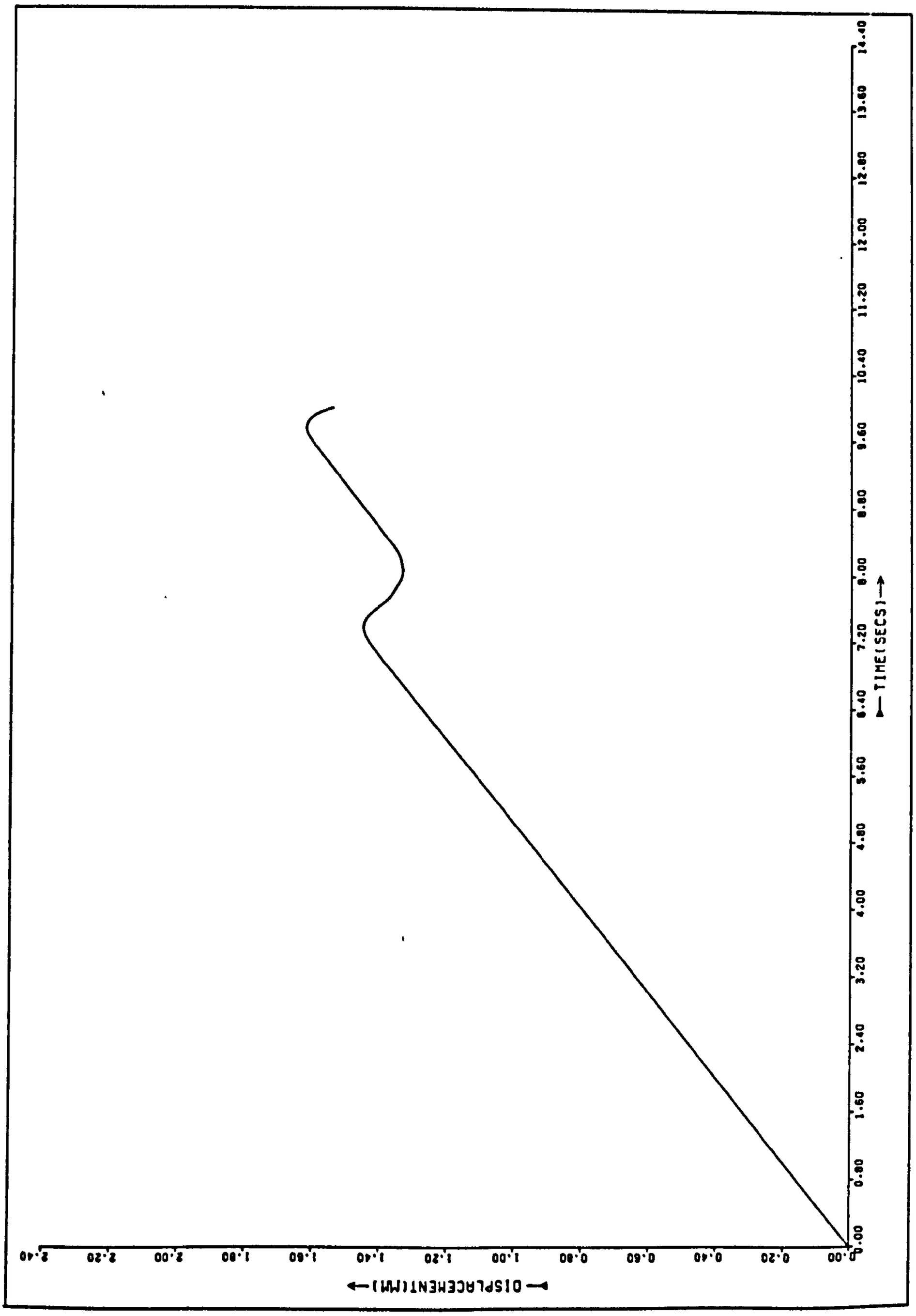

Fig. 5.21 x vs. t : k = 6.3 N/mm

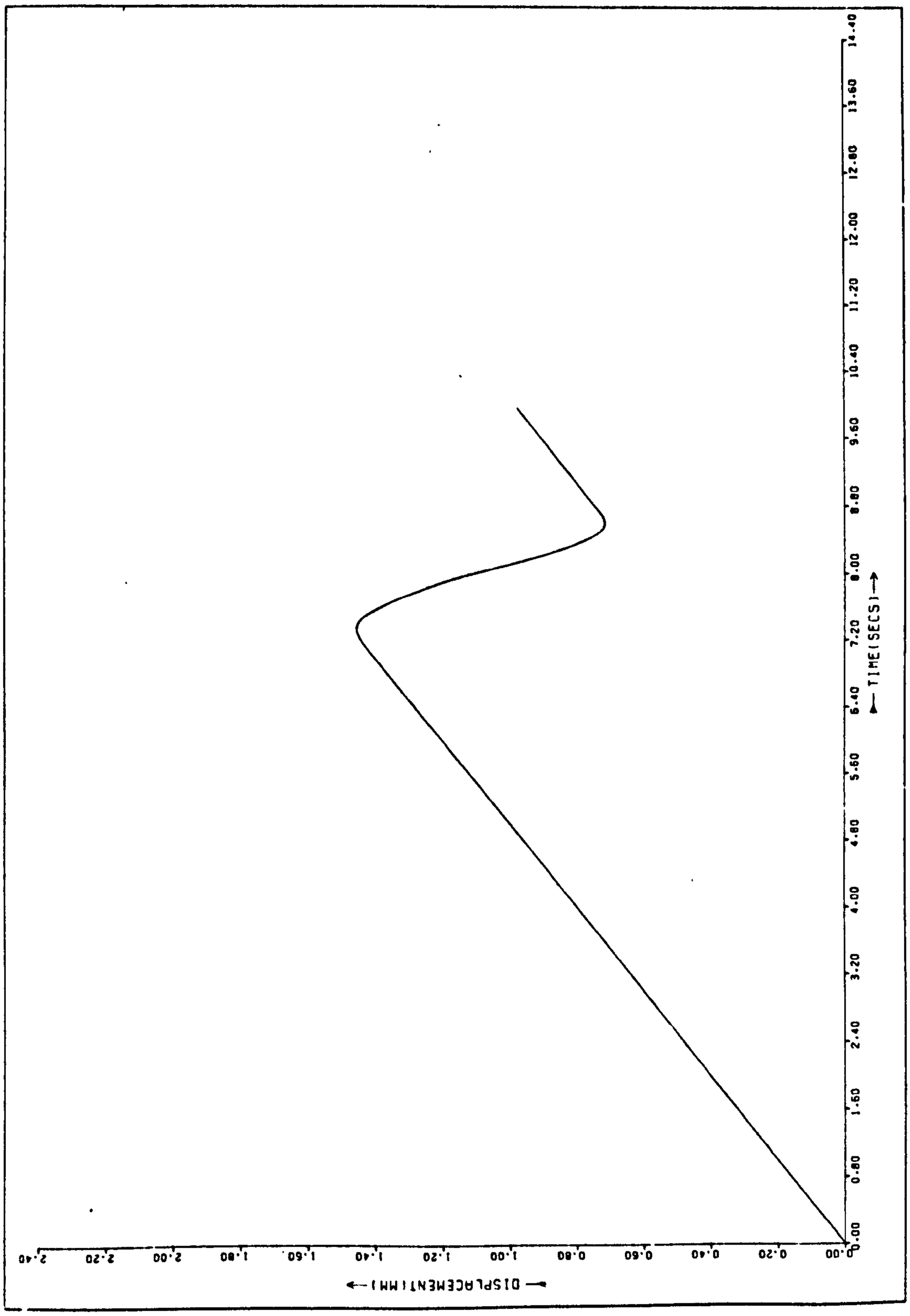

Fig. 5.22 x vs. t : k = 6.3 N/mm, C = 0.03

be seen, the amplitude has been reduced. This concurs with the experimental results in Chapter Four (e.g. section 4.3). The fact that a constant, plastic shear modulus in the contact was assumed in the model indicates that the simple mechanical explanation given for the results in section 4.3 (lower amplitude caused by lower kinetic energies) is probably correct.

Figure 5.22 shows stick-slip under identical conditions, except that c was set to 0.03. As would be intuitively expected, the system is very sensitive to small variations in c.

With the load, L, doubled to 60 N, the static contact pattern shown in fig. 5.23 resulted. Again, with V_o set to 0.2 and c set to 0.02, stick-slip of the form shown in fig. 5.24 resulted.

Fig. 5.23 Contact pattern with L set to 60 N

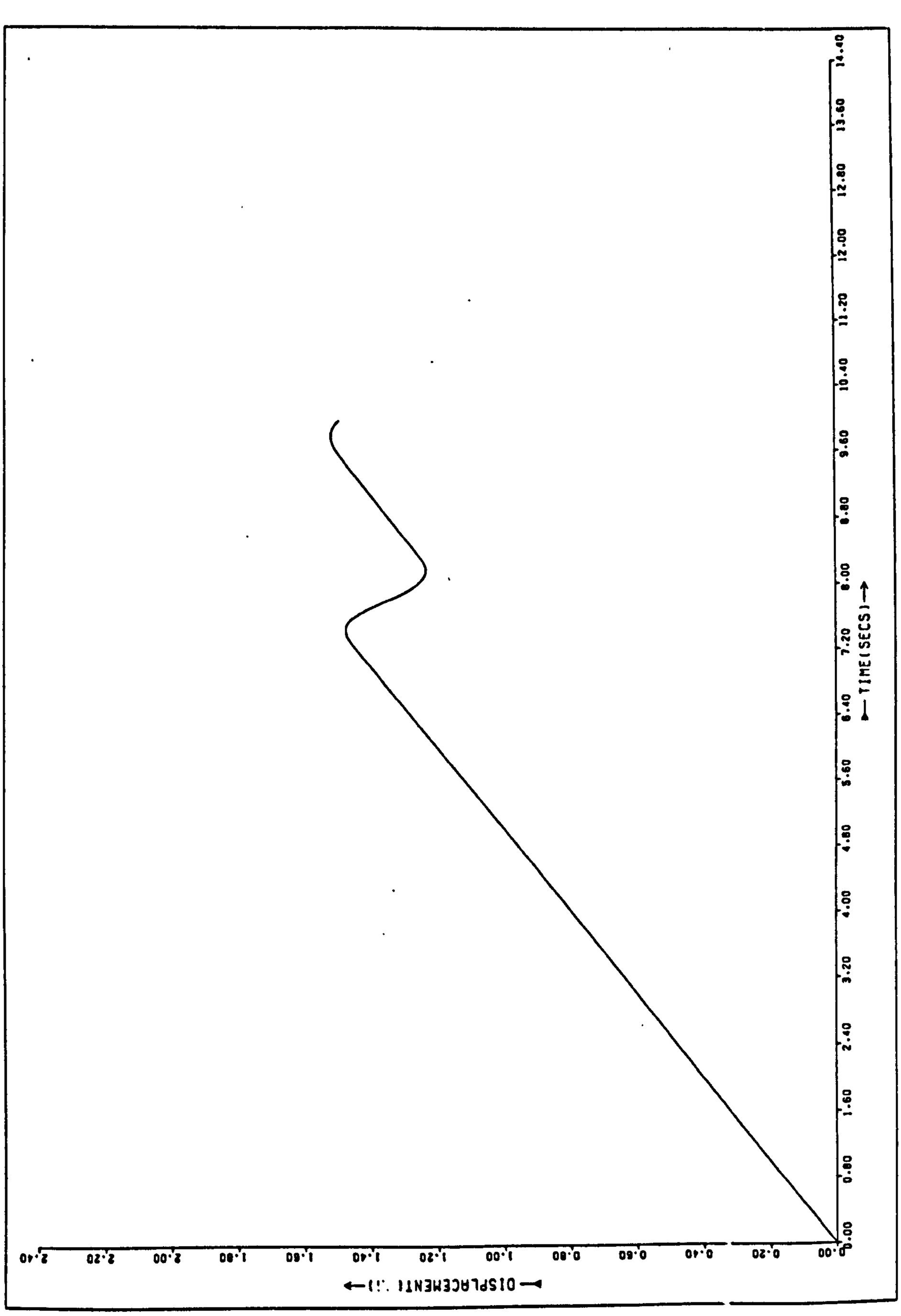

Fig. 5.24 x vs. t : L = 60 N

5.6 Conclusions

The computer model produces stick-slip of a very similar form to that seen in experiments. Quantitatively, the results are not perfect, but with so many constants set almost arbitrarily this is not surprising.

The fact that the model seems to be so good does not, of course, mean that the hypothesis advanced here concerning the separation of surfaces is necessarily the mechanism of stick-slip, though it makes it much more likely. Proof must wait on more experimental work.

The next chapter presents more detailed conclusions on the theoretical and experimental work, together with some suggestions for possible further research.

CHAPTER SIX

DISCUSSION, CONCLUSIONS AND SUGGESTIONS FOR FURTHER WORK

6.1 Experimental work

A computer programme has been developed that could be used to analyse any stick-slip experiment on any computer. The friction-velocity characteristics that were produced in Chapter Four exhibited the hysteresis observed by other workers.

The experimental apparatus worked reasonably adequately, with the possible exception of the frequency response of the charge amplifier. This could be much improved in any further work by the use of a more expensive, commercial amplifier.

The use of the U.V. recorder and digitising table to provide data for analysis was much more efficient than putting in the results by hand (9). However, improvements could be obtained by monitoring the voltages from the strain gauges and accelerometer with an A.D.C. connected on line to a mini-computer or micro-processor.

Depending on its sophistication, this device could partially process the data (say to the extent achieved in this work by the data preparation programme - Chapter Three and Appendix One), or even analyse it completely and produce results in the form of graphs on an on-line plotter or V.D.U.

This would retain the versatility and accuracy offered by digital techniques, but would have the convenience of the analogue system used by Brockley and Ko (15).

The hypothesis concerning the reasons for the vertical movement

of the slider could be tested by the method outlined at the end of Chapter Four. This movement was not measured here, as Tolstoi's method could not be applied. He used interferometry which requires the recording of a number of interference fringes accurately. The periods of stick-slip in his work (time axis, fig. 1.12) were very large (125 seconds) so this could easily be done. For the periods of fractions of a second used in this work, however, it would be very difficult, if not impossible, to make these measurements.

It has been recently suggested (54) that an LVDT (see Appendix Two) or a Talysurf machine could be used to detect this motion (fig. 6.1).

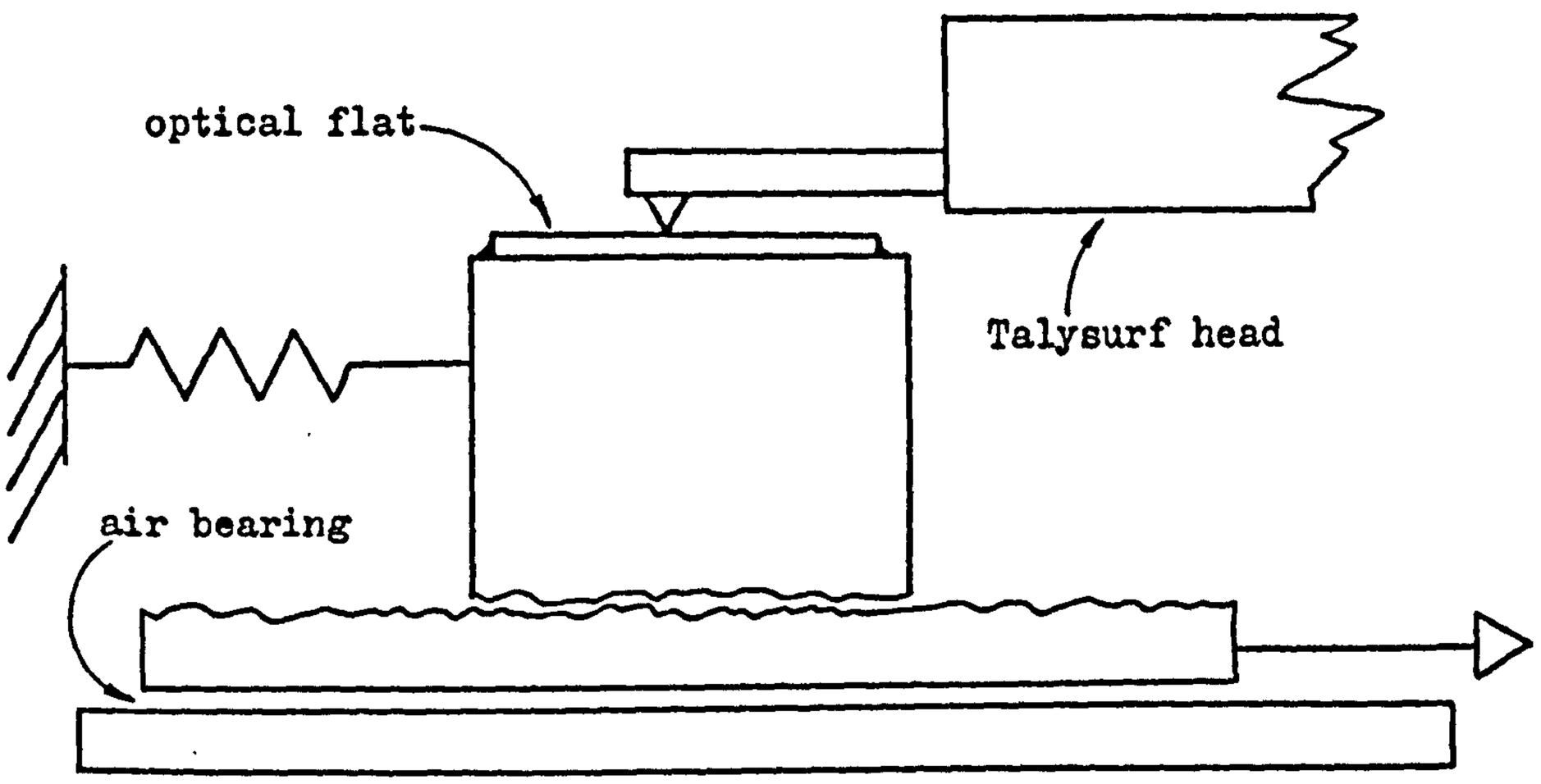

Fig. 6.1 Measurement of vertical movement

The Talysurf (or an LVDT with a diamond stylus) would run on an optical flat attached to the top of the slider. The lower surface would have to slide on an air bearing to minimise spurious vertical movements. As the system underwent stick-slip, the vertical movement of the flat would be measured by the Talysurf. The flat could not be made absolutely parallel to the direction of sliding, so some cross-talk would occur. This could be subtracted (fig. 6.2).

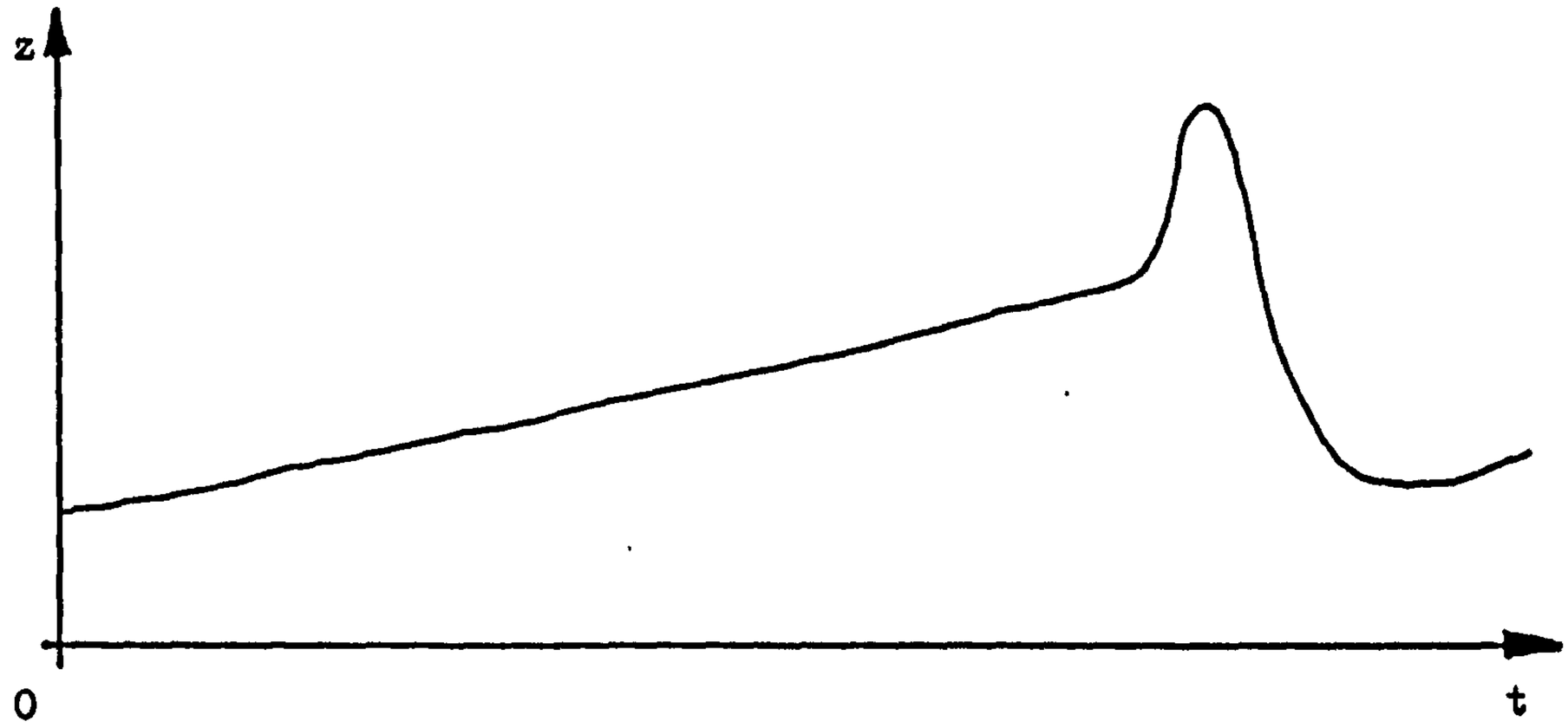

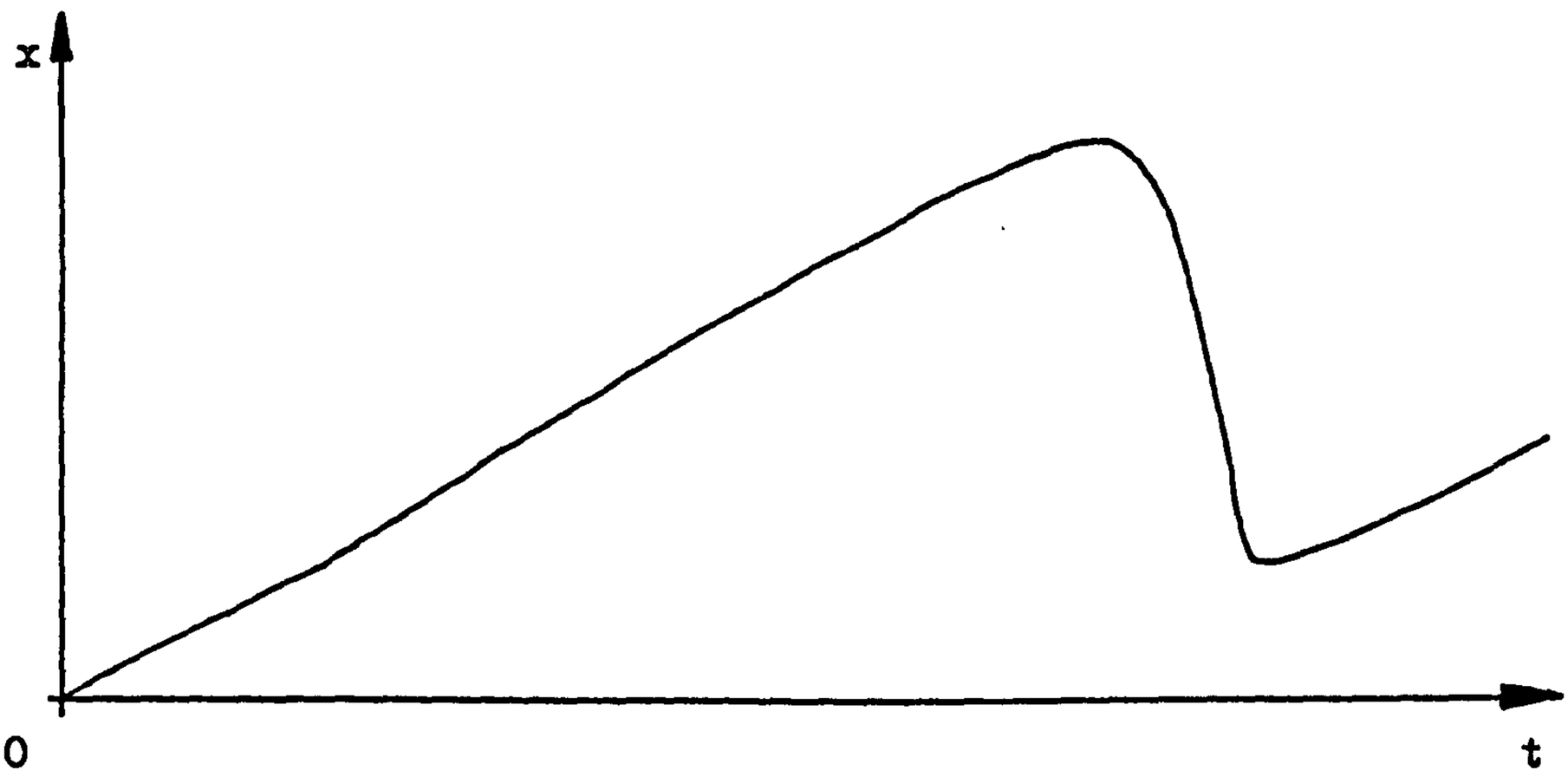

Fig. 6.2 Cross-talk in the system shown in fig. 6.1

6.2 Theoretical work

The computer model described in Chapter Five is potentially an extremely powerful method of friction investigation. Extensions to it are limited only by the amount of computer resources available. Some possible improvements are:-

6.2a) Giving the maps a memory

As it stands, the model assumes that the asperities resume their original shape after being distorted. This is despite the fact that the deformation was considered to be wholly plastic. It would be possible to calculate a mean height value for each overlap when it occurred and permanently to set both heights to this. In addition, a certain amount of elastic behaviour could be modelled by having these reset height values resume some fraction of their

initial heights after they came out of contact. Junction growth (37)(38) could be modelled by having the height values just ahead (in the direction of the shearing force) of the contacts raised (reversibly or irreversibly) by some amount proportional to such things as the shear force in the contact and, perhaps, the plasticity index (44) of the whole, or a local part of, the surface.

6.2b) Lubricants and additives

The voids between the contacts could be assumed to be filled by a viscous medium (Newtonian or non-Newtonian). The area out of contact would be easily calculated along with an average figure for the gap between those parts of the surfaces not in contact. This viscous force could be calculated from this area and gap, the assumed viscosity characteristics and the relative velocity between the surfaces.

The average asperity slope in the direction of sliding and the gap for those sections of the map not in contact could be calculated and used, along with the fluid characteristics, to calculate the hydrodynamic separating force between the surfaces (fig. 6.3).

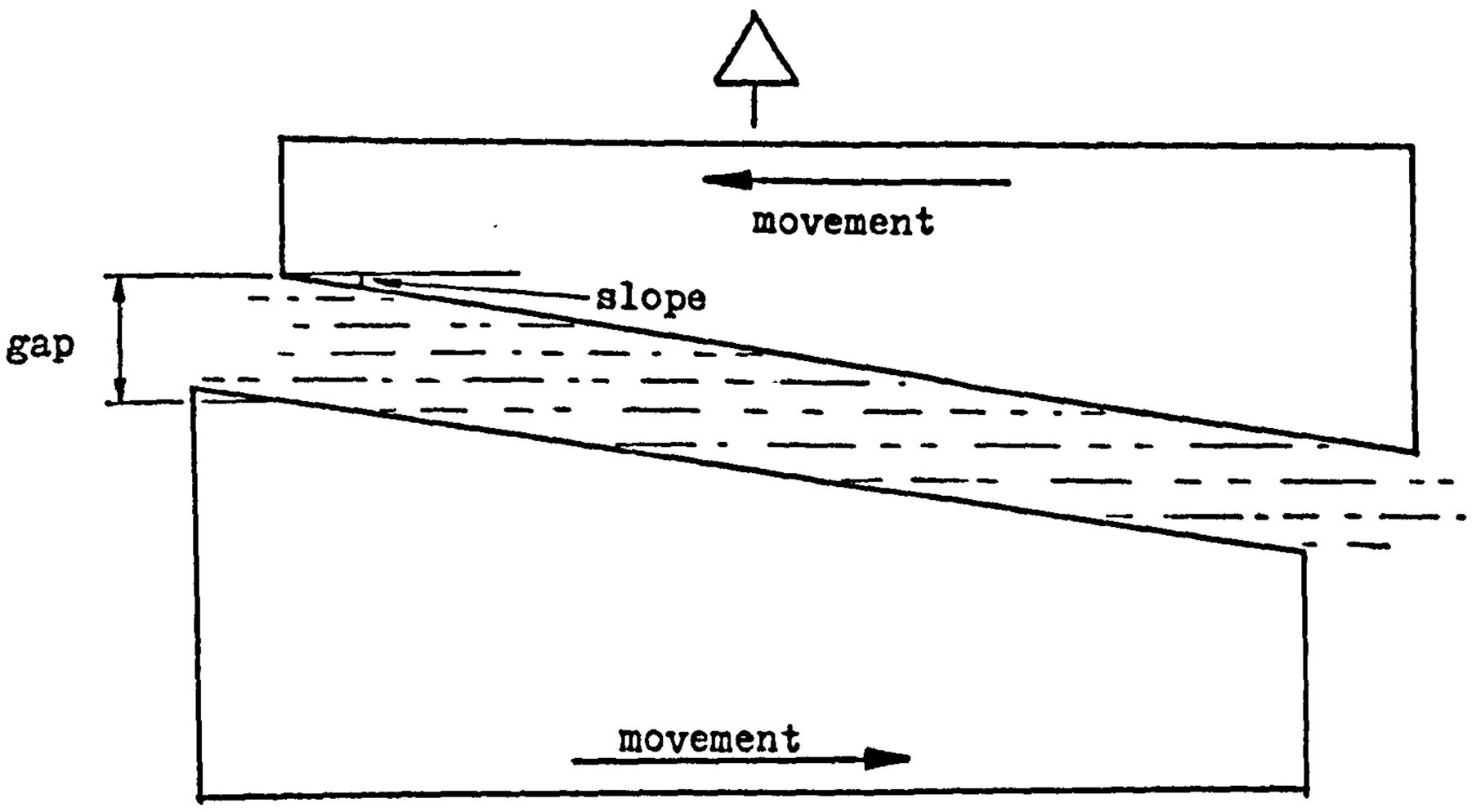

Fig. 6.3 Vertical force from the squeeze film

This separating force, along with the asperity contact force, the load, L, and mass, M, could be used to solve the vertical equation of motion of the slider at the same time as the horizontal equation. This would get rid of the linear assumption of separation with relative velocity.

The assumption that the contact has a constant shear strength could be dropped in favour of a more complex model. A certain fraction of the contact sites could be assumed to be covered with a low shear strength film of boundary additive or e.p. reaction products. This film could be made to behave thixotropically (Brockley (53)) or its fraction of coverage could be made inversely proportional to stick time (a possible explanation for Dokos (22)) or proportional to out-of-contact time.

6.2c) Creep

In solving the vertical equation of motion, the static loading equilibrium height, h_o, could be reset every few timesteps by the same process that it is initially found.

The deformed asperities could be assumed to creep together at some rate during stick time.

6.2d) Multiple passes

If the surfaces retained their deformations, the maps could be reset to their initial positions after sliding, and rubbed together again with the worn surfaces. When this is done experimentally, stick-slip amplitudes are found to decrease (28) (9). This offers further support to the idea that it is the separation of the surfaces that produces stick-slip behaviour, as it would be expected that surfaces which had had flats worn on them by wear (39) would separate less under the action of sliding. It would be instructive to see if the model displayed the same behaviour.

6.3 Conclusions

The analysis of experimental stick-slip could be improved by using an on-line computer and analogue to digital conversion. More experimental work needs to be done on the vertical movements present in sliding systems, especially in relating them to surface topography.

It might be said that friction will not be completely understood until the behaviour of lubricant, oxide and boundary shear films, and deforming asperities, can be predicted for a given pair of sliding surfaces. With the advent of large digital computers this has become realisable. It is hoped that the computer sliding model presented in this thesis constitutes a step towards this degree of understanding.

APPENDIX ONE

COMPUTER PROGRAMMES

A1.1 The operating system

All the programmes written for this thesis, with the exception of the PAL surface mapping programme mentioned in Appendix Three, were in FORTRAN IV and were run on the Imperial College/University of London computer centers' CDC installations, using either the Minnesota MNF or the FTN compilers. All used single precision floating point arithmetic throughout, which, with the sixty-bit word length of the CDC computers, gave truncations after fourteen decimal places.

A1.2 The experimental data preparation programme

This programme had to take the digitising table data of x and $\ddot{x}$ against t and convert it to actual values of x, $\ddot{x}$ and t in mm, mms^{-2} and s, performing an interpolation on the x vs. t curve so that its values of t corresponded with those on the $\ddot{x}$ vs. t curve (see Chapter Three).

A flow diagram for this programme is given in fig. A1.1.

A1.3 The experimental data analysis programme

This programme was required to take the data stored on disc by the above programme, calculate values of $\dot{x}$ vs. t and solve equation 5 for μ $(\dot{x} - V_o)$. A flow diagram is given in fig. A1.2, followed by a listing.

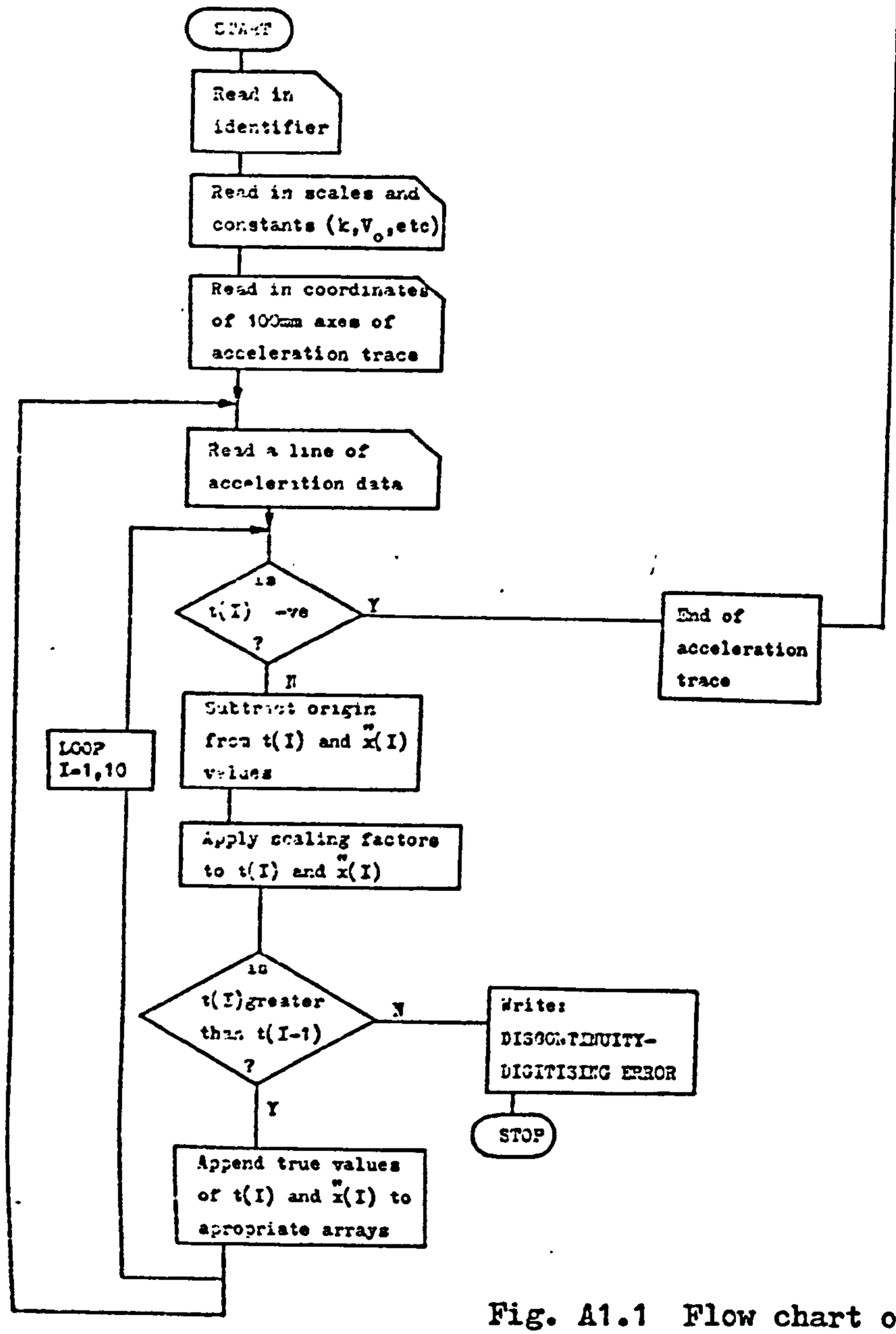

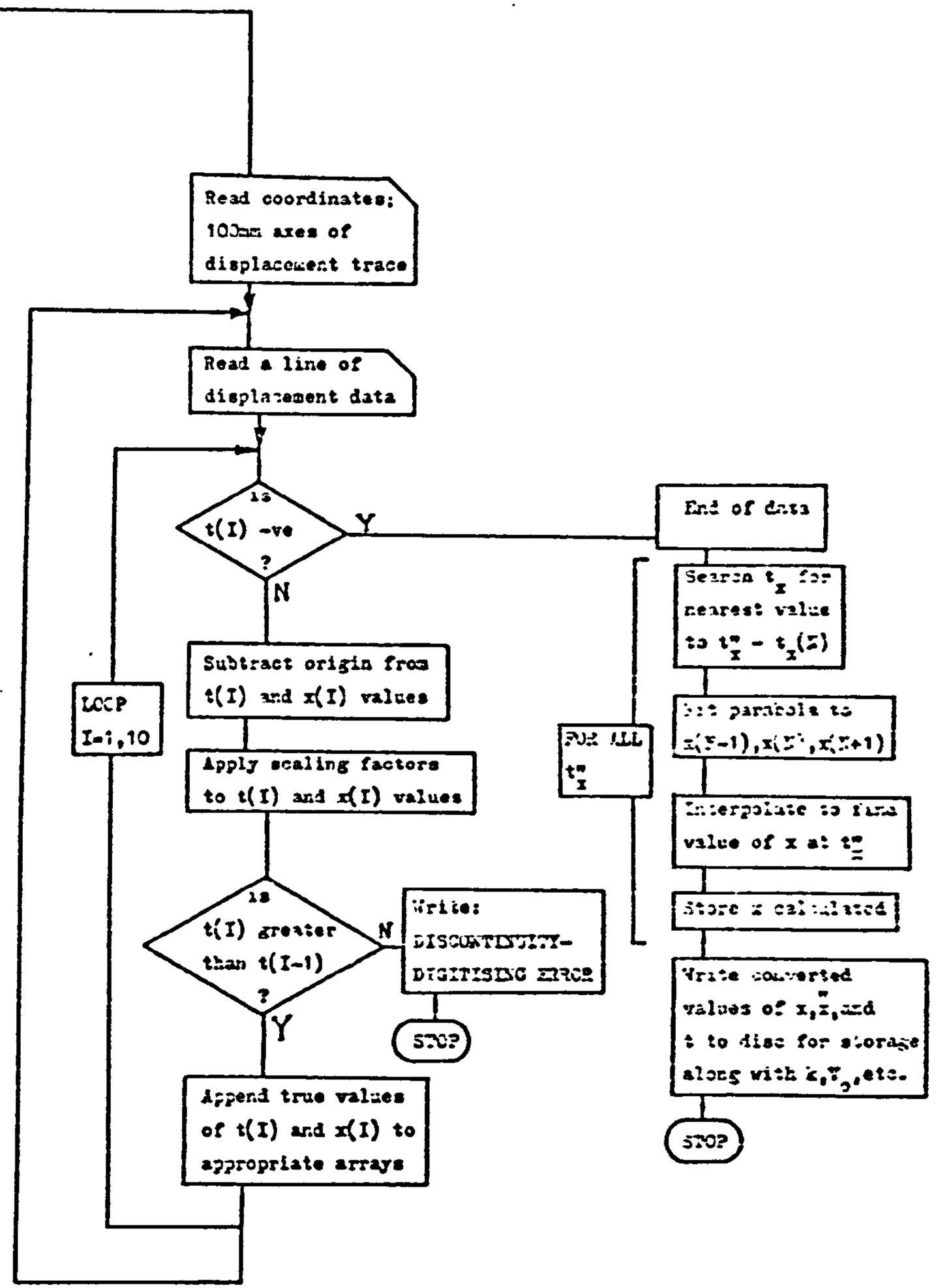

Fig. A1.1 Flow chart of the Data Preparation programme

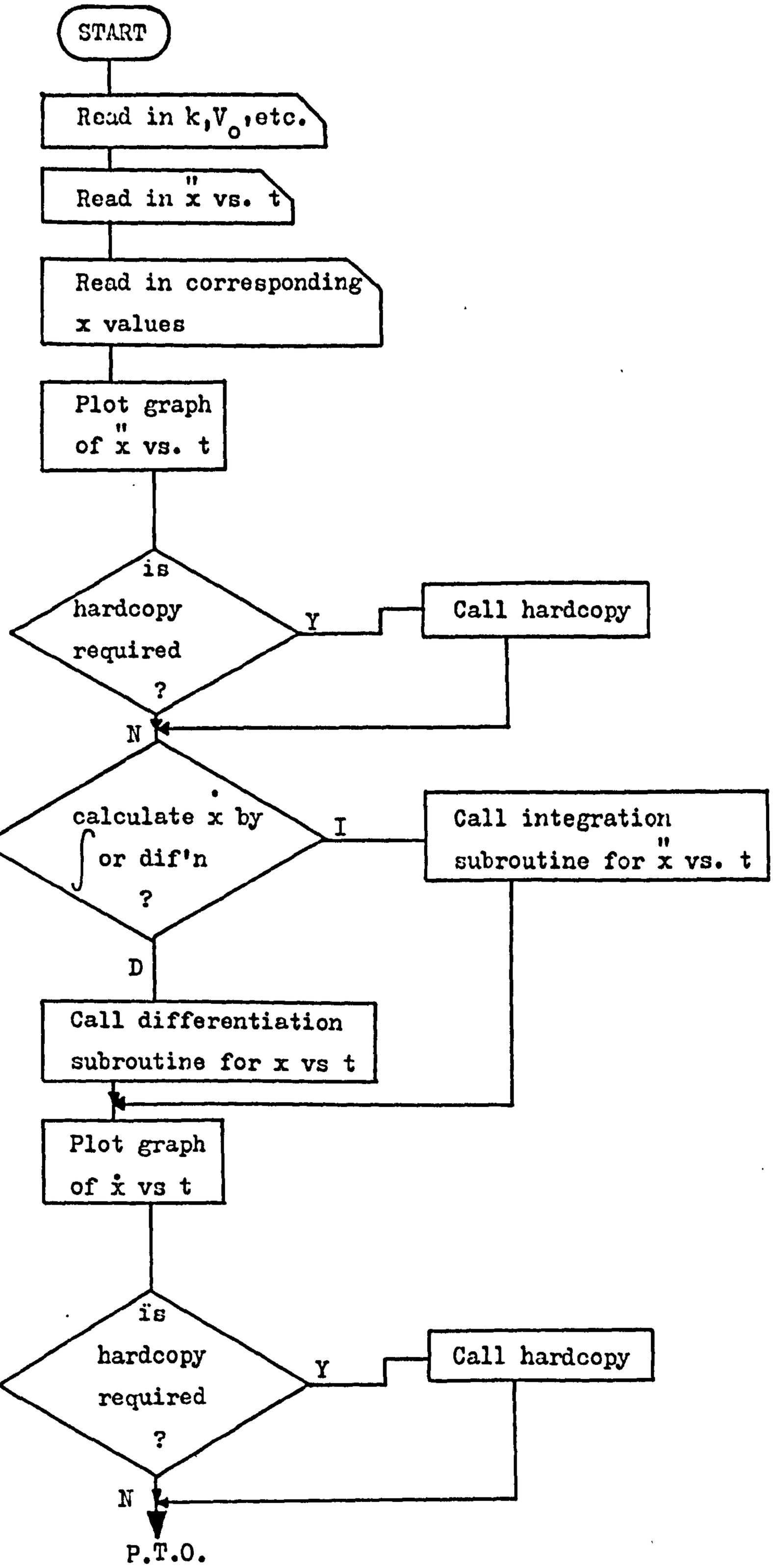

Fig. A1.2a Flow chart of the experimental analysis programme

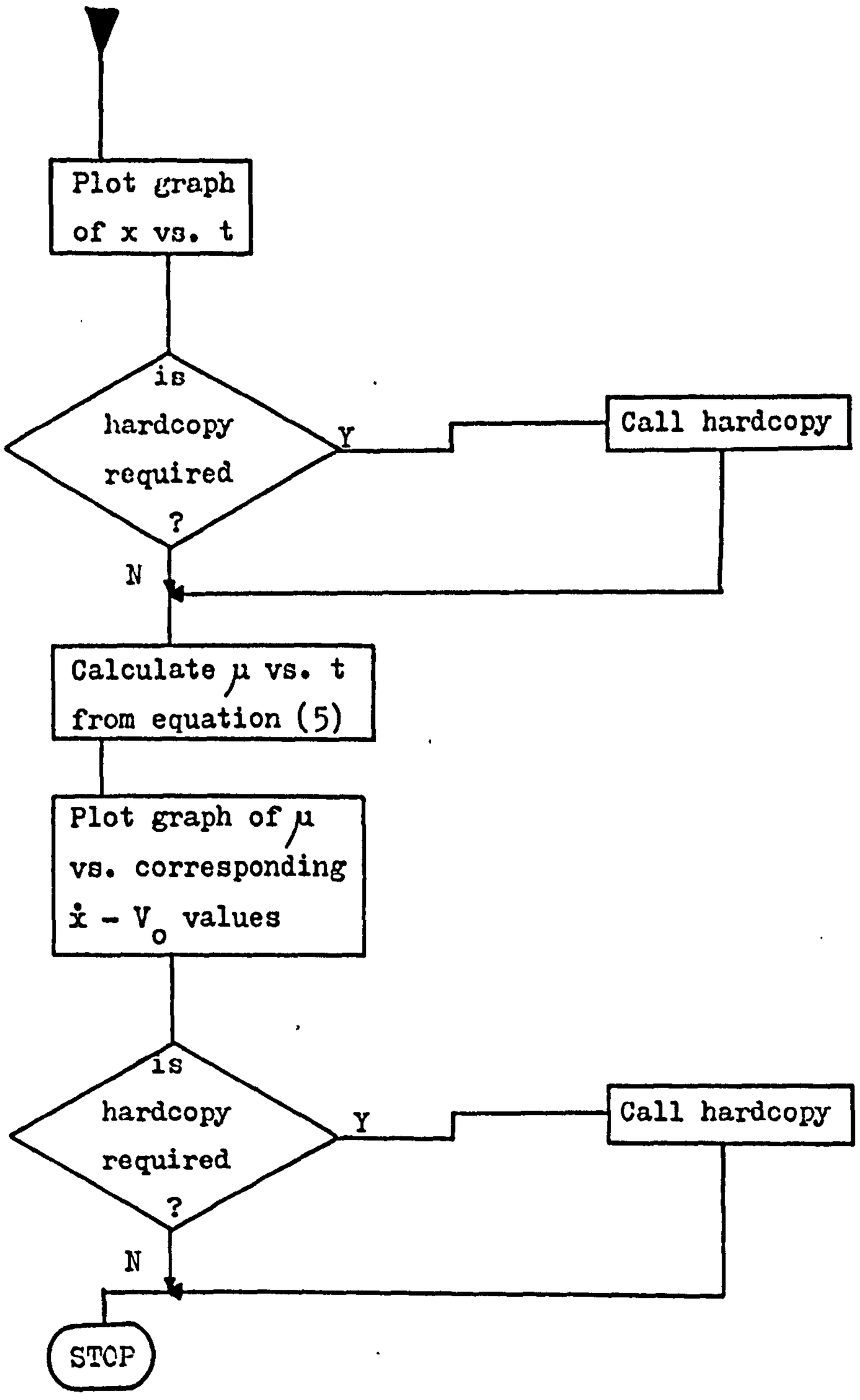
Plot graph of x vs. t
is hardcopy required ?
Y
Call hardcopy
N
Calculate μ vs. t from equation (5)
Plot graph of μ vs. corresponding ẋ - V_o values
is hardcopy required ?
Y
Call hardcopy
N
STOP

Fig. A1.2b

```
      PROGRAM SUS(INPUT=1318,TAPE5=INPUT,TAPE1=1318,TAPE2=1318,TAPE61=13
     +18,     TAPE64=1318,TAPE66=1318,OUTPUT=1318,TAPE20=1318)
C
C
C     ***************************************************************
C     *                                                             *
C     *          STICK-SLIP EXPERIMENTAL DATA ANALYSIS PROGRAMME    *
C     *                                                             *
C     *   THIS PROGRAMME TAKES DATA FROM AN EXPERIMENT ON STICK-SLIP *
C     *   CONDUCTED, FOR EXAMPLE, ON A BOWDEN-LEBEN MACHINE, AND SOLVES *
C     *   THE EQUATION OF MOTION OF THE SLIDER TO FIND THE VARIATION *
C     *   OF THE COEFFICIENT OF FRICTION WITH VELOCITY.             *
C     *                                                             *
C     *   THIS EQUATION OF MOTION IS:                               *
C     *                                                             *
C     *                    XM*A+XX*X=FMUX*XL .....(1)               *
C     *                                                             *
C     *   WHERE                                                     *
C     *          XM   IS THE MASS OF THE SLIDER                     *
C     *          A    IS THE ACCELERATION AT ANY INSTANT            *
C     *          XX   IS THE STIFFNESS OF THE RESTRAINING SPRING    *
C     *          X    IS THE DISPLACEMENT OF THE SLIDER AT ANY INSTANT *
C     *          FMUX IS THE FRICTION COEFFICIENT AT ANY INSTANT    *
C     *   AND    XL   IS THE NORMAL FORCE SQUASHING THE SLIDING     *
C     *                              COMPONENTS TOGETHER.           *
C     *                                                             *
C     ***************************************************************
C
C
      DIMENSION X(202),T(202),V(202),A(202),FMUX(202),DUMMY(202)
      LOGICAL NC,ND,NE
      REWIND 1,2
      NE=.F.
      G=9810.
      PIE=3.141592654
C
C     *   START INTERACTIVE GRAPHICS.......
C
      CALL START(2)
C
C     *   TURN ON MICROFILM HARDCOPIER......
C
      CALL SWITCH(9HHARDCPYON)
      CALL NEWPAGE
C
C     *   READ IN EXPERIMENTAL DATA: ACCELERATION AND DISPLACEMENT VS. TIME....
C
      CALL READER1(T,X,A,N,NC,INAME,V0,F,XX,XL,V1)
      V(1)=V1
C
C     *   PLOT GRAPH OF ACCELERATION VS. TIME....
C
      CALL GRAF(T,A,N,1.0,10HTIME(SECS),10,17HACCELEROMETER O/P,17,18.,1
     +2.)
      CALL SYMBOL(1.,0.3,.5,INAME,0.,10)
      CALL PROMPT(8HHARDCOPY,8)
      READ(5,1000) IRESP
 1000 FORMAT (A1)
      IF(IRESP.EQ.1HN) GO TO 3
      NE=.T.
      CALL HARDCPY
    3 CONTINUE
```

```
      IF(NC)GO TO 4
C
C     *   DECIDE UPON METHOD OF GENERATION OF VELOCITY TRACE.....
C
      CALL PROMPT(50HSHALL I GENERATE VELOCITY BY INTEGRATION OR DIFFERE
     +NTIATION,50)
      READ(5,1000)IRESP
      IF(IRESP.EQ.1HI)GO TO 4
C
C     *   DIFFERENTIATE DISPLACEMENT TO GIVE VELOCITY.....
C
      CALL DIF(T,X,DUMMY,N)
      DO 5 I=1,N
    5 V(I)=DUMMY(I)
C
C     *   PLOT GRAPH OF VELOCITY VS. TIME.......
C
    7 CALL GRAF(T,V,N,1.0,10HTIME(SECS),10,14HVELOCITY(MM/S),14,18.,12.)
     +
      CALL SYMBOL(1.,0.3,.5,INAME,0.,10)
      CALL PROMPT(8HHARDCOPY,8)
      READ(5,1000)IRESP
      IF(IRESP.EQ.1HN)GO TO 6
      ME=.T.
      CALL HARDCPY
      GO TO 6
C
C     *   INTEGRATE ACCELERATION TO GIVE VELOCITY....
C
    4 CALL INTX(T,A,V,N)
      GO TO 7
    6 IF(NC)GO TO 8
      GO TO 9
C
C     *   IF THERE IS NO DISPLACEMENT TRACE INTEGRATE THE VELOCITY TRACE
C     *   TO GIVE DISPLACEMENT. THIS IS NOT VERY RELIABLE......
C
    8 CALL INTX(T,V,X,N)
C
C     *   PLOT GRAPH OF DISPLACEMENT VS. TIME.......
C
    9 CALL GRAF(T,X,N,1.0,10HTIME(SECS),10,16HDISPLACEMENT(MM),16,18.,12
     +.)
      CALL SYMBOL(1.,0.3,.5,INAME,0.,10)
      CALL PROMPT(8HHARDCOPY,8)
      READ(5,1000)IRESP
      IF(IRESP.EQ.1HN)GO TO 10
      ME=.T.
      CALL HARDCPY
C
C     *   CALCULATE RELATIVE VELOCITY BETWEEN SLIDING SURFACES....
C
   10 DO 11 I=1,N
   11 V(I)=VO-V(I)
C
C     *   CALCULATE EFFECTIVE MASS OF THE SLIDER FROM ITS RESONANT FREQUENCY.
C     *   THIS IS GOVERNED BY THE EQUATIONO  F=(1/2*PIE)*(XK/XM)**0.5 ......
C
      XM=(XK*1000.)/(4.*((PIE*F)**2))
C
C     *   SOLVE EQUATION (1) FOR FRICTION COEFFICIENT.......
C
      DO 12 I=1,N
   12 FMUX(I)=(XM*A(I)/1000.+XK*X(I))/XL
```

```
C
C    *   PLOT GRAPH OF FRICTION VS. VELOCITY.....
C
      CALL GRAF(V,FMUX,N,1.0,14HVELOCITY(MM/S),14,14HFRICTION COEF.,14,1
     +0.,12.)
      CALL SYMBOL(1.,0.3,.5,INAME,0.,10)
      CALL PROMPT(8HHARDCOPY,8)
      READ(5,1000) IRESP
      IF(IRESP.EQ.1HN) GO TO 13
      NE=.T.
      CALL HARDCPY
C
C    *   WRITE FRICTION/VELOCITY CHARACTERISTIC TO FILE TAPE2.....
C
   13 WRITE(2,2000) INAME
 2000 FORMAT(A10)
      WRITE(2,) N
      DO 14 I=1,N
   14 WRITE(2,) V(I),FMUX(I)
C
C    *   IF MICROFILM HARDCOPY HAS BEEN GENERATED GIVE REMINDER TO
C    *   QUEUE IT FOR PROCESSING.....
C
      IF(NE)CALL PROMPT(34HCA-1LL POST-1P-1R0-1CESSORO-PROC61,34)
      STOP
      END
      SUBROUTINE INTX(X,Y,YI,N)
C
C    ***********************************************************************
C    *                                                                     *
C    *         THIS SUBROUTINE INTEGRATES A FUNCTION, Y=Y(X) AND           *
C    *         PUTS THE RESULT IN YI.                                      *
C    *                                                                     *
C    ***********************************************************************
C
      DIMENSION X(202),Y(202),YI(202)
      LOGICAL NZ
      NZ=.T.
      CALL PROMPT(42HSHALL I CORRECT FOR OFFSETS IN INTEGRATION,42)
      READ(5,1000) IRESP
 1000 FORMAT(A1)
      IF(IRESP.EQ.1HY) NZ=.F.
   10 DO 1 I=2,N
C
C    *   FIT A PARABOLA TO THE CURVE AND SUM THE AREA UNDER IT.....
C
      CALL QUADINT(N,AA,BB,CC,I,X,Y,AREA)
    1 YI(I)=YI(I-1)+AREA
C
C    *   RETURN IF CORRECTION NOT REQUIRED.....
C
      IF(NZ) RETURN
C
C    *   CALCULATE RMS VALUE OF INTEGRAL.....
C
      SUM=0.
      DO 2 I=1,N
    2 SUM=SUM+(YI(I)*YI(I))
      SUM=SQRT(SUM/FLOAT(N))
C
C    *   FIND DIFFERENCE BETWEEN ORDINATE VALUES AT THE BEGINNING AND
C    *   END OF THE CURVE. IF THERE WERE NO ERROR AND THE CURVE WERE A
C    *   PRECISE NUMBER OF WAVELENGTHS LONG THIS DIFFERENCE WOULD BE 0.
C    *   ITS ACTUAL VALUE REPRESENTS THE SLOPE ON THE INTEGRAL CAUSED BY
```

```
C    *   A SMALL OFFSET IN THE INTEGRAND.
C
      ERROR=YI(N)-YI(1)
C
C    *   IF ERROR IS LESS THAN 3 PERCENT OF RMS VALUE RETURN.....
C
      IF(ABS(ERROR).LT.0.03*SUM) RETURN
C
C    *   CALCULATE OFFSET IN INTEGRAND THAT IS CAUSING THE ERROR RAMP.....
C
      AER=ERROR/(X(N)-X(1))
C
C    *   SUBTRACT OFFSET......
C
      DO 3 I=1,N
    3 Y(I)=Y(I)-AER
C
C    *   LOOP BACK AND RE-EVALUATE INTEGRAL.....
C
      GO TO 10
      END
      SUBROUTINE DIF(X,Y,DY,N)
C
C    ************************************************************************
C    *                                                                      *
C    *          THIS SUBROUTINE EVALUATES THE DERIVATIVE OF A               *
C    *          FUNCTIONO  Y=Y(X) , AND PUTS THE RESULT IN DY.              *
C    *                                                                      *
C    ************************************************************************
C
      DIMENSION X(202),Y(202),DY(202)
      DO 1 I=1,N
C
C    *   FIT A PARABOLA TO THE DIFFERAND......
C
      CALL QUADINT(N,AA,BB,CC,I,X,Y,AREA)
C
C    *   CALCULATE DERIVATIVE OF PARABOLA.....
C
    1 DY(I)=2.*AA*X(I)+BB
      RETURN
      END
      SUBROUTINE READER1(T,X,A,N,MC,INAME,VO,F,XK,XL,V1)
C
C    ************************************************************************
C    *                                                                      *
C    *            THIS SUBROUTINE READS IN THE EXPERIMENTAL DATA            *
C    *                                                                      *
C    ************************************************************************
C
      DIMENSION A(202),X(202),T(202)
      LOGICAL MC
C
C    *   INAME IS A 10 CHARACTER IDENTIFIER.....
C
      READ(1,1) INAME
      MC=.F.
    1 FORMAT(A10)
      READ(1,) VO,F,XK,XL,V1,X(1)
C
C    *   VO IS THE CARRIAGE VELOCITY IN MM/S. F IS THE RESONANT FREQUENCY
C    *   OF THE SYSTEM IN HZ. XK IS THE SPRING STIFFNESS IN KGF/MM. XL IS THE
C    *   LOAD ON THE SYSTEM IN KGF. V1 IS THE SLIDER VELOCITY AT THE START
C    *   OF THE DATA AND X(1) IS THE DISPLACEMENT AT THE START.
```

```
C    *   N IS THE NUMBER OF POINTS OF DATA AND WLEN IS THE DATA
C    *   PERIOD IN SECONDS.
C
      READ(1,)N,WLEN
C
C    *   READ IN THE ACCELERATION TRACE....
C
      DO 3 I=1,N
    3 READ(1,)T(I),A(I)
C
C    *   CHECK FOR PRESENCE OF DISPLACEMENT TRACE.....
C
      READ(1,)IA
      IF(IA.EQ.1)GO TO 44
      NC=.T.
      RETURN
C
C    *   READ IN DISPLACEMENT TRACE (TIME VALUES THE SAME AS FOR
C    *   ACCELERATION TRACE).....
C
   44 DO 4 I=1,N
    4 READ(1,)X(I)
      RETURN
      END
      SUBROUTINE QUADINT(N,AA,BB,CC,NP,X,Y,AREA)
C
C    ********************************************************************
C    *                                                                  *
C    *          THIS SUBROUTINE FITS A PARABOLA TO THE FUNCTION         *
C    *          Y=Y(X) .                                                *
C    *                                                                  *
C    *   THE PARABOLA FITTED IS OF THE FORM                             *
C    *                                                                  *
C    *                    AA*(X**2)+BB*(X)+CC=Y                         *
C    *                                                                  *
C    *   THE FITTING IS DONE BY CONSIDERING THE VALUES OF X AND Y AT    *
C    *   EITHER SIDE OF THE POINT AT WHICH THE VALUES OF AA,BB AND CC   *
C    *   ARE REQUIRED. THIS GIVES THREE SIMULTANEOUS EQUATIONS IN AA,   *
C    *   BB AND CC THAT CAN BE SOLVED FOR THESE PARABOLA COEFFICIENTS.  *
C    *                                                                  *
C    *   THIS ROUTINE ALSO EVALUATES THE AREA UNDER THE CURVE BETWEEN   *
C    *   THE POINTS X(N-1) AND X(N) USING THE INTEGRAL                  *
C    *                                                                  *
C    *            AA*(X**3)/3.+BB*(X**2)/2.+CC*(X                       *
C    *                                                                  *
C    ********************************************************************
C
      DIMENSION X(300),Y(300)
C
C    *   CHECK FOR ENDS OF THE CURVE....
C
      NN=NP
      NNN=0
      IF(N.NE.NN)GO TO 2
      NN=NN-1
      NNN=1
    2 CONTINUE
      IF(NN.NE.1)GO TO 77
      NN=2
      NNN=-1
   77 CONTINUE
C
C    *   COMPUTE X**2 COEFFICIENT, AA ........
C
```

```
      A1=(X(NN)**2-X(NN-1)**2)/(X(NN-1)-X(NN))
      A2=(X(NN+1)**2-X(NN-1)**2)/(X(NN-1)-X(NN+1))
      A3=(Y(NN-1)-Y(NN+1))/(X(NN-1)-X(NN+1))
      A4=(Y(NN-1)-Y(NN))/(X(NN-1)-X(NN))
      AA=(A3-A4)/(A1-A2)
C
C     *   COMPUTE X COEFFICIENT, BB.......
C
      B1=AA*(X(NN)**2-X(NN-1)**2)
      B2=Y(NN-1)-Y(NN)
      B3=X(NN-1)-X(NN)
      BB=(B1+B2)/B3
C
C     *   COMPUTE CONSTANT TERM, CC .......
C
      CC=Y(NN-1)-AA*(X(NN-1)**2)-BB*(X(NN-1))
C
C     COMPUTE AREA OF SEGIENT  NN-1 TO NN
C
      IF(NNN.EQ.-1)GO TO 88
      NN=NN+NNN
   88 A1=AA*(X(NN-1)**3)/3.+BB*(X(NN-1)**2)/2.+CC*(X(NN-1))
      A2=AA*(X(NN)**3)/3.+BB*(X(NN)**2)/2.+CC*(X(NN))
      AREA=A2-A1
      RETURN
      END
```

```
      PROGRAM THEORY(OUTPUT=1318,TAPE20=10018,TAPE8=OUTPUT
     +          ,TAPE40,TAPE82)
C
C
C     ***************************************************************************
C     *                                                                         *
C     *              THEORETICAL STICK-SLIP PREDICTION PROGRAMME                *
C     *                                                                         *
C     *   THIS PROGRAMME TAKES TWO SURFACE MAPS (PRODUCED ON A TALLYSURF        *
C     *   PDP 8 MAPPING SYSTEM) AND RUBS THEM TOGETHER.                         *
C     *                                                                         *
C     *   IT FIRST MOVES THE TWO MAPS GRADUALLY TOGETHER IN A VERTICAL          *
C     *   DIRECTION, CALCULATING THE REAL AREA OF CONTACT AS IT DOES SO.         *
C     *   WHEN THIS AREA IS JUST ABLE TO SUPPORT THE APPLIED LOAD IT STOPS      *
C     *   THE MOVEMENT AND ASSUMES THAT IT HAS REACHED AN EQUILIBRIUM           *
C     *   POSITION.                                                             *
C     *                                                                         *
C     *   IT THEN STARTS TO MOVE THE LOWER SURFACE HORIZONTALLY AT A            *
C     *   CONSTANT VELOCITY,VO. IT CONSIDERS THE UPPER SURFACE TO BE            *
C     *   RESTRAINED BY A SPRING OF STIFFNESS XX,WHICH STRETCHES UNDER          *
C     *   THE ACTION OF A FRICTION FORCE WHICH IS CALCULATED FROM THE           *
C     *   REAL AREA OF CONTACT. WHEN THE SPRING FORCE EXCEEDS THE FRICTION      *
C     *   FORCE SLIDING COMMENCES AT AN ACCELERATION PROPORTIONAL TO THE         *
C     *   DIFFERENCE BETWEEN THE SPRING FORCE AND THE FRICTION FORCE,AND        *
C     *   TO THE MASS OF THE UPPER SLIDING SURFACE,XM.                           *
C     *                                                                         *
C     *   IN ORDER TO EXPLAIN THE PHENOMENON OF STICK-SLIP IT IS NECESSARY      *
C     *   THAT FRICTION FORCE DECREASE WITH INCREASING RELATIVE VELOCITY.       *
C     *   IN ORDER THAT THIS MODEL SHOULD DISPLAY THIS BEHAVIOUR IT IS          *
C     *   ASSUMED THAT THE SURFACES MOVE APPART SLIGHTLY WITH INCREACING        *
C     *   RELATIVE VELOCITY. THUS REDUCING THE REAL AREA OF CONTACT AND         *
C     *   HENCE REDUCING FRICTION.                                              *
C     *                                                                         *
C     ***************************************************************************
C
      COMMON F(100,100),G(100,100),X(1000),XD(1000),XDD(1000),Q(1000
     +     ),H(1000),T(1000),N,N1,N2,XP,YP,C,XL,XX,XM,PC,PS,DELTA,VO,
     +D,TS,          F1(100,100),INDEX(11),MM,A,ENAT,CONV,ASM,H1,HMM
      LOGICAL PIX
      EXTERNAL RESPLOT
      CALL BNTRAP(RESPLOT)
C
C     *   SET UP RANDOM ACCESS MASS STORAGE FOR LARGE SURFACE MAP (IE THE
C     *   LOWER ONE).......
C
      CALL OPENMS(40,INDEX,11,0)
      REWIND 20,40
      A=0.
      ENAT=2.718281828
      D=0.
C
C     *   READ IN MAPS AND PUT LARGE MAP ON RAMS.....
C
      READ(20,)N1,N2
      P1=P2=-1000000000.
      V1=V2=1000000000.
      DO 1 I=1,N1
      DO 2 J=1,N1
      READ(20,)G(I,J)
      IF(G(I,J).GT.P2)P2=G(I,J)
    2 IF(G(I,J).LT.V2)V2=G(I,J)
    1 CONTINUE
```

```
      DO 3 I=1,10
      DO 4 J=1,100
      DO 44 K=1,100
      READ(20,)F(J,K)
      IF(F(J,K).GT.P1)P1=F(J,K)
      IF(F(J,K).LT.V1)V1=F(J,K)
   44 CONTINUE
    4 CONTINUE
    3 CALL WRITMS(40,F,10000,I)
C
C     *   XK IS THE SPRING STIFFNESS IN N/MM.XL IS THE LOAD IN N. XM IS THE
C     *   MASS IN KG.PC IS THE PLASTIC COMPRESSION MODULUS OF THE MATERIALS
C     *   UNDER CONSIDERATION. PS IS THE PLASTIC SHEAR MODULUS OF THE MATERIALS
C     *   BOTH OF THESE FIGURES ARE IN N/MM**2. C IS THE GRADIENT OF THE H
C     *   VS. V CURVE. DELTA IS THE SAMPLE WIDTH OF THE MAP IN MM. VO IS THE
C     *   CONSTANT VELOCITY OF THE LOWER SLIDING SURFACE IN MM/S. CONV IS
C     *   THE CONVERGENCE CRITERION FOR STICKING. PIX IS A LOGICAL VARIABLE
C     *   THAT CONTROLS THE PLOTTING OF CONTACT PATTERNS.
C     *
C     *   READ IN THESE NUMBERS.......
C
      READ(20,)XK,XL,XM,PC,PS,C,DELTA,VO,ASM,CONV,PIX
C
C     *   LOWER BOTTOM SURFACE TO MAKE IT ALL -VE.....
C
      DO 33 I=1,10
      CALL READMS(40,F,10000,I)
      DO 55 J=1,100
      DO 66 K=1,100
   66 F(J,K)=F(J,K)-P1
   55 CONTINUE
   33 CALL WRITMS(40,F,10000,I)
C
C     *   INVERT TOP SURFACE AND RAISE IT TO MAKE IT ALL +VE.......
C
      DO 7 I=1,N1
      DO 8 J=1,N1
    8 G(I,J)=P2-G(I,J)
    7 CONTINUE
      V1=V1-P1
      V2=P2-V2
C
C     *   HM IS THE GAP BETWEEN THE 'HIGHEST' VALLEY IN THE TOP SURFACE
C     *   AND THE LOWEST VALLEY IN THE BOTTOM SURFACE.
C
      HM=V2-V1
      HMM=HM/1000.
      N=1
C
C     *   MOVE SURFACES TOGETHER UNTIL REAL CONTACT AREA IS JUST ABLE TO
C     *   SUPPORT THE APPLIED LOAD.......
C
      DO 9 I=1,1000
      MMM=-2
      H(1)=HMMM*FLOAT(I)
      CALL AREA(.F.)
      IF(PC*A.GE.XL)GO TO 10
    9 CONTINUE
   10 REWIND 20
      H1=H(1)
C
C     *   F1 CONTAINS THE STATIC CONTACT PATTERN: STORE IT FOR LATER PLOTTING...
C
      WRITE(20)F1
```

```
      REWIND 20
C
C   *   SET INITIAL CONDITIONS: X IS HORIZONTAL DISPLACEMENT,XD IS HORIZ.
C   *   VELOCITY, XDD IS HORIZ. ACCELERATION, Q IS THE FRICTION FORCE,
C   *   T IS THE TIME, TS IS THE TIME STEP.....
C
      X(1)=0.
      Q(1)=0.
      XDD(1)=0.
      XD(1)=VO
      T(1)=0.
      TS=DELTA/(VO*5.)
      WRITE(6,1000)
 1000 FORMAT(*D N        T             X             XD            XDD           H
     +                Q*)
C
C   *   MARCH PROBLEM FORWARD 999 TIME STEPS, OR UNTIL IT FALLS OFF THE EDGE
C   *   OF ITS WORLD, WHICHEVER IS SOONER....
C
   13 N=N+1
      CALL MARCH(PIX)
      IF(N.GE.999.OR.D.GE.(DELTA*FLOAT(N2-N1)))GO TO 14
      GO TO 13
C
C   *   PLOT OUT RESULTS......
C
   14 CALL RESPLOT
      STOP
      END
      SUBROUTINE RESPLOT
C
C   ***********************************************************************
C   *                                                                     *
C   *          THIS SUBROUTINE PLOTS GRAPHS OF THE ANSWERS                *
C   *          OBTAINED ONTO MICROFILM.                                   *
C   *                                                                     *
C   ***********************************************************************
C
      COMMON F(100,100),G(100,100),X(1000),XD(1000),XDD(1000),Q
     +       (1000),H(1000),T(1000),N,N1,N2,XP,YP,C,XL,XX,XM,PC,PS,DELT
     +A,VO,D,TS,      F1(100,100),INDEX(11),MMM,A,ENAT,CONV,ASM,H1,HMM
      N=N-1
C
C   *   SET UP MICROFILM PLOTTER......
C
      CALL START35
C
C   *   WRITE FRICTION CONDITIONS ONTO FIRST MICROFILM FRAME.....
C
      CALL SYMBOL(0.,12.,0.2,58HSTIFNESS  LOAD  MASS  COMP  SHEAR  C   G
     +RID  VO  CONV  ASM,0.,58)
      CALL NUMBER(0.,11.,0.2,XX,0.,4)
      CALL NUMBER(2.,11.,0.2,XL,0.,4)
      CALL NUMBER(4.,11.,0.2,XM,0.,4)
      CALL NUMBER(6.,11.,0.2,PC,0.,4)
      CALL NUMBER(8.,11.,0.2,PS,0.,4)
      CALL NUMBER(10.,11.,0.2,C,0.,4)
      CALL NUMBER(12.,11.,0.2,DELTA,0.,4)
      CALL NUMBER(14.,11.,0.2,VO,0.,4)
      CALL NUMBER(16.,11.,0.2,CONV,0.,4)
      CALL NUMBER(18.,11.,0.2,ASM,0.,4)
      CALL NEWPAGE
C
C   *   READ BACK INITIAL CONTACT PATTERN STORED PREVIOUSLY AND....
```

```
C
      READ(20)F1
      XP=20.5
      YP=15.5
      D=0.
C
C     *    ..... DRAW IT OUT...
C
      CALL DRAW
      CALL NEWPAGE
C
C     *    PLOT GRAPHS OF RESULTS.......
C
      CALL GRAF(T,X,N,1,0,10HTIME(SECS),10,16HDISPLACEMENT(MM),16,18.,12
     +.)
      CALL GRAF(T,XD,N,1,0,10HTIME(SECS),10,14HVELOCITY(MM/S),14,18.,12.
     +)
      CALL GRAF(T,XDD,N,1,0,10HTIME(SECS),10,21HACCELERATION(MM*S**-2),21
     +,18.,12.)
      CALL GRAF(T,H,N,1,0,10HTIME(SECS),10,25HVERTICAL DISPLACEMENT(MM),
     +25,18.,12.)
C
C     *    SET UP FRICTION VS. VELOCITY GRAPH.....
C
      VMAX=-100000000.
      DO 17 I=1,N
      XD(I)=VO-XD(I)
      IF(ABS(XD(I)).GT.VMAX)VMAX=ABS(XD(I))
   17 Q(I)=Q(I)/XL
C
C     *    .....AND PLOT IT....
C
      CALL GRAF(XD,Q,N,1,0,17HVELOCITY(MM*S**-1),17,14HFRICTION COEF.,14,
     +18.,12.)
C
C     *    SET UP SEPARATION VS. VELOCITY GRAPH.......
C
      XD(1)=0.
      VINC=VMAX/100.
      DO 100 I=1,100
      VEL=XD(I)
      H(I)=SEP(ASM,ENAT,VO,VEL,C,H1)
  100 XD(I+1)=XD(I)+VINC
C
C     *    ..... AND PLOT IT......
C
      CALL GRAF(XD,H,100,1,0,14HVELOCITY(MM/S),14,1HH,1,18.,12.)
C
C     *    ALL RESULTS RECORDED SO STOP MICROFILM PLOTTER AND THEN STOP
C     *    EXECUTION......
C
      CALL ENPL035
      STOP
      END
      SUBROUTINE AREA(PIX)
C
C     ***********************************************************
C     *                                                         *
C     *          THIS SUBROUTINE WORKS OUT THE REAL CONTACT AREA*
C     *          BETWEEN THE TWO SURFACES, GIVEN A VERTICAL SEPARATION,*
C     *          H, AND A HORIZONTAL DISPLACEMENT, D.           *
C     *                                                         *
C     ***********************************************************
C
```

```
      COMMON F(100,100),G(100,100),X(1000),XD(1000),XDD(1000),Q
     +       (1000),H(1000),T(1000),N,N1,N2,XP,YP,C,XL,XX,XM,PC,PS,DELT
     +A,VO,D,TS,      F1(100,100),INDEX(11),MMM,A,ENAT,CONV,ASM,H1,HMM
      LOGICAL PIX,SAME
      SAME=.F.
      AA=A
      A=0.
C
C    *   DETERMINE IF THERE HAS BEEN ANY RELATIVE MOVEMENT BETWEEN THE
C    *   SURFACES SINCE THIS SUBROUTINE WAS LAST CALLED......
C
      MM=INT(D/DELTA)+1
      IF(MM-1.EQ.MMM)SAME=.T.
      IF(N.EQ.1)GO TO 987
      IF(H(N).NE.H(N-1))SAME=.F.
  987 CONTINUE
      MMM=MM-1
C
C    *   IF THERE HAS BEEN NO RELATIVE MOVEMENT SKIP TO THE END OF THIS
C    *   SUBROUTINE.....
C
      IF(SAME)GO TO 200
      IREC1=(MMM*10)/1000+1
      IREC2=IREC1+1
C
C    *   IF MOVEMENT IS SUCH AS TO OVERRUN THE END OF THE MAP, PLOT THE
C    *   RESULTS SO FAR AND STOP.....
C
      IF(IREC2.GT.10)CALL RESPLOT
C
C    *   READ IN THE TWO ADJACENT SECTIONS OF THE MAP WHICH CONTAIN THE DES-
C    *   IRED SECTION.....
C
      CALL READMS(40,F,10000,IREC1)
      CALL READMS(40,F1,10000,IREC2)
C
C    *   EXTRACT THE DESIRED SECTION.....
C
      MM=MOD(MM,100)
      IF(MM.EQ.0)MM=100
      MM1=MM-1
      MM2=101-MM
      DO 4 I=1,MM2
      DO 5 J=1,100
    5 F(I,J)=F(I+MM1,J)
    4 CONTINUE
      IF(MM.EQ.1)GO TO 66
      DO 44 I=1,MM1
      DO 55 J=1,100
   55 F(I+MM2,J)=F1(I,J)
   44 CONTINUE
   66 CONTINUE
C
C    *   CALCULATE THE REAL AREA OF CONTACT.....
C
      DO 1 I=1,N1
      DO 2 J=1,N1
C
C    *   ZERO F1 SO THAT THE.....
C
      F1(I,J)=0.
      GG=G(I,J)-H(N)
      IF(GG.GT.F(I,J))GO TO 2
C
```

```
C    *    .....CONTACT PATTERN CAN BE PUT IN IT (F1 IS NO LONGER IN USE)....
C
     3 F1(I,J)=1.
       A=A+1.
     2 CONTINUE
     1 CONTINUE
   200 IF(PIX)CALL DRAW
       IF(SAME)A=AA
       IF(SAME)RETURN
       A=A*DELTA*DELTA
       RETURN
       END
       SUBROUTINE DRAW
C
C    ***************************************************************************
C    *                                                                         *
C    *              THIS SUBROUTINE DRAWS OUT THE CONTACT PATTERN              *
C    *                                                                         *
C    ***************************************************************************
C
       COMMON F(100,100),G(100,100),X(1000),XD(1000),XDD(1000),D
      +       (1000),H(1000),T(1000),M,N1,N2,XP,YP,C,XL,XK,XM,PC,PS,DELT
      +A,V0,D,TS,      F1(100,100),INDEX(11),MMM,A,ENAT,CONV,ASM,H1,HMM
       CALL NEWPAGE
       XMIC=0.1
       Z=YP/FLOAT(N1)
       DO 1 I=1,N1
       Y=FLOAT(I)*Z
       DO 2 J=1,N1
       XX=FLOAT(J)*Z
C
C    *    F1 CONTAINS THE CONTACT PATTERN. WHENEVER IT IS 1.0 DRAW A
C    *    LITTLE SQUARE AT XX,Y TO REPRESENT THE CONTACT......
C
     2 IF(F1(I,J).GT.0.5)CALL SQUARE(XX,Y,Z)
     1 CONTINUE
C
C    *    WRITE THE ELAPSED TIME AT ONE SIDE OF THE MICROFILM FRAME......
C
       CALL NUMBER(YP+0.25,YP-0.75,0.35,T(N),0.,4)
       CALL PLOT(YP,0.,-3)
C
C    *    DRAW A SERIES OF LINES 0.1MM APART DOWN ONE SIDE OF THE PATTERN TO
C    *    GIVE A SCALE TO THE PICTURE......
C
       SC=YP/(FLOAT(N1)*DELTA)
       GAP=SC*XMIC
       NUM=INT(D/XMIC)+1
       ST=(FLOAT(NUM)*XMIC-D)*SC-GAP
     3 ST=ST+GAP
       IF(ST.GT.YP-1.)RETURN
       CALL PLOT(0.,ST,3)
       CALL PLOT(1.,ST,2)
       GO TO 3
       END
       SUBROUTINE SQUARE(X,Y,Z)
C
C    ***************************************************************************
C    *                                                                         *
C    *        THIS SUBROUTINE DRAWS THE LITTLE SQUARES MENTIONED               *
C    *        ABOVE. THEY HAVE A SIDE OF LENGTH Z AND ARE PLOTTED              *
C    *        AT THE POINT X,Y.                                                *
C    *                                                                         *
C    ***************************************************************************
```

```
C
      X1=X-Z/2.
      Y1=Y-Z/2.
      X2=X1+Z
      Y2=Y1+Z
      CALL PLOT(X1,Y1,3)
      CALL PLOT(X1,Y2,2)
      CALL PLOT(X2,Y2,2)
      CALL PLOT(X2,Y1,2)
      CALL PLOT(X1,Y1,2)
      RETURN
      END
      SUBROUTINE MARCH(PIX)
C
C     ***************************************************************************
C     *                                                                         *
C     *        THIS SUBROUTINE MARCHES THE MODEL FORWARD IN TIME                *
C     *        USING A SIMPLE EULER TECHNIQUE. THAT IS TO SAY THAT,             *
C     *        IN ORDER TO FIND THE VALUE OF SOME VARIABLE, P, AT A             *
C     *        TIME T(N), THE VALUE OF DP/DT AT T(N-1) IS MULTIPLIED            *
C     *        BY THE TIMESTEP,TS (TS=T(N)-T(N-1)), AND THE RESULT IS           *
C     *        IS ADDED TO THE VALUE OF P AT T(N-1).                            *
C     *                                                                         *
C     ***************************************************************************
C
      COMMON F(100,100),G(100,100),X(1000),XD(1000),XDD(1000),Q
     +       (1000),H(1000),T(1000),N,N1,N2,XP,YP,C,XL,XK,XM,PC,PS,DELT
     +A,VO,D,TS,      F1(100,100),INDEX(11),MM1,A,ENAT,CONV,ASM,H1,HMM
      LOGICAL PIX
C
C     *   WRITE OUT THE VALUES OBTAINED AT THE LAST TIME STEP.......
C
      WRITE(6,1000)N-1,T(N-1),X(N-1),XD(N-1),XDD(N-1),H(N-1),Q(N-1)
 1000 FORMAT(1HO,I3,6(1X,E11.5))
C
C     *   INCREMENT THE TIME.......
C
      T(N)=T(N-1)+TS
C
C     *   MARCH FORWARD DISPLACEMENT AND VELOCITY USING EULER METHOD......
C
      X(N)=X(N-1)+XD(N-1)*TS
      XD(N)=XD(N-1)+TS*XDD(N-1)
C
C     *   CALCULATE RELATIVE MOVEMENT SO FAR.....
C
      D=T(N)*VO-X(N)
      IF(D.GE.0.)GO TO 2
C
C     *   WRITE WARNING IF ITS SLID TO FAR IN THE WRONG DIRECTION.....
C
      WRITE(6,) 'D=',D,' AT N=',N,' ++++WARNING---'
      D=0.
    2 VEL=XD(N)
C
C     *   WORK OUT SEPARATION WITH RELATIVE VELOCITY (IF ANY).....
C
      H(N)=SEP(ASM,ENAT,VO,VEL,C,H1)
C
C     *   STOP SURFACES FALLING TOGETHER IMMEDIATELY THEY HAVE MOVED APART
C     *   WHEN C& IS ACTIVATED.......
C
C&    IF(H(N).GT.H(N-1))H(N)=H(N-1)
C
```

```
C    *   WORK OUT REAL AREA OF CONTACT.......
C
       CALL AREA(PIX)
C
C    *   WORK OUT FRICTION FORCE......
C
       Q(N)=A*PS
C
C    *   IF THE RELATIVE VELOCITY IS -VE THE FRICTION MUST BE -VE......
C
       IF(VO-XD(N).LT.0.)Q(N)=-Q(N)
C
C    *   CALCULATE THE ACCELERATION FROM THE RESULTANT OF THE SPRING
C    *   AND FRICTION FORCES.......
C
       XDD(N)=(Q(N)-XK*X(N))/XM †
C
C    *   IF THE RELATIVE VELOCITY DROPS BELOW THE CONVERGENCE CRITERION
C    *   AND THE FRICTION FORCE IS GREATER THAN THAT DUE TO THE SPRING
C    *   ASSUME THAT THE RELATIVE VELOCITY IS 0. IE THAT THE SURFACES
C    *   HAVE JUST 'STUCK'.......
C
       IF(ABS(VO-XD(N)).LT.CONV.AND.ABS(Q(N)).GT.ABS(XK*X(N)))GO TO 1
       RETURN
     1 XDD(N)=0.
       XD(N)=VO
       H(N)=H1
       RETURN
       END
       SUBROUTINE START35
C
C    ************************************************************************
C    *                                                                      *
C    *          THIS SUBROUTINE STARTS THE MICROFILM PLOTTER                *
C    *                                                                      *
C    ************************************************************************
C
       CALL START(2)
       RETURN
       END
       SUBROUTINE ENPL035
C
C    ************************************************************************
C    *                                                                      *
C    *           THIS SUBROUTINE STOPS THE MICROFILM PLOTTER                *
C    *                                                                      *
C    ************************************************************************
C
       CALL ENPLOT
       RETURN
       END
       FUNCTION SEP(A,E,VO,V1,C,H)
C
C    ************************************************************************
C    *                                                                      *
C    *         THIS FUNCTION ROUTINE GIVES THE SEPARATION OF THE            *
C    *         SURFACES FOR A GIVEN RELATIVE VELOCITY.                      *
C    *                                                                      *
C    ************************************************************************
C
       Z=1.-C*ABS(V1-VO)
       SEP=H*Z
C
C    *   SUPRESS SEPARATION WHEN C2 IS ACTIVATED.......
```

† This value of XDD should be multiplied by 1000. See p159

```
C
C<      SEP=H
        RETURN
        END
```

A1.4 The theoretical model

This was required to take two surface maps and to model the sliding of one over the other. A listing is given after the listing of the experimental analysis programme.

A1.5 The subtraction of the least squares fit plane from the surface map

The equation of a plane is:-

$$z(x,y) = ax + by + c \quad \ldots\ldots\ldots (28)$$

If the height values of the surface map are:-

$$\begin{bmatrix} z'(x_1,y_1) & z'(x_2,y_1) \ldots\ldots z'(x_n,y_1) \\ z'(x_1,y_2) \ldots\ldots & \\ & \\ z'(x_1,y_m) \ldots\ldots & \ldots\ldots z'(x_n,y_m) \end{bmatrix}$$

then it is required that:-

$$\sum = \sum_{\substack{i=0 \\ j=0}}^{n,m} \left[z(x_i,y_j) - z'(x_i,y_j) \right]^2 \quad \ldots\ldots\ldots (29)$$

be a minimum. That is to say that:-

$$\sum = \sum_{0}^{n,m} \left[a.x_i + b.y_j + c - z'(x_i,y_j) \right]^2 \quad \ldots.(30)$$

be a minimum.

Now, from equation (30):-

$$\frac{\partial \Sigma}{\partial a} = \sum_{0}^{n,m} 2x_i \left[ax_i + by_j + c - z'(x_i,y_j) \right] \quad \ldots\ldots (31)$$

$$\frac{\partial \Sigma}{\partial b} = \sum_{0}^{n,m} 2y_j \left[ax_i + by_j + c - z'(x_i,y_j) \right] \quad \ldots\ldots (32)$$

and

$$\frac{\partial \Sigma}{\partial c} = \sum_{0}^{n,m} 2 \left[ax_i + by_j + c - z'(x_i,y_j) \right] \ldots\ldots\ldots (33)$$

When all these partial derivatives are zero, the least squares function, equation 30, must be either a minimum or a maximum. As it is a second-order function, there can be only one such point.

If it was a maximum, $\sum$ would have to go negative. As it is the sum of a set of squares of real (as opposed to complex) numbers, this is impossible. The point must therefore be a minimum. So, from equations 31, 32 and 33:-

$$\left.\begin{aligned} 2\sum x_i\left[ax_i + by_j + c - z'(x_i,y_j)\right] &= 0 \\ 2\sum y_j\left[ax_i + by_j + c - z'(x_i,y_j)\right] &= 0 \\ 2\sum\left[ax_i + by_j + c - z'(x_i,y_j)\right] &= 0 \end{aligned}\right\} \quad \ldots\ldots\ldots (34)$$

Rearranging these gives:-

$$\left.\begin{aligned} a\sum x_i^2 + b\sum x_i.y_j + c\sum x_i &= \sum z'(x_i,y_j) \\ a\sum x_i.y_j + b\sum y_j^2 + c\sum y_j &= \sum z'(x_i,y_j) \\ a\sum x_i + b\sum y_j + c &= \sum z'(x_i,y_j) \end{aligned}\right\} \quad \ldots\ldots\ldots (35)$$

If the computer is programmed to give figures for the coefficients in these linear simultaneous equations in a, b and c:-

$\sum x_i^2$, $\sum y_j^2$, $\sum x_i.y_j$, $\sum x_i$, $\sum y_j$ and $\sum z'(x_i,y_j)$

the set of equations, 35, can be solved for a, b and c. The plane $z = ax + by + c$ can then be subtracted from the initial data, z', to remove any tilt that is present on it.

A programme to do this was written. When run, the values of a, b and c for the data (measurements in all directions in mm) were:-

$$a = 0.2595987369 \times 10^{-3}$$

$$b = -0.1122315892 \times 10^{-2}$$

$$c = 0.2046317951 \times 10^{-2}$$

When the plane represented by these coefficients had been subtracted from the data, the resulting, corrected data were run through the programme again as a check. The new values of a, b and c were:-

$$a = 0.1468912067 \times 10^{-15}$$

$$b = -0.1232249907 \times 10^{-13}$$

$$c = 0.2756116542 \times 10^{-14}$$

As can be seen, these values are similar to the truncation limit of the computer (10^{-14}). The least squares fit plane of the new data was, as required, the x,y plane.

APPENDIX TWO

ELECTRONIC CIRCUITS

A2.1 Strain gauge power supply

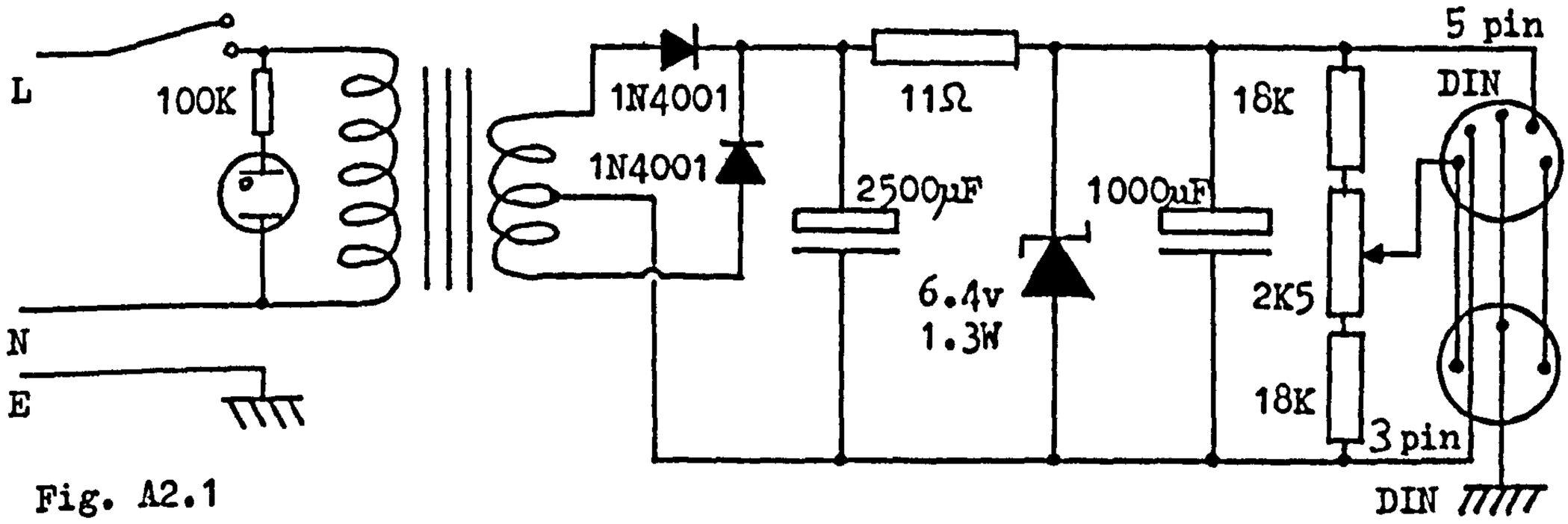

Fig. A2.1

A2.2 Charge Amplifier

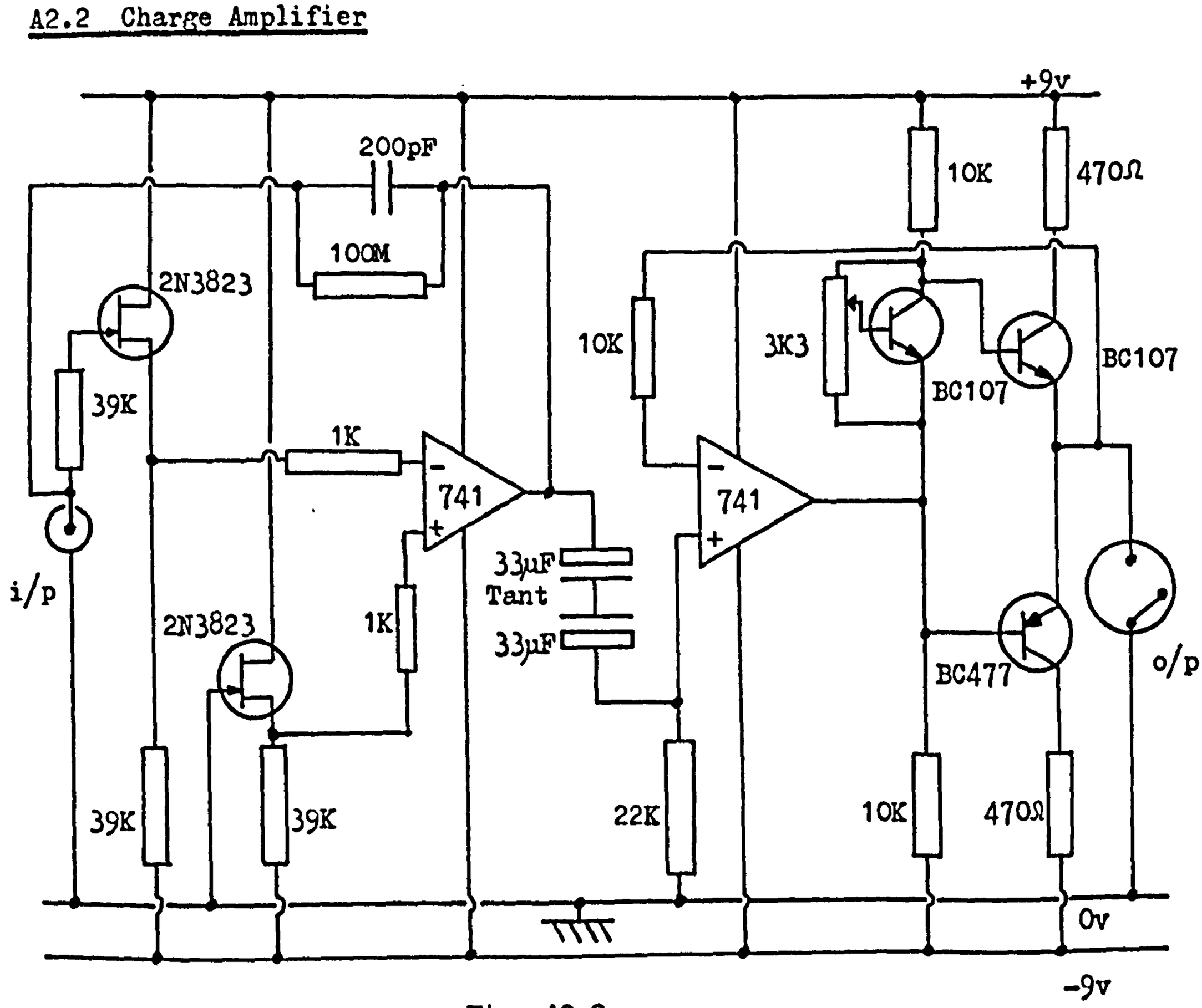

Fig. A2.2

A2.3 Linear variable displacement transducer (LVDT)

This device was used to calibrate the experimental apparatus (Chapter Two) and also forms the basis of the Talysurf machine (62).

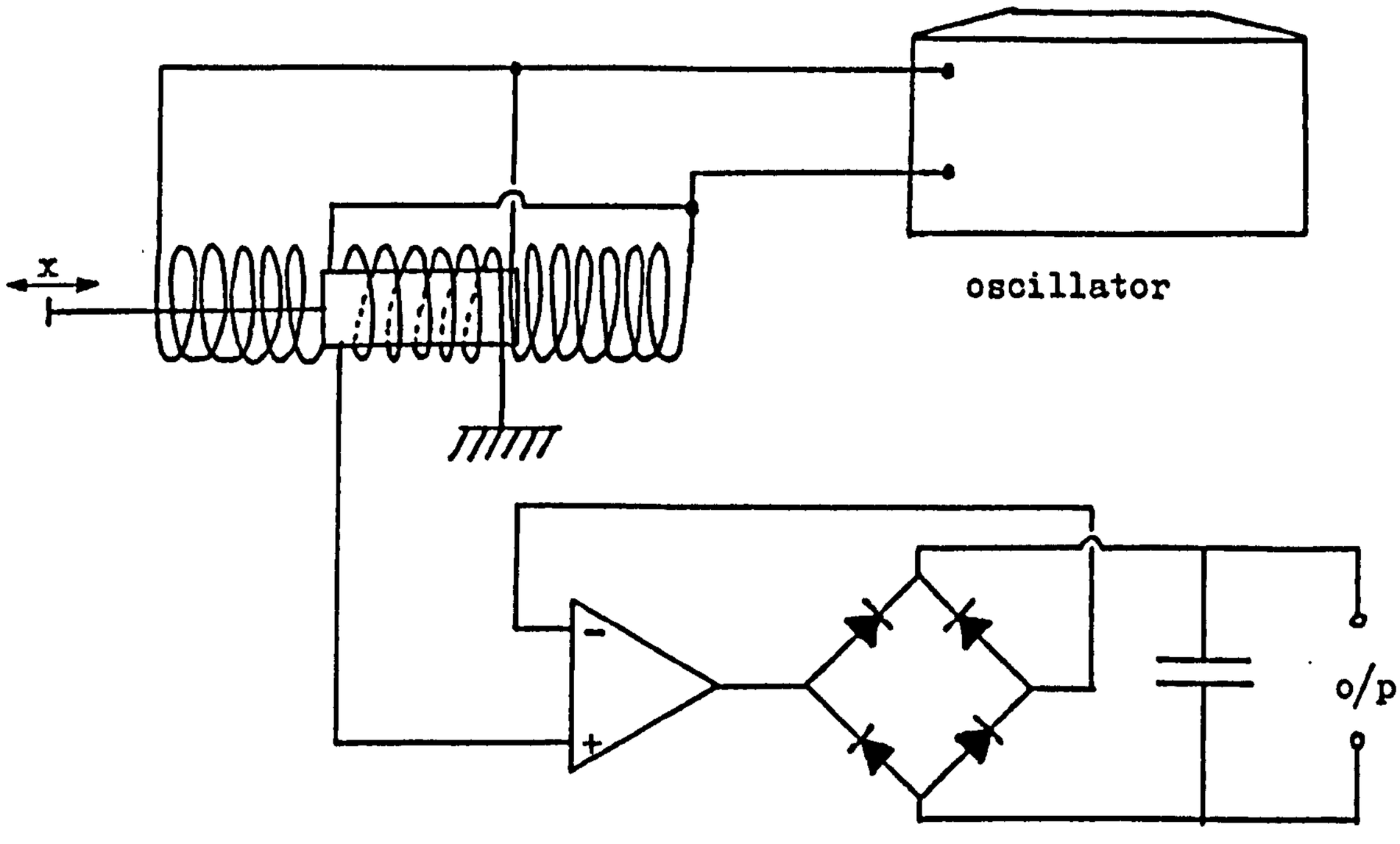

Fig. A2.3 LVDT

It comprises a variable transformer, the core of which is made to move through the displacement to be measured. The primary coils of the transformer form part of the resonant circuit of an oscillator. The voltage that appears on the secondary is rectified by a zero bias error rectifier to give a d.c. voltage which relies upon the mutual inductance of the system, which, in turn, relies upon the position of the core.

APPENDIX THREE

THE TALYSURF/PDP8 MAPPING SYSTEM

Fig. A3.1 General view of the Talysurf and PDP8

Figure A3.1 shows a general view of the system built by R. A. Hill and the author. The ADC and the quartz crystal timing circuitry were mounted in a CAMAC crate interfaced to the PDP8 mainframe. The timer was enabled by a microswitch in the Talysurf head. This ensured that the sampling of a surface profile began at the same point on each pass.

The controlling programme was written in PAL assembly language. The resolution of the ADC (i.e. the number of bits that a conversion comprised) could be set interactively before a profile was recorded. For this work, the resolution was set to 4,096 (12 bits). The sampling rate and the number of samples required could also be varied.

When a profile had been taken and was stored in the computer's memory, it was written out to the teletype and its associated paper tape punch in octal. The listing below shows a typical profile of three hundred samples taken at a spacing of 10 μm. The interactive setting up of the programme variables can be seen at the beginning.

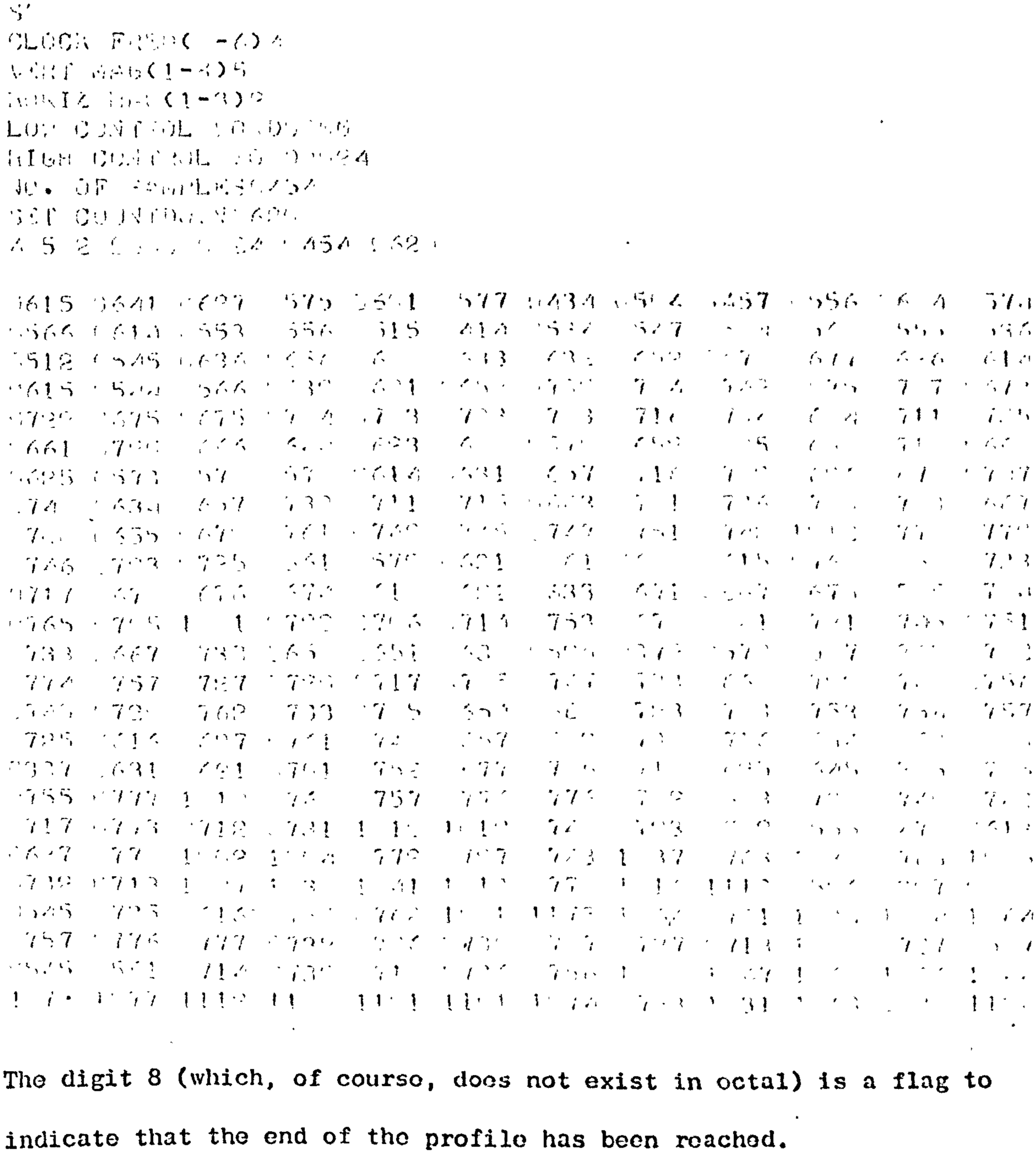

The digit 8 (which, of course, does not exist in octal) is a flag to indicate that the end of the profile has been reached.

When a number of parallel profiles had been recorded on a length of punched tape, this was used as input data for a programme run on the Imperial College CDC computer. This converted the octal integers into decimal height values in fractions of a millimeter and stored the whole map permanently on disc.

ADDENDUM

CORRECTIONS AND FURTHER INVESTIGATIONS

AD1.1 The Computer Model

There are two numerical errors in the computer model presented in Chapter five. They are:

1) The hardness of the stainless steel (used to calculate bearing areas) given on page 97 as 208 Nmm^{-2} is out by a factor of g. It should be 208 kgf mm^{-2}.
2) The force used to compute the accelerations of the slider in the computer model was calculated in Newtons, so accelerations computed where in ms^{-2} instead of mms^{-2}.

The effect of the first of these was to increace the load bearing area at which the surface maps, when brought together in the computer programme, where in equilibrium.

The principal effect of the second error was to alter the resonant frequency of the system. A spring/mass system with a mass of 0.6kg and a spring stiffness of $12.66x10^{3}Nm^{-1}$ would have a resonant frequency of 23.1Hz. The slip portion of a stick-slip cycle should (as a first approximation) be about half a cycle of the free resonant frequency, i.e., in the above case, 0.022s long. The effect of the error can be seen, for example, on fig. 5.11, where the slip time is about one second.

In view of these errors it was decided to re-run the computer

model with them corrected in order to to see if the hypotheses it incorporated were still tenable. In addition it was decided to make a more detailed investigation of the nature of the contact. The results of these two studies are presented in this addendum.

AD1.2 The Nature of the Contact

In the computer model presented in chapter five the contact between the rough surfaces was assumed to be entirely plastically deformed. Other work was quoted to justify this assumption for freshly created, un-run-in, surfaces of the type being considered, but no calculations were done on the data gathered on the surfaces: the surface maps.

Greenwood and Williamson (40) use a slightly different form of plasticity index from that used later by Hirst and Hollander (44 and p32) which is simpler to compute. The characteristic length that they use is the mean radius, R, of the curvature of the peaks of the surface profile. The Greenwood and Williamson plasticity index is given by

$$\psi = \frac{E'}{H}\sqrt{\frac{\sigma}{R}} \qquad \ldots\ldots (36)$$

where H is the hardness of the material of the surface, σ is the standard deviation of the heights of the peaks of the surface and E' is given by

$$E' = \frac{E}{2(1-\nu^2)} \qquad \ldots\ldots (37)$$

where E is Young's modulus for the material of the surface and ν is its Poisson's ratio. When ψ is less than about 0.6 asperity contact will be almost completely elastic except under

very high loads indeed. When ψ exeeds 1.0 plastic flow will occur under all but the lightest loads. This is not, of course, to say that all asperities in contact deform plastically for values of ψ greater than 1.0.

Another useful concept described by Greenwood and Williamson is that of elastic contact hardness, H', give by

$$H' = 0.25E'\sqrt{\frac{\sigma}{R}} \qquad \ldots. (38)$$

When two rough surfaces are loaded together and deform elastically the mean pressure between the asperities does not vary very much over a wide range of loads (typically by a factor of two for a load variation of 10^5). This is because, as the surfaces are forced together and the pressure between those asperities that were first in contact increases, new material and asperities come into contact under lower pressure and keep the mean pressure down. This means that the surfaces behave as though the contacts were, in a sense, plastic and deforming under roughly constant pressure. This is the justification for the idea of elastic contact hardness. If it was required to determine the real contact area for a given load when the deformation was elastic, it would be found to be that area which, when multiplied by the elastic contact hardness, gave a force equal to the load under consideration. Some of the areas of contact would be under greater pressure than the mean, some less, but the aggeregate effect would be the same as if the mean pressure were exerted throuought.

The behaviour of the elastic contact hardness and plasticity index outlined above is only valid for surfaces with a Gaussian height distribution. Surfaces that have been run-in almost

certainly do not have this distribution. However, freshly created surfaces would probably be closer to it (grit blasting or grinding, for example, produce height distributions that are very close to Gaussian).

The surfaces used in the experiments described in Chapter four and considered in the computer model were freshly created (though abraded with emery cloth - a process that would tend to remove the higher peaks).

A computer program was written to take the surface profiles that made up the surface map and to calculate values of σ and R from them. Five profiles, each 3mm long, were selected at random from the fifty that made up the map and run through the program, giving a total of 1500 height samples. The results (averaged appropriately across the five profiles) were as follows:

TABLE AD1

	mean	variance
CLA	2.32 μm	0.045 μm^2 (over 5 profiles)
RMS	3.26 μm	-
Peak height	-0.093 μm	5.64 μm^2 (over total of all peaks)
Peak radius	58.7 μm	-
Number of peaks	86	- (over 5 profiles)

As can be seen from the variance in the CLA values over the five profiles they were, in that respect at least, reasonably similar. σ, the standard deviation of the peak heights, is given by $\sqrt{5.64}$ = 2.37μm. R, the mean peak radius, was 58.7μm. Fig AD1 shows one of the profiles.

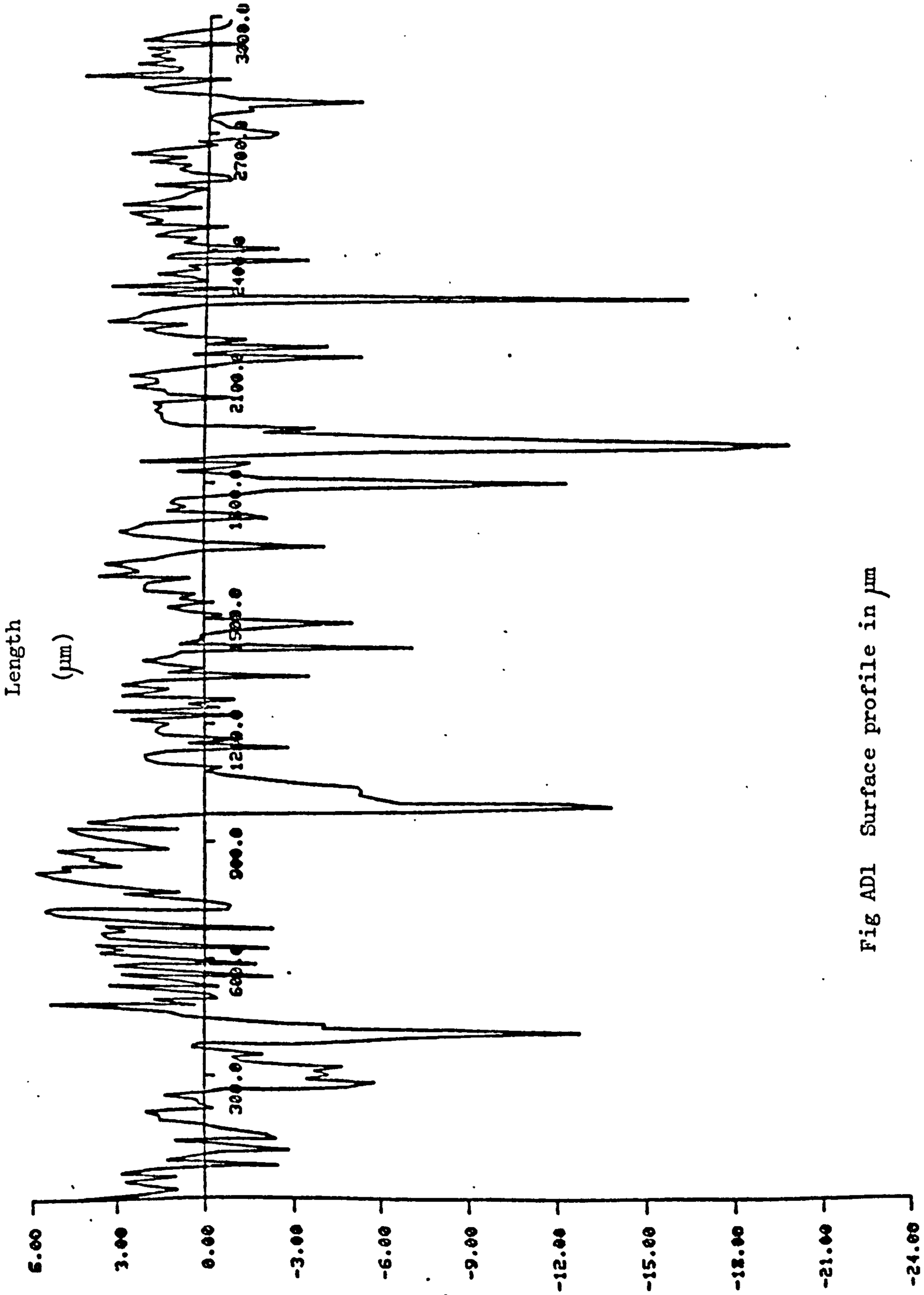

Fig AD1 Surface profile in μm

If the Young's modulus of the steel is taken to be 210kNmm^{-2} and its Poisson's ratio to be 0.3 then

$$E' = \frac{210}{2(1-0.3^2)}$$

$$= 115 \text{ kNmm}^{-2}$$

The elastic contact hardness is

$$H' = 0.25 \times 115 \sqrt{\frac{2.37}{58.7}}$$

$$= 5.78 \text{ kNmm}^{-2} \quad (=589 \text{ kgf mm}^{-2})$$

The plasticity index is

$$\psi = \frac{115 \times 10^3}{208 \times 9.81} \sqrt{\frac{2.37}{58.7}}$$

$$= 11.3$$

As can be seen the elastic contact hardness is about two and a half times greater than the plastic hardness measured for the surface (208 kgf mm^{-2}). This at first seems unreasonable. How can an elastically deforming surface give rise to mean pressures in exess of its elastic limit? The plasticity index of the surface, however, is 11.3. This means that a significant number of contacts will, in fact, be plastic, even under light loads. The analysis used by Greenwood and Williamson to give equation (38) is based, quite reasonably, on the assumption that the surfaces are deforming elastically when a value of H' is of interest.

AD1.3 The Revised Computer Model

In view of the high plasticity index obtained above it was decided to run the corrected computer model with the assumption that all

Fig AD2.1

Real Contact Area vs. Separation (mm^2/mm)

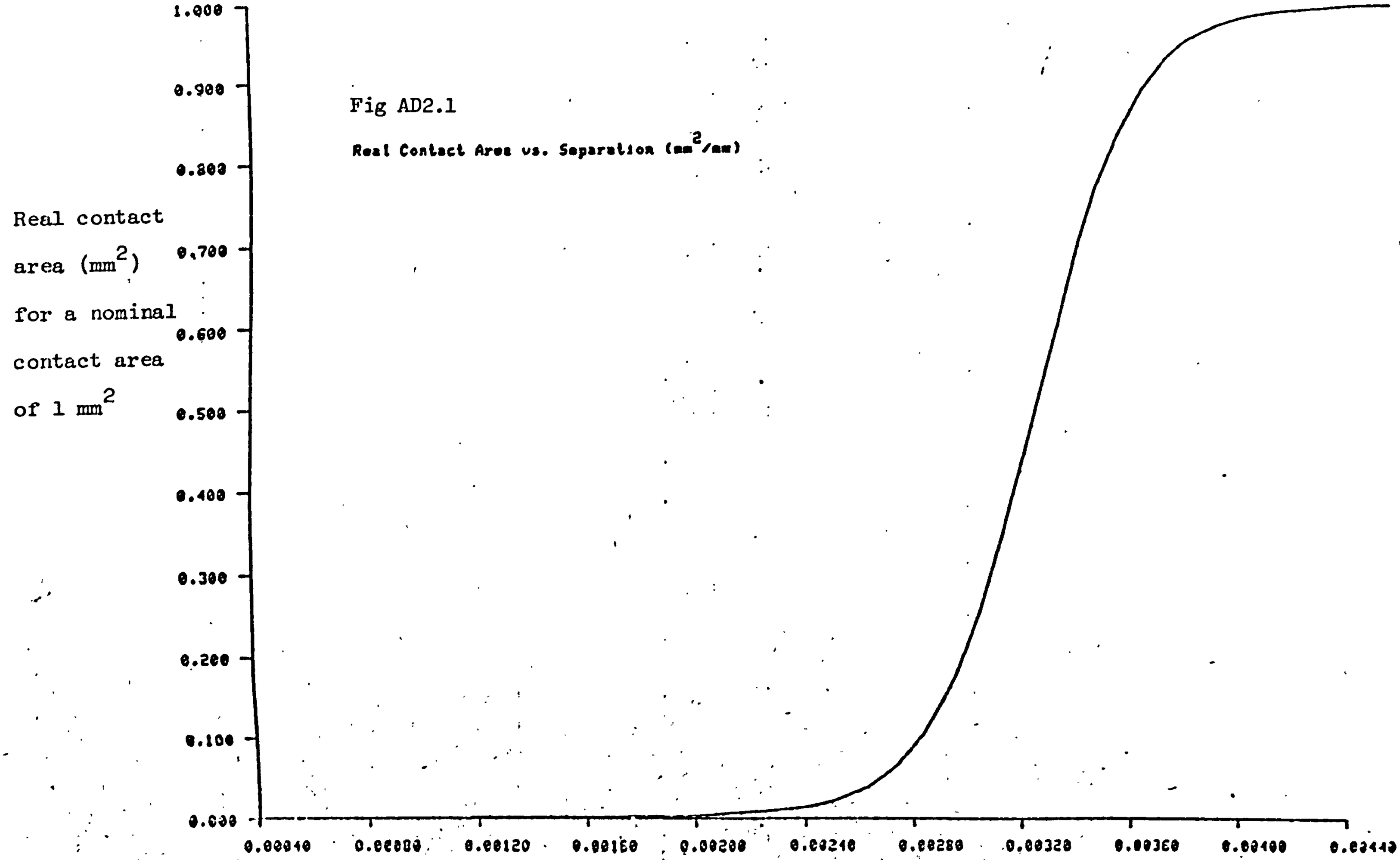

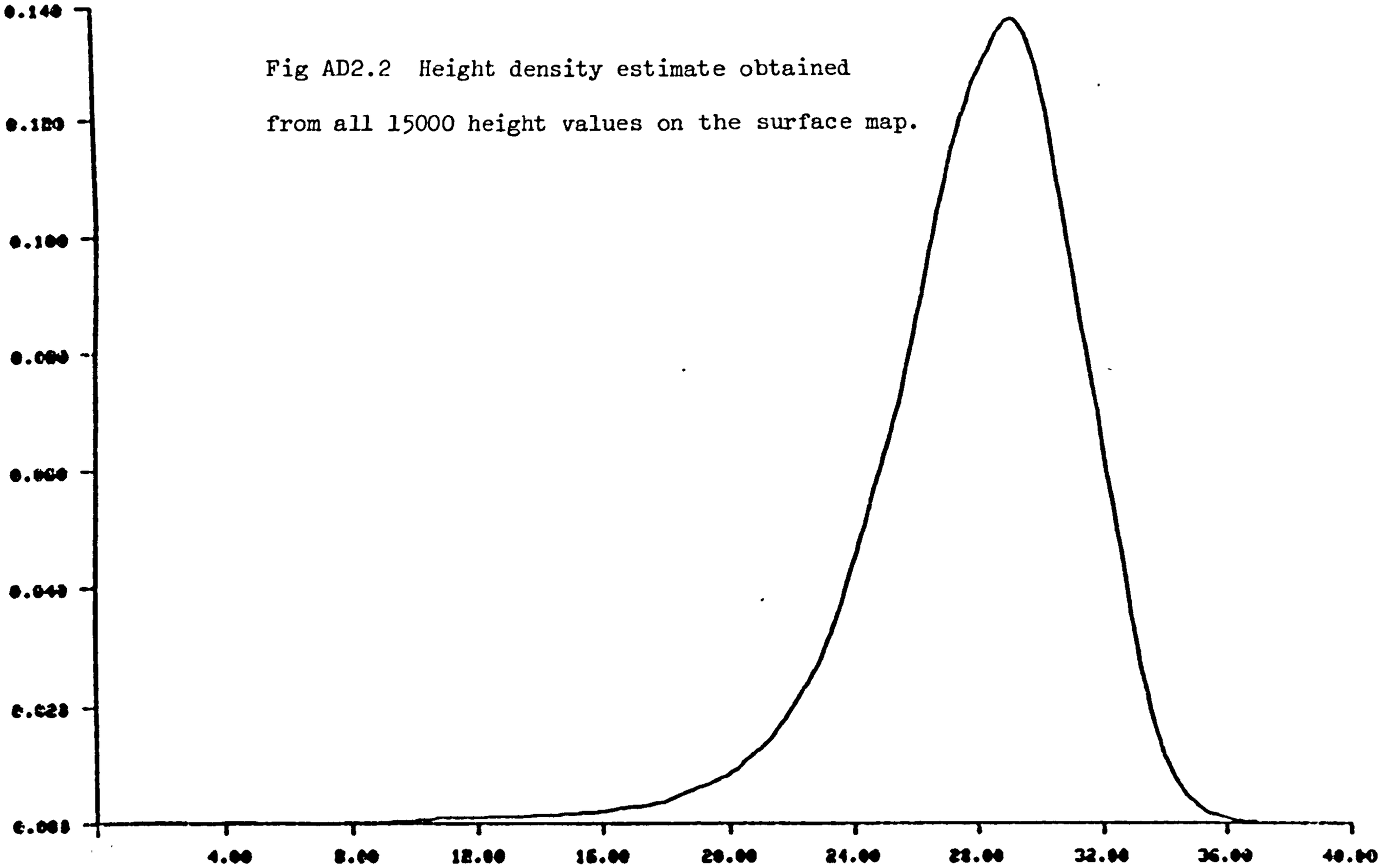

Fig AD2.2 Height density estimate obtained from all 15000 height values on the surface map.

contact deformation was plastic as before.

In order to reduce the workload on the computer an alteration was made to the part of the program that compared the two surface maps, looking for contacts, and gave an estimate of the true contact area between the surfaces. This was changed so that, instead of inspecting 10000 height values of the surface maps at each time-step in the marching process, it performed linear interpolation along a curve of bearing area vs. separation (obtained from the figures on the film of the contact under pressure that was mentioned in chapter five - see fig 5.6). A graph of the increase in area with increasing compression between the surface maps is shown in fig AD2.1. Fig AD2.2 shows the result of running a non-parametric density estimation program on all the height values of the surface map. The technique used was based on methods devised by Silverman (63,64) and implemented by him and the author.

As can be seen from the height density the parent distribution is skew. The abrasion of the surface has tended to remove the higher peaks while leaving the valleys largely untouched. The tails at the two ends of the density are thus very different. It was for this reason that it was considered best to use interpolation along the curve of cumulative contact area derived from the surface map. It would, of course, be possible to fit analytic expressions to this curve, or part of it, but, as the tails of the distribution were badly behaved (it is the right hand tail on fig AD2.2 that is of interest in contact under reasonable loads) it was thought that this might lead to some loss in accuracy, and, as linear interpolation on a function of a single variable defined at N points is an $O(\log_2 N)$ process the time savings involved would only be

marginal. In the case of fig AD2.1 N was about 50, most points being measured at the area of interest (the left hand tail).

Fig AD3 shows the result of running the friction modelling program with the variables set as in table AD2.

Table AD2

separation with relative velocity,	c	: 0.8
slider velocity,	V_o	: 0.01 ms^{-1}
mass,	M	: 0.6 kg
load,	L	: 30 N
spring stiffness ,	k	: 12.66 x 10^3 Nm^{-1}
Hardness		: 2.04 x 10^9 Nm^{-2}
shear strength		: 6.0 x 10^8 Nm^{-2}

Under these conditions the estimated real area of contact for a $1mm^2$ slider with no relative movement was 0.0147 mm^2.

Next the meaning of the variable, c, was modified to make it more robust. Instead of giving the gradient of the separation vs |relative velocity| when multiplied by the static loading separation of the surfaces it was set up to give the gradient when multiplied by the RMS surface roughness value (3.26 μm). Its effect was thus independant of the load under which the system was imagined to be operating.

As can be seen from fig AD3 the computer model still produces behaviour very similar to experimental stick-slip. The resonant frequency of the system (taken from the slip time on this figure) is about 20Hz. The resonant frequency from values of spring stiffness and mass in the model system was calculated to be 23.1Hz which is in reasonable agreement with this value.

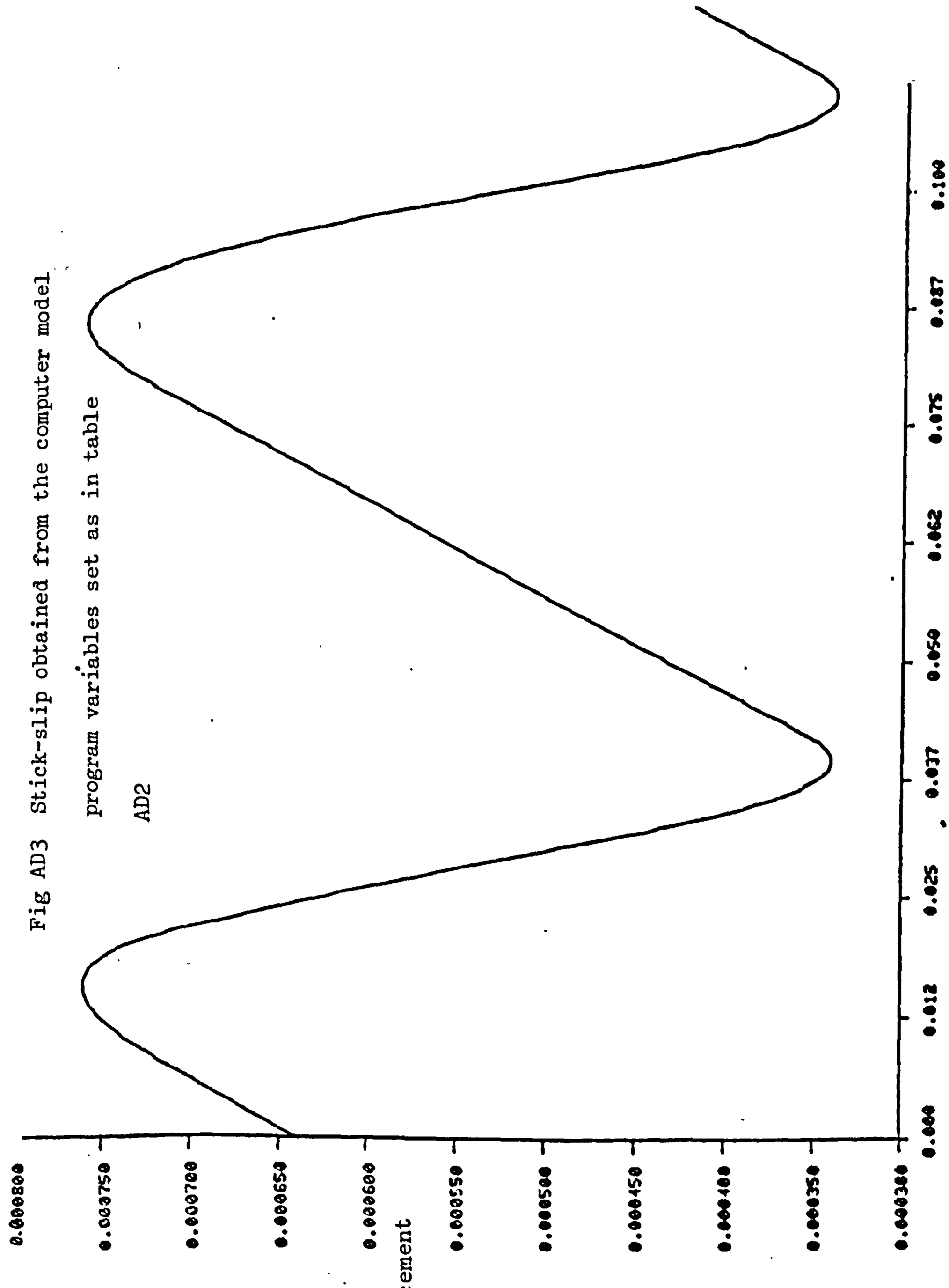

Fig AD3 Stick-slip obtained from the computer model program variables set as in table AD2

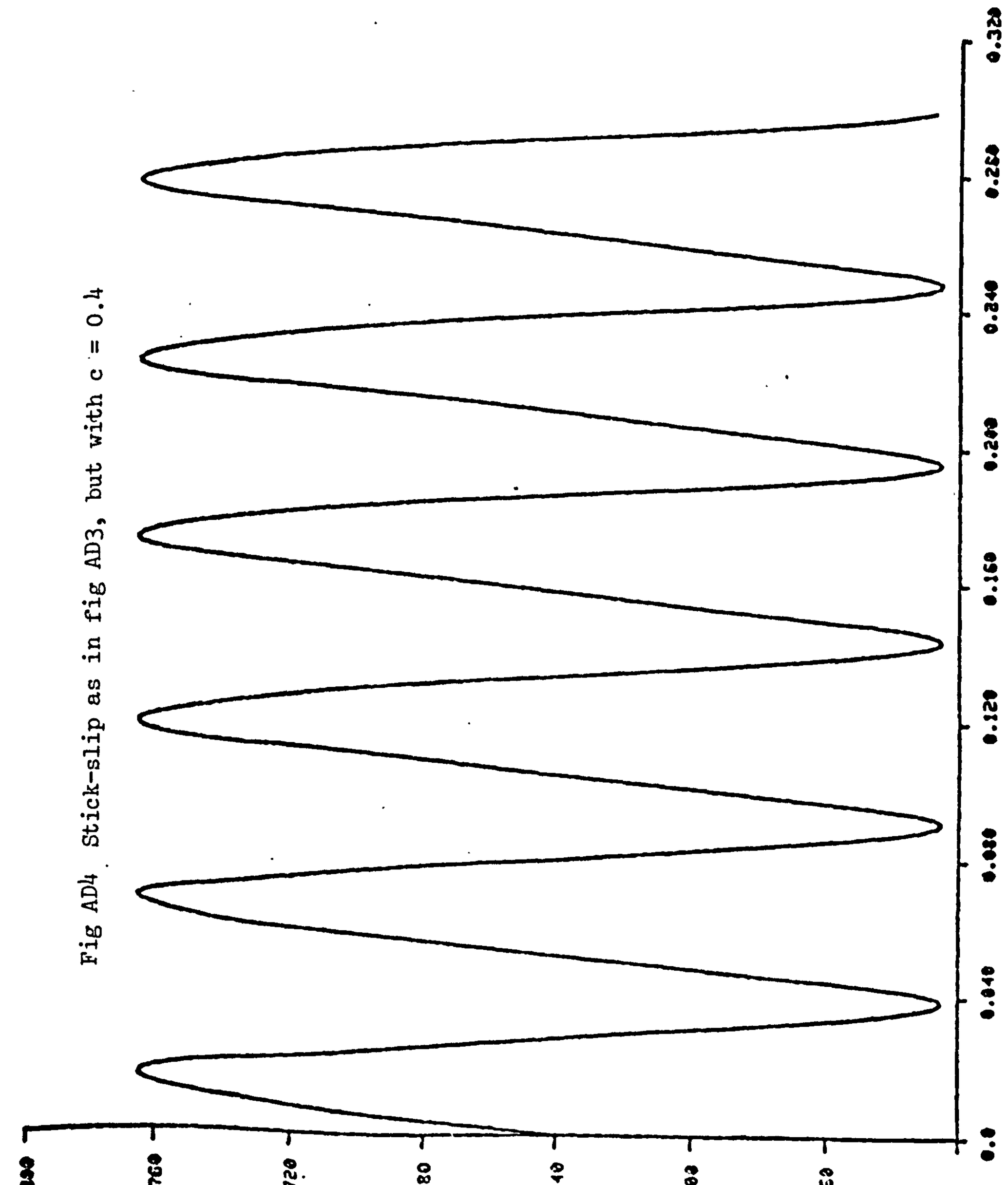

Fig AD4 Stick-slip as in fig AD3, but with c = 0.4

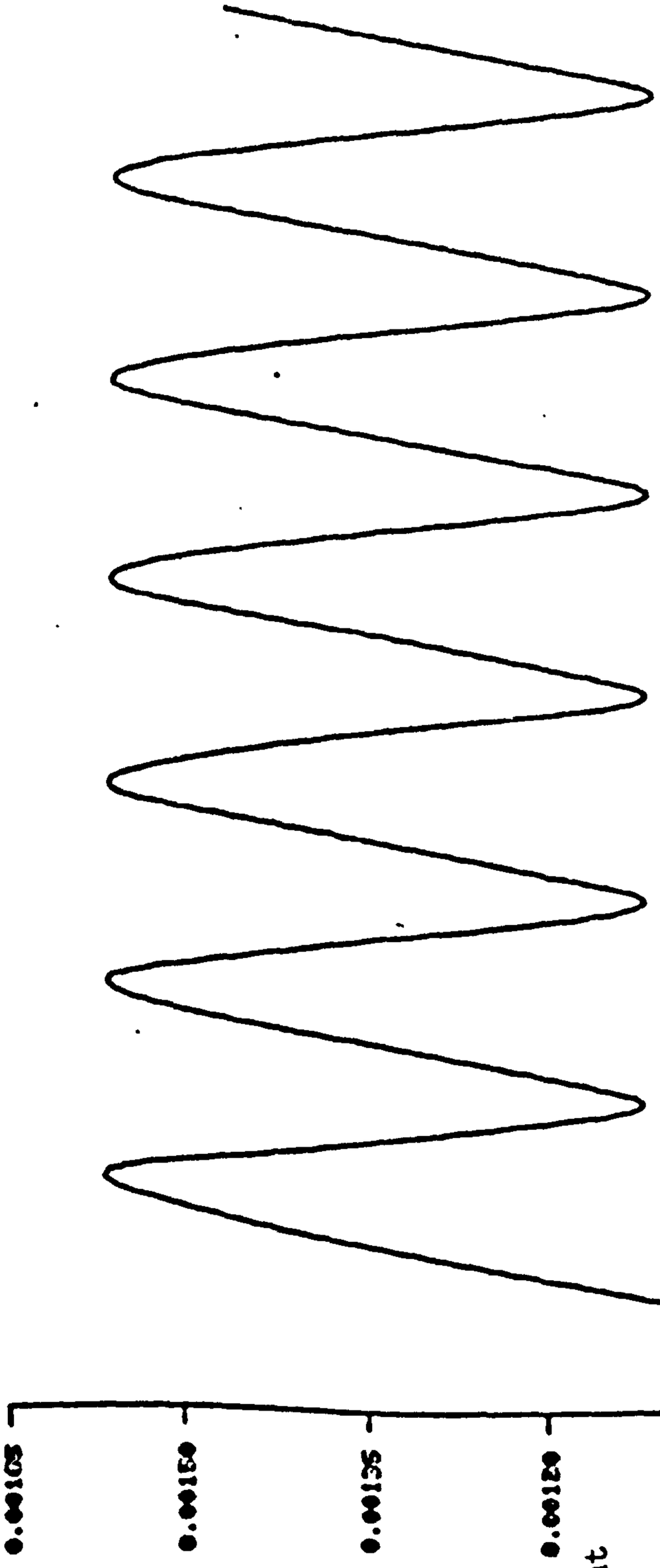

Fig AD5 As fig AD4 but with k = 6.0×10^{3} Nm^{-1}

Fig AD4 shows the result of reducing the value of c from 0.8 to 0.4, all other conditions being the same as for fig AD3. As would be expected this has reduced the amplitude of the stick-slip. In this case the computer model was run for a longer time to check its stability. As can be seen it has produced very regular, repeatable stick-slip. This would be expected if the program were working well, as, unlike the version of the model described in Chapter five, where true area of contact between the sliding surfaces depended not only upon relative velocity, but also, to a certain extent, upon the local nature of the surface maps, the true area of contact for a given relative velocity in the later version of the model was always the same, as it resulted from simple interpolation on a fixed curve (fig AD2.1).

Fig AD5 shows the result of reducing the spring stiffness in the system from 12.66×10^3 Nm^{-1} to 6.0×10^3 Nm^{-1}, other conditions remaining the same as for figure AD4. Again, behaviour is as would be expected. The theoretical resonant frequency of the model system should now be 16Hz. That calculated from the slip time displayed by the model is 14Hz. The displacement reached before slipping starts is about 1.58mm. With $k=6 \times 10^3 Nm^{-1}$ and L=30N this represents a friction coefficient of 0.32. Dividing the shear strength assumed by the hardness gives a value of 0.34.

The revised computer model was run under a variety of combinations of values of spring stiffness, velocity and separation coefficient, c. Except under extreme conditions, where the Euler technique for solving the differential equation of motion was either too costly or too unstable, it produced results similar to experimental stick-slip.

Finally, it was decided to attempt to use the computer model

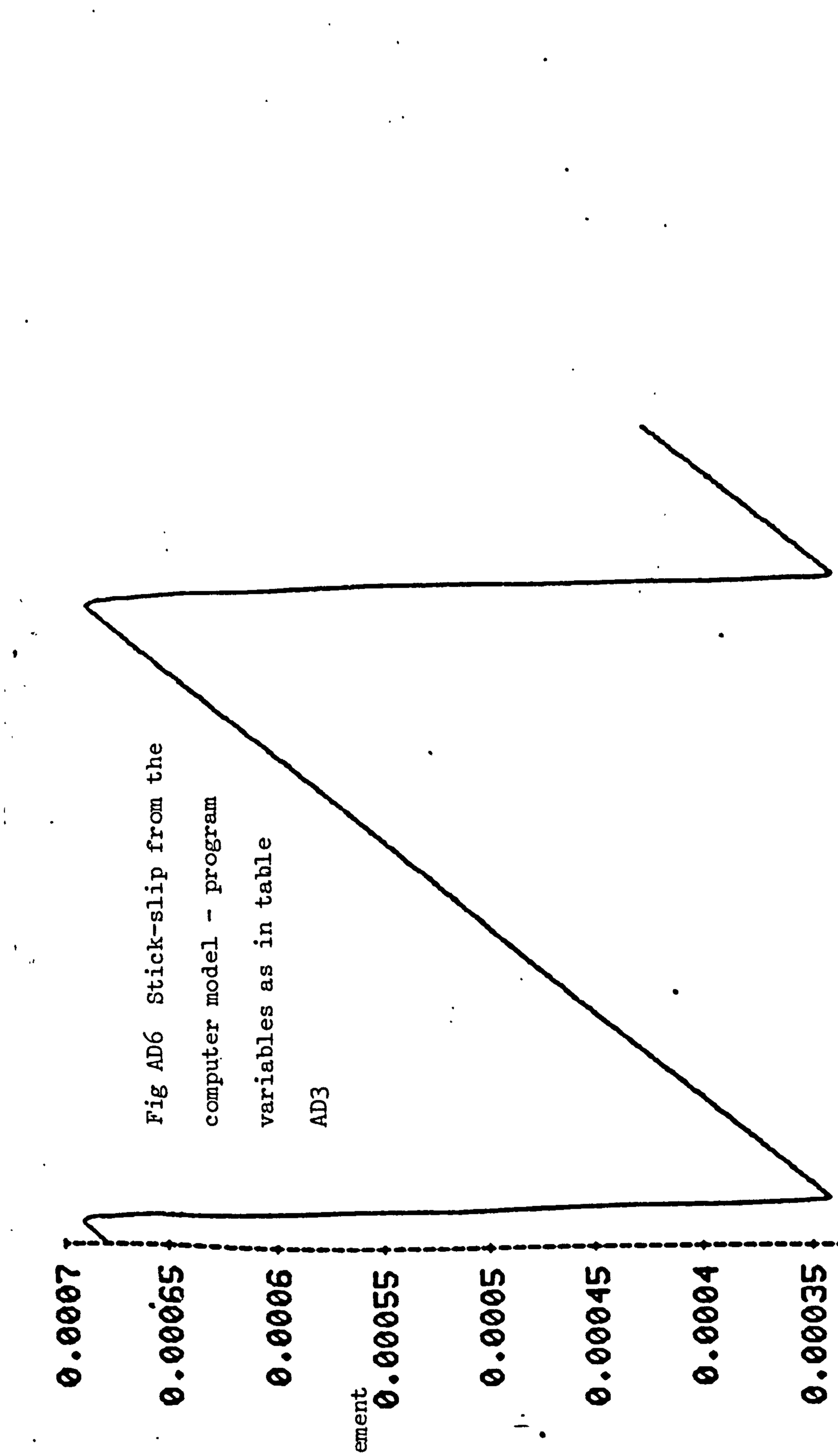

Fig AD6 Stick-slip from the computer model - program variables as in table AD3

to reproduce experimental results quantitatively. Figure AD6 shows the result of running the model under the following conditions:

Table AD3

c : 1.72

V_o : 0.42 mms^{-1}

M : 0.6kg

L : 30N

K : $17.1x10^{3}Nm^{-1}$

Hardness : $2.04x10^{9}Nm^{-2}$

shear strength : $7.94x10^{8}Nm^{-2}$

These equal the conditions of the experiment reported in fig 4.1a (page 63) (the velocity during the experiment ($0.42mms^{-1}$) measured from the gradient of the stuck portion of the curve, was slightly lower than the nominal $0.5mms^{-1}$ reported at the side of fig 4.1). The shear strength was set to give the required displacement just before the start of sliding. As comparison between fig AD6 and fig 4.1a will show, the output of the computer model and the experimental result are very similar.

AD1.4 Discussion and Conclusions

Computations done on the statistics obtained from the surface map justified the assumption, that was used in the computer model, that contact between the surfaces was largely plastic.

The vertical movement between the sliding surfaces required to make the model work agrees reasonably with reported results. For example in fig AD3 the peak relative velocity between the sliding surfaces is about $0.06ms^{-1}$. At this relative velocity the surfaces were considered to have moved appart by 0.16μm. As

inspection of fig AD1 will show, this is not a great deal when compared with the overall structure of the surface. Quite small relative movements, therefore, are sufficient to produce changes in contact area (and hence friction force) that lead to reasonably lifelike stick-slip. In Tolstoi's experiments (27 and p23) vertical slider movements of about 0.2 - 0.5 μm were measured for stick-slip amplitudes of about 0.5mm. This is similar to the stick-slip amplitude in fig AD3. The steel used by Tolstoi had a roughness of 1.25μm CLA. However the mass, sliding velocity and bulk geometry of his apparatus were all different from those assumed for the computer model presented here, so any comparisons should be treated with caution.

In the attempt to reproduce experimental results (figs AD6/4.1a) the peak relative velocity was about 0.01ms^{-1} (cf fig4.1b). With c set to 1.72 this would imply a maximum separation of the surfaces from their rest position of about 0.06μm. This is tolerably small when compared with the scale of the surface asperities (fig AD1), and it would not be unreasonable to expect their interaction to produce movements of this magnitude.

When the computer model had been corrected, and performed acceleration and true contact area calculations properly it gave results very similar to experimental stick-slip, lending support to the various hypotheses it incorporated.

REFERENCES

1) Bowden, F.P., Leben, L.: The Nature of Sliding and the Analysis of Friction: Proc. Roy. Soc. (Lond.) A169(1939)371

2 Schelling, J.C.: The Physics of the Bowed String: Scientific American Jan.(1974)87

3 Swanson, S.A.V.: Engineering Dynamics: English Universities Press (1963)207

4 Morin, A.: Nouvelles experiances sur le frottement .... Faites a Metz en 1833 Paris (cited in (8))

5 Wells, J.H.: Kinetic Boundary Friction: The Engineer 147(1929)454

6 Thomas, S.: Vibrations Damped by Solid Friction: Phil. Mag. Ser.7 9(1930)329

7 Rowson, D.M.: Analysis of Stick-Slip Motion: Wear 31,2(1975)213

8 Rabinowicz, E: Stick and Slip: Scientific American 194,5(1956)109

9 Antoniou, S.S.: The Mechanisim of Frictional Oscillations: Ph.D. Thesis, Univ. of Lond. Nov. 1971

10 Michel, JCG.L., Porter, A.: The Effect of Friction on the Behaviour of Servomechanisims at Creep Speeds: Proc. Inst. Elec. Engrs. 98,2(1951)297

11 Halling, J.: Principles of Tribology: Macmillan 1975 Ch. 7

12 Block, H.: Fundamental Mechanical Aspects of Boundary Lubrication: SAE Journal (Trans.) 46(1940)54

13 Kaidanovsky, N.L., Haykin, S.E.: Zeits f. Tech. Physik 3(1933)91 (cited in (14))

14 Sampson, J.B.; Morgan, F., Reed, D.W., Muskat, M.: Friction Behaviour During the Slip Portion of the Stick-Slip Process: J. App. Phys. 14(1943)689

15 Brockley, C.A., Ko, P.L.: The Measurement of Friction and Friction Induced Vibration: Trans. ASME J. Lub. Tech. F92(1970)543

16 Lienard, P.: Representation graphique de la resonance d'un oscillateur utilisable pour l'etude de systems non lineaires: La Rech. Aeron 29(1952)45

17 Brockley, C.A., Ko, P.L.: Quasi-Harmonic Friction Induced Vibration: Trans. ASME J. Lub. Tech. F92(1970)550

18 Brockley, C.A., Cameron, R., Potter, A.F.: Friction Induced Vibration: Trans ASME J. Lub. Tech. F89 F89(1967)101

19 Banerjee, A.K., Influence of Kinetic Friction on the Critical Velocity of Stick-Slip Motion: Wear 12(1968)107

20 Cockerham, G., Cole, M.: Stick-Slip Stability by Analogue Simulation: Wear 36,2(1966)189

21 Rabinowicz, E.: The Intrinsic Variables Affecting the Stick-Slip Process: Proc. Phys. Soc. 71(1958)668

22 Dokos, S.J.: J. App. Mech. A148(1946)13 (cited in (21))

23 Bowden, F.P., Tabor, D.: The Friction and Lubrication of Solids: Oxford University Press Part 2, Ch. 4 (1964)

24 Tabor, D.: Junction Growth in Metalic Friction: Proc. Roy. Soc. (Lond.) A251(1959)378

25 Syrop, A.N.: Lubricant Activity in Slow Speed Friction Tests: p Ph.DD Thesis, Univ. Lond. 1976

26 Green, M.A.?EBrockley, C.A.: Visco-elastic Effects in Boundary Lubrication

27 Tolstoi, D.M.: Significance of the Normal Degree of Freedom and Natural Normal Vibration in Contact Friction: Wear 10(1967)199

28 Elder, J.A., Eiss jr., N.S.: A Study of the Effect of Normal Stiffness on Kinetic Friction Forces Between Two Bodies in Sliding Contact: Trans. ASLE 12(1969)234

29 Leather, J.A.: A Short Introduction to the Study of Rough Surfaces: Surfacing J. Jan.(1976)7

30 Thomas, T.R., King, M.: Surface Topography in Engineering: British Hydrodynamic Res. Assoc., Fluid Eng. Ser. 3(1971)

31 Thomas, T.R.: Private Communication, Lubrication Lab., I.C. May 1977

32 Dyson, J., Hirst, W.: The True Contact Area Between Solids: Proc. Phys. Soc. B67(1954)309

33 Uppal, A.H., Probert, S.T., Thomas, T.R.: The Real Area of Contact Between a Rough and a Flat Surface: Wear 22(1972)163

34 Archard, J.F.: Elastic Deformation and the Laws of Friction: Proc. Roy. Soc. (Lond)) A243(1957)190

35 Greenwood, J.A.: The Real Area of Contact Between Rough Surfaces and Flats: Trans. ASME J. Lub. Tech. F89,1(1967)81

36 Pullen, J., Williamson, J.P.B.: On the Plastic Contact of Rough Surfaces: Proc. Roy. Soc. (Lond.) A327(1972)159

37 Courtney-Pratt, J.S., Eisner: The Effect of Tangential Force on the Contact of Metalic Bodies: Proc. Roy. Soc. (Lond.) A238(1957)529

38 Tabor, D.: Junction Growth in Metallic Friction - The role of Combined Stresses and Surface Contamination: Proc. Roy. Soc. (Lond.) A251(1959)378

39 Thomas, T.R.: Computer Simulation of Wear: Wear 22(1972)83

40 Greenwood, J.A., Williamson, J.P.B.: Contact of Nominally Flat Surfaces: Proc. Roy. Soc. (Lond.) A253(1966)300

41 Greenwood, J.A., Tripp, J.H.: The Contact of Two Nominally Flat Rough Surfaces: Proc. I. Mech. E. 185(1970)625

42 Williamson J.P.B.: The Microtopography of Surfaces: Proc. I. Mech. E. 182,3K(1967)21

43 Whitehouse, D.J., Archard, J.F.: The Properties of Random

Surfaces of Significance in Their Contact: Proc. Roy. Soc. (Lond.) A316(1970)97

44 Hirst, W., Hollander, A.E.: Surface Finish and Damage in Sliding: Proc. Roy. Soc. (Lond.) A337(1974)379

45 Sayles, R.S.: Ph.D. Thesis, Teesside Polytechnic 1976

46 Sayles, R.S., Thomas, T.R.: Microtopometry of Engineering Surfaces: Course Notes, Mech. Eng. Dept., Teesside Poly., Middlesbrough.

47 Sayles, R.S., Thomas, T.R.: Private communication, Lubrication Lab., I.C. 1975. To be published.

48 Hill, R.A.: Private Communication, Lubrication Lab., I.C. 1976

49 Barwell, F.T.: Tribological Implications of Surfaces: Proc. I. Mech. E. 182,3K(1967)1

50 Williamson, J.P.B., Hunt, R.T.: Relocation Profilometry: J. Phys. E. Sci. Instrum. 1(1968)749

51 Takahashi, N., Okada, K., Yoshida, M.: Electron Microscope Study of the Intermittent Motion of Friction: Wear 28(1974)285

52 Gregory, J.N.: Radioactive Tracers in the Study of Friction and Lubrication: Nature 157(1946)443

53 Brockley, C.A.: Private Communication, Lubrication Lab., I.C. 1977

54 Thomas, T.R.: Private Communication, Lubrication Lab., I.C. 1977

55 Hiley, R.W.: Private Communication, Lubrication Lab., I.C. 1976

56 James, N.W.: Ph.D. Thesis in preparation, Univ. of Lond. 1977

57 Kazamaki, T.: An Investigation of Air Leakage Between Contact Surfaces: Bul. JSME 17(1974)1321

58 Armand, G., Pujoulade, J.L.A., Paigne, J.: A Theoretical and Experimental Relationship Between the Leakage of Gases Through the Interface of Two Metals in Contact and Their Superficial Microgeometry: Vacuum 14(1964)53

59 Brockley, C.A.: Private communication, Lubrication Lab., I.C. 1977

60 Fowles, P.E.: The Application of EHL Theory to individual asperity - asperity collisions: Trans. ASME, J. Lub. Tech. F91,3(1969)464

61 Coates, T.: Private Communication, Lubrication Lab., I.C. 1977

62 Chinick, H.P.: LVDT Puts Precision in Surface Texture Measurement: Cutting Tool Engning. 20(1968)13

63 Silverman, B.W.: Choosing the window width when estimating a density: Biometrika 65(1978)1

64 Silverman, B.W.: Density estimation. Are theoretical results useful in practice?: Proc. of the Advanced Int. Symp. on Asymptotic Stats. Chapel Hill, North Carolina, USA. Apr 79 A.P. in press